

A Thesis Submitted for the Degree of PhD at the University of Warwick

Permanent WRAP URL:

<http://wrap.warwick.ac.uk/116327>

**Copyright and reuse:**

This thesis is made available online and is protected by original copyright.

Please scroll down to view the document itself.

Please refer to the repository record for this item for information to help you to cite it.

Our policy information is available from the repository home page.

For more information, please contact the WRAP Team at: [wrap@warwick.ac.uk](mailto:wrap@warwick.ac.uk)

**Synthesis and properties of novel  
polyester-based materials**

by

**Patrick Adrianus Johannes Maria de Jongh**

**A thesis submitted for the degree of  
Doctor of Philosophy in Chemistry**

**Department of Chemistry**

**University of Warwick**

**August 2018**

---

*I am among those who think science has great beauty. A scientist in a laboratory is not only a technician, he is also a child placed before natural phenomena which impress him like a fairy tale.*

Marie Curie

---

# Table of contents

Table of contents	ii
Table of figures	vii
Table of tables	xvii
Table of schemes	xxi
Table of equations	xxv
Abbreviations and symbols	xxvi
Acknowledgements / Dankwoord	xxxii
Declaration	xxxiii
Abstract	xxxiv
Lekensamenvatting	xxxv
<b>Chapter 1 - Synthetic strategies for polyester-based materials</b>	<b>1</b>
1.1 Biodegradable materials	2
1.2 Synthetic strategies for polyesters, poly(ester amide)s and poly(aminoester)s	2
1.3 Polycondensation	3
1.3.1 Monomers from renewable resources	5
1.3.2 Carothers and Flory-Stockmayer equations	7
1.3.3 Catalysts	10
1.4 Ring-opening polymerisation	11
1.4.1 Monomers for ring-opening polymerisation	12
1.4.2 Thermodynamics of ring-opening polymerisation	13
1.4.3 Catalysts for ring-opening polymerisation	14
1.5 Radical ring-opening polymerisation	16
1.5.1 RROP monomers and their polymerisation	16
1.5.2 Introducing additional functionalities	19
1.5.3 Post-polymerisation functionalisation, controlled polymerisation and applications	21
1.6 Chain-growth condensation polymerisation	22
1.7 Spontaneous zwitterionic copolymerisation	25

---

1.7.1 SZWIP of cyclic imino ethers	27
1.7.2 SZWIP of aziridines	33
1.8 Miscellaneous strategies	34
1.9 Conclusions	35
1.10 References	36
<b>Chapter 2 – <i>N</i>-Acylated poly(aminoester) macromonomers by spontaneous zwitterionic copolymerisation</b>	<b>48</b>
2.1 Introduction	49
2.2 Results and discussion	51
2.2.1 Initial synthesis of NPAE macromonomers	51
2.2.2 Screening experimental parameters	52
2.2.3 Expanding the library of NPAE macromonomers	54
2.2.4 Manipulating the $\omega$ -end group	57
2.2.5 MALDI-ToF analysis	58
2.2.6 Elemental analysis	60
2.2.7 Thermal analysis of NPAE macromonomers	61
2.3 Conclusions	63
2.4 Experimental details	64
2.4.1 Materials	64
2.4.2 Instruments and analysis	65
2.4.3 Synthetic procedures	66
2.5 References	67
<b>Chapter 3 – Mechanistic studies on the spontaneous zwitterionic copolymerisation of cyclic imino ethers and acrylic acid</b>	<b>71</b>
3.1 Introduction	72
3.2 Results and discussion	74
3.2.1 Macromonomer synthesis	74
3.2.2 ESI MS analysis of macromonomers	75
3.2.3 Tandem mass spectrometry	81
3.2.4 Evidencing microstructures	82

---

---

3.2.5 Semi-quantification of homopropagation and $\omega$ -end groups	87
3.2.6 Mechanism for SZWIP of cyclic imino ethers and acrylic acid	95
3.3 Conclusions	98
3.4 Experimental	99
3.4.1 Materials	99
3.4.2 Instruments and analysis	100
3.4.3 Synthetic procedures	101
3.5 References	106
<b>Chapter 4 – Dual-stimuli responsive comb polymer scaffold from <i>N</i>-acylated poly(aminoester) macromonomers</b>	<b>108</b>
4.1 Introduction	109
4.2 Results and discussion	112
4.2.1 Macromonomer synthesis	112
4.2.2 Comb polymer synthesis	113
4.2.2.1 Free radical polymerisation	113
4.2.2.2 Redox-initiated RAFT polymerisation	114
4.2.2.3 Triple detection SEC analysis	118
4.2.3 Thermal analysis	120
4.2.4 LCST studies	122
4.2.5 Comb polymer functionalisation	126
4.3 Conclusions	130
4.4 Experimental details	130
4.4.1 Materials	130
4.4.2 Instruments and analysis	131
4.4.3 Synthetic procedures	132
4.5 References	138
<b>Chapter 5 – Evaluating the potential of <i>N</i>-acylated poly(aminoester)-based comb polymers for biological applications</b>	<b>143</b>
5.1 Introduction	144
5.2 Results and discussion	146

---

---

5.2.1 Degradation studies	148
5.2.2 Cell toxicity studies	151
5.2.3 Haemolysis studies	153
5.2.4 Comb polymers for cell association and uptake studies	154
5.2.5 Cell association studies	157
5.2.6 Cell uptake studies	159
5.2.7 Film formation and anti-fouling properties	160
5.3 Conclusions	166
5.4 Experimental	166
5.4.1 Materials	166
5.4.2 Instruments and analysis	168
5.4.3 Synthetic procedures	169
5.4.4 Degradation studies	176
5.4.5 Cell viability studies	178
5.4.6 Haemolysis studies	179
5.4.7 Cell association studies	180
5.4.8 Cell uptake studies	180
5.4.9 Anti-fouling properties	181
5.5 References	182
<b>Chapter 6 – Thermal study on polyester networks based on the renewable monomers citric acid and gluconolactone</b>	<b>186</b>
6.1 Introduction	187
6.2 Results and discussion	188
6.2.1 Citric acid and D-glucono- $\delta$ -lactone	189
6.2.2 Aliphatic bifunctional co-monomers	190
6.2.3 Aliphatic polyfunctional co-monomers	195
6.2.4 Aromatic co-monomers	197
6.2.5 Effect of ring-structured monomers	199
6.2.6 Catalysts	201
6.3 Conclusions	202
6.4 Experimental	203

---

---

6.4.1 Materials	203
6.4.2 Differential scanning calorimetry (DSC)	203
6.4.3 Synthetic procedures	204
6.5 References	205
<b>Chapter 7 – High <math>T_g</math> poly(ester amide)s by melt polycondensation of monomers from renewable resources; citric acid, D-glucono-<math>\delta</math>-lactone and amino acids: A DSC study</b>	<b>207</b>
7.1 Introduction	208
7.2 Results and discussion	211
7.2.1 Hydrophobic, non-reactive side chains	213
7.2.2 Hydroxyl and thiol side chains	214
7.2.3 Carboxylic acid side chains	216
7.2.4 Amine and guanidine side chains	217
7.2.5 Cyclic amino acids	218
7.3 Conclusions	220
7.4 Experimental	220
7.4.1 Materials	220
7.4.2 Differential scanning calorimetry (DSC)	221
7.4.3 Synthetic procedures	221
7.5 References	221
<b>Chapter 8 – Conclusions and outlook</b>	<b>225</b>
8.1 The potential of polyester-based materials	226
8.2 <i>N</i> -acylated poly(aminoester)s by SZWIP	226
8.3 Branched polyesters from renewable materials	228
8.4 Overall outlook	229
8.5 References	229
About the author	230
List of publications	231
Appendix – Supplementary information for Chapter 3	233

---

---

## List of figures

- Figure 1.1** Evolution of molecular weight versus monomer conversion for uncontrolled chain-growth, step-growth and living polymerisations. Adapted from ref. 34. 3
- Figure 1.2** Schematic of a step-growth polymerisation illustrating the formation of a broad molecular weight distribution. White circles are bifunctional monomers, black circles are dimers, trimers and longer oligomers. 4
- Figure 1.3** Conversion of cellulose to sugars and other common hydroxy monomers. Adapted from ref. 44. 6
- Figure 1.4** Monomers suitable for polycondensation reactions that can be derived from 5-hydroxymethylfurfural. Adapted from ref. 45. 6
- Figure 2.1** Analysis of EtOx/AA 1/1 macromonomer by  $^1\text{H}$  NMR (a) and SEC (b). R = H,  $\text{CH}_2\text{CH}_2\text{NHCOEt}$ . 52
- Figure 2.2** SEC molecular weight distributions for NPAE macromonomers synthesised from EtOx and AA under various conditions (Table 2.1): a) entries 1-5, and b) entries 6-10. 53
- Figure 2.3** Structures of the monomers employed in this work. 54
- Figure 2.4** Structures of the NPAE macromonomers investigated. 54
- Figure 2.5**  $^1\text{H}$  NMR spectra ( $\text{CDCl}_3$ ) of macromonomers synthesised from MeOx/AA (a), EtOx/AA (b), EtOx/CEA (c) and EtOz/AA (d). R = H or  $\text{CH}_2\text{CH}_2\text{NHCOMe}$  (MeOx), H or  $\text{CH}_2\text{CH}_2\text{NHCOEt}$  (EtOx), H or  $\text{CH}_2\text{CH}_2\text{CH}_2\text{NHCOEt}$  (EtOz). 55
- Figure 2.6** SEC analysis of macromonomers synthesised from MeOx/AA (a), EtOx/AA (b), EtOx/CEA (c) and EtOz/AA (d). 56
- Figure 2.7** MALDI-ToF spectra for MeOx/AA synthesised from (a) 1/1 and (b) 1/2 feed ratios. Rectangular symbols denote alternating compositions, circular symbols indicate distributions that deviate from an alternating composition. 58
- Figure 2.8** MALDI-ToF spectra for EtOx/AA synthesised from (a) 1/1 and (b) 1/2 feed ratios. Rectangular symbols denote alternating compositions, 59

---

circular symbols indicate distributions that deviate from an alternating composition.

**Figure 2.9** MALDI-ToF spectra for EtOz/AA synthesised from (a) 1/1 and (b) 1/2 feed ratios. Rectangular symbols denote alternating compositions, circular symbols indicate distributions that deviate from an alternating composition. 60

**Figure 2.10** Elemental analysis results for NPAE macromonomers. 61

**Figure 2.11** Thermogravimetric analysis of NPAE macromonomers synthesised from MeOx/AA (a), EtOx/AA (b), EtOx/CEA (c) and EtOz/AA (d). 62

**Figure 2.12** DSC analysis (second heating curve) of NPAE macromonomers synthesised from MeOx/AA (a), EtOx/AA (b), EtOx/CEA (c) and EtOz/AA (d). 63

**Figure 3.1** Overview ESI MS spectra for oligo(MeOx-*alt*-AA)<sub>n</sub>A copolymers from MeOx:AA 1:1 (a), 1:2 (b) and 2:1 (c) feed ratios. Purple circles correspond to ω-carboxylic acid terminated H<sup>+</sup> ionised species, green circles correspond to ω-amide terminated H<sup>+</sup> ionised species. 76

**Figure 3.2** Overview ESI MS spectra for oligo(EtOx-*alt*-AA)<sub>n</sub>A copolymers from EtOx:AA 1:1 (a) and 1:2 (b) feed ratios. Purple circles correspond to ω-carboxylic acid terminated H<sup>+</sup> ionised species, green circles correspond to ω-amide terminated H<sup>+</sup> ionised species. 76

**Figure 3.3** Overview ESI MS spectra for oligo(EtOz-*alt*-AA)<sub>n</sub>A copolymers from EtOz:AA 1:1 (a) and 1:2 (b) feed ratios. Purple circles correspond to ω-carboxylic acid terminated H<sup>+</sup> ionised species, green circles correspond to ω-amide terminated H<sup>+</sup> ionised species. 77

**Figure 3.4** Expanded ESI MS spectra for oligo(MeOx-*alt*-AA)<sub>n</sub>A macromonomers from MeOx:AA 1:1 (a), 1:2 (b) and 2:1 (c) feed ratios, showing all species within one repeat unit. A generalised peak assignment is shown in Table 3.2. 77

**Figure 3.5** Expanded ESI MS spectra for oligo(EtOx-*alt*-AA)<sub>n</sub>A macromonomers from EtOx:AA 1:1 (a) and 1:2 (b) feed ratios, showing all species within one repeat unit. A generalised peak assignment is shown in 79

---

Table 3.3.	
<b>Figure 3.6</b> Expanded ESI MS spectra for oligo(EtOz- <i>alt</i> -AA) <sub>n</sub> A macromonomers from EtOz:AA 1:1 (a) and 1:2 (b) feed ratios, showing all species within one repeat unit. A generalised peak assignment is shown in Table 3.4.	80
<b>Figure 3.7</b> ESI MS/MS spectrum for MeOx/AA of $m/z^{\text{exp}} = 328.1861$ with an HCD of 25 eV. The corresponding peak assignments can be found in Table 3.5 and Scheme 3.4.	83
<b>Figure 3.8</b> Fragmentation of MeOx/AA $m/z^{\text{exp}} = 472.2295$ . a) Possible microstructures and their key fragment ions. b) ESI MS/MS spectrum showing the fragmentation of various isobaric structures at an HCD of 18 eV and the presence of key fragment ions for two possible microstructures.	85
<b>Figure 3.9</b> ESI MS/MS spectra for EtOx/AA $m/z^{\text{exp}} = 365.1670$ (a) and EtOz/AA $m/z^{\text{exp}} = 393.1995$ (b).	86
<b>Figure 3.10</b> Calibration curves for the AA-MeOx-AA small molecule analogue. a) Calibration based on protonated species ( $m/z^{\text{exp}} = 230.1019$ ). b) Calibration based on sodiated species ( $m/z^{\text{exp}} = 252.0835$ ).	88
<b>Figure 3.11</b> Semi-quantitative results for the homopropagation. Comparison between MeOx/AA oligomers (a), EtOx/AA oligomers (b), EtOz/AA oligomers (c) and different oligomers from 1:1 feed ratios (d).	90
<b>Figure 3.12</b> Semi-quantitative $\omega$ -end group analysis of MeOx/AA oligomers. a) $\omega$ -carboxylic acid groups, H <sup>+</sup> ionised. b) $\omega$ -carboxylic acid groups, Na <sup>+</sup> ionised. c) $\omega$ -amide groups, H <sup>+</sup> ionised. d) $\omega$ -amide groups, Na <sup>+</sup> ionised.	92
<b>Figure 3.13</b> Semi-quantitative $\omega$ -end group analysis of EtOx/AA oligomers. a) $\omega$ -carboxylic acid groups, H <sup>+</sup> ionised. b) $\omega$ -carboxylic acid groups, Na <sup>+</sup> ionised. c) $\omega$ -amide groups, H <sup>+</sup> ionised. d) $\omega$ -amide groups, Na <sup>+</sup> ionised.	93
<b>Figure 3.14</b> Semi-quantitative $\omega$ -end group analysis of EtOz/AA oligomers. a) $\omega$ -carboxylic acid groups, H <sup>+</sup> ionised. b) $\omega$ -carboxylic acid groups, Na <sup>+</sup> ionised. c) $\omega$ -amide groups, H <sup>+</sup> ionised. d) $\omega$ -amide groups, Na <sup>+</sup> ionised.	94

---

---

<b>Figure 3.15</b> Semi-quantitative comparison of $\omega$ -end group of CIE/AA oligomers. a) $\omega$ -carboxylic acid groups, $H^+$ ionised. b) $\omega$ -carboxylic acid groups, $Na^+$ ionised. c) $\omega$ -amide groups, $H^+$ ionised. d) $\omega$ -amide groups, $Na^+$ ionised.	95
<b>Figure 3.16</b> $^1H$ NMR spectra and SEC molecular weight distributions of the macromonomers.	102
<b>Figure 3.17</b> NMR analysis ( $CDCl_3$ ) of compound (2). Left: $^1H$ NMR. Right: $^{13}C$ NMR.	105
<b>Figure 3.18</b> $^1H$ NMR analysis ( $CDCl_3$ ) of compound (3).	105
<b>Figure 3.19</b> NMR analysis ( $D_2O$ ) of compound (4). Left: $^1H$ NMR. Right: $^{13}C$ NMR.	105
<b>Figure 4.1</b> Overview of physical, chemical and biological stimuli that can be implemented in polymer design. Adapted from ref. 3.	109
<b>Figure 4.2</b> $^1H$ NMR spectra ( $CDCl_3$ ) of macromonomer M3 (a) and the corresponding comb polymer (b) and SEC analysis of the comb polymer (c). $R = H, CH_2CH_2NHCOEt$ .	114
<b>Figure 4.3</b> $^1H$ NMR spectra (MeOD) for the comb polymers synthesised from NPAE macromonomers MeOx/AA (a), EtOx/AA (b), EtOx/CEA (c) and EtOz/AA (d). $R = H$ or $CH_2CH_2NHCOMe$ (MeOx), $H$ or $CH_2CH_2NHCOEt$ (EtOx), $H$ or $CH_2CH_2CH_2NHCOEt$ (EtOz).	116
<b>Figure 4.4</b> Conventional SEC analysis of the macromonomers and comb polymers. Molecular weights and dispersity values are summarised in Tables 4.2 and 4.3.	117
<b>Figure 4.5</b> Triple detection SEC analysis results for selected comb polymers.	119
<b>Figure 4.6</b> Thermogravimetric analysis of comb polymers P1 <sub>x</sub> (a), P2 <sub>10</sub> (b), P3 <sub>x</sub> (c), P4 <sub>100</sub> (d), P5 <sub>100</sub> (e) and P6 <sub>100</sub> (f).	120
<b>Figure 4.7</b> DSC analysis (second heating curve) of comb polymers P1 <sub>x</sub> (a), P2 <sub>10</sub> (b), P3 <sub>x</sub> (c), P4 <sub>100</sub> (d), P5 <sub>100</sub> (e) and P6 <sub>100</sub> (f).	121
<b>Figure 4.8</b> Cloud point studies on comb polymer P3 at pH 4.0, 5 mg mL <sup>-1</sup> in HPLC grade H <sub>2</sub> O, unless otherwise stated. a) Heating and cooling cycle of P3 <sub>100</sub> at pristine pH. b) Reproducibility studies on P3 <sub>100</sub> . c) Effect of	123

---

---

concentration of P3 <sub>100</sub> on the cloud point. d). Effect of DP of P3 on the cloud point.	
<b>Figure 4.9</b> Dual-responsive aqueous solubility of NPAE comb polymers.	124
a) The cloud point of P3 <sub>100</sub> is dependent on the pH of the solution and decreases with decreasing pH. b) Decrease of cloud point with increase $\omega$ -carboxylic acid end groups on the comb polymer side chain.	
<b>Figure 4.10</b> Cloud point measurements of P6 <sub>100</sub> at varying pH (a) and compared to P3 <sub>100</sub> (b) in HPLC grade H <sub>2</sub> O (5 mg mL <sup>-1</sup> ).	125
<b>Figure 4.11</b> Cloud point measurements of P3 <sub>100</sub> (a) and P6 <sub>100</sub> (b) in HPLC grade H <sub>2</sub> O and PBS buffer, demonstrating a salting out effect.	126
<b>Figure 4.12</b> pH-dependent aqueous solubility of P3 <sub>100</sub> , P5 <sub>100</sub> and P6 <sub>100</sub> in HPLC grade H <sub>2</sub> O and PBS buffer at 25 °C.	126
<b>Figure 4.13</b> SEC analysis for the functionalisation of P1 <sub>10</sub> and P2 <sub>10</sub> with selected amines. PME = phenylalanine methyl ester.	128
<b>Figure 4.14</b> DSC analysis of the functionalisation of P1 <sub>10</sub> and P2 <sub>10</sub> with selected amines. PME = phenylalanine methyl ester.	129
<b>Figure 4.15</b> Thermogravimetric analysis of the functionalisation of P1 <sub>10</sub> and P2 <sub>10</sub> with selected amines. PME = phenylalanine methyl ester.	129
<b>Figure 4.16</b> <sup>1</sup> H NMR spectra (CDCl <sub>3</sub> ) of the macromonomers: a) MeOx/AA, b) EtOx/AA, c) EtOx/CEA, and d) EtOz/AA. R = H or CH <sub>2</sub> CH <sub>2</sub> NHCOMe (MeOx), H or CH <sub>2</sub> CH <sub>2</sub> NHCOEt (EtOx), H or CH <sub>2</sub> CH <sub>2</sub> CH <sub>2</sub> NHCOEt (EtOz).	133
<b>Figure 5.1</b> Polymers investigated as alternative to poly(ethylene glycol) in biomedical applications. a) Poly( <i>L</i> -glutamic acid). b) Poly(glycerol). c) Poly(acrylamide). d) Poly( <i>N</i> -vinylpyrrolidone). e) Poly( <i>N</i> -(2-hydroxypropyl)methacrylamide). f) Poly(2-oxazoline)s.	145
<b>Figure 5.2</b> Structure of a poly(2-oxazoline) functionalised with ritogotine, a drug used in treatment of Parkinson's disease. Reproduced from ref. 23.	145
<b>Figure 5.3</b> Overview of the comb polymers studied in this chapter.	146
<b>Figure 5.4</b> HPLC calibration for comb polymers P2 <sub>50</sub> , P3 <sub>50</sub> , P4 <sub>50</sub> and P5 <sub>50</sub> .	148
<b>Figure 5.5</b> HPLC traces illustrating the degradation of P2 <sub>50</sub> (a), P3 <sub>50</sub> (b), P4 <sub>50</sub> (c) and P5 <sub>50</sub> (d) in 0.1 M KOH at 80 °C. The boxes highlight the comb	149

---

---

polymer (blue), internal standard (orange) and solvent elution (green) peaks.	
<b>Figure 5.6</b> Degradation of comb polymers P2 <sub>50</sub> , P3 <sub>50</sub> , P4 <sub>50</sub> and P5 <sub>50</sub> in PBS at pH 7.4 (a) and pH 5.0 (b).	150
<b>Figure 5.7</b> Degradation of comb polymers P2 <sub>50</sub> (a), P3 <sub>50</sub> (b), P4 <sub>50</sub> (c) and P5 <sub>50</sub> (d) in the presence of amylase.	151
<b>Figure 5.8</b> Cell viability results for macromonomers M2, M3 and M5 and their corresponding comb polymers for NIH 3T3 cells. All values are averaged from triplicates.	152
<b>Figure 5.9</b> Cell viability results for macromonomers M2, M3 and M5 and their corresponding comb polymers for A549 cells. All values are averaged from triplicates.	153
<b>Figure 5.10</b> Haemolysis results at pH 7.4 (a) and pH 5.0 (b). All values are averaged from triplicates.	154
<b>Figure 5.11</b> DLS size analysis of comb polymers P2 <sub>50</sub> , P2 <sub>400</sub> , P3 <sub>50</sub> and P5 <sub>50</sub> in water (a) and PBS (b) at 1 mg mL <sup>-1</sup> .	155
<b>Figure 5.12</b> Fluorescence spectroscopy spectra for Cy5-functionalised comb polymers.	156
<b>Figure 5.13</b> Concentration dependant cell association results for comb polymers P2 <sub>50</sub> , P2 <sub>400</sub> , P3 <sub>50</sub> and P5 <sub>50</sub> , shown on a linear (a) and logarithmic scale (b).	158
<b>Figure 5.14</b> Kinetic study of the cell association of comb polymers P2 <sub>50</sub> , P2 <sub>400</sub> , P4 <sub>50</sub> and P5 <sub>50</sub> at 37 °C (a) and 4 °C (b).	158
<b>Figure 5.15</b> Cell uptake experiments with lysosomal staining for comb polymers P2 <sub>50</sub> (a), P2 <sub>400</sub> (b), P3 <sub>50</sub> (c) and P5 <sub>50</sub> (d). Polymers, cell nuclei and lysosomes are labelled red, blue and green, respectively.	159
<b>Figure 5.16</b> Cell uptake experiments with mitochondrial staining for comb polymers P2 <sub>50</sub> (a), P2 <sub>400</sub> (b), P3 <sub>50</sub> (c) and P5 <sub>50</sub> (d). Polymers, cell nuclei and mitochondria are labelled red, blue and green, respectively.	160
<b>Figure 5.17</b> QCM-D traces for the film formation optimisation results with P1 <sub>100</sub> . The polymer solutions were added at t = 0 s and unbound material was washed away at the time point marked with an asterisk.	161

---

---

<b>Figure 5.18</b> QCM-D traces for the anti-fouling behaviour of P1 <sub>100</sub> against BSA (a) and lysozyme (b). The protein solutions were added at $t = 0$ s and unbound enzyme was washed away at the time point marked with an asterisk.	164
<b>Figure 5.19</b> <sup>1</sup> H NMR spectra (CDCl <sub>3</sub> ) of the macromonomers: a) MeO <sub>x</sub> /AA, b) EtO <sub>x</sub> /AA, c) EtO <sub>x</sub> /CEA and d) EtO <sub>z</sub> /AA. R = H or CH <sub>2</sub> CH <sub>2</sub> NHCOMe (MeO <sub>x</sub> ), H or CH <sub>2</sub> CH <sub>2</sub> NHCOEt (EtO <sub>x</sub> ), H or CH <sub>2</sub> CH <sub>2</sub> CH <sub>2</sub> NHCOEt (EtO <sub>z</sub> ).	170
<b>Figure 5.20</b> <sup>1</sup> H NMR spectra (MeOD) of the comb polymers: a) P1 <sub>x</sub> /P2 <sub>x</sub> , b) P3 <sub>x</sub> , c) P4 <sub>50</sub> and d) P5 <sub>x</sub> . R = H or CH <sub>2</sub> CH <sub>2</sub> NHCOMe (P1 <sub>x</sub> /P2 <sub>x</sub> ), H or CH <sub>2</sub> CH <sub>2</sub> NHCOEt (P3 <sub>x</sub> , P4 <sub>50</sub> ), H or CH <sub>2</sub> CH <sub>2</sub> CH <sub>2</sub> NHCOEt (P5 <sub>x</sub> ).	174
<b>Figure 5.21</b> SEC analysis of macromonomers M1 – M5 and their corresponding comb polymers P1 <sub>x</sub> – P5 <sub>x</sub> .	175
<b>Figure 6.1</b> Structures of citric acid and D-glucono- $\delta$ -lactone.	188
<b>Figure 6.2</b> Polycondensation of CA and GL followed by DSC. a) The reaction mixture of CA and GL (1/1) melts and reacts at a lower temperature than the individual monomers. b) On the second heating cycle a glass transition temperature can be observed, which increases with increasing reaction time ( $T_{\text{react}} = 160$ °C). c) The glass transition temperature increases with increasing reaction temperatures, with a minimum of 130 °C required (10 min ITS). d) The melt onset temperature of CA and GL mixtures revealed a eutectic melt behaviour.	190
<b>Figure 6.3</b> Structures of aliphatic bifunctional co-monomers.	191
<b>Figure 6.4</b> DSC polymerisation of CA and GL with glycolic acid. a) First heating cycle. b) Second heating cycle.	191
<b>Figure 6.5</b> DSC polymerisation of CA and GL with 1,6-hexanediol. a) First heating cycle. b) Second heating cycle.	192
<b>Figure 6.6</b> DSC polymerisation of CA and GL with L-lactic acid. a) First heating cycle. b) Second heating cycle.	192
<b>Figure 6.7</b> DSC polymerisation of CA and GL with 2-hydroxyisobutyric acid. a) First heating cycle. b) Second heating cycle.	193
<b>Figure 6.8</b> DSC polymerisation of CA and GL with methylmalonic acid.	193

---

---

a) First heating cycle. b) Second heating cycle.	
<b>Figure 6.9</b> DSC polymerisation of CA and GL with glutaric acid. a) First heating cycle. b) Second heating cycle.	193
<b>Figure 6.10</b> Comparison of glass transition temperatures obtained by polycondensation of CA and GL with aliphatic bifunctional co-monomers.	194
<b>Figure 6.11</b> DSC polymerisation of CA and GL with excess glycolic acid. a) First heating cycle. b) Second heating cycle.	194
<b>Figure 6.12</b> DSC polymerisation of CA and GL with glycolic acid at higher temperature (180 °C). a) First heating cycle. b) Second heating cycle.	195
<b>Figure 6.13</b> Structures of aliphatic polyfunctional co-monomers.	195
<b>Figure 6.14</b> DSC polymerisation of CA and GL with 1,1,1-trimethylolpropane. a) First heating cycle. b) Second heating cycle.	196
<b>Figure 6.15</b> DSC polymerisation of CA and GL with DL-malic acid. a) First heating cycle. b) Second heating cycle.	196
<b>Figure 6.16</b> DSC polymerisation of CA and GL with L-tartaric acid. a) First heating cycle. b) Second heating cycle.	197
<b>Figure 6.17</b> Comparison of glass transition temperatures obtained by polycondensation of CA and GL with aliphatic polyfunctional monomers.	197
<b>Figure 6.18</b> Structures of aromatic co-monomers.	198
<b>Figure 6.19</b> DSC polymerisation of CA and GL with 4-hydroxybenzoic acid. a) First heating cycle. b) Second heating cycle.	198
<b>Figure 6.20</b> DSC polymerisation of CA and GL with terephthalic acid. a) First heating cycle. b) Second heating cycle.	198
<b>Figure 6.21</b> DSC polymerisation of CA and GL with 1,3,5-trihydroxybenzene. a) First heating cycle. b) Second heating cycle.	199
<b>Figure 6.22</b> Comparison of glass transition temperatures obtained by polycondensation of CA and GL with aromatic monomers.	199
<b>Figure 6.23</b> Structures of the ring-structured monomers.	200
<b>Figure 6.24</b> DSC polymerisation of CA and D-glucose. a) First heating cycle. b) Second heating cycle.	200
<b>Figure 6.25</b> DSC polymerisation of CA and D-fructose. a) First heating cycle. b) Second heating cycle.	201

---

---

cycle. b) Second heating cycle.	
<b>Figure 6.26</b> Comparison of glass transition temperatures obtained by polycondensation of CA and ring-structured monomers.	201
<b>Figure 6.27</b> Glass transition temperatures for the polycondensation of CA and GL in the presence of zinc catalysts (a) and other catalysts (b).	202
<b>Figure 7.1</b> Monomers studied and their melting ( $T_{\text{melt}}$ ) or decomposition ( $T_{\text{dec}}$ ) temperatures.	210
<b>Figure 7.2</b> Polycondensation of CA and GL with amino acids containing hydrophobic, non-reactive side chains. a) Glycine. b) L-alanine. c) L-leucine. d) L-phenylalanine. e) Comparison of the different amino acid co-monomers. The reaction times refer to the ITS.	214
<b>Figure 7.3</b> Polycondensation of CA and GL with amino acids containing hydroxyl or thiol side chains. a) L-serine. b) L-tyrosine. c) L-cysteine. d) Comparison of the different amino acid co-monomers. The reaction times refer to the ITS.	215
<b>Figure 7.4</b> Polycondensation of CA and GL with amino acids containing carboxylic acid side chains. a) L-aspartic acid. b) L-glutamic acid. c) Comparison of the different amino acid co-monomers. The reaction times refer to the ITS.	216
<b>Figure 7.5</b> Polycondensation of CA and GL with amino acids containing amine side chains. a) L-lysine. b) L-arginine. c) L-histidine. d) Comparison of the different amino acid co-monomers. The reaction times refer to the ITS.	218
<b>Figure 7.6</b> Polycondensation of CA and GL with cyclic amino acids. a) L-proline. b) PIPERCOLINIC acid. c) Azetidine-2-carboxylic acid. d) Comparison of the different amino acid co-monomers. The reaction times refer to the ITS.	219
<b>Figure A.1</b> Mole fractions of the various microstructures of MeOx/AA oligomers. a) $\text{H}^+$ ionised $\bullet$ species. b) $\text{Na}^+$ ionised $\triangle$ species. c) $\text{H}^+$ ionised $\blacktriangledown$ species. d) $\text{H}^+$ ionised $\bullet$ species. e) $\text{H}^+$ ionised $\blacktriangledown$ species.	239
<b>Figure A.2</b> ESI MS/MS (positive mode) of MeOx/AA (1/1) isolating a species at $m/z^{\text{exp}} = 337.1368$ with an HCD of 20 eV.	240

---

---

<b>Figure A.3</b> ESI MS/MS (positive mode) of MeOx/AA (1/1) isolating a species at $m/z^{\text{exp}} = 400.2072$ with an HCD of 20 eV.	241
<b>Figure A.4</b> ESI MS/MS (positive mode) of MeOx/AA (1/1) isolating a species at $m/z^{\text{exp}} = 409.1574$ with an HCD of 20 eV.	243
<b>Figure A.5</b> ESI MS/MS (positive mode) of MeOx/AA (1/1) isolating a species at $m/z^{\text{exp}} = 422.1891$ with an HCD of 20 eV.	246
<b>Figure A.6</b> ESI MS/MS (positive mode) of MeOx/AA (1/1) isolating a species at $m/z^{\text{exp}} = 472.2295$ with an HCD of 20 eV.	247
<b>Figure A.7</b> ESI MS/MS (positive mode) of MeOx/AA (1/1) isolating a species at $m/z^{\text{exp}} = 481.1797$ with an HCD of 18 eV.	248
<b>Figure A.8</b> ESI MS/MS (positive mode) of MeOx/AA (1/1) isolating a species at $m/z^{\text{exp}} = 490.2400$ with an HCD of 15 eV.	249
<b>Figure A.9</b> ESI MS/MS (positive mode) of MeOx/AA (1/1) isolating a species at $m/z^{\text{exp}} = 494.2101$ with an HCD of 18 eV.	250
<b>Figure A.10</b> ESI MS/MS (positive mode) of MeOx/AA (1/1) isolating a species at $m/z^{\text{exp}} = 507.2419$ with an HCD of 20 eV.	252
<b>Figure A.11</b> ESI MS/MS (positive mode) of EtOx/AA (1/1) isolating a species at $m/z^{\text{exp}} = 437.1882$ with an HCD of 20 eV.	256
<b>Figure A.12</b> ESI MS/MS (positive mode) of EtOx/AA (1/1) isolating a species at $m/z^{\text{exp}} = 442.2538$ with an HCD of 20 eV.	257
<b>Figure A.13</b> ESI MS/MS (positive mode) of EtOx/AA (1/1) isolating a species at $m/z^{\text{exp}} = 464.2353$ with an HCD of 20 eV.	259
<b>Figure A.14</b> ESI MS/MS (positive mode) of EtOx/AA (1/1) isolating a species at $m/z^{\text{exp}} = 482.2463$ with an HCD of 25 eV.	260
<b>Figure A.15</b> ESI MS/MS (positive mode) of EtOz/AA (1/1) isolating a species at $m/z^{\text{exp}} = 465.2210$ with an HCD of 20 eV.	264
<b>Figure A.16</b> ESI MS/MS (positive mode) of EtOz/AA (1/1) isolating a species at $m/z^{\text{exp}} = 472.3010$ with an HCD of 18 eV.	265
<b>Figure A.17</b> ESI MS/MS (positive mode) of EtOz/AA (1/1) isolating a species at $m/z^{\text{exp}} = 484.3023$ with an HCD of 18 eV.	265

---

---

## List of tables

<b>Table 1.1</b> Thermodynamic properties for ROP of lactones with different ring sizes.	14
<b>Table 1.2</b> Monomer pairs for the synthesis of polyesters by SZWIP of CIEs with (meth)acrylate type $M_E$ .	31
<b>Table 1.3</b> Monomer pairs for SZWIP of CIEs with lactones and cyclic anhydrides.	32
<b>Table 1.4</b> Monomer pairs for SZWIP of aziridines.	34
<b>Table 2.1</b> Screening of experimental parameters for the SZWIP of EtOx and AA.	53
<b>Table 2.2</b> Results for the synthesis of NPAE macromonomers from various CIEs and $M_E$ .	57
<b>Table 2.3</b> Amount of $\omega$ -carboxylic acid groups of macromonomers from various CIEs and AA as determined by acid-base titration.	58
<b>Table 2.4</b> Elemental analysis results for NPAE macromonomers.	61
<b>Table 2.5</b> Glass transition temperatures for NPAE macromonomers.	63
<b>Table 2.6</b> Quantities for the synthesis of the macromonomers.	66
<b>Table 3.1</b> Overview of the macromonomers studied in this work.	75
<b>Table 3.2</b> Peak assignment for the MeOx:AA ESI MS spectra (Figure 3.4).	78
<b>Table 3.3</b> Peak assignment for the EtOx:AA ESI MS spectra (Figure 3.5).	79
<b>Table 3.4</b> Peak assignment for the EtOz:AA ESI MS spectra (Figure 3.6).	80
<b>Table 3.5</b> Overview of peaks observed upon fragmentation of MeOx/AA $m/z^{\text{exp}}=328.1861$ (Figure 3.7). Structural assignment of the peaks is presented in Scheme 3.4.	83
<b>Table 3.6</b> Overview of species associated with homopropagation in MeOx/AA spectra and their respective mole fractions.	89
<b>Table 3.7</b> Quantities for the synthesis of the macromonomers.	101
<b>Table 4.1</b> Structures and cloud points of water-soluble POx and POz.	111
<b>Table 4.2</b> Macromonomers employed for the synthesis of NPAE comb polymers.	113

---

<b>Table 4.3</b> Overview of comb polymers prepared by redox-initiated RAFT polymerisation.	118
<b>Table 4.4</b> Triple detection SEC analysis results for selected comb polymers.	119
<b>Table 4.5</b> Glass transition temperatures for comb polymers from NPAE macromonomers.	122
<b>Table 4.6</b> Results for the functionalisation of DP10 comb polymers with selected amines.	128
<b>Table 4.7</b> Quantities for the synthesis of the macromonomers.	132
<b>Table 4.8</b> Quantities for the synthesis of comb polymers by redox-initiated RAFT.	135
<b>Table 4.9</b> Quantities for the functionalisation of P1 <sub>10</sub> and P2 <sub>10</sub> with selected amines.	137
<b>Table 5.1</b> Overview of the macromonomers and comb polymers studied in this chapter.	147
<b>Table 5.2</b> Viscosity, size and zeta potential analysis of comb polymers.	155
<b>Table 5.3</b> Fluorescence spectroscopy analysis results for Cy5-functionalised comb polymers.	157
<b>Table 5.4</b> Overview of the QCM-D results for comb polymers P1 <sub>x</sub> and P2 <sub>x</sub> .	162
<b>Table 5.5</b> Anti-fouling behaviour of comb polymers P1 <sub>x</sub> and P2 <sub>x</sub> against BSA.	164
<b>Table 5.6</b> Anti-fouling behaviour of comb polymers P1 <sub>x</sub> and P2 <sub>x</sub> against lysozyme.	165
<b>Table 5.7</b> Quantities for the synthesis of the macromonomers.	169
<b>Table 5.8</b> Quantities for the synthesis of comb polymers by RRAFT.	172
<b>Table 5.9</b> Quantities for the synthesis of comb polymers by organic RRAFT.	173
<b>Table 5.10</b> Quantities for the functionalisation of comb polymers with Cy5-amine.	176
<b>Table A.1</b> Quantitative calculations for MeOx:AA 1:1 based on the calibration curve (Figure 3.10) referred to the overview spectrum (Figure 3.1a). Calculated using Equation 3.1.	234

---

---

<b>Table A.2</b> Quantitative calculations for MeOx:AA 1:2 based on the calibration curve (Figure 3.10) referred to the overview spectrum (Figure 3.1b). Calculated using Equation 3.1.	234
<b>Table A.3</b> Quantitative calculations for MeOx:AA 2:1 based on the calibration curve (Figure 3.10) referred to the overview spectrum (Figure 3.1c). Calculated using Equation 3.1.	235
<b>Table A.4</b> Quantitative calculations for MeOx:AA 1:1 based on the calibration curve (Figure 3.10) referred to the overview spectrum (Figure 3.2a). Calculated using Equation 3.1.	236
<b>Table A.5</b> Quantitative calculations for MeOx:AA 1:2 based on the calibration curve (Figure 3.10) referred to the overview spectrum (Figure 3.2b). Calculated using Equation 3.1.	237
<b>Table A.6</b> Quantitative calculations for MeOx:AA 2:1 based on the calibration curve (Figure 3.10) referred to the overview spectrum (Figure 3.2c). Calculated using Equation 3.1.	238
<b>Table A.7</b> Peak assignment of ESI MS/MS experiment of a MeOx/AA species at $m/z^{\text{exp}} = 337.1368$ (Figure A.2).	240
<b>Table A.8</b> Peak assignment of ESI MS/MS experiment of a MeOx/AA species at $m/z^{\text{exp}} = 400.2072$ (Figure A.3).	242
<b>Table A.9</b> Peak assignment of ESI MS/MS experiment of a MeOx/AA species at $m/z^{\text{exp}} = 409.1574$ (Figure A.4).	244
<b>Table A.10</b> Peak assignment of ESI MS/MS experiment of a MeOx/AA species at $m/z^{\text{exp}} = 422.1891$ (Figure A.5).	246
<b>Table A.11</b> Peak assignment of ESI MS/MS experiment of a MeOx/AA species at $m/z^{\text{exp}} = 472.2295$ (Figure A.6).	248
<b>Table A.12</b> Peak assignment of ESI MS/MS experiment of a MeOx/AA species at $m/z^{\text{exp}} = 481.1797$ (Figure A.7).	249
<b>Table A.13</b> Peak assignment of ESI MS/MS experiment of a MeOx/AA species at $m/z^{\text{exp}} = 490.2400$ (Figure A.8).	250
<b>Table A.14</b> Peak assignment of ESI MS/MS experiment of a MeOx/AA species at $m/z^{\text{exp}} = 494.2101$ (Figure A.9).	251
<b>Table A.15</b> Peak assignment of ESI MS/MS experiment of a MeOx/AA	252

---

---

species at $m/z^{\text{exp}} = 507.2419$ (Figure A.10).	
<b>Table A.16</b> Quantitative calculations for EtOx:AA 1:1 based on the calibration curve (Figure 3.10) referred to the overview spectrum (Figure 3.2a). Calculated using Equation 3.1.	253
<b>Table A.17</b> Quantitative calculations for EtOx:AA 1:2 based on the calibration curve (Figure 3.10) referred to the overview spectrum (Figure 3.2b). Calculated using Equation 3.1.	253
<b>Table A.18</b> Overview of species associated with homopropagation in EtOx/AA spectra and their respective mole fractions.	254
<b>Table A.19</b> Peak assignment of ESI MS/MS experiment of an EtOx/AA species at $m/z^{\text{exp}} = 365.1670$ (Figure 3.9a).	254
<b>Table A.20</b> Peak assignment of ESI MS/MS experiment of an EtOx/AA species at $m/z^{\text{exp}} = 437.1882$ (Figure A.11).	256
<b>Table A.21</b> Peak assignment of ESI MS/MS experiment of an EtOx/AA species at $m/z^{\text{exp}} = 442.2538$ (Figure A.12).	258
<b>Table A.22</b> Peak assignment of ESI MS/MS experiment of an EtOx/AA species at $m/z^{\text{exp}} = 464.2353$ (Figure A.13).	259
<b>Table A.23</b> Peak assignment of ESI MS/MS experiment of an EtOx/AA species at $m/z^{\text{exp}} = 482.2463$ (Figure A.14).	260
<b>Table A.24</b> Quantitative calculations for EtOz:AA 1:1 based on the calibration curve (Figure 3.10) referred to the overview spectrum (Figure 3.3a). Calculated using Equation 3.1.	261
<b>Table A.25</b> Quantitative calculations for EtOz:AA 1:2 based on the calibration curve (Figure 3.10) referred to the overview spectrum (Figure 3.3b). Calculated using Equation 3.1.	262
<b>Table A.26</b> Overview of species associated with homopropagation in EtOz/AA spectra and their respective mole fractions.	262
<b>Table A.27</b> Peak assignment of ESI MS/MS experiment of an EtOz/AA species at $m/z^{\text{exp}} = 393.1995$ (Figure 3.9b).	263
<b>Table A.28</b> Peak assignment of ESI MS/MS experiment of an EtOz/AA species at $m/z^{\text{exp}} = 465.2210$ (Figure A.15).	264

---

---

## List of schemes

<b>Scheme 1.1</b> Two-step PEA synthesis. a) Condensation of L-alanine with 1,12-dodecanediol to form a bisamine monomer. b) Interfacial polycondensation of the bisamine monomer with sebacoyl chloride to form the PEA. Adapted from ref. 51.	7
<b>Scheme 1.2</b> General mechanism for anionic ROP of cyclic esters. a) Initiation with a hydroxide anion. b) Propagation by consecutive addition of monomers. c) Termination by an electrophile. Adapted from ref. 72.	11
<b>Scheme 1.3</b> General synthesis of <i>O</i> -carboxyanhydrides from $\alpha$ -hydroxy acids.	13
<b>Scheme 1.4</b> Synthesis of the CKA 2-methylene-1,3-dioxepane (MDO) by acetal exchange followed by dehydrohalogenation. <sup>106</sup>	16
<b>Scheme 1.5</b> Mechanism for the RROP of MDO. a) Generation of radicals from a common initiator ( <i>e.g.</i> AIBN). b) Reaction of a radical with MDO forms a tertiary radical which isomerises into a primary radical. c) Reaction with other MDO monomers furnishes higher molecular weight polyesters.	17
<b>Scheme 1.6</b> Radical ring-opening polymerisation of 2-methylene-1,3-dioxepane, ring-opening polymerisation of $\epsilon$ -caprolactone and polycondensation of 6-hydroxyhexanoic acid all yield poly( $\epsilon$ -caprolactone).	18
<b>Scheme 1.7</b> Ring-retention in RROP leads to the introduction of acetal functionalities in the polymer backbone.	18
<b>Scheme 1.8</b> RROP of 2-methylene-1,3-dioxepane. Rearrangements at high temperatures lead to multiple backbone structures and the formation of 3-vinyl-1,4-butyrolactone. Adapted from ref. 7, 112.	20
<b>Scheme 1.9</b> Schematic of chain-growth condensation polymerisation <i>via</i> substituent effects. Adapted from ref. 162.	23
<b>Scheme 1.10</b> Synthesis of poly(4-hydroxybenzoate)s by CGCP, using triethylsilane, caesium fluoride and 18-crown-6 as base system. R = octyl or 4,7-dioxaoctyl. Reproduced from ref. 164.	24
<b>Scheme 1.11</b> Synthesis of poly(4-bromo-2-octylphenol) by palladium(II)-catalysed CO copolymerisation with 4-bromo-2-octylphenol by CGCP. Adapted	24

---

from ref. 166.	
<b>Scheme 1.12</b> Polymerisation of 4-bromomethyl-2-octyloxybenzoate <i>via</i> phase transfer catalysis. Reproduced from ref. 167.	25
<b>Scheme 1.13</b> General mechanism for SZWIP. a) Michael addition between $M_N$ and $M_E$ forms the genetic zwitterion. b) Propagation into oligomers and polymers. c) Homopropagation of $M_N$ and $M_E$ to produce non-alternating structures. d). Propagation followed by cyclisation.	26
<b>Scheme 1.14</b> SZWIP of HOx with BPL and AA. a) Formation of the genetic zwitterion between HOx and BPL. b) Formation of the genetic zwitterion between HOx and AA. c) Propagation of the genetic zwitterion to form a <i>N</i> -formylated poly(aminoester).	27
<b>Scheme 1.15</b> SZWIP between CIEs and AA leads to the introduction of $\alpha$ -acrylate groups and carboxylic acid and amide $\omega$ -end groups. Adapted from ref. 179.	28
<b>Scheme 1.16</b> SZWIP of Ox with 2-bromoacrylic acid leads to <i>N</i> -acylated poly(amino ester)s with pendant bromine groups. Adapted from ref. 182.	29
<b>Scheme 1.17</b> SZWIP of 2-methyl-2-thiazoline with AA. a) Initiation by formation of the carbanion and subsequent proton transfer. b) Propagation of both the carbanion and genetic zwitterion with AA to form a poly(ester imino thioether) with pendant carboxylic acid groups.	30
<b>Scheme 1.18</b> SZWIP of HOx and glutaric anhydride (GAn). a) Reaction between HOx and GAn at low temperatures leads to a bicyclic intermediate, which after reaction with another HOx monomer forms an $A_2B$ type genetic zwitterion. b) Propagation of this genetic zwitterion produces an $A_2B$ type <i>N</i> -formylated poly(amino amido ester). Adapted from ref. 197.	32
<b>Scheme 1.19</b> SZWIP of aziridine and AA. a) Initiation takes place by Michael addition of the aziridine to AA to form the genetic zwitterion. b) Propagation leads to a poly(amino ester). Adapted from ref. 204.	33
<b>Scheme 2.1</b> Proposed mechanism for the SZWIP of MeOx and AA: formation of the genetic zwitterion (a), propagation to form oligomers (b) and termination into a macromonomer (c).	50
<b>Scheme 2.2</b> SZWIP of EtOx with AA yielding <i>N</i> -acylated poly(aminoester)	51

---

---

macromonomers. R = H, CH <sub>2</sub> CH <sub>2</sub> NHCOEt.	
<b>Scheme 3.1</b> Mechanism for the SZWIP of MeOx and AA as proposed by Saegusa <i>et al.</i> <sup>3</sup>	73
<b>Scheme 3.2</b> Fragmentation pathways for NPAAE macromonomers in MS/MS <i>via</i> a concerted mechanism (a) and a ring-closure mechanism (b).	81
<b>Scheme 3.3</b> Fragmentation of two isobaric structures for MeOx/AA at $m/z^{\text{exp}} = 328.1867$ .	82
<b>Scheme 3.4</b> Fragmentation of MeOx/AA $m/z^{\text{exp}} = 328.1867$ as observed in Figure 3.7.	84
<b>Scheme 3.5</b> Synthesis of the AA-MeOx-AA dimer for semi-quantification.	87
<b>Scheme 3.6</b> Initiation of SZWIP <i>via</i> an aza-Michael addition to form the genetic zwitterion (i, ii) or an acid-base reaction to form the [HCIE] <sup>+</sup> [AA] <sup>-</sup> ion pair (iii).	96
<b>Scheme 3.7</b> Propagation reactions for SZWIP. a) The addition reaction of two zwitterions leads to alternating structures. b) Reaction of a zwitterion with a CIE monomer introduces copolymers with defects from CIE homopropagation. c) The reaction of a [HCIE] <sup>+</sup> [AA] <sup>-</sup> ion pair with a CIE monomer produces poly(CIE) homopolymers.	97
<b>Scheme 3.8</b> Termination pathways for SZWIP. a) Reaction of a growing oligomer with AA introduces an $\alpha$ -acrylate and $\omega$ -carboxylic acid group. b) Reaction with a [HCIE] <sup>+</sup> [AA] <sup>-</sup> ion pair introduces an $\alpha$ -acrylate and $\omega$ -amide group. c) Reaction with ambient water introduces a $\alpha$ -hydroxyl and $\omega$ -carboxylic acid group.	98
<b>Scheme 4.1</b> Reaction conditions for the synthesis of macromonomers. SZWIP of EtOx with AA shown as example.	112
<b>Scheme 4.2</b> Synthesis of comb polymers by redox-initiated free radical polymerisation of <i>N</i> -acylated poly(amino ester) macromonomer M3. R = H, CH <sub>2</sub> CH <sub>2</sub> NHCOEt.	114
<b>Scheme 4.3</b> Synthesis of comb polymers by redox-initiated RAFT (RRAFT) polymerisation of <i>N</i> -acylated poly(aminoester) macromonomer M3. R = H, CH <sub>2</sub> CH <sub>2</sub> NHCOEt.	115
<b>Scheme 5.1</b> Labelling of comb polymers with cyanine 5 dye.	156

---

- 
- Scheme A.1** Fragmentation scheme for MeOx/AA precursor at  $m/z^{\text{exp}} = 241$   
337.1368.
- Scheme A.2** Fragmentation scheme for MeOx/AA precursor at  $m/z^{\text{exp}} = 242$   
400.2072 based on an AABA oligomer (A=MeOx, B=AA).
- Scheme A.3** Fragmentation scheme for MeOx/AA precursor at  $m/z^{\text{exp}} = 243$   
400.2072 based on an AAAB oligomer (A=MeOx, B=AA).
- Scheme A.4** Fragmentation scheme for MeOx/AA precursor at  $m/z^{\text{exp}} = 243$   
400.2072 based on an ABAA oligomer (A=MeOx, B=AA).
- Scheme A.5** Fragmentation scheme for MeOx/AA precursor at  $m/z^{\text{exp}} = 245$   
409.1574.
- Scheme A.6** Fragmentation scheme for MeOx/AA precursor at  $m/z^{\text{exp}} = 247$   
422.1898.
- Scheme A.7** Fragmentation scheme for EtOx/AA precursor at  $m/z^{\text{exp}} = 255$   
365.1683.
- Scheme A.8** Fragmentation scheme for EtOx/AA precursor at  $m/z^{\text{exp}} = 257$   
437.1894.
- Scheme A.9** Fragmentation scheme for EtOx/AA precursor at  $m/z^{\text{exp}} = 258$   
442.2538.
- Scheme A.10** Fragmentation scheme for EtOx/AA precursor at  $m/z^{\text{exp}} = 261$   
482.2463.
- Scheme A.11** Fragmentation scheme for EtOz/AA precursor at  $m/z^{\text{exp}} = 263$   
393.1995.

---

## List of equations

<b>Equation 1.1</b> Carothers equation for linear polymers.	8
<b>Equation 1.2</b> Calculation of $X_n$ for linear polymers.	8
<b>Equation 1.3</b> Calculation of conversion for linear polymers.	8
<b>Equation 1.4</b> Calculation of $X_w$ for linear polymers.	8
<b>Equation 1.5</b> Calculation of $M_n$ for linear polymers.	8
<b>Equation 1.6</b> Calculation of $M_w$ for linear polymers.	9
<b>Equation 1.7</b> Calculation of dispersity for linear polymers.	9
<b>Equation 1.8</b> Calculation of average functionality for branched monomers.	9
<b>Equation 1.9</b> Calculation of conversion for multifunctional monomers.	9
<b>Equation 1.10</b> Calculation of $X_n$ for branched polymers.	9
<b>Equation 1.11</b> Calculation of critical branching degree.	9
<b>Equation 1.12</b> Calculation of conversion at gel point.	10
<b>Equation 1.13</b> Gibbs free energy equation for ROP.	13
<b>Equation 3.1</b> Calculation of mole fractions in MS spectra.	88
<b>Equation 5.1</b> Sauerbrey equation.	163
<b>Equation 5.2</b> Calculation of the cell viability.	179
<b>Equation 5.3</b> Calculation of the haemolysis.	180
<b>Equation 7.1</b> Calculation of conversion for multifunctional monomers.	211
<b>Equation 7.2</b> Calculation of average functionality for branched monomers.	211
<b>Equation 7.3</b> Calculation of $X_n$ for branched polymers.	212
<b>Equation 7.4</b> Calculation of critical branching degree.	212
<b>Equation 7.5</b> Calculation of conversion at gel point for citric acid.	212
<b>Equation 7.6</b> Calculation of conversion at gel point for D-glucono- $\delta$ -lactone.	212

---

## Abbreviations and symbols

$\alpha$	Mark-Houwink constant
A549	human lung carcinoma cells
AA	acrylic acid
AA	amino acid
ACA	azetidine-2-carboxylic acid
Ala	L-alanine
Arg	L-arginine
AsAc	ascorbic acid
Asp	L-aspartic acid
BSA	bovine serum albumin
CA	citric acid
CEA	2-carboxyethyl acrylate
CIE	cyclic imino ether
CGCP	chain growth condensation polymerisation
CKA	cyclic ketene acetal
CROP	cationic ring-opening polymerisation
CTA	chain transfer agent
Cys	L-cysteine
Cy5	cyanine 5 dye
$\Delta D$	dissipation shift
$\mathcal{D}$	dispersity ( $\mathcal{D} = M_w / M_n$ )
DF	degree of functionalisation
DIPEA	<i>N,N</i> -diisopropylethylamine
DLS	dynamic light scattering
DMEM	Dulbecco's modified Eagle's medium
DMF	<i>N,N</i> -dimethylformamide

---

DMTMM	(4-(4,6-dimethoxy-1,3,5-triazin-2-yl)-4-methyl-morpholinium chloride
DNS	3,5-dinitrosalicylic acid
DP	degree of polymerisation
dRI	differential refractive index
DSC	differential scanning calorimetry
EA	elemental analysis
equiv.	equivalents
ESI	electrospray ionisation
EtOx	2-ethyl-2-oxazoline
EtOz	2-ethyl-2-oxazine
$\Delta f$	frequency shift
FBS	foetal bovine serum
FDA	Food and Drug Administration
Fru	D-fructose
GA	glycolic acid
GL	D-glucono- $\delta$ -lactone
GLA	glutaric acid
Glc	D-glucose
Glu	L-glutamic acid
Gly	glycine
GRAS	generally recognised as safe
h	hours
HATU	1-[bis(dimethylamino)methylene]-1 <i>H</i> -1,2,3-triazolo[4,5- <i>b</i> ]pyridinium 3-oxid hexafluorophosphate
HBA	4-hydroxybenzoic acid
HCD	higher-energy collision dissociation
HD	1,6-hexanediol
HIBA	2-hydroxyisobutyric acid
His	L-histidine

---

---

HPLC	high performance liquid chromatography
ITS	isothermal segment
IV	intrinsic viscosity
$k_p$	rate of propagation
$\lambda_{em}$	emission wavelength
$\lambda_{ex}$	excitation wavelength
LA	L-lactic acid
LCST	lower critical solution temperature
Leu	L-leucine
LS	light scattering
Lys	L-lysine
MA	DL-malic acid
MALDI-ToF	matrix-assisted laser desorption-ionisation time-of-flight
MDO	2-methylene-1,3-dioxepane
$M_E$	electrophilic monomer
MEHQ	<i>p</i> -methoxyphenol
MeOx	2-methyl-2-oxazoline
MMA	methylmalonic acid
$M_N$	nucleophilic monomer
$M_n$	number-average molecular weight
MS	mass spectrometry
MS/MS	tandem mass spectrometry
$M_w$	weight-average molecular weight
MWCO	molecular weight cut-off
$m/z$	mass-over-charge
NIH 3T3	mouse fibroblast cells
NIH 3T3 COX8A	3T3 cells modified for mitochondrial staining
NIH 3T3 LAMP1	3T3 cells modified for lysosomal staining (lysosome associated membrane protein 1)

---

---

NMR	nuclear magnetic resonance
NPAE	<i>N</i> -acylated poly(aminoester)
OCA	<i>O</i> -carboxyanhydride
PAE	poly(aminoester)
PBS	phosphate buffered saline
PCA	pipecolinic acid
PEA	poly(ester amide)
Phe	L-phenylalanine
pI	isoelectric point
PI	propidium iodide
PME	phenylalanine methylester hydrochloride
PO <sub>x</sub>	poly(2-oxazoline)
PO <sub>z</sub>	poly(2-oxazine)
ppm	parts per million
Pro	L-proline
QCM-D	quartz crystal microbalance with dissipation monitoring
RAFT	reversible addition-fragmentation chain transfer
RBCs	red blood cells
R <sub>g</sub>	radius of gyration
R <sub>h</sub>	solvodynamic radius
ROP	ring-opening polymerisation
RRAFT	redox-initiated reversible addition-fragmentation chain transfer
SEC	size exclusion chromatography
Ser	L-serine
SZWIP	spontaneous zwitterionic copolymerisation
TA	L-tartaric acid
<i>t</i> BuOOH	<i>tert</i> -butylhydroperoxide
<i>T</i> <sub>CP</sub>	cloud point temperature
<i>T</i> <sub>dec</sub>	decomposition temperature

---

---

TD SEC	triple detection size exclusion chromatography
TFA	trifluoroacetic acid
$T_g$	glass transition temperature
TGA	thermogravimetric analysis
THB	1,3,5-trihydroxybenzene
$T_{\text{melt}}$	melting temperature
TMP	1,1,1-trimethylolpropane
TPA	terephthalic acid
$T_{\text{react}}$	reaction temperature
Tyr	L-tyrosine
UV-Vis	ultraviolet-visible
VS	viscometry
$\chi$	mole fraction
$\chi^{\text{avg}}$	average mole fraction

## Acknowledgements / Dankwoord

At the age of 13 I said I would never go study a laboratory subject. Fast-forward a few years and here I am finishing a PhD in chemistry. Time to thank the people who made that possible.

First of all, I would like to thank my supervisors Dave Haddleton and Kristian Kempe. Dave, you gave me the opportunity to come to Warwick for my PhD. Your *Just do it* mentality is well-known within and outside the group and plays an important role in the success of your group. Why is Nike not sponsoring your research? You provided all the freedom someone could wish for while also being there whenever I needed advice and allowed me to travel around the globe in pursuit of science (and post-conference holidays). Perhaps most importantly, you allowed me to work with Kristian. Speaking (writing?) of you, Kristian, I still remember how I assumed you were just going to be another postdoc when you left for Warwick. Instead, you became Dave's senior researcher and somewhat later my co-supervisor. Under your leadership we brought SZWIP back to the attention of the scientific community and it has been a great pleasure working with you these past years. I especially want to thank you for getting me to Monash and letting me co-supervise some of your students. Vielen Dank!

My thanks also go to Prem Paul, Ezat Khoshdel and Unilever for funding my PhD and providing me with an interesting project. I have always found it fitting that a Dutch-British company was sponsoring a Dutch PhD researcher in the UK. Thank you to Paul Wilson for all the useful advice over the years, the chats about the (too often disappointing) results of our football teams and the opportunity to work with many of your students as well – it almost made me a part of the Wilson group too.

I am also thankful for all people I have collaborated with. Thanks to Jan Steinkoenig, Anja Goldmann and Christopher Barner-Kowollik for a successful collaboration on the results in Chapter 3. Most of the results in Chapter 5 would not have been possible without the help of Angus Johnston, Moore Chen and Ayaat Mahmoud. Thanks also to all the undergraduate students that I was fortunate to co-supervise: Greg, Alice,

Mechelle, Alex and Alex. Some of your results have made it into this thesis, but most of all, it was a pleasure to work with you.

Thank you to all members of the Haddleton group, in particular the legends of Office C210 and its associated members: Sam, Danielle, Nuttapol, Dan, Rachel, Jenny, Sam, Chris S., Alan, Gavin, Chris A., Tammie, Emily and Yujing. There are many stories that can be told and it is probably best to keep them between us, but this PhD was definitely made better by you all. A special mention should also go to the others who started at the same time as me and have been here for the whole journey: Richard, Glen and Nikos. Thank you as well to all other Haddleton group members over the past years. Thanks also to the members of the Perrier, Bon and Scott groups for many a drink after work. I would also like to thank the members of the Kempe group and in particular Ayaat for (too) many coffee breaks and laughs. Thanks to Mikey for letting me stay with him and all members of the Nanomedicine and Johnston groups for being so welcoming and helpful during my visit to Monash. A special mention also to Tobi as biology partner-in-crime.

One cannot do good science without the right equipment, so thanks should also go to those maintaining that equipment. Likewise, thanks to all other support staff in their administrative roles and the team at Chemistry Stores.

Dit proefschrift zou ook niet tot stand zijn gekomen zonder support van het thuisfront. Om te beginnen Opa Radings, met al zijn verhalen over Indië ongetwijfeld de verantwoordelijke voor al mijn gereis. Dank ook aan de familie Vissers, Mark en Sven die altijd in de buurt zijn als ik weer eens terug ben in Nederland.

Stephan, de andere chemicus in de familie. We werken dan wellicht wel aan verschillende aspecten van chemie, maar het is fijn om iemand te hebben die echt begrijpt wat ik doe. Pa en ma, hoeveel jullie nu daadwerkelijk begrijpen van wat ik doe maakt niet uit. Jullie hebben mij en Stephan altijd gesteund en hoewel het niet altijd even makkelijk is dat ik wat verder weg woon, dit proefschrift was er zonder jullie niet geweest. Dankjulliewel.

## Declaration

Experimental work contained in this thesis is original research carried out by the author, unless otherwise stated, in the Department of Chemistry, University of Warwick, between October 2014 and June 2018, and at the Monash Institute of Pharmaceutical Sciences, Monash University, between March 2017 and June 2017.

The mechanistic studies on the spontaneous zwitterionic copolymerisation mechanism described in Chapter 3 were carried out in collaboration with Jan Steinkoenig, Dr. Anja Goldmann and Prof. Christopher Barner-Kowollik (Karlsruhe Institute of Technology and Queensland University of Technology) and form part of a PhD thesis submitted by Jan Steinkoenig to the Karlsruhe Institute of Technology (2018). The cell uptake images in Chapter 5 were obtained by Ayaat Mahmoud (Monash University). The QCM-D studies in Chapter 5 were carried out by Mechelle Bennett under supervision of the author at the University of Warwick and have previously been submitted as part of a MChem thesis at the University of Warwick (2016).

Patrick de Jongh

August 2018

## Abstract

Polyester-based materials have received significant attention from the scientific community for a plethora of applications. This thesis investigated the synthesis and properties of novel polyester-based materials synthesised by spontaneous zwitterionic copolymerisation (SZWIP) and melt polycondensation.

The synthesis of *N*-acylated poly(aminoester) (NPAE) macromonomers by SZWIP of cyclic imino ethers (CIEs) and acrylic acid (AA) was investigated in Chapter 2, revealing the limited effect of different reaction conditions, but interestingly demonstrated a facile way to tune the  $\omega$ -end groups on the NPAE macromonomers. A post-mortem ESI MS/MS study on a small library of NPAE macromonomers was conducted in Chapter 3 to investigate the microstructures formed during SZWIP of CIEs and AA. This demonstrated the presence of homopropagation of CIEs as a side reaction to the alternating copolymerisation of the CIEs with AA and led to an extended mechanism for SZWIP.

Next, the synthesis of well-defined comb polymers by aqueous redox-initiated RAFT polymerisation of these NPAE macromonomers was investigated in Chapter 4. The resulting comb polymers showed a dual stimuli-responsive behaviour in aqueous solution with a pH-dependant LCST behaviour. Furthermore, the efficient post-polymerisation functionalisation with model amines was demonstrated. Chapter 5 discusses early investigations into the potential of these comb polymers for biomedical applications, demonstrating the absence of cytotoxicity and haemolysis, their cellular uptake and low-fouling behaviour, amongst others.

Finally, Chapters 6 and 7 discuss the synthesis of branched polyesters and poly(ester amide)s by melt polycondensation of safe and renewable materials, focussing on citric acid and gluconolactone. The simple tuneability of the glass transition temperatures of the resulting polymers through variation of reaction conditions and co-monomers was demonstrated, leading to new insights in monomer structure-thermal property relationships.

## Lekensamenvatting

Er is veel potentieel for materialen gebaseerd op polyesters voor een verscheidenheid aan toepassingen. In dit proefschrift zijn de synthese en eigenschappen van nieuwe polyesters gemaakt via *spontane zwitterionische copolymerisatie* en klassieke smelt polymerisatie onderzocht.

De spontane zwitterionische copolymerisatie produceert alternerende poly(aminoester)s. In Hoofdstuk 2 wordt het effect van verschillende reactie condities onderzocht en het gemakkelijk aanpassen van één van de eindgroepen aangetoond. Massa spectrometrie studies geven een eerste indicatie dat bijreacties plaatsvinden die resulteren in defecten in de alternerende structuur van de polymeren. Dit is verder onderzocht en bewezen in Hoofdstuk 3, waar deze bijreacties eveneens gekwantificeerd worden. Dit leidt uiteindelijk tot een vernieuwde mechanisme voor de spontane zwitterionische copolymerisatie.

Deze polymeren kunnen zelf ook weer gepolymeriseerd kunnen worden en dit is vervolgens onderzocht in Hoofdstuk 4. De resulterende ‘kampolymeren’ vertonen interessant gedrag in waterigge oplossingen: bij lagere temperaturen zijn ze volledig oplosbaar, maar als de oplossing opgewarmd wordt, worden de polymeren onoplosbaar. Deze eigenschap biedt interessante mogelijkheden voor biomedische toepassingen. Daarnaast kunnen deze kampolymeren simpel gefunctionaliseerd worden met andere moleculen. Hoofdstuk 5 bestudeert vervolgens het potentieel van deze kampolymeren voor biomedische toepassingen en het is onder meer aangetoond dat deze polymeren niet schadelijk zijn voor de cellen en dat ze in staat zijn opgenomen te worden in deze cellen.

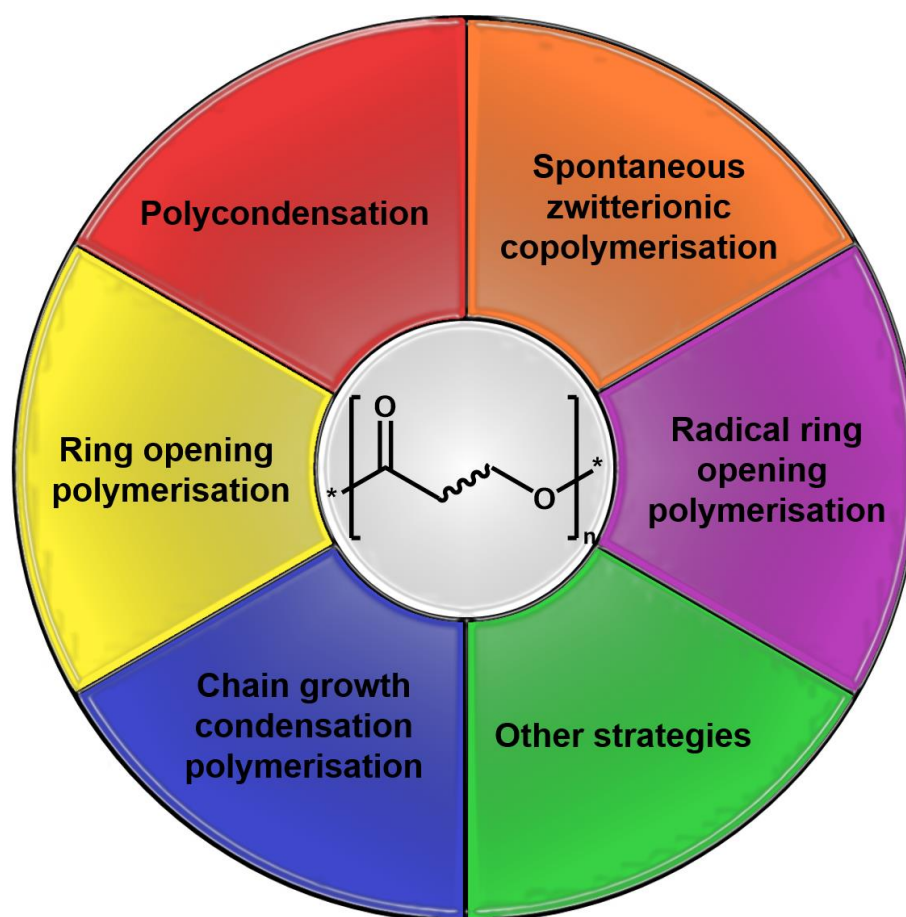
De laatste twee hoofdstukken beschouwen relatief simpele chemie: de smelt polymerisatie van veilige en hernieuwbare monomeren voor vertakte polymeren gebaseerd op citroenzuur en gluconolacton (een broertje van glucose) waarbij de focus ligt op de thermische eigenschappen van de resulterende polymeren. Het is gedemonstreerd dat deze simpel gevarieerd kunnen worden door middel van de reactiecondities, alsmede het gebruik van co-monomeren en katalysatoren.

## Chapter 1

---

# Synthetic strategies for polyester-based materials

---



Parts of this chapter have been published:

P.A.J.M. de Jongh, D.M. Haddleton, K. Kempe, *Prog. Polym. Sci.* **2018**, DOI: 10.1016/j.prog-polymsci.2018.08.002.

## 1.1. Biodegradable materials

The development of biocompatible and biodegradable materials has received a significant amount of attention over the last decades (a Web of Science search on “biodegradable polymer\*” in August 2018 revealed over 4,000 articles and 500 reviews since 2012). In order to be classified as biodegradable, microorganisms need to be able to completely degrade and catabolise the polymer to carbon dioxide and water under natural environmental conditions. Moreover, any products generated during the degradation process should not be harmful.<sup>1</sup> The applications of these materials are wide ranging, from packaging materials to drug delivery systems, and each application comes with its own specific requirements for the materials used.

Over the years a broad range of biodegradable polymers has been investigated. Their primary classification is most commonly by their origin; natural, microbial or synthetic polymers.<sup>2</sup> Natural polymers can be divided into polysaccharides, including starch, cellulose and chitosan, and proteins, such as collagen and albumin. Microbial polymers include poly(hydroxyl alkananoate)s and poly( $\gamma$ -glutamic acid). The largest class of biodegradable polymers are based on synthetic polymers. Polyesters,<sup>3–13</sup> including poly( $\alpha$ -hydroxy acid)s,<sup>10,11</sup> polylactones,<sup>4,5,12,13</sup> polyorthoesters,<sup>14</sup> polyphosphoesters<sup>15</sup> and polycarbonates,<sup>7,16–18</sup> have been given significant attention in literature as a result of their straightforward synthesis and good degradability. Polyanhydrides,<sup>19</sup> polyurethanes,<sup>20,21</sup> polyphosphazenes,<sup>22–24</sup> as well as poly(amino acid)s<sup>25–27</sup> and poly(ester amide)s<sup>28–30</sup> are other types of biodegradable synthetic polymers which have frequently been studied.

## 1.2. Synthetic strategies for polyesters, poly(ester amide)s and poly(aminoester)s

Biodegradable polymers can be synthesised both by step-growth polymerisations, such as polyadditions or polycondensations,<sup>31,32</sup> and chain-growth polymerisations, such as ring-opening polymerisations (ROPs).<sup>33</sup> Polyadditions and polycondensations generally need higher temperatures and longer reaction times to reach higher molecular weights and the resulting polymers typically have relatively broad molecular weight

distributions as a result of the limited control over the reaction. Conversely, chain-growth strategies allow for good control over the target molecular weight and yields narrower molecular weight distributions. However, ROP is only applicable to certain monomers, limiting its use. The various techniques, however, do all have their own levels of control over the reaction and molecular weight build up, as illustrated in Figure 1.1. In this Chapter, the synthetic strategies available for the synthesis of (functional) polyesters, poly(ester amide)s (PEAs) and poly(aminoester)s (PAEs) are discussed, illustrating the monomers required for the various polymerisation mechanisms and methods to introduce additional functionalities into the polymers.

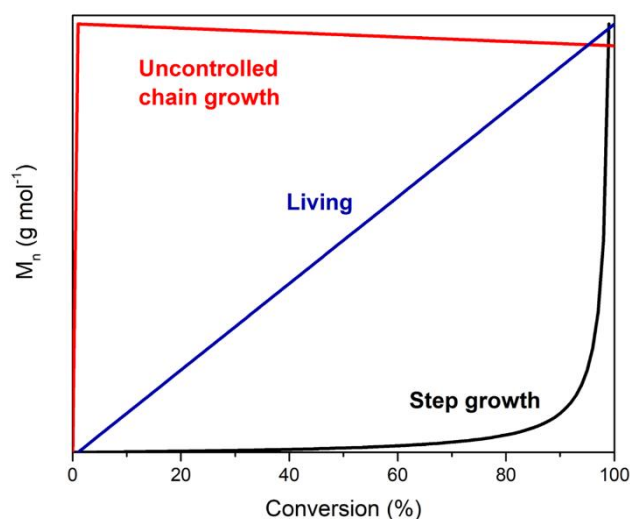


**Figure 1.1** Evolution of molecular weight versus monomer conversion for uncontrolled chain-growth, step-growth and living polymerisations. Adapted from ref. 34.

### 1.3. Polycondensation

The very first polyesters were made by polycondensation, a technique that is still widely used by industry to fabricate a wide range of commodity polyesters. Dating back as far as 1833 when Gay-Lussac and Pelouze polymerised lactic acid,<sup>35</sup> this technique was later picked up by Von Baeyer<sup>36</sup> and, most notably, Leo Baekeland who used this technique to produce Bakelite by reaction of phenol with formaldehyde in 1909.<sup>37</sup>

The textbook examples of synthesising polyesters by polycondensation typically involve the reaction of a dicarboxylic acid with a diol (AA + BB), such as adipic acid

with 1,6-hexanediol, or condensation of hydroxy acids (AB) such as lactic acid. In all cases, polycondensation is a step-growth polymerisation and therefore follows the standard mechanism as depicted in Figure 1.2, and consequently leads to the formation of broad molecular weight distributions.

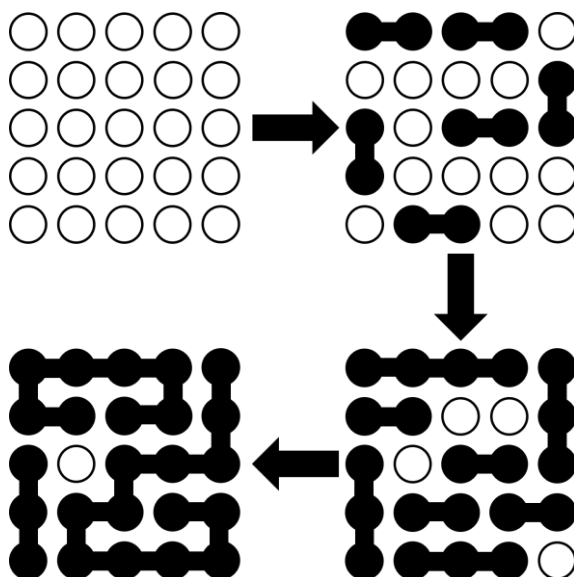


**Figure 1.2** Schematic of a step-growth polymerisation illustrating the formation of a broad molecular weight distribution. White circles are bifunctional monomers, black circles are dimers, trimers and longer oligomers.

The polycondensation approach is often divided into three categories: (a) melt polycondensation which takes place in the absence of any solvents and is therefore considered a “green” approach, (b) solution synthesis, which takes place with all reagents dissolved in a single solvent or a mixture of miscible solvents, and (c) interfacial polymerisation, a method based on Schotten-Baumann reaction conditions where two immiscible solvents are used and the reaction takes place at the interface of both solvents.<sup>28,29</sup>

An essential aspect of this polymerisation technique is the stoichiometric production of a small molecule condensate (*e.g.* water or small alcohols) which can initiate the depolymerisation to reproduce the monomer and, if not removed during the reaction, can limit the molecular weights obtained by polycondensation. Some methods to remove this condensate include temperature, vacuum and gas.<sup>13</sup>

This section does not aim to provide an all-inclusive overview of polyesters obtained by polycondensation since the first example back in 1833, but instead highlights several interesting monomers from renewable resources, the Carothers and Flory-Stockmayer equations and catalysis in polycondensation reactions.

### 1.3.1. Monomers from renewable resources

The majority of polyesters used commercially today are made from non-renewable fossil sources. As a result of fluctuating oil prices and their ultimate depletion, polyesters derived from renewable resources have attracted significant attention in recent years. In particular, their biodegradability, potential biocompatibility and the relatively easy access to bio-based/biomass monomers makes them highly interesting next generation sustainable materials. The polycondensation of lactic acid by Gay-Lussac and Pelouze<sup>35</sup> was not only the first example of polycondensation, but also the first one of a renewable resource as lactic acid can be sourced from corn and wheat.<sup>38</sup>

In recent years an ever-increasing list of monomers that can be obtained from biomass has been reported.<sup>39–41</sup> An important subclass is the oxygen-rich monomers such as carboxylic acids, polyols, dianhydroalditols and furans.<sup>42</sup> Vilela *et al.* highlighted succinic acid, fumaric acid, itaconic acid, and furandicarboxylic acid as promising diacids, and isosorbide, isomannide, isoidide, 1,3-propanediol and 1,4-butanediol as diol monomers for the synthesis of polyesters.<sup>42</sup> The polysaccharide cellulose is the main precursor for aliphatic renewable monomers, including carbohydrate monomers recently reviewed by Galbis and co-workers (Figure 1.3).<sup>43,44</sup>

Lignin is a source for aromatic monomers such as vanillic acid and 5-(hydroxymethyl)furfural; the latter is the precursor to 2,5-furandicarboxylic acid and several other renewable furan monomers that can be employed in the synthesis of polyesters and PEAs, amongst others (Figure 1.4). In particular 2,5-furandicarboxylic acid has received significant interest over recent years as a result of its polycondensation product with ethylene glycol, poly(ethylene furanoate), which demonstrated superior properties compared to the fossil fuel derived poly(ethylene terephthalate).<sup>45–49</sup>

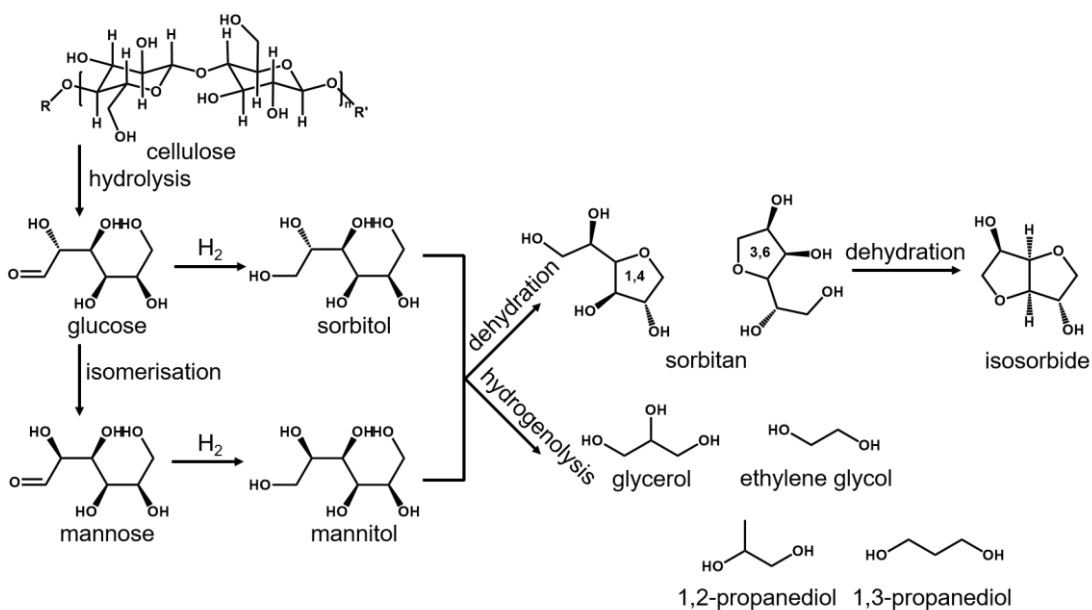


**Figure 1.3** Conversion of cellulose to sugars and other common hydroxy monomers. Adapted from ref. 44.

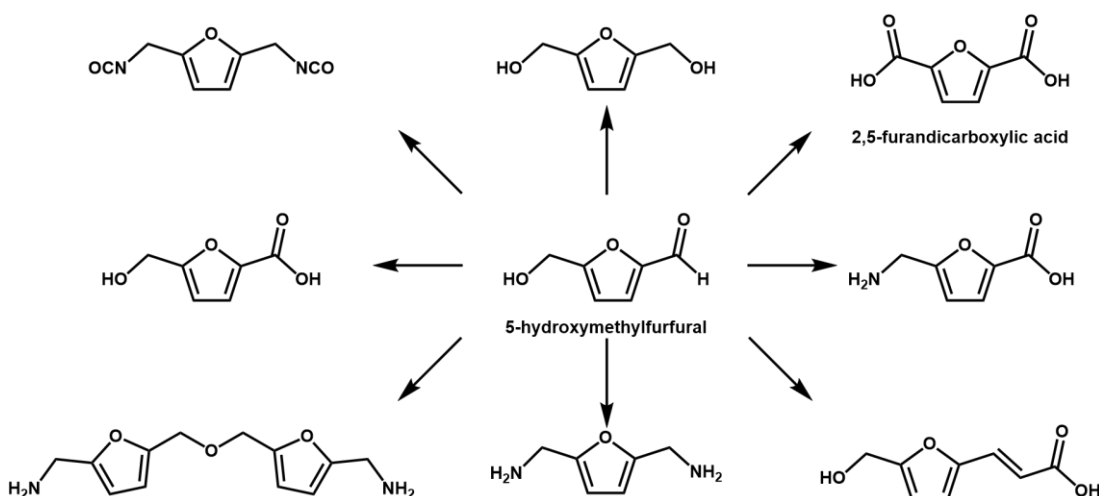
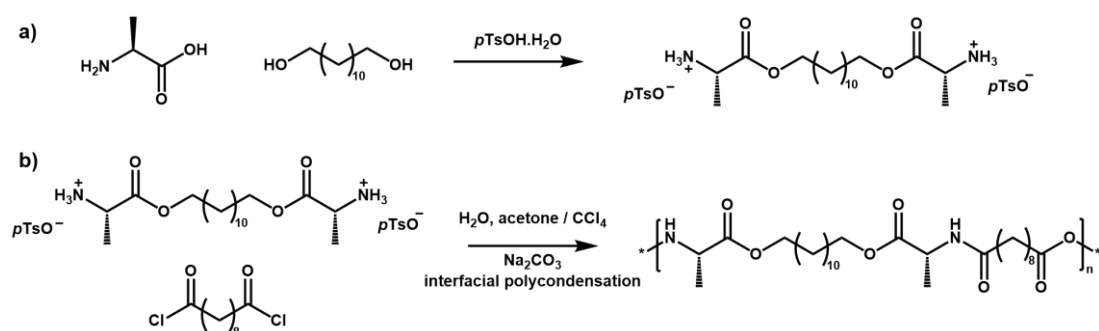


**Figure 1.4** Monomers suitable for polycondensation reactions that can be derived from 5-hydroxymethylfurfural. Adapted from ref. 45.

When considering renewable monomers containing amines for the synthesis of PEAs, amino acids have received significant interest.<sup>1,28–30,50</sup> The benefit of amino acids over other amine-containing monomers lies in their biocompatibility, enzymatic degradability, interactions with other biological materials and the introduction of additional functionalities, for example for post-polymerisation functionalisation.<sup>29</sup>

Although it is possible to directly copolymerise a dicarboxylic acid with diol and amino acid monomers, for example, this may lead to an uneven incorporation of the diol and amino acid monomers as a result of the different reactivities of hydroxyl and amine groups. A common strategy to overcome this is by converting the synthesis into a two or three step procedure. Scheme 1.1 illustrates such an example in which Puig-gali and co-workers synthesised PEAs from sebacoyl chloride, 1,10-dodecanediol and L-alanine. In the presence of *p*-toluenesulfonic acid (*p*TsOH), the diol and glycine were reacted to form a new bis( $\alpha$ -(L-alanine)- $\alpha,\omega$ -dodecanediol diester) monomer as the *p*TsO<sup>-</sup> salt. This intermediate was subsequently reacted with sebacoyl chloride in an interfacial polycondensation to form the resulting PEA with a  $M_n$  of 24 kg mol<sup>-1</sup>.<sup>51</sup> Other examples not only synthesise an intermediate from the diol and amino acid, but also further activate the dicarboxylic acid (chloride) through esterification with a better leaving group such as nitrophenol esters. This was for example demonstrated by Pang *et al.* for the synthesis of a series of novel water-soluble polycationic polymers incorporating arginine moieties.<sup>52</sup>



**Scheme 1.1** Two-step PEA synthesis. a) Condensation of L-alanine with 1,12-dodecanediol to form a bisamine monomer. b) Interfacial polycondensation of the bisamine monomer with sebacoyl chloride to form the PEA. Adapted from ref. 51.

### 1.3.2. Carothers and Flory-Stockmayer equations

Some important theoretical understanding of polycondensation reactions is provided through the Carothers and Flory-Stockmayer equations. Wallace Carothers, known for his iconic review “Polymerization” in 1931,<sup>31</sup> related the conversion of a polyconden-

sation to the average degree of polymerisation (DP) of the formed polymers.<sup>53</sup> An important requirement for this is the assumption of equal reactivity between all functional groups of a certain type, *i.e.* all hydroxyl groups on monomers have the same reactivity as hydroxyl groups on growing polymer chains. Equation 1.1 shows the Carothers equation for linear polymers. In this equation, the average DP ( $X_n$ ) is calculated from the molar ratio between the two bifunctional monomers ( $r$ ) and the conversion ( $p$ ). The molar ratio is obtained by simple division of two monomers, using the monomer in excess as denominator such that  $0 < r < 1$ . If the two monomers are present in stoichiometric ratio  $r = 0$  and the Carothers equation reduces to Equation 1.2. The conversion ( $p$ ) is calculated according to Equation 1.3, in which  $N_0$  is the initial number of monomers and  $N_t$  is number of molecules (monomers, oligomers and polymers) at a given time ( $t$ ).

$$X_n = \frac{1 + r}{1 + r - 2rp} \quad (1.1)$$

$$X_n = \frac{1}{1 - p} \quad (1.2)$$

$$p = \frac{N_0 - N_t}{N_0} \quad (1.3)$$

The extended Carothers equation (Equation 1.1) enables to control the target molecular weight at full conversion by adding one monomer in excess. In both cases the Carothers equation demonstrates the slow build-up of molecular weight until high conversions as illustrated in Figure 1.1. Furthermore, Carothers established the relationship between the conversion and the weight-average DP (Equation 1.4), number-average molecular weight ( $M_n$ , Equation 1.5), weight-average molecular weight ( $M_w$ , Equation 1.6) and dispersity ( $D$ , Equation 1.7), in which  $M_0$  is the molecular weight of the repeating unit.

$$X_w = \frac{1 + p}{1 - p} \quad (1.4)$$

$$M_n = M_0 \cdot \frac{1}{1 - p} \quad (1.5)$$

$$M_w = M_0 \cdot \frac{1+p}{1-p} \quad (1.6)$$

$$\mathbb{D} = \frac{M_w}{M_n} = 1+p \quad (1.7)$$

This theory has also been extended to monomers with a functionality greater than two. In this case the average degree of functionality of the monomers ( $f_{av}$ ) is calculated according to Equation 1.8, in which  $N_i$  is the number of molecules of type  $i$  and  $f_i$  the functionality of monomer  $i$ .

$$f_{av} = \frac{\sum N_i \cdot f_i}{\sum N_i} \quad (1.8)$$

The conversion  $p$  is then calculated using Equation 1.9 and the number-average DP results from Equation 1.10. When bifunctional monomers are used,  $f_{av} = 2$  and Equations 1.9 and 1.10 reduce back to Equations 1.3 and 1.2, respectively.

$$p = \frac{2(N_0 - N_t)}{N_0 \cdot f_{av}} \quad (1.9)$$

$$X_n = \frac{2}{2 - p \cdot f_{av}} \quad (1.10)$$

In addition to the Carothers equation, another important equation for the polymerisation of multifunctional monomers by step-growth polymerisations is given by the Flory-Stockmayer equation.<sup>54–58</sup> The introduction of a polyfunctional monomer ( $f > 2$ ) leads to gel formation at high conversions. With the Flory-Stockmayer equation it is possible to calculate the critical branching degree ( $\alpha_c$ ) based on the functionality of the monomers ( $f$ ) and from there the monomer conversion at the gel point (Equations 1.11 and 1.12). The ratio between the two monomers is given by  $r$ .

$$\alpha_c = \frac{1}{f - 1} \quad (1.11)$$

---

$$p_{gel\ point} = \sqrt{\frac{\alpha_c}{r}} \quad (1.12)$$

This equation demonstrates that for the reaction of a trifunctional with a bifunctional monomer, the conversion at gel point lies at  $p = \sqrt{1/2r}$  for the trifunctional monomer and  $p = \sqrt{2/r}$  for the bifunctional monomer.

### 1.3.3. Catalysts

One common problem in polycondensation strategies is the slow build-up of higher molecular weight species (Figure 1.1), a challenge that is typically addressed by utilising catalysts.<sup>3,4</sup> Organometal or metal-oxide compounds have been widely explored and enable the synthesis of significantly higher molecular weight polymers. In particular titanium catalysts, such as titanium(IV) isopropoxide, have been extensively employed for the synthesis of for example poly(butylene succinate) where they demonstrate high catalytic activity.<sup>59</sup> Scandium catalysts have emerged as a milder alternative to titanium catalysts. Takasu *et al.* demonstrated the polycondensation of sebacic acid dimethyl ester with 1,4-butanediol at 35 °C,<sup>60</sup> as well as the polycondensation between adipic acid and 3-methyl-1,5-pentanediol at 60 °C<sup>61</sup> in the presence of several scandium catalysts. A systematic study on catalysts for the synthesis of poly(butylene succinate) revealed the following trend: Ti > Ge > Zr ~ Sn > Hf > Sb > Bi.<sup>62</sup> This highlights the potential of germanium and zirconium catalysts as an alternative for titanium catalysts. Closely related to the organometal and metal-oxide catalysts are the corresponding triflates, with different groups reporting good results under mild conditions with scandium triflate<sup>63</sup> and lanthanide triflate,<sup>64</sup> amongst others. Alternatively, inorganic acids (H<sub>3</sub>PO<sub>4</sub> or H<sub>2</sub>SO<sub>4</sub>) have been reported at mild temperatures and low vacuum to produce polyesters with molecular weights close to 55 kg mol<sup>-1</sup>.<sup>65</sup>

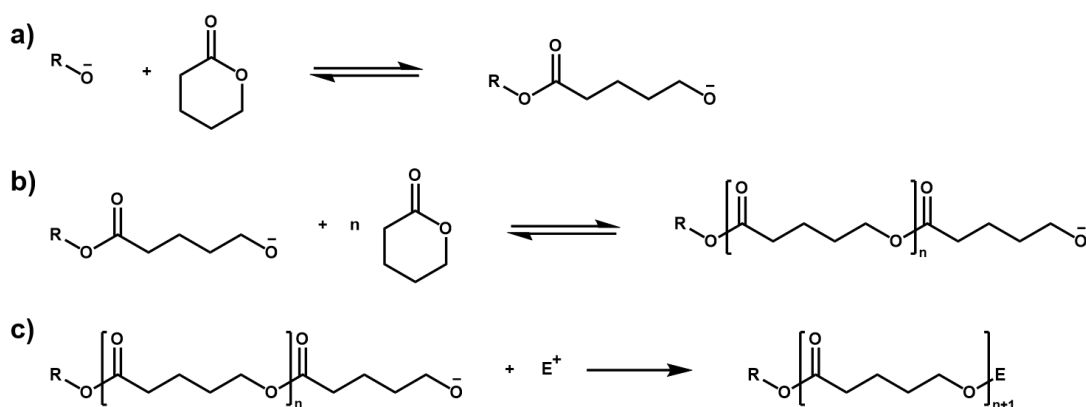
A “greener” approach to catalysis lies in the use of enzymes as it can avoid the use of toxic metal-based catalysts and organic solvents.<sup>3,4</sup> A popular choice is *Candida antarctica* lipase B (CalB),<sup>4,42,66,67</sup> which is selective towards primary hydroxyl groups and thus enables the synthesis of linear polyesters from unprotected sugar monomers,<sup>68</sup>

but also other enzymes such as lipases from *Mucor miehei*,<sup>69,70</sup> *Pseudomonas aeruginosa*, *Candida cylindracea* and *Klebsiella* have been investigated for polycondensations involving sebacic acid.<sup>71</sup> Even though good results can be obtained by enzymatic catalysis, the main drawback is the relatively high prices of enzymes compared to metal-based catalysts.

## 1.4. Ring-opening polymerisation

Following polycondensation, ring-opening polymerisation (ROP) is the second main strategy for the synthesis of polyesters. In contrast to polycondensation, ROP is a chain growth polymerisation technique and consequently allows for significantly more control of the molecular weight distribution and polymer end groups.

The general mechanism for ROP is shown in Scheme 1.2, using a hydroxide anion as initiator, but this reaction can also be initiated by cationic species. Ring-opening of the monomers to add to the growing polymer chain is a reversible process determined by the thermodynamics of the reaction (*vide infra*). Cyclisation and backbiting are side reactions leading to the formation of cyclic species, whereas transesterification reactions between two polymer chains leads to polymers that deviate from the targeted chain lengths.<sup>72</sup>



**Scheme 1.2** General mechanism for anionic ROP of cyclic esters. a) Initiation with a hydroxide anion. b) Propagation by consecutive addition of monomers. c) Termination by an electrophile. Adapted from ref. 72.

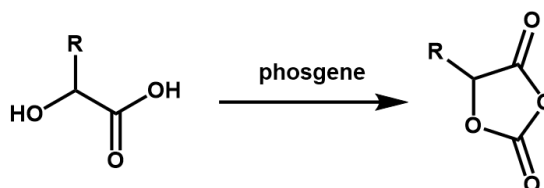
### 1.4.1. Monomers for ring-opening polymerisation

The two main classes of monomers employed for the synthesis of polyester-based materials by ROP are cyclic esters, *i.e.* lactones, and *O*-carboxyanhydrides (OCAs). This section provides a brief overview of synthetic strategies for these monomers, with a focus on monomers derived from renewable resources. Although most monomers cannot be directly obtained from biomass, they can often be prepared in a few steps from bio-renewable resources.

The six-membered monomer lactide is typically prepared through a two-step process. First, lactic acid is polymerised into oligomers (1 – 5 kg mol<sup>-1</sup>) by polycondensation. Subsequently, selective depolymerisation through an intramolecular transesterification process in the presence of a catalyst and continual removal of lactide by distillation produces the monomer in good yield.<sup>73</sup> A similar strategy is utilised for the synthesis of glycolide from glycolic acid.<sup>72</sup> The most investigated seven-membered lactone,  $\epsilon$ -caprolactone, is obtained by Baeyer-Villiger oxidation of cyclohexanone,<sup>12</sup> which in turn can be obtained from lignin.<sup>74</sup> This approach has also been used for a menthol-derived monomer,<sup>75</sup> amongst others. An alternative approach is the catalytic hydrogenation of diacids, which has been reported by Budroni and Corma to produce  $\gamma$ -butyrolactone from succinic acid.<sup>76</sup> Blake and Waymouth recently reported the synthesis of morpholine-2,5-dione derivatives *via* oxidative lactonization from *N*-substituted diethanolamines as an alternative method for lactones that can be polymerised into *N*-substituted PAEs.<sup>77</sup> Gregory *et al.* recently published a comprehensive review on the synthesis of carbohydrate-derived monomers for ROP using various strategies.<sup>78</sup>

The second group of monomers suitable for the synthesis of polyesters by ROP consists of *O*-carboxyanhydrides (OCAs) and has started to receive more attention over the last decade.<sup>79</sup> In analogy to the more popular *N*-carboxyanhydrides (NCAs),<sup>27</sup> OCAs can be synthesised from  $\alpha$ -hydroxy acids by reacting them with phosgene or phosgene derivatives (Scheme 1.3).<sup>79</sup> Many  $\alpha$ -hydroxy acids can be found in renewable resources and additionally can be obtained through the reaction of amino acids with sodium nitrite.<sup>80</sup> An interesting benefit of OCAs compared to lactones is that their ROP

is more thermodynamically favourable, as both the ring-opening process and subsequent decarboxylation contribute to the overall change in Gibbs free energy for the ROP, allowing faster polymerisation under milder conditions.<sup>79</sup> Although there is still much progress to be made in the field of OCAs compared to lactones, in particular the OCA derived from lactic acid has been given considerable attention.<sup>78</sup>



**Scheme 1.3** General synthesis of *O*-carboxyanhydrides from  $\alpha$ -hydroxy acids.

### 1.4.2. Thermodynamics of ring-opening polymerisation

The Gibbs free energy equation for ROP of lactones is given in Equation 1.13. In this equation,  $\Delta G$  is the change in Gibbs free energy, which needs to be negative for polymerisation to occur,  $\Delta H$  the change in enthalpy,  $T$  the temperature and  $\Delta S$  the change in entropy.<sup>81</sup>

$$\Delta G = \Delta H - T\Delta S \quad (1.13)$$

The driving force behind ROP of small lactones (< 8 membered rings) is the release of ring strain, which overcomes the entropic contributions during the polymerisation. Table 1.1 shows an overview of common monomers employed in ROP and their thermodynamic properties.<sup>72</sup> It can be observed that the enthalpic values for four-, six- and seven-membered rings are favourable for ROP, whereas the five-membered  $\gamma$ -butyrolactone has long been considered non-polymerisable under ‘normal’ conditions as a result of its low ring strain.<sup>82</sup> However, Hong and Chen recently reported its controlled polymerisation up to high conversions (> 90 %) under ambient pressure at -40 °C using  $\text{La}[\text{N}(\text{SiMe}_3)_2]$  as catalyst.<sup>83</sup> ROP of large lactones, on the other hand, is no longer driven by enthalpy, but rather by entropy (increase in conformational freedom) where their polymerisation has been demonstrated by various groups.<sup>84–86</sup>

**Table 1.1** Thermodynamic properties for ROP of lactones with different ring sizes.

Monomer <sup>a</sup>	Ring size	$\Delta H$	$\Delta S$	$[M]_{eq}$ <sup>b</sup>
		[kJ mol <sup>-1</sup> ]	[J mol <sup>-1</sup> K <sup>-1</sup> ]	[mol L <sup>-1</sup> ]
$\beta$ -propiolactone	4	- 82.3	- 74	$3 \cdot 10^{-11}$
$\gamma$ -butyrolactone	5	- 5.4	- 39.6 <sup>c</sup>	13.24 <sup>c</sup>
$\delta$ -valerolactone	6	- 8.4	- 14.7 <sup>d</sup>	0.18 <sup>d</sup>
L-lactide	6	- 22.9	- 41.1 <sup>e</sup>	$1.2 \cdot 10^{-2e}$
$\epsilon$ -caprolactone	7	- 14.0	- 6.0 <sup>f</sup>	$7.0 \cdot 10^{-3f}$
Tridecanolide	14	- 8	26	$2.3 \cdot 10^{-2g}$
Pentadecanolide	16	3	23	0.70 <sup>h</sup>

<sup>a</sup> Data reproduced from ref. 72. <sup>b</sup> Equilibrium monomer concentration at 25 °C. <sup>c</sup> Determined in CD<sub>2</sub>Cl<sub>2</sub>, [M]<sub>0</sub> = 10 M. <sup>d</sup> Determined in CH<sub>2</sub>Cl<sub>2</sub>/toluene (70/30 v/v), [M]<sub>0</sub> = 0.35 M. <sup>e</sup> Determined in 1,4-dioxane, [M]<sub>0</sub> = 1.0 M. <sup>f</sup> Determined in CH<sub>2</sub>Cl<sub>2</sub>/toluene (70/30 v/v), [M]<sub>0</sub> = 2.0 M. <sup>g</sup> Determined at 157 °C. <sup>h</sup> Determined at 97 °C.

### 1.4.3. Catalysts for ring-opening polymerisation

ROP can take place in the absence of catalysts, but is relatively slow under non-catalysed conditions, allowing side reactions such as backbiting to take place. In order to speed up the ROP and minimise these side reactions, many catalytic systems have been developed over the years. A recent review by Waymouth and co-workers provides an excellent overview of their development.<sup>72</sup> In this section only some of the more interesting catalytic advances are highlighted.

Traditionally, metal-based catalysts such as tin(II) 2-ethylhexanoate, have received significant attention as they are a cheap yet effective way to polymerise lactones. These catalysts are proposed to function through a coordination-insertion mechanism. However, they are not highly selective or stereospecific and therefore other, more well-defined single-site catalysts have been developed, equipped with ancillary ligands to fine-tune the electronic and steric properties of the catalysts and thereby improve control over the polymerisation. For example, a Ln-phosSALEN complex has been employed for the synthesis of high molecular weight (> 100 kg mol<sup>-1</sup>) isotactic polylactide.<sup>87</sup> Another interesting example is a zinc complex with chiral ligands that is able to

produce *iso*-enriched stereoblock polylactide from *rac*-lactide monomer.<sup>88</sup> Recently, there has been a drive towards the development of switchable catalysts. In this context, Wang *et al.* reported on redox-switchable group 4 metal catalysts for the one-pot block copolymerisation of lactide and  $\epsilon$ -caprolactone with minor defects.<sup>89</sup> Williams and co-workers developed a CO<sub>2</sub>-switchable catalyst. In the presence of CO<sub>2</sub>, selective, alternating copolymerisation of an epoxide and CO<sub>2</sub> was observed, without any polymerisation of  $\epsilon$ -caprolactone, but once the CO<sub>2</sub> was removed from the reaction by purging with N<sub>2</sub>, epoxide polymerisation ceased and polymerisation of  $\epsilon$ -caprolactone took place to form a poly(carbonate-*b*-ester).<sup>90</sup>

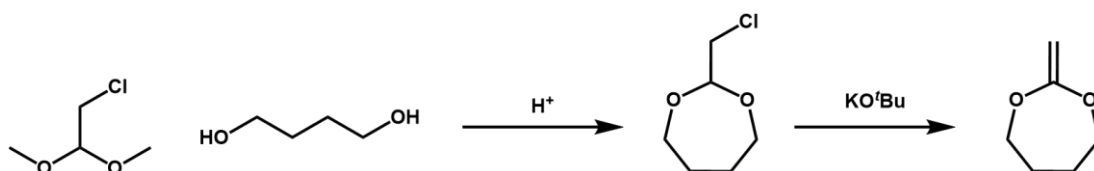
Another important advancement in the field of ROP catalysis is the move from metal-based catalysts to organocatalytic strategies<sup>91-94</sup> and much work in this field was done by the groups of Hedrick and Waymouth. Following the first example in 2001, in which 4-(dimethylamino)pyridine (DMAP) was used for ROP of lactide,<sup>95</sup> attention shifted to *N*-heterocyclic carbenes (NHCs) as highly active catalysts.<sup>91-93</sup> Amongst others, they allow for the selective synthesis of cyclic homo- and gradient polyesters by zwitterionic ring-opening polymerisation.<sup>96-98</sup> A dual-catalytic system consisting of thiourea and 1,8-diazabicyclo(5.4.0)undec-7-ene (DBU) was developed which allowed additional activation of the lactones through hydrogen bonding with the thiourea co-catalyst to enable efficient polymerisation.<sup>99</sup> This strategy was later expanded by Kiesewetter and co-workers who designed similar catalysts containing two or three of these thiourea moieties, which are up to 100 times faster than the mono-thiourea catalytic system with similar selectivity.<sup>100,101</sup> The single thiourea catalyst also formed the inspiration for a thiourea anion (thioimidate) family of catalysts that are able to polymerise lactones (and cyclic carbonates) selectively into the corresponding polymers in the timespan of only seconds to several minutes.<sup>102,103</sup> More recently, *N*-heterocyclic olefins (NHOs) were introduced by the Dove group as an alternative class of very fast and selective catalysts for the ROP of lactones.<sup>104</sup> Altogether, catalysis is an important subtopic in ROP and development of new catalysts, able to polymerise faster, more selective and/or from mixed feedstocks is essential to allow this technique to compete with the more industrially popular polycondensation processes.

## 1.5. Radical ring-opening polymerisation

The ROP strategies discussed in Section 1.4 proceed through ionic mechanisms and are typically catalysed by metal complexes or organic catalysts. A different ROP approach is radical ring-opening polymerisation (RROP). Unlike ionic ROP strategies, this is a radical polymerisation technique which allows to combine the characteristics of ROP with the possibilities offered by controlled radical polymerisation techniques. The RROP technique encompasses a wide variety of monomers,<sup>7</sup> but will here only be discussed in the context of polyester-based materials.

### 1.5.1. RROP monomers and their polymerisation

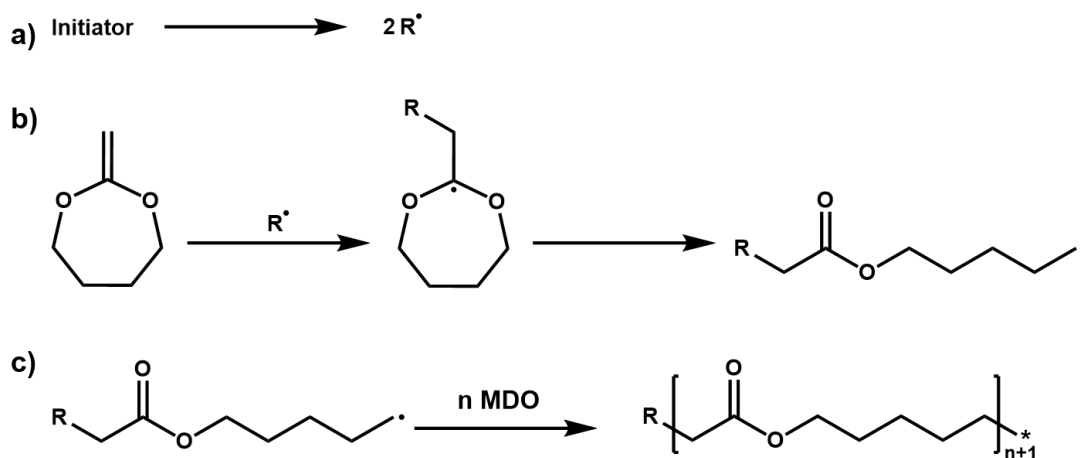
The main class of monomers investigated in the context of RROP consists of cyclic ketene acetals (CKAs). These monomers are typically synthesised by an acid catalysed acetal exchange reaction of a halogenated acetaldehyde acetal with a diol, followed by dehydrohalogenation with a strong base, such as potassium *tert*-butoxide (KO<sup>*t*</sup>Bu) as originally reported by McElvain.<sup>105</sup> Scheme 1.4 shows this for the most popular CKA monomer, 2-methylene-1,3-dioxepane (MDO).<sup>106</sup>



**Scheme 1.4** Synthesis of the CKA 2-methylene-1,3-dioxepane (MDO) by acetal exchange followed by dehydrohalogenation.<sup>106</sup>

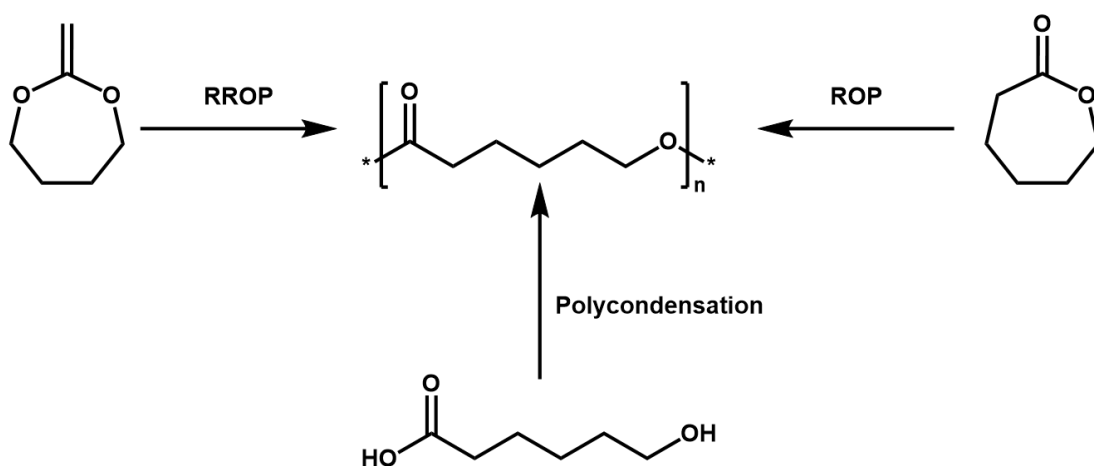
By varying the diol reagent employed, the ring size can be easily tuned and other functionalities can be introduced. It should of course be kept in mind that any pendant groups need to be compatible with the experimental conditions of CKA synthesis and subsequent RROP. Some other synthetic strategies for CKAs involve the acid catalysed reaction of acetonitrile with ethylene glycol, followed by sodium methoxide,<sup>107</sup> and the olefination of cyclic carbonates in the presence of dimethyltitalocene.<sup>108</sup> CKAs can be polymerised *via* cationic polymerisation, however, this yields polyacetals instead of polyesters and is therefore not further discussed here.<sup>7</sup>

Much of the pioneering work on RROP of CKAs was performed by Bailey and co-workers. Scheme 1.5 illustrates the RROP of MDO, one of the early examples of RROP of CKAs.<sup>106</sup> They used di-*tert*-butyl peroxide and 2,2'-azobisisobutyronitrile (AIBN) as radical sources in a free radical process. After the radical (R) reacts with the first CKA molecule, initially a tertiary radical is formed, which then isomerises into a primary radical while the acetal rearranges to introduce the ester functionality. The reactive primary radical rapidly reacts with another monomer to propagate into a high molecular weight polyester, which is terminated by typical termination mechanisms observed for radical polymerisations.



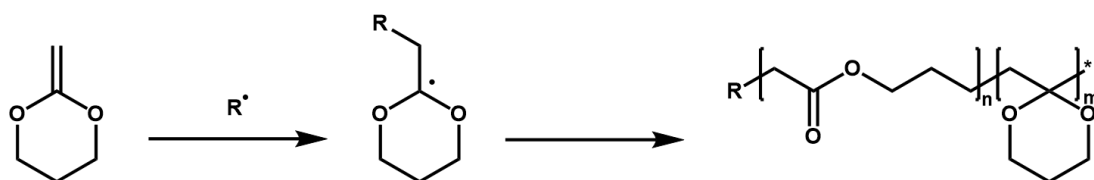
**Scheme 1.5** Mechanism for the RROP of MDO. a) Generation of radicals from a common initiator (*e.g.* AIBN). b) Reaction of a radical with MDO forms a tertiary radical which isomerises into a primary radical. c) Reaction with other MDO monomers furnishes higher molecular weight polyesters.

It is interesting to note that the RROP of MDO yields poly( $\epsilon$ -caprolactone) (PCL), similar to ROP of  $\epsilon$ -caprolactone and the polycondensation of 6-hydroxyhexanoic acid (Scheme 1.6), but with the experimental versatility of radical polymerisations, rather than the stringent anhydrous conditions required for ROP or the limited control associated with polycondensations.



**Scheme 1.6** Radical ring-opening polymerisation of 2-methylene-1,3-dioxepane, ring-opening polymerisation of  $\epsilon$ -caprolactone and polycondensation of 6-hydroxyhexanoic acid all yield poly( $\epsilon$ -caprolactone).

Although RROP works well for MDO, evaluation of other monomers and reaction conditions revealed side reactions that accompany the RROP process. The most prominent is ring-retention, which occurs when the tertiary radical reacts with another CKA monomer before the isomerisation into the primary radical. This results in the introduction of an acetal functionality in the polymer backbone (Scheme 1.7).



**Scheme 1.7** Ring-retention in RROP leads to the introduction of acetal functionalities in the polymer backbone.

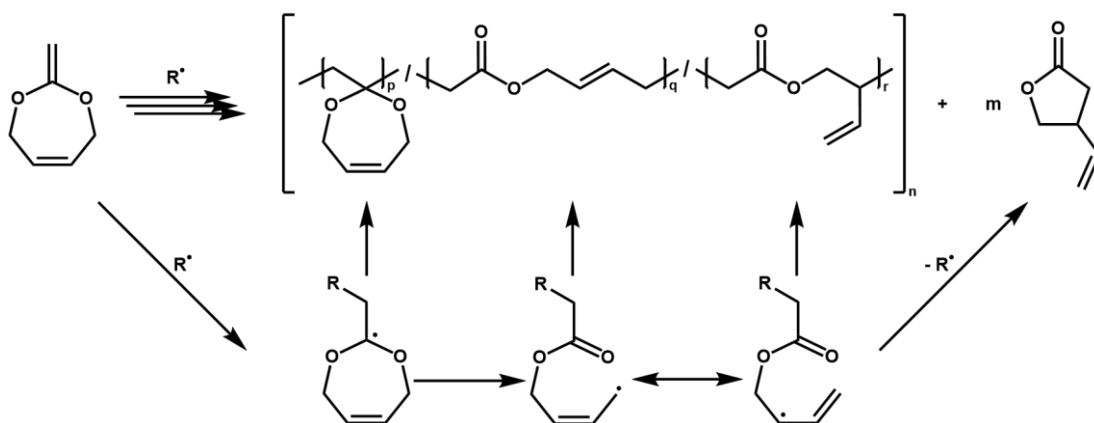
For example, whereas MDO and 5,6-benzo-2-methylene-1,3-dioxepane (BMDO) proceed via quantitative ring-opening in a wide range of conditions, RROP of the five-membered 2-methylene-1,3-dioxolane (MDL) suffered from ring-retention. Bailey *et al.* demonstrated that the number of ring-opened units increased from 50 % for a reaction at 60 °C to 83 % for a reaction at 125 °C. When the temperature was further increased to 160 °C ring-retention was no longer observed. The problem of ring-retention could be resolved by introducing substituents on MDL. The polymerisation of 2-

methylene-4-hexyl-1,3-dioxolane and 2-methylene-4-phenyl-1,3-dioxalane proceeded with quantitative ring-opening at temperatures from 60 to 150 °C.<sup>109,110</sup> Another common side-reaction is 1,4- and 1,7-hydrogen transfer leading to branched polymers, which was shown to be a temperature-dependant side reaction that was suppressed at higher temperatures.<sup>109,111</sup>

Based on the available literature, some general conclusions can be made on the relation between CKA monomers, their RROP conditions and the resulting extent of ring-retention in the final product. Five-membered CKAs have a significant amount of ring-retention at moderate reaction temperatures, whereas six-membered CKAs result in an increased amount of ring-opened structures. For seven-membered CKAs generally no ring-retention is observed. Furthermore, as shown for the MDL example, increasing the temperature generally lowers the presence of side reactions, as does stabilisation of the radical by introduction of side chains. However, it should be noted that much work has been done under varying experimental conditions and these are therefore only general conclusions.

### **1.5.2. Introducing additional functionalities**

As mentioned above, the appropriate choice of diol in the CKA synthesis directly enables the introduction of functional groups. Despite this, at first sight, seemingly straightforward accessibility to a library of functional CKAs, only a small variety of functional CKAs has been investigated as a result of the synthetic requirements for CKAs (*vide supra*). Albertsson and co-workers investigated the RROP of 2-methylene-1,3-dioxo-5-pene (MDOP), an analogue of MDO containing a double bond in the ring. When polymerised at low temperatures (50 °C) a polyester containing pendant vinyl groups was obtained (Scheme 1.8), alongside some ring-retention (not quantified). However, at high temperatures (150 °C) instead of forming the polyester, a rearrangement leads to the formation of 3-vinyl-1,4-butyrolactone (Scheme 1.8), demonstrating the importance of reaction temperature in this reaction.<sup>112</sup>



**Scheme 1.8** RRPOP of 2-methylene-1,3-dioxane-5-pene. Rearrangements at high temperatures lead to multiple backbone structures and the formation of 3-vinyl-1,4-butanolactone. Adapted from ref. 7, 112.

As an alternative way to introduce vinyl groups into a polyester, Cho and Kim demonstrated the RRPOP of 4-phenyl-2-propenyl-1,3-dioxolane.<sup>113</sup> In both cases, the pendant vinyl groups open up the possibility for post-polymerisation functionalisation by thiol-ene chemistry. Furthermore, several partially and fully fluorinated CKAs have been investigated by Liu *et al.*,<sup>114</sup> although they proved more difficult to polymerise as a result of the high polarity of the C–F<sub>2</sub> bond, so that consequently the radical adduct preferred propagation over the β-scission required for RRPOP.

Another strategy to introduce other functionalities via RRPOP is the copolymerisation of CKAs with conventional vinyl monomers,<sup>8</sup> which cannot be directly achieved by ROP of the corresponding lactones and therefore shows a potential major benefit of RRPOP over ROP. Sun *et al.* polymerised MDO with styrene and methyl acrylate (MA), but observed that the reactivity ratio of MDO was significantly lower ( $r_{\text{MDO}} = 0.024$ ) than the reactivity ratio of MA ( $r_{\text{MA}} = 26.54$ ), resulting in a strong gradient copolymer and a relatively low introduction of ester groups in the polymer backbone.<sup>115</sup> This difference in reactivity ratios is a general observation for the copolymerisation of CKAs with common activated vinyl monomers and has also been observed for the copolymerisation with other monomers.<sup>116–118</sup> However, when less activated vinyl monomers are used, such as vinyl acetate (VAc), the reactivity ratios are closer to each other ( $r_{\text{MDO}} = 0.47$ ,  $r_{\text{VAc}} = 1.53$ ) and consequently more random structures are formed.<sup>119</sup> In order to further address this issue, Tardy *et al.* recently employed density functional theory

(DFT) to identify *n*-butyl vinyl ether (BVE) as a vinyl monomer with closer-to-equal reactivity as MDO. Experimental results confirmed  $r_{\text{MDO}} = 0.73$  and  $r_{\text{BVE}} = 1.61$ , in line with the DFT calculations.<sup>120</sup>

### 1.5.3. Post-polymerisation functionalisation, controlled polymerisation and applications

With respect to the post-polymerisation functionalisation of RROP copolymers, Tardy *et al.* also demonstrated the versatile platform provided by RROP of MDO with BVE and its derivatives. RROP of MDO with chloroethyl vinyl ether (CEVE) enables subsequent nucleophilic substitution of the chlorines by Rose Bengal dye or sodium azide, followed by copper(I)-catalysed alkyne-azide cycloaddition (CuAAC). They also cast films of the MDO/CEVE copolymers and transformed the chlorines into quaternary amines. The resulting films shows antimicrobial properties against *Pseudomonas aeruginosa*, *Staphylococcus aureus* and the multi-resistant *S. aureus* strain MRSA USA300. Furthermore, they demonstrated the facile synthesis of crosslinked bioelastomers by RROP of MDO with the difunctional di(ethylene glycol) divinyl ether.<sup>120</sup> Maji *et al.* demonstrated that the copolymerisation of propargyl acrylate with MDO allows subsequent functionalisation by CuAAC,<sup>121</sup> whereas copolymerisation with glycidyl methacrylate introduced epoxides enables the binding of heparin as shown by Albertsson and co-workers.<sup>122</sup>

Whereas most work on RROP of CKAs has involved free radical polymerisations, the advent of controlled radical polymerisation techniques such as nitroxide mediated polymerisation (NMP),<sup>123–125</sup> transition metal-mediated polymerisation<sup>126,127</sup> (including atom transfer radical polymerisation (ATRP)<sup>128–131</sup> and Cu(0)-mediated reversible deactivation radical polymerisation<sup>132–137</sup>), as well as reversible addition-fragmentation chain-transfer (RAFT) polymerisation (including macromolecular design via the interchange of xanthates (MADIX)),<sup>138–147</sup> has enabled the synthesis of more well-defined polymers by RROP.

In the late 1990s, Wei *et al.* reported the first controlled RROP, using NMP to mediate the RROP of MDO. They demonstrated a linear relationship between monomer con-

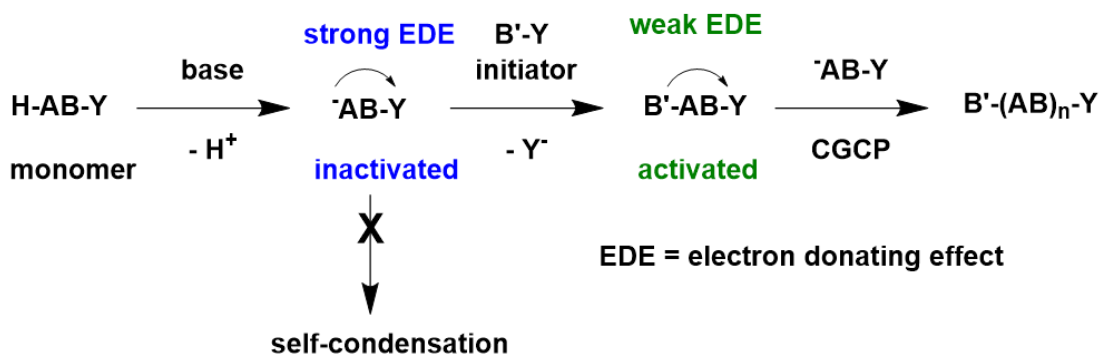
version and molecular weight, with the final polymers having low to moderate molecular weight distributions ( $D_{\text{SEC}} = 1.2 - 1.5$ ).<sup>148,149</sup> Several CKAs have been polymerised with ATRP, for example 2-methylene-4-phenyl-1,3-dioxolane.<sup>150</sup> An early example of RAFT polymerisation was provided by the same group for the RROP of BMDO, furnishing polyesters with varying dispersity values ( $D_{\text{SEC}} = 1.29 - 1.76$ ).<sup>151</sup> More recently, Hedir *et al.* used MADIX to copolymerise MDO with vinyl acetates.<sup>152-157</sup> When vinyl chloroacetate was used, selective hydrolysis of the acetate furnished a degradable poly(vinyl alcohol), which demonstrated ice recrystallisation inhibition for copolymers containing up to 24 % MDO.<sup>157</sup> Furthermore, when a block copolymer was synthesised using *N*-vinylpyrrolidone as the hydrophilic component and a copolymer of MDO and VAc as the hydrophobic block, well-defined, degradable micelles were obtained.<sup>155</sup>

## 1.6. Chain-growth condensation polymerisation

Conventional condensation polymerisation (Section 1.3) benefits from the wide range of monomers that can be used, but suffers from poor control over the reaction, whereas the controlled aspects of (radical) ROP can only be applied to suitable monomers. Chain-growth condensation polymerisation (CGCP) combines these techniques to provide a condensation polymerisation strategy with the control of chain-growth polymerisations. The key element is the use of A-B type polycondensation monomers that do not undergo self-condensation, but only undergo polycondensation in the presence of an activating initiator. This can be controlled through substituent effects, catalyst transfer and phase transfer catalysts. Although primarily used for the synthesis of polyamides and conjugated polymers, there are a few examples of polyesters synthesised by CGCP. This number is limited as a result of monomers being able to cause transesterification of the polymer backbone and so far has only been used for aromatic polyesters.<sup>158-162</sup>

CGCP via the substituent effect takes place via deprotonation of the H-AB-Y monomer to form the  $\bar{\text{A}}\text{B-Y}$  anion, which is unable to self-condense as a result of a strong electron donating effect (EDE) of the anion onto the Y chain end (Scheme 1.9). Addi-

tion of a B'-Y type initiator without a reaction-limiting EDE, can then initiate the reaction and form B'-AB-A. This product can then propagate with additional  $\text{AB-Y}^-$  monomer anions to form a well-defined B'-(AB)<sub>n</sub>-Y polymer.<sup>162</sup>

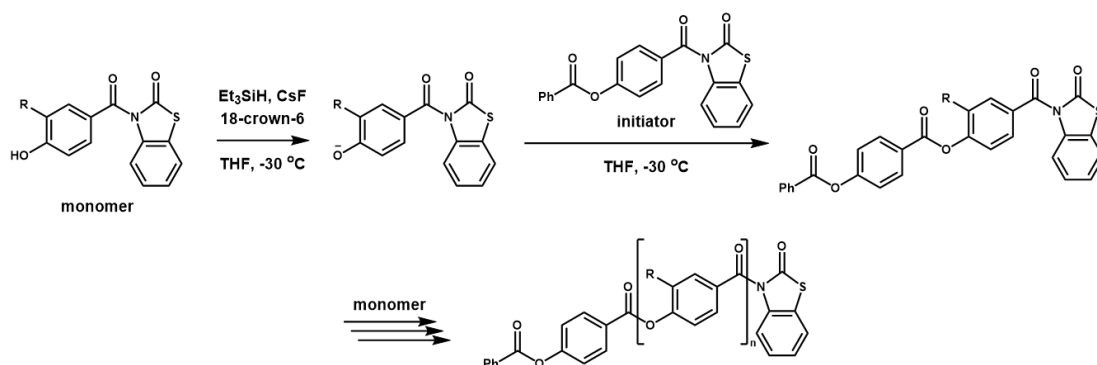


**Scheme 1.9** Schematic of chain-growth condensation polymerisation *via* substituent effects. Adapted from ref. 162.

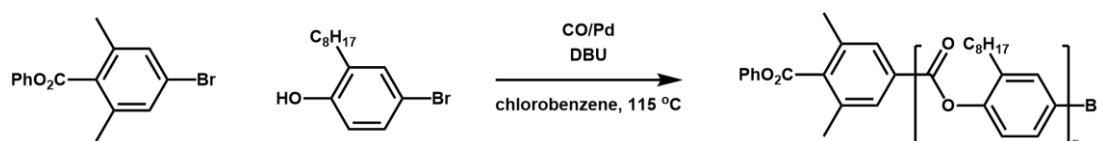
Yokozawa and co-workers used this strategy for the synthesis of a poly(4-hydroxy-3-R-benzoate)s, with R being either an *n*-octyl or a 4,7-dioxaoctyl group. In an initial optimisation study on the octyl-bearing monomer, they obtained well-controlled polyesters *via* CGCP, but only short chain lengths (DP = 5) after which transesterification became a significant problem.<sup>163</sup> In order to enable the synthesis of higher DP polyesters, they changed the base from *N,N*-diisopropylethylamine to a mixture of triethylsilane, caesium fluoride and 18-crown-6 and performed the reactions at -30 °C in THF (Scheme 1.10). This allowed for the synthesis of homopolymers up to DP 30, as well as chain extensions with the same monomer or a different monomer to produce block copolymers.<sup>164</sup>

The same group also investigated the palladium(II)-catalysed polycondensation of 4-bromophenols with carbon monoxide. Following a series of model<sup>165</sup> and optimisation studies due to polymer precipitation and side reactions during the polymerisation, a suitable monomer, 4-bromo-2-octylphenol, was identified. In the presence of 4-bromo-1,6-dimethylphenylbenzoate as initiator and DBU as base in chlorobenzene at 115 °C, they were able to polymerise this monomer in a controlled fashion into short

oligomers (Scheme 1.11). At prolonged reaction times, the molecular weights observed by SEC analysis decreased, suggesting ester exchange reactions in the polymer backbone, which is a typical problem for the synthesis of polyesters by CGCP.<sup>166</sup>

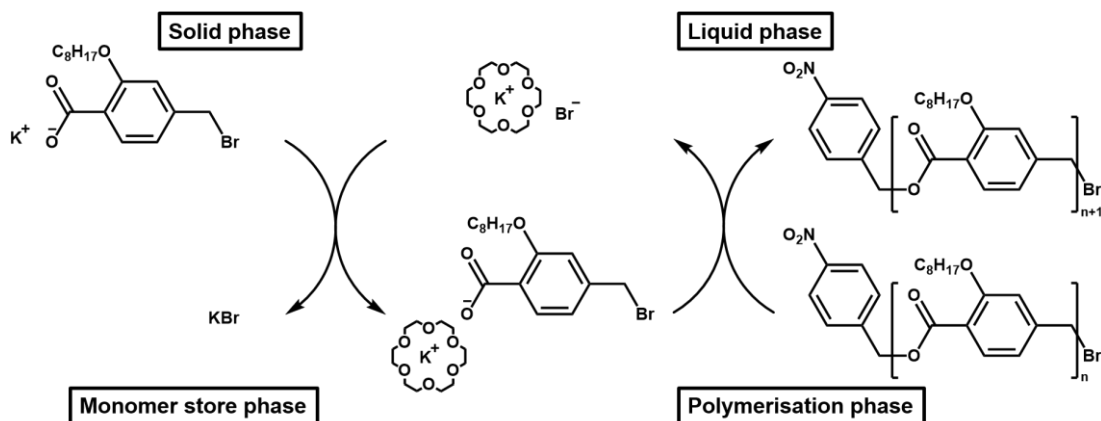


**Scheme 1.10** Synthesis of poly(4-hydroxybenzoate)s by CGCP, using triethylsilane, caesium fluoride and 18-crown-6 as base system. R = octyl or 4,7-dioxaoctyl. Reproduced from ref. 164.



**Scheme 1.11** Synthesis of poly(4-bromo-2-octylphenol) by palladium(II)-catalysed CO copolymerisation with 4-bromo-2-octylphenol by CGCP. Adapted from ref. 166.

Phase-transfer catalysis is another version of CGCP, in which the monomers are dispersed in an organic solvent which should prevent self-condensation. By introducing a phase-transfer catalyst (PTC) a fraction of the monomers is rendered soluble and available for polymerisation. Yokozawa and co-workers investigated this method for the polymerisation of potassium 4-bromomethyl-2-octyloxybenzoate in acetone, employing 18-crown-6 as PTC and 4-nitrobenzyl bromide as initiator (Scheme 1.12). They found that that an equimolar amount of PTC to initiator resulted in the narrowest molecular weight distributions ( $D_{SEC} = 1.36$ ). Kinetic studies demonstrated the chain growth nature of this polymerisation, which was tested up to DP 15.<sup>167</sup> In a follow-up study they evaluated ammonium salts as PTC and managed to further narrow the molecular weight distribution under optimised conditions ( $D_{SEC} = 1.21$ , 0.5 equiv. of tetrabutylammonium iodide to initiator).<sup>168</sup>



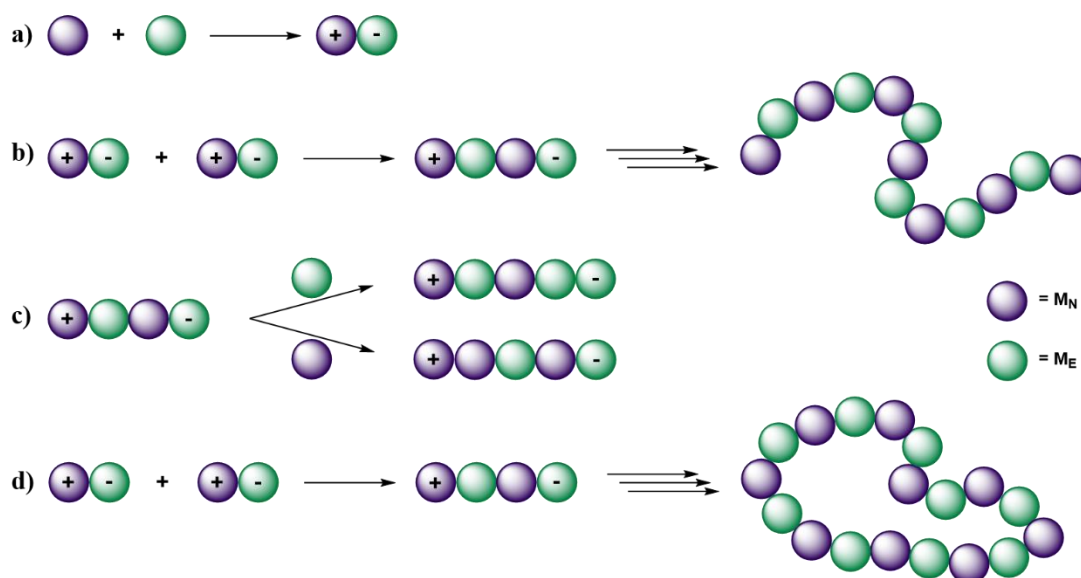
**Scheme 1.12** Polymerisation of 4-bromomethyl-2-octyloxybenzoate via phase transfer catalysis. Reproduced from ref. 167.

As previously mentioned, CGCP has mainly been used for the synthesis of polyamides and conjugated systems. The main drawback of CGCP in polyester synthesis comes from transesterification reactions, which have so far prevented the synthesis of high molecular weight polymers *via* this method. Furthermore, although derived from classical polycondensation chemistry, the monomers have to be modified in order to introduce the control associated with chain growth polymerisation and consequently this has limited CGCP to a small group of aromatic polyesters. However, the concept has proven to be an interesting alternative and further exploration of CGCP might lead to a wider applicability of the technique.

## 1.7. Spontaneous zwitterionic copolymerisation

The spontaneous zwitterionic copolymerisation (SZWIP) of nucleophilic ( $M_N$ ) and electrophilic monomers ( $M_E$ ) is a relatively unknown technique for the synthesis of a wide range of polymers, including polyesters, poly(aminoester)s and polyphosphoesters, amongst others. The technique was pioneered by Saegusa and co-workers following their initial example of the SZWIP of 2-oxazoline (HOx) with  $\beta$ -propiolactone in 1972.<sup>169</sup> Scheme 1.13 shows a general schematic for SZWIP. The first step involves a Michael addition between the  $M_N$  and  $M_E$  to form a zwitterionic species, commonly referred to as the *genetic zwitterion*. These genetic zwitterions can then propagate in a polyaddition type fashion to produce alternating copolymers. This will occur if the dipole-dipole interactions between the  $M_N$  and  $M_E$  to form the genetic zwitterion is

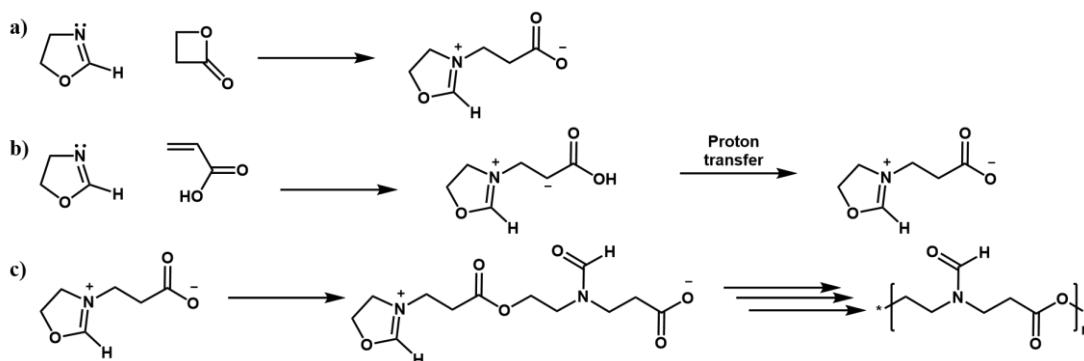
favoured over ion-dipole interactions between zwitterions and unreacted monomers. When the ion-dipole interactions become more significant, homopropagation of the  $M_N$  or  $M_E$  can take place, leading to non-alternating structures. If the ion-dipole interactions are very significant, it is possible for one monomer to effectively become the initiator for the homopolymerisation of the other. Finally, it is possible to form cyclic structures, although there is no evidence in literature that this takes place.<sup>170,171</sup>



**Scheme 1.13** General mechanism for SZWIP. a) Michael addition between  $M_N$  and  $M_E$  forms the genetic zwitterion. b) Propagation into oligomers and polymers. c) Homopropagation of  $M_N$  and  $M_E$  to produce non-alternating structures. d) Propagation followed by cyclisation.

As mentioned above, much of the pioneering work on SZWIP was done by Saegusa and co-workers. In 1972 they reported the SZWIP between 2-oxazoline (HOx) and  $\beta$ -propiolactone (BPL).<sup>169</sup> The genetic zwitterion formed by the Michael addition of the two monomers consists of an oxazolinium ring and a carboxylate group (Scheme 1.14a). Propagation takes place through ring-opening of the oxazolinium ring by the carboxylate of another genetic zwitterion and produces a *N*-formylated poly(aminoester) (Scheme 1.14c). However, this reaction suffers from (significant) homopropagation of BPL under most reaction conditions, producing non-alternating copolymers. In 1974 the same group reported on the SZWIP of HOx with acrylic acid (AA). After Michael addition a genetic zwitterion containing a carbanion is formed, which quickly

rearranges *via* a proton transfer to form the same genetic zwitterion as HOx with BPL (Scheme 1.14b). Interestingly, no homopropagation of AA was observed, thereby forming *N*-formylated poly(aminoester)s that only have homopropagation of HOx under some reaction conditions.<sup>172</sup>



**Scheme 1.14** SZWIP of HOx with BPL and AA. a) Formation of the genetic zwitterion between HOx and BPL. b) Formation of the genetic zwitterion between HOx and AA. c) Propagation of the genetic zwitterion to form a *N*-formylated poly(aminoester).

The monomers evaluated for SZWIP can most easily be classified by the  $M_N$  used: cyclic imino ethers (CIEs), such as 2-oxazolines (Ox), dioxaphospholanes (which lead to poly(phosphoester)s), aziridines and miscellaneous monomers. In this section only monomer pairs that lead to polyesters, poly(aminoester)s (PAEs) and poly(ester amide)s (PEAs) will be discussed.

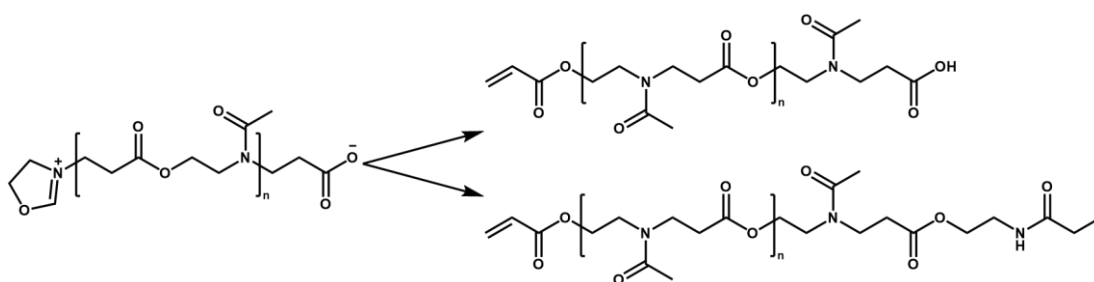
### 1.7.1. SZWIP of cyclic imino ethers

The largest class of SZWIP copolymers constitutes those synthesised from cyclic imino ethers (CIEs), a versatile monomer class that can be polymerised via chain and step growth polymerisations.<sup>173–176</sup> In the context of SZWIP, Ox and 2-oxazines (Oz) have been extensively studied in combination with (meth)acrylate co-monomers.

Most of the initial studies not only focused on identifying new monomers that can partake in the SZWIP reaction, but also investigated the effect of reaction conditions on the resulting polymers, with a particular focus being placed on the alternating nature of the copolymers. Dipolar aprotic solvents, in particular acetonitrile and *N,N*-dimethylformamide (DMF), not only enhanced an alternating copolymerisation, but also

increased the yields of the polymers after purification. Various reaction temperatures, typically ranging from 40 to 80 °C, but sometimes as high as 130 °C, have been evaluated, but no significant effect of the reaction temperature on the resulting products was identified when comparing a range of different co-monomer systems. The monomer sequence in the polymers is also dependent on the monomers employed (their relative reactivities and ability to homopolymerise) and therefore a range of stoichiometries has often been evaluated, with equimolar feed ratios typically yielding a more equimolar incorporation of the two monomers in the copolymer (as determined by NMR and elemental analysis) as well as higher yields after purification. Although these initial optimisation studies from Saegusa and co-workers provide a useful starting point,<sup>169,172,177,178</sup> the optimal conditions will vary from monomer combination to monomer combination and therefore a screening of polymerisation conditions for each new monomer combination is recommended to optimise their SZWIP reaction.

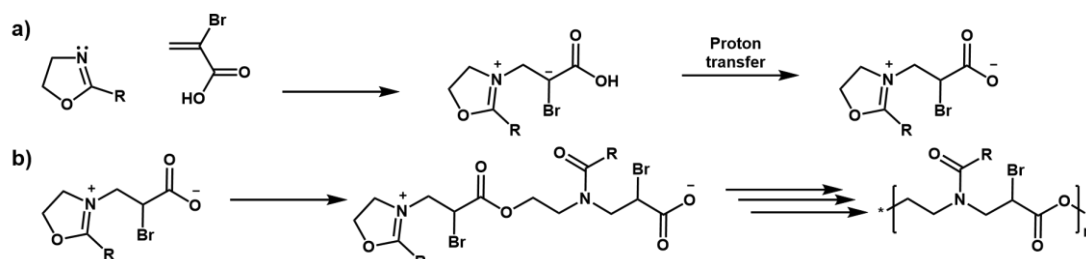
It was reported by Odian and Gunatillake that one termination mechanism for the SZWIP of Ox/Oz and (meth)acrylic acid results in the introduction of an  $\alpha$ -(meth)acrylic end group. They also discussed the introduction of two possible  $\omega$ -end groups, carboxylic acids or amides, but only investigated this qualitatively (Scheme 1.15).<sup>179</sup>



**Scheme 1.15** SZWIP between CIEs and AA leads to the introduction of  $\alpha$ -acrylate groups and carboxylic acid and amide  $\omega$ -end groups. Adapted from ref. 179.

SZWIP between CIEs and other (meth)acrylate monomer systems follow mechanisms similar to that in Scheme 1.14. For 2-hydroxyethyl acrylate (HEA) the transferred proton originates from the hydroxyl group, leading to the formation of poly(aminoester ether)s.<sup>180</sup> The structurally related 2-bromoacrylic acid was polymerised in an alternating fashion with MeOx and EtOx if an equimolar feed ratio is employed, providing

a *N*-acylated poly(aminoester) (NPAE) with a pendant bromine group that can facilitate straightforward post-polymerisation functionalisation (Scheme 1.16).<sup>181</sup>



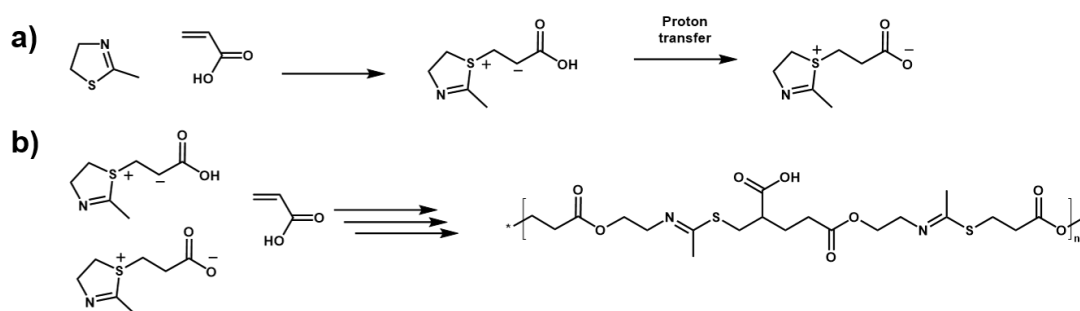
**Scheme 1.16** SZWIP of Ox with 2-bromoacrylic acid leads to *N*-acylated poly(amino ester)s with pendant bromine groups. Adapted from ref. 181.

The SZWIP is not limited to acrylate monomers but can also take place with methacrylates. Balakrishnan and Periyasamy reported the SZWIP of MeOx and methacrylic acid (MAA) whereby they claimed that a NPAE is formed in alternating fashion.<sup>182</sup> This was challenged by Odian and co-workers who repeated the reactions and reported different results. Not only did they obtain significantly lower yields, but they also found after separation of the products by preparative HPLC and subsequent NMR analysis of the fractions, that many by-products were formed that deviated from an ideal alternating structure as a result of homopropagation of the MeOx monomer. The generally lower molecular weights obtained from the SZWIP of MeOx/MAA compared to MeOx/AA is attributed to the lower acidity of MAA compared to AA.<sup>183</sup> The only other report on the use of a methacrylic monomer (phenyl methacrylate) was from Kadokawa *et al.* who copolymerised it with MeOx and 2-phenyl-2-oxazoline (PhOx).<sup>184</sup> For both Ox homopropagation was observed (PhOx > MeOx) and low molecular weights (< 1500 Da) were obtained, which is in line with the observations of Odian and co-workers.

Moreover, these reactions are not only limited to CIEs with an endocyclic imine, such as Ox, but also are applicable to exocyclic imines, which increases its potential. The SZWIP of 2-benzyliminotetrahydrofuran with BPL or AA produces alternating copolymers, but interestingly the exocyclic imine yields poly(ester amide)s instead of poly(aminoester)s.<sup>177</sup> Unsubstituted and 4-methyl substituted 5-oxazolone have been copolymerised with AAm and HEA to furnish poly(amino imide)s and *N*-formylated

poly(aminoester)s, respectively,<sup>185</sup> and cyclohexane-2-oxazoline (*cis*- and *trans*-CHOx) has been copolymerised with AA and HEA to yield poly(aminoester)s and poly(aminoester ether)s.<sup>186</sup> Only *cis*-CHOx with HEA did not yield alternating copolymers, but a HEA based poly(ester ether) homopolymer initiated by *cis*-CHOx instead. Phenyl cinnamate and methylhydrogenitaconate have been copolymerised with Ox as more exotic monomers based on the acrylate functionality, whereby only the latter results in degradable polymers and neither has an alternating structure.<sup>184,187</sup> NPAEs with additional methyl esters in the side chains were obtained by SZWIP of MeOx with methyl maleate.<sup>188</sup>

A rather remarkable example was reported by Rivas and co-workers who investigated the SZWIP of 2-methyl-2-thiazoline (MTIA) with AA.<sup>189</sup> Unlike other Ox-type M<sub>N</sub>, MTIA forms the genetic zwitterion via its sulphur atom instead of its nitrogen (Scheme 1.17).

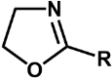
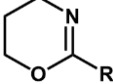
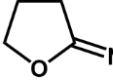
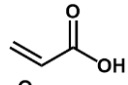
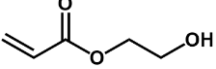
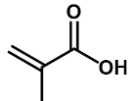
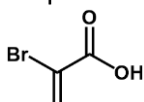
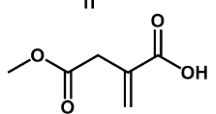
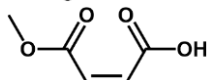


**Scheme 1.17** SZWIP of 2-methyl-2-thiazoline with AA. a) Initiation by formation of the carbanion and subsequent proton transfer. b) Propagation of both the carbanion and genetic zwitterion with AA to form a poly(ester imino thioether) with pendant carboxylic acid groups.

Detailed <sup>13</sup>C NMR analysis revealed that the genetic zwitterion reacts through both the carbanion (before proton transfer) and the carboxylate anion (after proton transfer), effectively having two propagation sites. Regardless of the monomer feed ratios, all copolymers obtained were rich in AA, which is attributed to the carbanion intermediate being able to homopolymerise AA. The authors reasoned that different ion-dipole interactions in this system compared to Ox/AA allowed for this homopropagation *via* two reaction sites, although this is the only example in literature where this behaviour

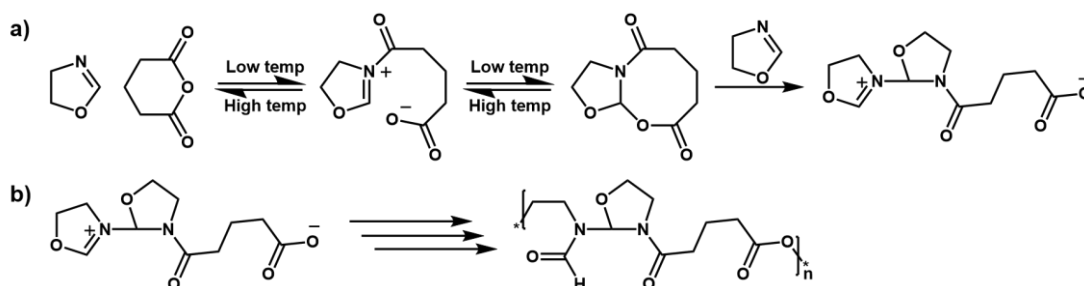
is observed in a SZWIP reaction. The resulting copolymer can be considered a poly(ester imino thioether) which has pendent carboxylic acid groups and can be degraded via its ester and imine bonds.

**Table 1.2** Monomer pairs for the synthesis of polyesters by SZWIP of CIEs with (meth)acrylate type ME.

Entry	ME			
1		R=H, <sup>172</sup> Me, <sup>172,179</sup> Et <sup>190</sup>	R=H, <sup>191</sup> Me, <sup>191</sup> Ph <sup>191</sup>	R=Bn <sup>177</sup>
2		R=Me <sup>180</sup>	R=H <sup>180</sup>	
3		R=Me <sup>182,183</sup>		
4		R=Me, <sup>181</sup> Et <sup>181</sup>		
5		R=Me <sup>187</sup>		
6		R=Me <sup>188</sup>		

The SZWIP of Ox and Oz extends further than only (meth)acrylates. Cyclic anhydrides are a well-explored class of M<sub>E</sub> that have been copolymerised with Ox and Oz. Copolymerisations between MeOx, EtOx and PhOx with succinic (SAn), glutaric (GAn) and phthalic anhydride (PhAn) yield poly(ester amide)s. Under diverse reaction conditions homopropagation of the CIE can be observed, providing poly(aminoester amide)s, but at equimolar monomer feed ratios alternating poly(ester amide)s are obtained.<sup>192–195</sup> Interestingly, Kobayashi *et al.* reported that SZWIP of HOx and unsubstituted Oz (HOz) with SAn and GAn resulted in the formation of M<sub>N</sub>:M<sub>E</sub> 2:1 sequence controlled copolymers, independent of the monomer feed ratios and reaction conditions employed. They explained this by the formation of a bicyclic intermediate between the M<sub>N</sub> and M<sub>E</sub>, as shown in Scheme 1.18, prior to ring opening of that intermediate by a second M<sub>N</sub> to yield the genetic zwitterion. This genetic zwitterion can then react as

previously described for Ox/AA type genetic zwitterions. Their hypothesis was confirmed by reaction of Ox and GAn at 0 °C, which led to the formation of the bicyclic intermediate which could be successfully isolated and characterised. The first step is reversible and temperature controlled. Upon heating the bicyclic intermediate, the 2:1 copolymer could be obtained.<sup>196</sup>



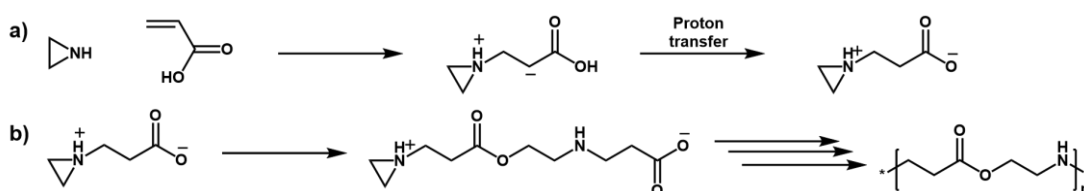
**Scheme 1.18** SZWIP of HOx and glutaric anhydride (GAn). a) Reaction between HOx and GAn at low temperatures leads to a bicyclic intermediate, which after reaction with another HOx monomer forms an A<sub>2</sub>B type genetic zwitterion. b) Propagation of this genetic zwitterion produces an A<sub>2</sub>B type N-formylated poly(amino amido ester). Adapted from ref. 196.

**Table 1.3** Monomer pairs for SZWIP of CIEs with lactones and cyclic anhydrides.

Entry	ME			
1		R=H <sup>169,197</sup>	R=H, <sup>191</sup> Me, <sup>191</sup> Ph <sup>191</sup>	R=Bn <sup>177</sup>
2		R,R'=Me, R''=H <sup>198</sup> R=Et, R'=Me, R''=H <sup>199</sup>		
3		R=H, <sup>170,196</sup> Me, <sup>192</sup> Ph <sup>193</sup>		
4		R=H <sup>196</sup>	R=H <sup>196</sup>	
5		R=Me, <sup>200</sup> Et, <sup>201</sup> Ph <sup>193</sup>		
6		R=Me, <sup>194</sup> Et, <sup>195</sup> Ph <sup>193</sup>		

### 1.7.2. SZWIP of aziridines

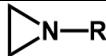
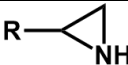
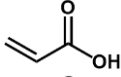
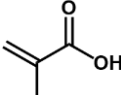
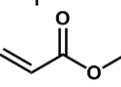
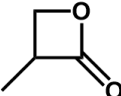
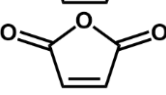
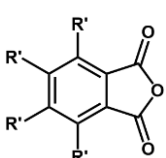
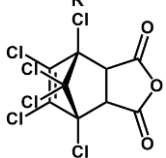
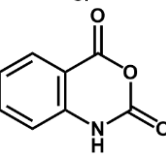
Aziridines (Azs) are the second class of  $M_N$  that have been investigated in the context of polyester-type materials by SZWIP. Unsubstituted Az (HAz) was the very first  $M_N$  to be used in a SZWIP reaction with carbonyl sulphide (SCO) as  $M_E$  by Yokota and Kondo, although they questioned their own results and put their own results down to potential catalytic impurities in the monomers.<sup>202</sup> Several years later Takahashi copolymerised HAz with AA and MAA to obtain poly(aminoester)s,<sup>203</sup> and with a broad range of cyclic anhydrides to yield alternating poly(ester amide)s.<sup>204</sup> The mechanism for Azs is similar to that for CIEs. The Az nitrogen can undergo a Michael addition with AA followed by a proton transfer to generate a comparable genetic zwitterion. The carboxylate can ring-open another genetic zwitterion and propagate to form higher molecular weight oligomers and polymers (Scheme 1.19).<sup>203</sup>



**Scheme 1.19** SZWIP of aziridine and AA. a) Initiation takes place by Michael addition of the aziridine to AA to form the genetic zwitterion. b) Propagation leads to a poly(aminoester). Adapted from ref. 203.

A significant amount of work on the SZWIP of Azs was performed by Rivas, Canessa and Pooley. They demonstrated that *N*-alkylated poly(aminoester)s could be obtained by SZWIP of 2-methylaziridine (MeAz) with AA and MAA. An equimolar feed ratio of the monomers was identified as the key to obtaining alternating structures.<sup>205</sup> Several Azs have also been copolymerised with a range of cyclic anhydrides<sup>200,204,206–212</sup> as well as 3-methyl- $\beta$ -propiolactone (MBPL), as shown in Table 1.4.<sup>213,214</sup> Interesting to note is the use of *N*-acetylaziridine which after copolymerisation with maleic anhydride produces the same polymer as the SZWIP of MeOx with maleic anhydride.<sup>200</sup> Furthermore, there is one example of an azetidines, the four-membered ring equivalent of Az, that has been copolymerised via SZWIP: 1,3,3-trimethylazetidines was successfully copolymerised with AA into an alternating structure.<sup>215</sup>

**Table 1.4** Monomer pairs for SZWIP of aziridines.

Entry	M <sub>E</sub>			
1		R=H, <sup>203</sup> Me <sup>205</sup>		215
2		R=H <sup>203,205</sup>		
3		R=H <sup>216</sup>		
4		R=H, <sup>214</sup> EtOH <sup>213</sup>		
5		R=H, <sup>204,209</sup> EtOH <sup>206</sup>		
6		R=H, <sup>204,211</sup> EtOH, <sup>208</sup> tBu, <sup>212</sup> Ac <sup>200</sup>		
7		R=H, R'=H, <sup>204,210</sup> R'=Br, <sup>204</sup> R'=Cl <sup>204</sup>	R=H or Me, R'=H <sup>210</sup>	
8		R=H <sup>204</sup>		
9		R=EtOH <sup>207</sup>		
10	S=C=O	R=H <sup>202</sup>		

## 1.8. Miscellaneous strategies

In addition to the five main strategies discussed in the previous sections, there are several miscellaneous strategies that have been employed for the synthesis of polyester-based materials. This section provides a few selected examples to illustrate some promising alternative strategies.

Wilsens *et al.* synthesised a bis(2-oxazoline) monomer from 2,5-furandicarboxylic acid in a three-step process and subsequently reacted it with sebacic acid in a melt polymerisation process to form a PEA. They observed that the amide nitrogen in the resulting PEA was able to react with other oxazoline moieties to generate branched

structures, which could be catalysed by addition of triphenylphosphite and/or an increase in reaction temperature.<sup>217</sup>

Another strategy involves the aza-Michael addition between amines and diacrylates to produce *N*-substituted poly(aminoester)s. This method has been investigated by the Langer group to generate a library of materials for binding DNA.<sup>218–220</sup> Zhou *et al.* explored this chemistry to synthesise hyperbranched PAEs with dual-responsiveness (temperature and pH) that demonstrated selective binding behaviour to HeLa.<sup>221</sup>

One last method worth discussing is the synthesis of polyesters, specifically poly(hydroxy alkanate)s (PHAs), *via* microbial fermentation, which is used on industrial scale for the production of bioplastics.<sup>222</sup> Organic waste is digested to CO<sub>2</sub> and/or methane and subsequently converted in PHA precursors.<sup>223</sup> Biotic polymerisation then produces intracellular PHAs that can be used after extraction from the microorganisms. However, the lack of control and the need to extract the PHAs from the bacteria are the main drawbacks for this process.<sup>224</sup>

## 1.9. Conclusions

The development of (bio)degradable materials, in particular polyester-based materials from renewable monomers, has received significant attention over the last decades as an alternative to current, fossil-fuel derived polymers. Several strategies have been developed that allow the synthesis of these materials, all accompanied with their own advantages and disadvantages. This section summarises the various synthetic strategies and discusses their potential.

The direct polycondensation has been, and still is, the most popular technique for producing polyesters and related polymers as a result of the readily available monomers and simple chemistry. However, the lack of control over the reaction leads to broad molecular weight distributions, and high temperatures and/or vacuum are required for the synthesis of high molecular weight materials. Its main competitor, especially on laboratory scale, is ROP. In contrast to polycondensation, it offers significantly better control over the molecular weight of the polymers and their end groups and good control through the use of catalysts. The monomer scope is mostly limited to 4, 6 and 7-membered rings as a result of the polymerisation thermodynamics. Moreover, the

range of monomers that can be derived from renewable resources is lower than for polycondensation monomers and the introduction of additional functionalities is more challenging. RROP benefits from the possibilities offered by controlled radical polymerisation techniques, but the requirements for the monomer synthesis make the introduction of additional functionalities difficult. Furthermore, the reactivity differences between RROP monomers and common vinyl monomers differs significantly, which is a problem for their direct copolymerisation. DFT calculations have recently been shown to be a potential solution for this problem. CGCP is an interesting technique that attempts to combine the control of ROP with the monomer scope of polycondensation, but in the context of polyester synthesis suffers from transesterification reactions that limit the production of high molecular weight materials. SZWIP is a relatively unknown technique that allows the (alternating) copolymerisation of compatible nucleophilic and electrophilic monomers into a broad range of polymers, including polyesters, PEAs and PAEs. Despite the synthetic versatility and potential to access a wide range of functional and degradable polymers, this method has received limited attention, mainly as a result of the typically low molecular weight polymers obtained by this technique. Finally, there are several miscellaneous strategies of which microbial fermentation is the most interesting one when considering bio-renewable, cradle-to-cradle processes.

In conclusion, a large range of synthetic techniques for the synthesis of polyesters and related materials is available that all come with their own advantages and disadvantages, which ultimately dictate their synthetic and industrial applicability. Further investigation of these synthetic strategies and overcoming their current challenges will broaden the scope of their applicability in the future.

## 1.10. References

- 1 M. Okada, *Prog. Polym. Sci.*, 2002, **27**, 87–133.
- 2 S. Doppalapudi, A. Jain, W. Khan and A. J. Domb, *Polym. Adv. Technol.*, 2014, **25**, 427–435.
- 3 A. Díaz, R. Katsarava and J. Puiggalí, *Int. J. Mol. Sci.*, 2014, **15**, 7064–7123.
- 4 S. Kobayashi, *Polym. Adv. Technol.*, 2015, **26**, 677–686.

- 
- 5 R. J. Pounder and A. P. Dove, *Polym. Chem.*, 2010, **1**, 260.
- 6 W. Amass, A. Amass and B. Tighe, *Polym. Int.*, 1998, **47**, 89–144.
- 7 A. Tardy, J. Nicolas, D. Gigmes, C. Lefay and Y. Guillaneuf, *Chem. Rev.*, 2017, **117**, 1319–1406.
- 8 S. Agarwal, *Polym. Chem.*, 2010, **1**, 953–964.
- 9 V. Delplace and J. Nicolas, *Nat. Chem.*, 2015, **7**, 771–784.
- 10 Q. Yin, L. Yin, H. Wang and J. Cheng, *Acc. Chem. Res.*, 2015, **48**, 1777–1787.
- 11 Y. Yu, J. Zou and C. Cheng, *Polym. Chem.*, 2014, **5**, 5854–5872.
- 12 M. Labet and W. Thielemans, *Chem. Soc. Rev.*, 2009, **38**, 3484.
- 13 C. K. Williams, *Chem. Soc. Rev.*, 2007, **36**, 1573–1580.
- 14 J. Heller, J. Barr, S. Y. Ng, K. S. Abdellauoi and R. Gurny, *Adv. Drug Deliv. Rev.*, 2002, **54**, 1015–1039.
- 15 T. Steinbach and F. R. Wurm, *Angew. Chem. Int. Ed.*, 2015, **54**, 6098–6108.
- 16 S. Tempelaar, L. Mespouille, O. Coulembier, P. Dubois and A. P. Dove, *Chem. Soc. Rev.*, 2013, **42**, 1312–1336.
- 17 S. Paul, Y. Zhu, C. Romain, R. Brooks, P. K. Saini and C. K. Williams, *Chem. Commun.*, 2015, **51**, 6459–6479.
- 18 J. Xu, E. Feng and J. Song, *J. Appl. Polym. Sci.*, 2014, **131**, 39822.
- 19 K. L. Poetz and D. A. Shipp, *Aust. J. Chem.*, 2016, **69**, 1223–1239.
- 20 J. O. Akindoyo, M. D. H. Beg, S. Ghazali, M. R. Islam, N. Jeyaratnam and A. R. Yuvaraj, *RSC Adv.*, 2016, **6**, 114453–114482.
- 21 G. Rokicki, P. G. Parzuchowski and M. Mazurek, *Polym. Adv. Technol.*, 2015, **26**, 707–761.
- 22 M. Gleria and R. De Jaeger, *Top. Curr. Chem.*, 2005, **250**, 165–251.
- 23 I. Teasdale and O. Brüggemann, *Polymers*, 2013, **5**, 161–187.
- 24 S. Rothmund and I. Teasdale, *Chem. Soc. Rev.*, 2016, **45**, 5200–5215.
- 25 S. Maude, L. R. Tai, R. P. W. Davies, B. Liu, S. A. Harris, P. J. Kocienski and A. Aggeli, *Top. Curr. Chem.*, 2012, **310**, 27–70.
- 26 J. M. Palomo, *RSC Adv.*, 2014, **4**, 32658–32672.
- 27 H. R. Kricheldorf, *Angew. Chem. Int. Ed.*, 2006, **45**, 5752–5784.
- 28 A. Rodriguez-Galan, L. Franco and J. Puiggali, *Polymers*, 2011, **3**, 65–99.
-

- 
- 29 A. C. Fonseca, M. H. Gil and P. N. Simões, *Prog. Polym. Sci.*, 2014, **39**, 1291–1311.
- 30 M. Winnacker and B. Rieger, *Polym. Chem.*, 2016, **7**, 7039–7046.
- 31 W. H. Carothers, *Chem. Rev.*, 1931, **8**, 353–426.
- 32 P. J. Flory, *Chem. Rev.*, 1946, **39**, 137–197.
- 33 O. Nuyken and S. D. Pask, *Polymers*, 2013, **5**, 361–403.
- 34 G. Odian, in *Principles of Polymerization*, John Wiley & Sons, Inc., Fourth edi., 2014, pp. 1–38.
- 35 J. Gay-Lussac and J. Pelouze, *Ann. Pharm.*, 1833, **7**, 40–44.
- 36 A. Baeyer, *Ber. Dtsch. Chem. Ges.*, 1872, 1094–1100.
- 37 L. H. Baekeland, *Ind. Eng. Chem.*, 1909, **1**, 545–549.
- 38 A. J. Ragauskas, C. K. Williams, B. H. Davison, G. Britovsek, J. Cairney, C. A. Eckert, W. J. F. Jr, J. P. Hallett, D. J. Leak, C. L. Liotta, J. R. Mielenz, R. Murphy, R. Templer and T. Tschaplinski, *Science*, 2006, **311**, 484–489.
- 39 H. Kobayashi and A. Fukuoka, *Green Chem.*, 2013, **15**, 1740–1763.
- 40 R. T. Mathers, *J. Polym. Sci. A Polym. Chem.*, 2012, **50**, 1–15.
- 41 K. Yao and C. Tang, *Macromolecules*, 2013, **46**, 1689–1712.
- 42 C. Vilela, A. F. Sousa, A. C. Fonseca, A. C. Serra, J. F. J. Coelho, C. S. R. Freire and A. J. D. Silvestre, *Polym. Chem.*, 2014, **5**, 3119–3141.
- 43 J. A. Galbis, M. de Gracia García-Martin, M. Violante de Paz and E. Galbis, *Chem. Rev.*, 2016, **116**, 1600–1636.
- 44 Q. Liu, Y. Liao, T. Wang, C. Cai, Q. Zhang, N. Tsubaki and L. Ma, *Ind. Eng. Chem. Res.*, 2014, **53**, 12655–12664.
- 45 A. Gandini, *Polym. Chem.*, 2010, **1**, 245–251.
- 46 A. Gandini and T. M. Lacerda, *Prog. Polym. Sci.*, 2015, **48**, 1–39.
- 47 A. Gandini, T. M. Lacerda, A. J. F. Carvalho and E. Trovatti, *Chem. Rev.*, 2016, **116**, 1637–1669.
- 48 A. F. Sousa, C. Vilela, A. C. Fonseca, M. Matos, C. S. R. Freire, G.-J. M. Gruter, J. F. J. Coelho and A. J. D. Silvestre, *Polym. Chem.*, 2015, **6**, 5961–5983.
- 49 A. Gandini and M. N. Belgachem, *Prog. Polym. Sci.*, 1997, **22**, 1203–1379.
- 50 W. Khan, S. Muthupandian, S. Farah, N. Kumar and A. J. Domb, *Macromol.*
-

- Biosci.*, 2011, **11**, 1625–1636.
- 51 N. Paredes, A. Rodriguez-Galan, J. Puiggali and C. Peraire, *J. Appl. Polym. Sci.*, 1998, **69**, 1537–1549.
- 52 X. Pang, J. U. N. Wu, C. Reinhart-king and C. Chu, *J. Polym. Sci. A Polym. Chem.*, 2010, **48**, 3758–3766.
- 53 W. H. Carothers, *Trans. Faraday Soc.*, 1936, **32**, 39–49.
- 54 P. J. Flory, *J. Am. Chem. Soc.*, 1941, **63**, 3083–3090.
- 55 P. J. Flory, *J. Am. Chem. Soc.*, 1941, **63**, 3091–3096.
- 56 P. J. Flory, *J. Am. Chem. Soc.*, 1941, **63**, 3096–3100.
- 57 W. H. Stockmayer, *J. Chem. Phys.*, 1943, **11**, 45–55.
- 58 W. H. Stockmayer, *J. Chem. Phys.*, 1944, **12**, 125–131.
- 59 J. Yang, S. Zhang, X. Liu and A. Cao, *Polym. Degrad. Stab.*, 2003, **81**, 1–7.
- 60 A. Takasu, Y. Iio, Y. Oishi, Y. Narukawa and T. Hirabayashi, *Macromolecules*, 2005, **38**, 1048–1050.
- 61 A. Takasu, T. Makino and S. Yamada, *Macromolecules*, 2010, **43**, 144–149.
- 62 N. Jacquel, F. Freyermouth, A. Rousseau, J. P. Pascault and P. Fuertes, *J. Polym. Sci. A Polym. Chem.*, 2011, **49**, 5301–5312.
- 63 A. Takasu, Y. Oishi, Y. Iio, Y. Inai and T. Hirabayashi, *Macromolecules*, 2003, **36**, 1772–1774.
- 64 M. Garaleh, M. Lahcini, H. R. Kricheldorf and S. M. Weidner, *J. Polym. Sci. A Polym. Chem.*, 2009, **47**, 170–177.
- 65 M. Sokolsky-Papkova, R. Langer and A. J. Domb, *Polym. Adv. Technol.*, 2011, **22**, 502–511.
- 66 F. Binns, P. Harffey, S. M. Roberts and A. Taylor, *J. Polym. Sci. A Polym. Chem.*, 1998, **36**, 2069–2080.
- 67 H. Uyama, K. Inada and S. Kobayashi, *Polym. J.*, 2000, **32**, 440–443.
- 68 R. A. Gross, M. Ganesh and W. Lu, *Trends Biotechnol.*, 2010, **28**, 435–443.
- 69 F. Binns, S. M. Roberts, A. Taylor and C. F. Williams, *J. Chem. Soc. Perkin Trans. 1*, 1993, **1**, 899–904.
- 70 Y. Linko, Z. Wang and J. Seppd, *J. Biotechnol.*, 1995, **40**, 133–140.
- 71 S. Kobayashi, H. Uyama and S. Namekawab, *Polym. Degrad. Stab.*, 1998, 195–201.

- 
- 72 X. Zhang, M. Fevre, G. O. Jones and R. M. Waymouth, *Chem. Rev.*, 2018, **118**, 839–885.
- 73 M. Dusselier, P. Van Wouwe, A. Dewaele, E. Makshina and B. F. Sels, *Energy Environ. Sci.*, 2013, **6**, 1415–1442.
- 74 Q. Meng, M. Hou, J. Song, H. Liu and B. Han, *Nat. Commun.*, 2017, **8**, 14190–14197.
- 75 D. Zhang, M. A. Hillmyer and W. B. Tolman, *Biomacromolecules*, 2005, **6**, 2091–2095.
- 76 G. Budroni and A. Corma, *J. Catal.*, 2008, **257**, 403–408.
- 77 T. R. Blake and R. M. Waymouth, *J. Am. Chem. Soc.*, 2014, **136**, 9252–9255.
- 78 G. L. Gregory, E. M. López-Vidal and A. Buchard, *Chem. Commun.*, 2017, **53**, 2198–2217.
- 79 B. M. Vaca and D. Bourissou, *ACS Macro Lett.*, 2015, **4**, 792–798.
- 80 N. Cohen-Arazi, J. Katzhendler, M. Kolitz and A. J. Domb, *Macromolecules*, 2008, **41**, 7259–7263.
- 81 A. Duda and A. Kowalski, in *Handbook of Ring-Opening Polymerization*, eds. P. Dubois, O. Coulembier and J.-M. Raquez, Wiley-VCH Verlag GmbH & Co. KGaA, 2009, pp. 1–51.
- 82 P. Olsén, K. Odelius and A. C. Albertsson, *Biomacromolecules*, 2016, **17**, 699–709.
- 83 M. Hong and E. Y. X. Chen, *Nat. Chem.*, 2016, **8**, 42–49.
- 84 I. van der Meulen, E. Gubbels, S. Huijser, C. E. Koning, A. Heise and R. Duchateau, *Macromolecules*, 2011, **44**, 4301–4305.
- 85 J. A. Wilson, S. A. Hopkins, P. M. Wright and A. P. Dove, *Polym. Chem.*, 2014, 2691–2694.
- 86 D. Myers, T. Witt, A. Cyriac, M. Bown, S. Mecking and C. K. Williams, *Polym. Chem.*, 2017, **8**, 5780–5785.
- 87 C. Bakewell, T.-P.-A. Cao, N. Long, X. F. Le, A. Au and C. K. Williams, *J. Am. Chem. Soc.*, 2012, **134**, 20577–20580.
- 88 H. Wang and H. Ma, *Chem. Commun.*, 2013, **49**, 8686–8688.
- 89 X. Wang, A. Thevenon, J. L. Brosmer, I. Yu, S. I. Khan, P. Mehrkhodavandi and P. L. Diaconescu, *J. Am. Chem. Soc.*, 2014, **136**, 11264–11267.
-

- 
- 90 C. Romain and C. K. Williams, *Angew. Chem. Int. Ed.*, 2014, **53**, 1607–1610.
- 91 N. E. Kamber, W. Jeong, R. M. Waymouth, R. C. Pratt, B. G. G. Lohmeijer and J. L. Hedrick, *Chem. Rev.*, 2007, **107**, 5813–5840.
- 92 M. K. Kiesewetter, E. J. Shin, J. L. Hedrick and R. M. Waymouth, *Macromolecules*, 2010, **43**, 2093–2107.
- 93 A. P. Dove, *ACS Macro Lett.*, 2012, **1**, 1409–1412.
- 94 W. Nzahou Ottou, H. Sardon, D. Mecerreyes, J. Vignolle and D. Taton, *Prog. Polym. Sci.*, 2016, **56**, 64–115.
- 95 F. Nederberg, E. F. Connor, M. Möller, T. Glauser and J. L. Hedrick, *Angew. Chem. Int. Ed.*, 2001, **40**, 2712–2715.
- 96 D. A. Culkin, W. Jeong, S. Csihony, E. D. Gomez, N. P. Balsara, J. L. Hedrick and R. M. Waymouth, *Angew. Chem. Int. Ed.*, 2007, **46**, 2627–2630.
- 97 H. A. Brown and R. M. Waymouth, *Acc. Chem. Res.*, 2013, **46**, 2585–2596.
- 98 E. J. Shin, H. A. Brown, S. Gonzalez, W. Jeong, J. L. Hedrick and R. M. Waymouth, *Angew. Chem. Int. Ed.*, 2011, **50**, 6388–6391.
- 99 A. P. Dove, R. C. Pratt, B. G. G. Lohmeijer, R. M. Waymouth, J. L. Hedrick and S. U. V, *J. Am. Chem. Soc.*, 2005, **127**, 13798–13799.
- 100 S. S. Spink, O. I. Kazakov, E. T. Kiesewetter and M. K. Kiesewetter, *Macromolecules*, 2015, **48**, 6127–6131.
- 101 K. V Fastnacht, S. S. Spink, N. U. Dharmaratne, J. U. Pothupitiya, P. P. Datta, E. T. Kiesewetter and M. K. Kiesewetter, *ACS Macro Lett.*, 2016, **5**, 982–986.
- 102 X. Zhang, G. O. Jones, J. L. Hedrick and R. M. Waymouth, *Nat. Chem.*, 2016, **8**, 1047–1053.
- 103 B. Lin and R. M. Waymouth, *J. Am. Chem. Soc.*, 2017, **139**, 1645–1652.
- 104 S. Naumann, A. W. Thomas and A. P. Dove, *ACS Macro Lett.*, 2016, **5**, 134–138.
- 105 S. M. McElvain and M. J. Curry, *J. Am. Chem. Soc.*, 1948, **70**, 3781–3786.
- 106 W. J. Bailey, Z. Ni and S.-R. Wu, *J. Polym. Sci. A Polym. Chem.*, 1982, **20**, 3021–3030.
- 107 A. B. Argade and B. R. Joglekar, *Synth. Commun.*, 1993, **23**, 1979–1984.
- 108 N. A. Petasis and S. P. Lu, *Tetrahedron Lett.*, 1995, **36**, 2393–2396.
- 109 W. J. Bailey, S. Wu and Z. Nib, *Macromol. Chem. Phys.*, 1982, **183**, 1913–
-

- 1920.
- 110 W. J. Bailey, S. R. Wu and Z. Ni, *J. Macromol. Sci. A Chem.*, 1982, **18**, 973–986.
- 111 S. Agarwal, *Polym. J.*, 2007, **39**, 163–174.
- 112 P. Plikk, T. Tyson, A. Finne-Wistrand and A.-C. Albertsson, *J. Polym. Sci. A Polym. Chem.*, 2009, **47**, 4587–4601.
- 113 I. Cho and S. K. Kim, *J. Polym. Sci. C Polym. Lett.*, 1990, **28**, 417–421.
- 114 W. Liu, F. Mikeš, Y. Guo, Y. Koike and Y. Okamoto, *J. Polym. Sci. A Polym. Chem.*, 2004, **42**, 5180–5188.
- 115 L. F. Sun, R. X. Zhuo and Z. L. Liu, *J. Polym. Sci. A Polym. Chem.*, 2003, **41**, 2898–2904.
- 116 W. J. Bailey, T. Endo, B. Gapud, Y.-N. Lin, Z. Ni, C.-Y. Pan, S. E. Shaffer, S.-R. Wu, N. Yamazaki and K. Yonezawa, *J. Macromol. Sci. A Chem.*, 1984, **21**, 979–995.
- 117 S. Agarwal, *J. Polym. Res.*, 2006, **13**, 403–412.
- 118 G. E. Roberts, M. L. Coote, J. P. A. Heuts, L. M. Morris and T. P. Davis, *Macromolecules*, 1999, **32**, 1332–1340.
- 119 S. Agarwal, R. Kumar, T. Kissel and R. Reul, *Polym. J.*, 2009, **41**, 650–660.
- 120 A. Tardy, J. C. Honoré, J. Tran, D. Siri, V. Delplace, I. Bataille, D. Letourneur, J. Perrier, C. Nicoletti, M. Maresca, C. Lefay, D. Gigmes, J. Nicolas and Y. Guillaneuf, *Angew. Chem. Int. Ed.*, 2017, **56**, 16515–16520.
- 121 S. Maji, M. Zheng and S. Agarwal, *Macromol. Chem. Phys.*, 2011, **212**, 2573–2582.
- 122 J. Undin, A. Finne-Wistrand and A. C. Albertsson, *Biomacromolecules*, 2013, **14**, 2095–2102.
- 123 M. K. Georges, R. P. N. Veregin, P. M. Kazmaier and G. K. Hamer, *Macromolecules*, 1993, **26**, 2987–2988.
- 124 C. J. Hawker, A. W. Bosman and E. Harth, *Chem. Rev.*, 2011, **101**, 3661–3688.
- 125 J. Nicolas, Y. Guillaneuf, D. Bertin, D. Gigmes and B. Charleux, *Prog. Polym. Sci.*, 2013, **38**, 63–235.
- 126 M. Kamigaito, T. Ando and M. Sawamoto, *Chem. Rev.*, 2001, **101**, 3689–

- 3745.
- 127 M. Ouchi and M. Sawamoto, *Macromolecules*, 2017, **50**, 2603–2614.
- 128 M. Kato, M. Kamigaito, M. Sawamoto and T. Higashimuras, *Macromolecules*, 1996, **28**, 1721–1723.
- 129 J. S. Wang and K. Matyjaszewski, *J. Am. Chem. Soc.*, 1995, **117**, 5614–5615.
- 130 K. Matyjaszewski and J. Xia, *Chem. Rev.*, 2001, **101**, 2921–2990.
- 131 K. Matyjaszewski, *Macromolecules*, 2012, **45**, 4015–4039.
- 132 V. Percec, A. V. Popov, E. Ramirez-Castillo, M. Monteiro, B. Barboiu, O. Weichold, A. D. Asandei and C. M. Mitchell, *J. Am. Chem. Soc.*, 2002, **124**, 4940–4941.
- 133 V. Percec, T. Guliashvili, J. S. Ladislaw, A. Wistrand, A. Stjerndahl, M. J. Sienkowska, M. J. Monteiro and S. Sahoo, *J. Am. Chem. Soc.*, 2006, **128**, 14156–14165.
- 134 B. M. Rosen and V. Percec, *Chem. Rev.*, 2009, **109**, 5069–5119.
- 135 Q. Zhang, P. Wilson, Z. Li, R. McHale, J. Godfrey, A. Anastasaki, C. Waldron and D. M. Haddleton, *J. Am. Chem. Soc.*, 2013, **135**, 7355–7363.
- 136 A. Anastasaki, V. Nikolaou, G. Nurumbetov, P. Wilson, K. Kempe, J. F. Quinn, T. P. Davis, M. R. Whittaker and D. M. Haddleton, *Chem. Rev.*, 2016, **116**, 835–877.
- 137 A. Anastasaki, V. Nikolaou and D. M. Haddleton, *Polym. Chem.*, 2016, **7**, 1002–1026.
- 138 J. Chiefari, Y. K. B. Chong, F. Ercole, J. Krstina, J. Jeffery, T. P. T. Le, R. T. A. Mayadunne, G. F. Meijs, C. L. Moad, G. Moad, E. Rizzardo and S. H. Thang, *Macromolecules*, 1998, **31**, 5559–5562.
- 139 G. Moad, E. Rizzardo and S. H. Thang, *Aust. J. Chem.*, 2005, **58**, 379–410.
- 140 G. Moad, E. Rizzardo and S. H. Thang, *Aust. J. Chem.*, 2006, **59**, 669–692.
- 141 G. Moad, E. Rizzardo and S. H. Thang, *Aust. J. Chem.*, 2009, **62**, 1402–1472.
- 142 G. Moad, E. Rizzardo and S. H. Thang, *Aust. J. Chem.*, 2012, **65**, 985–1076.
- 143 S. Perrier and P. Takolpuckdee, *J. Polym. Sci. A Polym. Chem.*, 2005, **43**, 5347–5393.
- 144 C. Boyer, V. Bulmus, T. P. Davis, V. Ladmiral, J. Liu and S. Perrier, *Chem. Rev.*, 2009, **109**, 5402–5436.

- 
- 145 A. Gregory and M. H. Stenzel, *Prog. Polym. Sci.*, 2012, **37**, 38–105.
- 146 M. R. Hill, R. N. Carmean and B. S. Sumerlin, *Macromolecules*, 2015, **48**, 5459–5469.
- 147 S. Perrier, *Macromolecules*, 2017, **50**, 7433–7447.
- 148 Y. Wei, E. J. Connors, X. Jia and B. Wang, *Chem. Mater.*, 1996, **8**, 604–606.
- 149 Y. Wei, E. J. Connors, X. Jia and C. Wang, *J. Polym. Sci. A Polym. Chem.*, 1998, **36**, 761–771.
- 150 C.-Y. Pan and X.-D. Lou, *Macromol. Chem. Phys.*, 2000, **201**, 1115–1120.
- 151 T. He, Y.-F. Zou and C.-Y. Pan, *Polym. J.*, 2002, **34**, 138–143.
- 152 G. G. Hedir, C. A. Bell, N. S. Jeong, E. Chapman, I. R. Collins, R. K. O'Reilly and A. P. Dove, *Macromolecules*, 2014, **47**, 2847–2852.
- 153 C. A. Bell, G. G. Hedir, R. K. O'Reilly and A. P. Dove, *Polym. Chem.*, 2015, **6**, 7447–7454.
- 154 G. G. Hedir, C. A. Bell, R. K. O'Reilly and A. P. Dove, *Biomacromolecules*, 2015, **16**, 2049–2058.
- 155 G. G. Hedir, A. Pitto-Barry, A. P. Dove and R. K. O'Reilly, *J. Polym. Sci. A Polym. Chem.*, 2015, **53**, 2699–2710.
- 156 G. G. Hedir, M. C. Arno, M. Langlais, J. T. Husband, R. K. O'Reilly and A. P. Dove, *Angew. Chem. Int. Ed.*, 2017, **56**, 9178–9182.
- 157 G. Hedir, C. Stubbs, P. Aston, A. P. Dove and M. I. Gibson, *ACS Macro Lett.*, 2017, **6**, 1404–1408.
- 158 T. Yokozawa and A. Yokoyama, *Polym. J.*, 2004, **36**, 65–83.
- 159 A. Yokoyama and T. Yokozawa, *Macromolecules*, 2007, **40**, 4093–4101.
- 160 T. Yokozawa and A. Yokoyama, *Prog. Polym. Sci.*, 2007, **32**, 147–172.
- 161 T. Yokozawa and A. Yokoyama, *Chem. Rev.*, 2009, **109**, 5595–5619.
- 162 T. Yokozawa and Y. Ohta, *Chem. Rev.*, 2016, **116**, 1950–1958.
- 163 A. Yokoyama, K. I. Iwashita, K. Hirabayashi, K. Aiyama and T. Yokozawa, *Macromolecules*, 2003, **36**, 4328–4336.
- 164 K. I. Iwashita, A. Yokoyama and T. Yokozawa, *J. Polym. Sci. A Polym. Chem.*, 2005, **43**, 4109–4117.
- 165 T. Yokozawa and S. Horio, *Polym. J.*, 1999, **28**, 633–636.
- 166 T. Yokozawa and H. Shimura, *J. Polym. Sci. A Polym. Chem.*, 1999, **37**,
-

- 2607–2618.
- 167 T. Yokozawa and H. Suzuki, *J. Am. Chem. Soc.*, 1999, **121**, 11573–11574.
- 168 T. Yokozawa, D. Maeda, N. Hiyama and S. Hiraoka, *Macromol. Chem. Phys.*, 2001, **202**, 2181–2186.
- 169 T. Saegusa, H. Ikeda and H. Fujii, *Macromolecules*, 1972, **5**, 354–359.
- 170 T. Saegusa, *Angew. Chem. Int. Ed.*, 1977, **16**, 826–835.
- 171 M. Suzuki, in *Encyclopedia of Polymer Science and Technology*, John Wiley and Sons, Inc., 2013.
- 172 T. Saegusa, S. Kobayashi and Y. Kimura, *Macromolecules*, 1974, **7**, 139–140.
- 173 K. Aoi and M. Okada, *Prog. Polym. Sci.*, 1996, **21**, 151–208.
- 174 B. M. Culbertson, *Prog. Polym. Sci.*, 2002, **27**, 579–626.
- 175 S. Kobayashi and H. Uyama, *J. Polym. Sci. A Polym. Chem.*, 2002, **40**, 192–209.
- 176 K. Kempe, *Macromol. Chem. Phys.*, 2017, **218**, 1700021.
- 177 T. Saegusa, Y. Kimura, K. Sano and S. Kobayashi, *Macromolecules*, 1974, **7**, 546–549.
- 178 T. Saegusa, S. Kobayashi and Y. Kimura, *Macromolecules*, 1975, **8**, 374–376.
- 179 G. Odian and P. A. Gunatillake, *Macromolecules*, 1984, **17**, 1297–1307.
- 180 T. Saegusa, Y. Kimura and S. Kobayashi, *Macromolecules*, 1977, **10**, 239–242.
- 181 B. L. Rivas, G. S. Canessa and S. A. Pooley, *Eur. Polym. J.*, 1992, **28**, 43–47.
- 182 T. Balakrishnan and M. Periyasamy, *Macromol. Rapid Commun.*, 1980, **1**, 307–312.
- 183 G. Odian, P. Gunatillake and D. Tomalia, *Macromolecules*, 1985, **18**, 605–611.
- 184 J. Kadokawa, S. Nishizawa and S. Kobayashi, *Acta Polym.*, 1994, **45**, 419–423.
- 185 L. L. Bryant Jr, J. F. Kinstle, T. Saegusa and S. Kobayashi, *Polym. Bull.*, 1986, **15**, 227–231.
- 186 S. Kobayashi, M. Miyamoto and T. Saegusa, *Macromolecules*, 1981, **14**, 1582–1584.
- 187 B. L. Rivas and G. del C. Pizzaro, *Polym. Bull.*, 1993, **30**, 515–520.

- 
- 188 K. I. Lee and M. H. Lee, *Polymer*, 1993, **34**, 650–654.
- 189 B. L. Rivas, G. S. Canessa and S. A. Pooley, *Eur. Polym. J.*, 1993, **29**, 1089–1093.
- 190 B. L. Rivas, G. S. Canessa and S. A. Pooley, *Eur. Polym. J.*, 1989, **25**, 225–230.
- 191 T. Saegusa, Y. Kimura and S. Kobayashi, *Macromolecules*, 1977, **10**, 236–239.
- 192 B. L. Rivas, G. S. Canessa and S. A. Pooley, *Polym. Bull.*, 1983, **9**, 417–422.
- 193 P. I. C. Guimarães and A. P. Monteiro, *Polym. Bull.*, 1995, **34**, 393–395.
- 194 G. S. Canessa, S. A. Pooley, M. Parra and B. L. Rivas, *Polym. Bull.*, 1984, **11**, 465–470.
- 195 B. L. Rivas, G. S. Canessa and S. A. Pooley, *Polym. Bull.*, 1985, **13**, 65–70.
- 196 S. Kobayashi, M. Isobe and T. Saegusa, *Macromolecules*, 1982, **15**, 703–707.
- 197 T. Saegusa, S. Kobayashi and Y. Kimura, *Macromolecules*, 1974, **7**, 1–4.
- 198 B. L. Rivas, G. S. Canessa and S. A. Pooley, *Makromol. Chem.*, 1986, **187**, 71–79.
- 199 B. L. Rivas, G. S. Canessa and S. A. Pooley, *Makromol. Chem.*, 1987, **188**, 149–154.
- 200 B. L. Rivas, G. S. Canessa and S. A. Pooley, *Polym. Bull.*, 1985, **13**, 103–107.
- 201 B. L. Rivas, G. S. Canessa and S. A. Pooley, *Polym. Bull.*, 1985, **13**, 519–523.
- 202 H. Yokota and M. Kondo, *J. Polym. Sci. A Polym. Chem.*, 1971, **9**, 13–25.
- 203 A. Takahashi, *J. Macromol. Sci. A Chem.*, 1977, **11**, 421–430.
- 204 A. Takahashi, *J. Macromol. Sci. A Chem.*, 1977, **11**, 411–420.
- 205 B. L. Rivas, G. del C. Pizzaro, L. H. Tagle and D. Radic, *Angew. Makromol. Chem.*, 1995, **231**, 199–211.
- 206 S. A. Pooley, G. S. Canessa, B. L. Rivas and E. Espejo, *Polym. Bull.*, 1995, **35**, 271–277.
- 207 S. A. Pooley, G. S. Canessa, B. L. Rivas and E. Espejo, *Polym. Bull.*, 1997, **39**, 407–414.
- 208 S. A. Pooley, G. S. Canessa, B. L. Rivas and E. Espejo, *Polym. Bull.*, 1996, **36**, 415–422.
- 209 S. A. Pooley, G. S. Canessa and B. L. Rivas, *Eur. Polym. J.*, 1993, **29**, 1239–
-

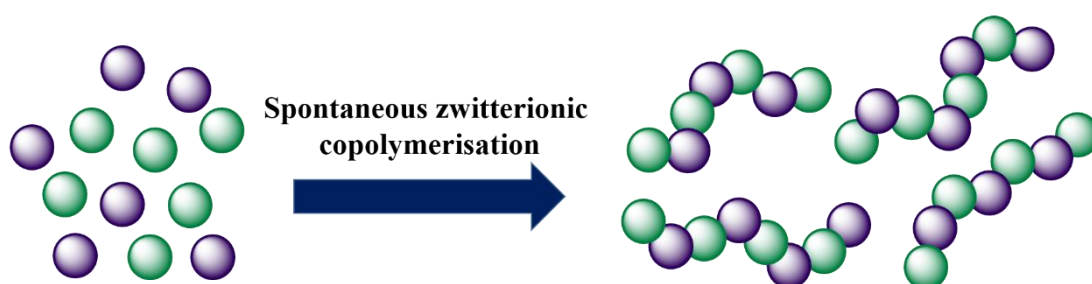
- 
- 1242.
- 210 S. A. Pooley, G. S. Canessa and B. L. Rivas, *Eur. Polym. J.*, 1995, **31**, 547–553.
- 211 B. L. Rivas, G. S. Canessa, S. A. Pooley, H. A. Maturana and U. Angne, *Eur. Polym. J.*, 1985, **21**, 939–942.
- 212 D. C. Christova, R. S. Velichkova and I. M. Panayotov, *Macromol. Chem. Phys.*, 1995, **196**, 3605–3613.
- 213 B. L. Rivas, G. S. Canessa and S. A. Pooley, *Makromol. Chem.*, 1989, **190**, 2665–2671.
- 214 B. L. Rivas, G. S. Canessa and S. A. Pooley, *Macromol. Rapid Commun.*, 1987, **8**, 365–372.
- 215 T. Saegusa, Y. Kimura, S. Sawada and S. Kobayashi, *Macromolecules*, 1974, **7**, 956–958.
- 216 B. L. Rivas, G. S. Canessa, S. A. Pooley and H. A. Maturana, *Polym. Bull.*, 1989, **22**, 169–173.
- 217 C. H. R. M. Wilsens, N. J. M. Wullems, E. Gubbels, Y. Yao, S. Rastogi and B. A. J. Noordover, *Polym. Chem.*, 2015, **6**, 2707–2716.
- 218 D. M. Lynn and R. Langer, *J. Am. Chem. Soc.*, 2000, **122**, 10761–10768.
- 219 A. Akinc, D. G. Anderson, D. M. Lynn and R. Langer, *Bioconjug. Chem.*, 2003, **14**, 979–88.
- 220 J. J. Green, R. Langer and D. G. Anderson, *Acc. Chem. Res.*, 2008, **41**, 749–759.
- 221 D. Zhou, L. Pierucci, Y. Gao, J. O’Keeffe Ahern, X. Huang, A. Sigen and W. Wang, *ACS Appl. Mater. Interfaces*, 2017, **9**, 5793–5802.
- 222 B. H. A. Rehm, *Nat. Rev. Microbiol.*, 2010, **8**, 578–592.
- 223 Y. Poirier, C. Nawrath and C. Somerville, *Nat. Biotechnol.*, 1995, **13**, 142–150.
- 224 G.-Q. Chen, *Chem. Soc. Rev.*, 2009, **38**, 2434–2446.
-

## Chapter 2

---

# *N*-Acylated poly(aminoester) macromonomers by spontaneous zwitterionic copolymerisation

---



Parts of this chapter have been published:

K. Kempe, P.A.J.M. de Jongh, A. Anastasaki, P. Wilson, D.M. Haddleton, *Chem. Commun.* **2015**, 51, 16213-16216; P.A.J.M. de Jongh, A. Mortiboy, G.S. Sulley, M.R. Bennett, A. Anastasaki, P. Wilson, D.M. Haddleton, K. Kempe, *ACS Macro Lett.* **2016**, 5, 321-325; P.A.J.M. de Jongh, M.R. Bennett, G.S. Sulley, P. Wilson, T.P. Davis, D.M. Haddleton, K. Kempe, *Polym. Chem.* **2016**, 7, 6703-6707; J. Steinkoenig, P.A.J.M. de Jongh, D.M. Haddleton, A.S. Goldmann, C. Barner-Kowollik, K. Kempe, *Macromolecules* **2018**, 51, 318-327

## 2.1. Introduction

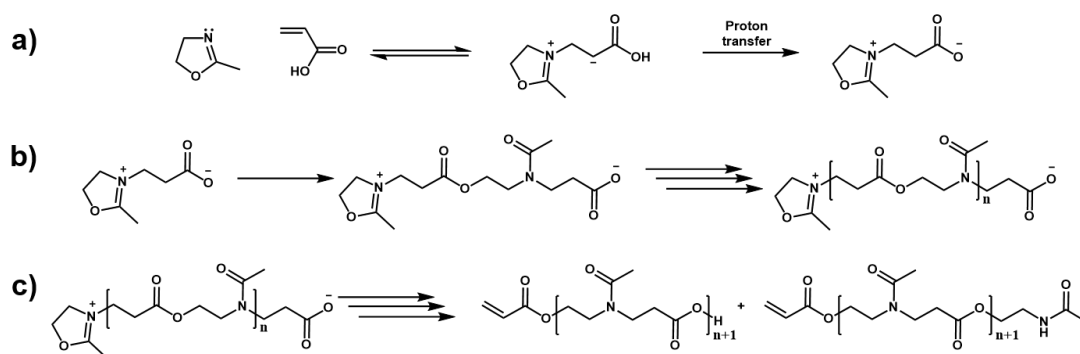
Poly(ester amide)s (PEAs) are a highly attractive polymer class which offer new design avenues for biomedical materials as they combine the degradability of polyesters with the thermomechanical stability of polyamides in one system.<sup>1,2</sup> As a result they allow for a high level of functionality and fine-tuning of their properties and consequently have received significant attention as potential biomedical materials.<sup>3-5</sup> PEAs are typically obtained by step-growth polymerisations such as polycondensations or polyadditions,<sup>2,3,5-7</sup> which generally do not allow for a high control of end group functionality, or ring-opening polymerisation (ROP) of (functionalised) morpholine-2,5-diones to form depsipeptides (peptides with alternating ester and amide bonds), which represent an elegant though demanding strategy.<sup>2-6,8,9</sup>

Poly(aminoester)s (PAEs), more specifically *N*-acylated poly(aminoester)s (NPAEs), are closely related to PEAs, but instead of constituting a part of the polymer backbone, the amide moieties connect the polymer backbone to the side chains. Similar to PEAs, PAEs have been given considerable attention by the scientific community for potential biomedical applications,<sup>10,11</sup> for example for DNA and gene delivery.<sup>12,13</sup> PAEs, including NPAEs, have previously been synthesised *via* various strategies, including aza-Michael polyadditions of di- and triacrylates with amines,<sup>10-14</sup> polycondensation of dicarboxylic acids (or acid chlorides) with *N*-substituted dihydroxyamines,<sup>15-19</sup> transesterification of carboxylic esters with hydroxyamines<sup>20</sup> and the ROP of functionalised lactones such as 2-morpholinones.<sup>21</sup>

Cyclic imino ethers (CIEs), such as 2-oxazolines (Ox), are well known for their ability to undergo various polyaddition reactions<sup>22,23</sup> as well as for their polymerisation into *N*-acylated poly(ethyleneimine)s (better known as poly(2-oxazoline)s (POx)) by cationic ring-opening polymerisation (CROP).<sup>23-27</sup> Since their initial discovery in 1966,<sup>28-30</sup> POx have received significant attention as highly functional and tuneable materials,<sup>31-33</sup> which, in combination with the biocompatibility of systems based on 2-methyl- (MeOx)<sup>34</sup> and 2-ethyl-2-oxazoline (EtOx),<sup>35</sup> are considered as a potential alternative to poly(ethylene glycol) for biomedical applications.<sup>36-43</sup>

In combination with electrophilic monomers ( $M_E$ ) such as acrylic acid (AA) and lactones, CIEs are able to undergo spontaneous zwitterionic copolymerisations (SZWIP) to form NPAEs, as previously reported by the groups of Saegusa,<sup>44–47</sup> Rivas<sup>48–50</sup> and Odian.<sup>51</sup> In case of a defect-free copolymerisation, SZWIP of CIEs with AA and  $\beta$ -propiolactone (BPL) results in the same copolymer backbone (with different end groups). However, under many reaction conditions homopolymerisation by anionic ROP of BPL has been observed, whereas AA has been reported to not undergo homopolymerisation, furnishing AB-type alternating copolymers, making AA the preferred  $M_E$  of choice over BPL.

According to the proposed mechanism for the SZWIP between CIEs and AA (Scheme 2.1),<sup>45</sup> the CIE nitrogen lone pair initiates a reversible Michael addition on the AA, followed by a proton transfer from the carboxylic acid to the carbanion to form the *genetic zwitterion* (a). The carboxylate can ring-open the oxazolinium ring of another genetic zwitterion to form dimers, trimers and other oligomers (b). Termination of the  $\alpha$ -chain end is presumed to take place by ring-opening of the oxazolinium ring by AA, whereas the  $\omega$ -chain end can be terminated by protonation to form a  $\omega$ -carboxylic acid group or by ring-opening of a CIE monomer to form a  $\omega$ -amide end group (c). The end groups have only been discussed qualitatively previously, but have not been quantified.<sup>51</sup>



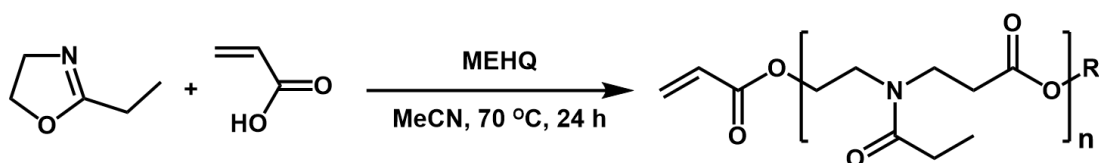
**Scheme 2.1** Proposed mechanism for the SZWIP of MeOx and AA: formation of the genetic zwitterion (a), propagation to form oligomers (b) and termination into a macromonomer (c).

Previous work on the SZWIP of CIEs with AA focussed on determining the influence of various solvents, feed ratios and screening monomers capable of undergoing SZWIP. However, the work by the groups of Saegusa,<sup>44,45</sup> Rivas<sup>48</sup> and Odian<sup>51</sup> demonstrated similar results, independent of the reaction conditions employed, although it should be noted that their work only included limited analysis, *i.e.* most of the conclusions are based on <sup>1</sup>H NMR analysis, vapour pressure osmometry and elemental analysis. Herein, the SZWIP between a small library of CIEs and AA is re-evaluated and new insights into their products are presented, including end group quantification and initial results of side-reactions.

## 2.2. Results and discussion

### 2.2.1. Initial synthesis of NPAE macromonomers

Rivas and co-workers previously reported the SZWIP of EtOx with AA (Scheme 2.2).<sup>48</sup> Following their procedure, EtOx and AA were mixed in an equimolar ratio in MeCN in the presence of *p*-methoxyphenol (MEHQ) as a radical inhibitor and the resulting mixture was heated to 70 °C for 24 h. After purification by precipitating in diethyl ether, a yellowish oil was obtained.



**Scheme 2.2** SZWIP of EtOx with AA yielding *N*-acylated poly(aminoester) macromonomers. R = H, CH<sub>2</sub>CH<sub>2</sub>NHCOEt.

<sup>1</sup>H NMR analysis of the resulting product shows peaks consistent with an alternating structure of the ring-opened EtOx and AA monomers, with the product consequently

classified as *N*-acylated poly(aminoester)s (NPAEs; Figure 2.1a). The quantitative introduction of an  $\alpha$ -acrylate end group was previously suggested by Odian and Gunatillake<sup>51</sup> and was used to determine the degree of polymerisation (DP) by comparing the relative integration values for the  $\alpha$ -acrylate end group ( $\delta = 5.5 - 6.5$  ppm) compared to the backbone signals from EtOx ( $\delta = 4 - 4.5$  ppm) and AA ( $\delta = 2 - 2.25$  ppm), which is typically 3 to 4, corresponding to molecular weights of 543 to 701 g mol<sup>-1</sup>. The ratio of the two possible  $\omega$ -end groups cannot be directly determined from <sup>1</sup>H NMR analysis as a result of overlapping signals, but can be determined via other methods (see Section 2.2.4). Size exclusion chromatography (SEC) analysis of the product revealed  $M_n$  values around 1500 g mol<sup>-1</sup> ( $D_{SEC} = 1.2 - 1.3$ ), which is consistent with the formation of short oligomers (Figure 2.1b).

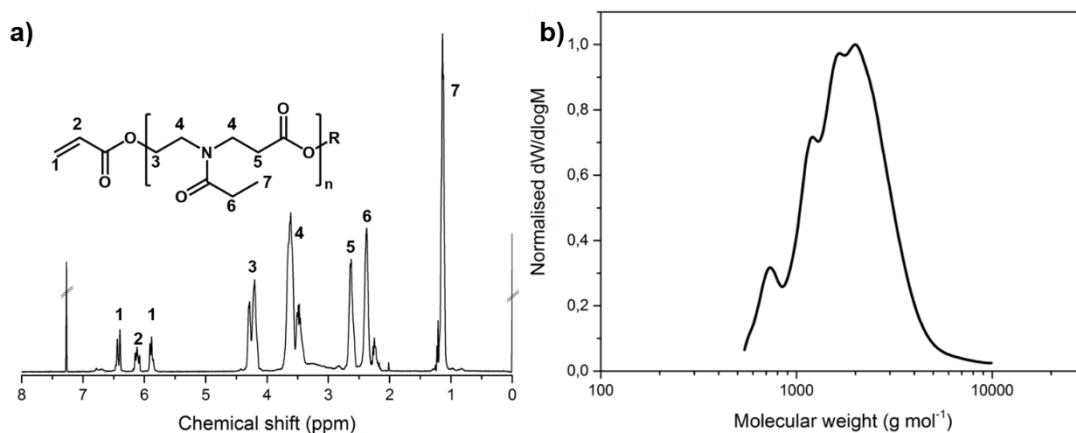


**Figure 2.1** Analysis of EtOx/AA 1/1 macromonomer by <sup>1</sup>H NMR (a) and SEC (b). R = H, CH<sub>2</sub>CH<sub>2</sub>NHCOEt.

### 2.2.2. Screening experimental parameters

Various experimental parameters were evaluated to determine if higher molecular weight NPAE macromonomers could be synthesised by SZWIP. The reaction appears to be uninfluenced by reaction temperature (40 or 70 °C), source of heating (conventional *vs.* microwave), reaction time (2 h – 1 week), multiple monomer additions or monomer ratios. As the monomers are also the terminating agents for this reaction, it was reasoned that the fast self-terminating nature of this reaction prevents the synthesis

of higher molecular weight NPAE macromonomers. Switching the solvent lead to higher dispersity values or interference with the reaction (Table 2.1).

**Table 2.1** Screening of experimental parameters for the SZWIP of EtOx and AA.

Entry <sup>a</sup>	Solvent	Temp. [°C]	Reaction time	DP <sub>NMR</sub>	M <sub>n,NMR</sub> [g mol <sup>-1</sup> ]	M <sub>n,SEC</sub> [g mol <sup>-1</sup> ]	Đ <sub>SEC</sub>
1	MeCN	70	24 h	3/3	543	1500	1.27
2	MeCN	40	24 h	2.5/2.5	500	1300	1.22
3 <sup>b</sup>	MeCN	120	2 h	1.5/1.5	260	800	1.27
4 <sup>b</sup>	MeCN	70	2 h	2.5/2.5	500	1300	1.30
5	MeCN	70	1 week	3.5/3.5	671	1800	1.30
6 <sup>c</sup>	MeCN	70	2 x 24 h	3.5/3.5	671	1500	1.30
7 <sup>d</sup>	MeCN	70	24 h	2/2	414	1300	1.16
8 <sup>e</sup>	MeCN	70	24 h	2.5/2.5	500	1500	1.30
9	DMF	70	24 h	2/2	414	2100	2.04
10	Acetone	40	24 h	n.d. <sup>f</sup>	n.d. <sup>f</sup>	800	1.09

<sup>a</sup> Standard conditions: EtOx/AA 1/1 feed ratio, MeCN, 70 °C, 24 h. <sup>b</sup> Microwave reaction.

<sup>c</sup> Double monomer feed; second batch added after 24 h. <sup>d</sup> EtOx/AA 1/2 feed ratio. <sup>e</sup> EtOx/AA 2/1 feed ratio. <sup>f</sup> n.d. = not determined. <sup>1</sup>H NMR spectrum does not match Figure 2.1a

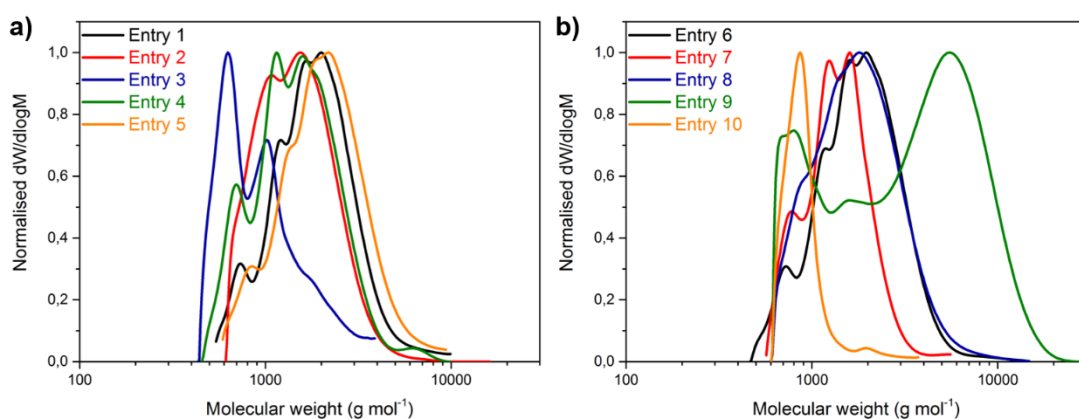


**Figure 2.2** SEC molecular weight distributions for NPAE macromonomers synthesised from EtOx and AA under various conditions (Table 2.1): a) entries 1-5, and b) entries 6-10.

### 2.2.3. Expanding the library of NPAE macromonomers

In order to further explore the potential of SZWIP to synthesise NPAE macromonomers, a small library was synthesised from three CIEs and two electrophilic monomers ( $M_E$ , Figure 2.3). The three different CIEs including different ring sizes and side chains allow tuning of the hydrophobicity, whereas 2-carboxyethyl acrylate (CEA) acts as the dimer of AA in SZWIP and thereby allows for the synthesis of  $AB_2$ -type macromonomers. The monomers were copolymerised in various ratios by SZWIP to produce four types of macromonomers (Figure 2.4).

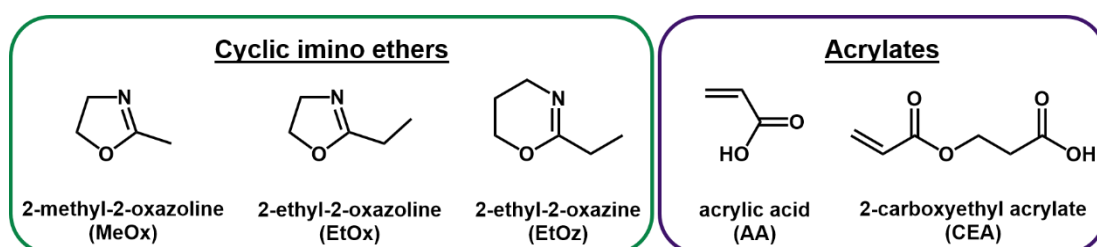


Figure 2.3 Structures of the monomers employed in this work.

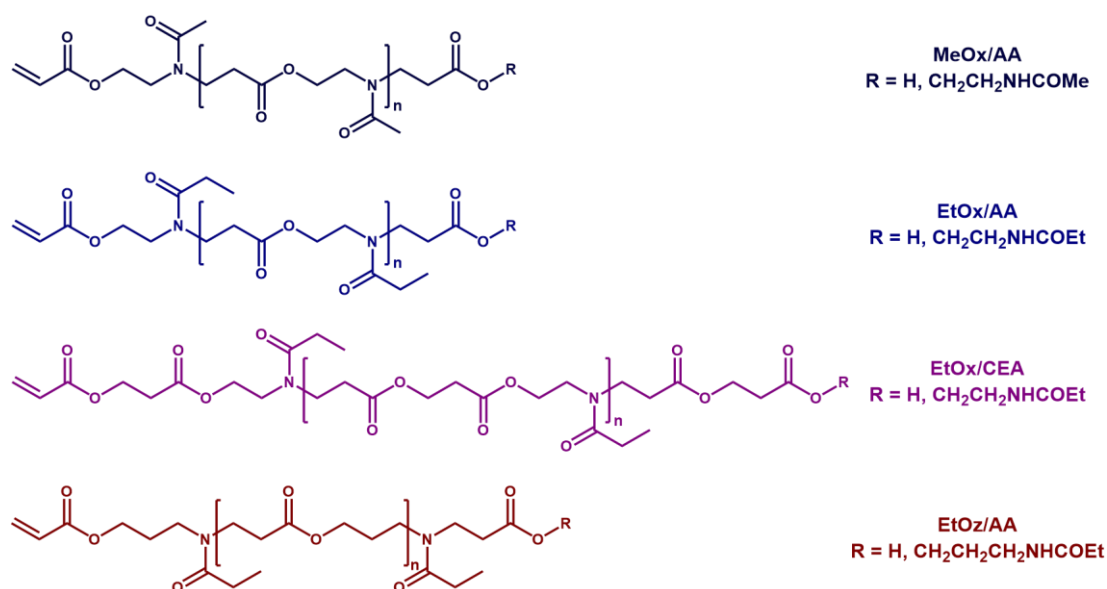
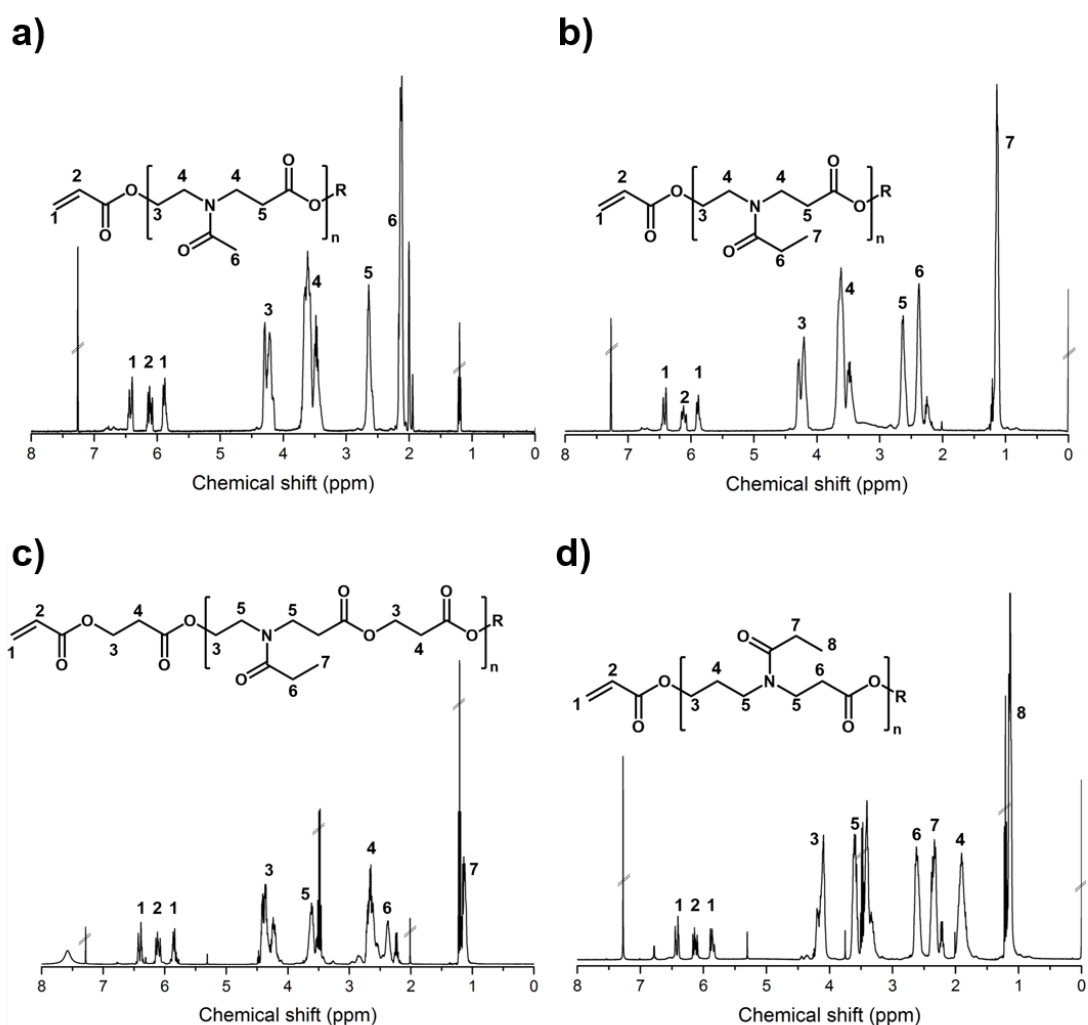


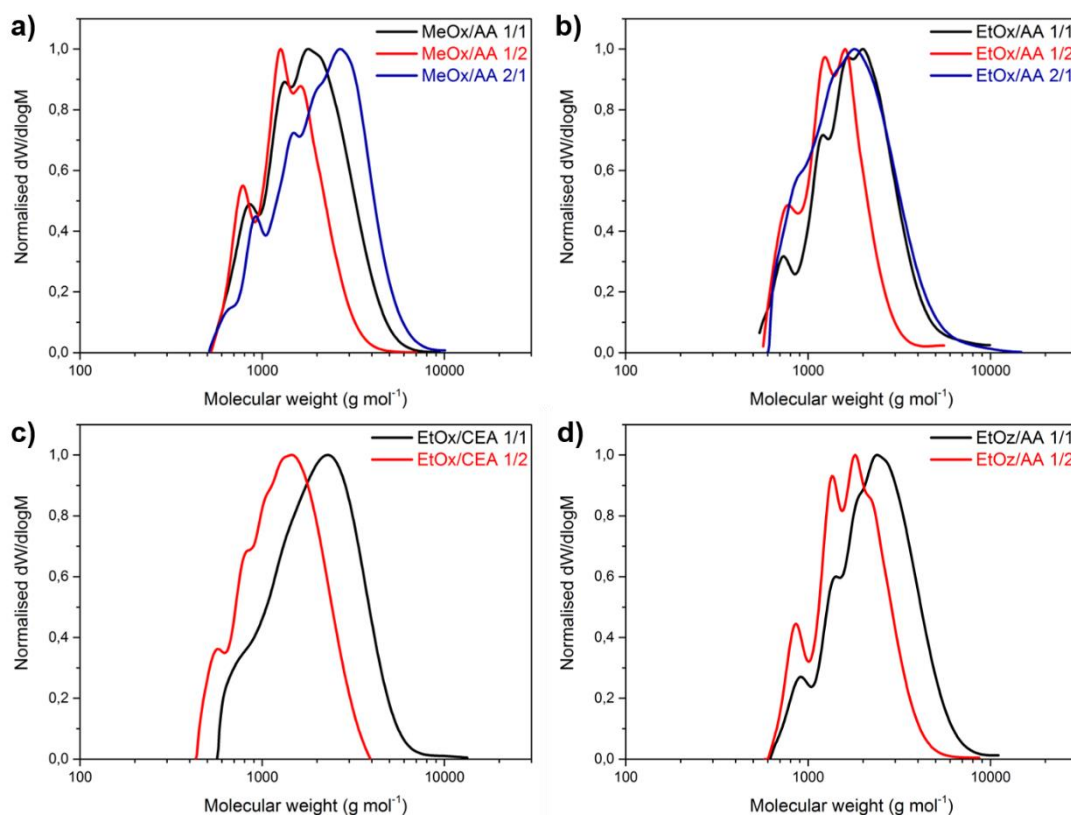
Figure 2.4 Structures of the NPAE macromonomers investigated.

Figure 2.5 shows the  $^1\text{H}$  NMR spectra for the macromonomers. Integration of the relevant peaks allows for determination of the DPs, revealing short oligomers. The results are generally comparable for all monomer combinations and feed ratios employed, although a trend can be observed in which an excess of the acrylate in the monomer feed results in slightly lower DPs. The higher concentration of  $\text{M}_E$  in the SZWIP most likely promotes faster termination of the reaction and consequently lower DPs.



**Figure 2.5**  $^1\text{H}$  NMR spectra ( $\text{CDCl}_3$ ) of macromonomers synthesised from MeOx/AA (a), EtOx/AA (b), EtOx/CEA (c) and EtOz/AA (d). R = H or  $\text{CH}_2\text{CH}_2\text{NHCOMe}$  (MeOx), H or  $\text{CH}_2\text{CH}_2\text{NHCOEt}$  (EtOx), H or  $\text{CH}_2\text{CH}_2\text{CH}_2\text{NHCOEt}$  (EtOz).

SEC analysis revealed molecular weights ranging from 1300 to 2200 g mol<sup>-1</sup>, which is consistent with the formation of oligomers. The discrepancies in molecular weights between <sup>1</sup>H NMR and SEC analysis are most likely the result of the difference in solvodynamic volume between the analytes and the PMMA calibrants. However, SEC analysis was mainly employed to confirm the absence of side reactions, such as the formation of high molecular weight species by free radical polymerisation of AA, and to determine the dispersity values (*D*), which are generally between 1.2 – 1.3 (Figure 2.6). Table 2.2 provides a summary of the NPAE macromonomer synthesised, including their DPs and molecular weights.



**Figure 2.6** SEC analysis of macromonomers synthesised from MeOx/AA (a), EtOx/AA (b), EtOx/CEA (c) and EtOz/AA (d).

**Table 2.2** Results for the synthesis of NPAE macromonomers from various CIEs and M<sub>E</sub>.

Entry	CIE	M <sub>E</sub>	Feed ratio	DP <sub>NMR</sub> [M <sub>N</sub> /M <sub>E</sub> ]	M <sub>n,NMR</sub> [g mol <sup>-1</sup> ]	M <sub>n,SEC</sub> [g mol <sup>-1</sup> ]	Đ <sub>SEC</sub>
<b>1</b>	MeOx	AA	1 : 1	3/3	543	1500	1.27
<b>2</b>	MeOx	AA	1 : 2	2.5/2.5	465	1300	1.18
<b>3</b>	MeOx	AA	2 : 1	2.5/2.5	465	1800	1.32
<b>4</b>	EtOx	AA	1 : 1	3/3	585	1600	1.22
<b>5</b>	EtOx	AA	1 : 2	2/2	414	1300	1.16
<b>6</b>	EtOx	AA	2 : 1	2.5/2.5	500	1500	1.30
<b>7</b>	EtOx	CEA	1 : 1	3.5/3.5	996	1700	1.32
<b>8</b>	EtOx	CEA	1 : 2	3/3	730	2200	1.32
<b>9</b>	EtOz	AA	1 : 1	3/3	627	2000	1.27
<b>10</b>	EtOz	AA	1 : 2	2.5/2.5	535	1600	1.20

<sup>a</sup> All macromonomers synthesised using standard conditions: MeCN, 70 °C, 24 h.

#### 2.2.4. Manipulating the ω-end group

Odian and Gunatillake previously reported the introduction of two possible ω-end groups, a carboxylic acid or an amide, but only discussed this in a qualitative context.<sup>51</sup> As shown in the previous section and work by Rivas and co-workers,<sup>48</sup> the feed ratio of the two monomers during the SZWIP does not have a significant effect on the DP and molecular weight, but its effect on the ω-end groups has not been previously investigated. In order to quantify the effect of monomer feed ratios on the ω-end groups, several macromonomers were analysed by acid-base titration against 0.1 M aqueous NaOH. An equimolar CIE:AA feed ratio results in the introduction of approximately 50 % ω-carboxylic acid groups and therefore also approximately 50 % ω-amide groups, whereas an excess of AA in the monomer feed enables near-quantitative introduction of ω-carboxylic acid end groups, thereby furnishing heterotelechelic materials (Table 2.3).

**Table 2.3** Amount of  $\omega$ -carboxylic acid groups of macromonomers from various CIEs and AA as determined by acid-base titration.

CIE : acrylate feed	CIE/acrylate			
	MeOx/AA	EtOx/AA	EtOx/CEA	EtOz/AA
1 : 1	48 %	46 %	49 %	53 %
1 : 2	99 %	98 %	n.d. <sup>a</sup>	n.d. <sup>a</sup>

<sup>a</sup> n.d. = not determined.

### 2.2.5. MALDI-ToF analysis

The macromonomers were further analysed by MALDI-ToF mass spectrometry. The spectra for MeOx/AA from 1/1 and 1/2 feed ratios are shown in Figure 2.7. Multiple distributions can be observed. Rectangular symbols correspond to distributions with alternating composition of MeOx and AA, whereas circular symbols correspond to distributions that deviate from an alternating structure. Furthermore, within the alternating distributions, species with  $\omega$ -carboxylic acid (green) and  $\omega$ -amide end groups (blue) can be distinguished.

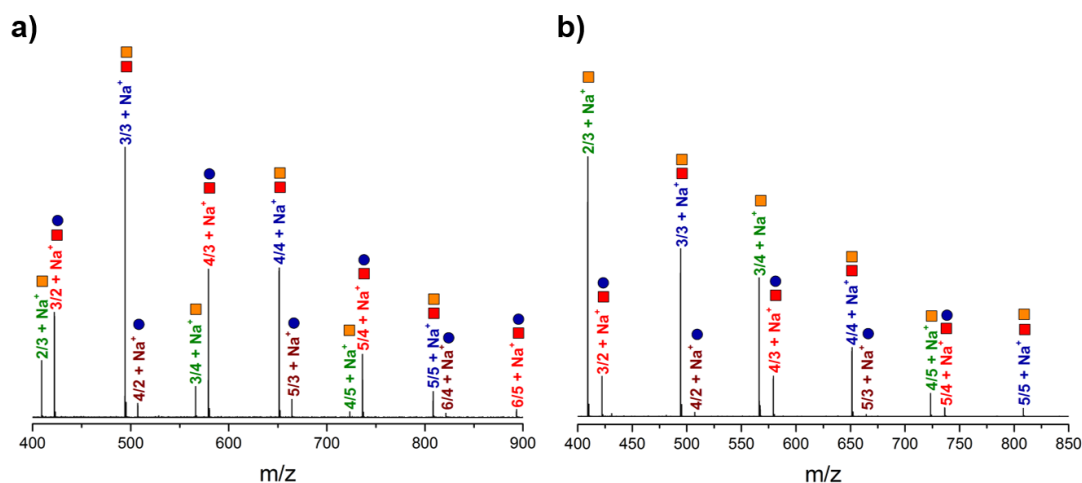


**Figure 2.7** MALDI-ToF spectra for MeOx/AA synthesised from (a) 1/1 and (b) 1/2 feed ratios. Rectangular symbols denote alternating compositions, circular symbols indicate distributions that deviate from an alternating composition.

When comparing the spectra for the two different feed ratios, it can be observed that an increased AA feed results in a significant increase in signals corresponding to alternating macromonomers with  $\omega$ -carboxylic acid end groups, while the species with  $\omega$ -amide groups reduce in intensity. Even with only approximately 1 %  $\omega$ -amide end groups present (as determined by acid-base titration), their signals are still clearly present in the spectra, which is most likely explained by the relative ionisation efficiencies of the two  $\omega$ -end groups, which is further explored in Chapter 3. The MALDI-ToF spectra for macromonomers from EtOx/AA (Figure 2.8) and EtOz/AA (Figure 2.9) show the same types of signals as MeOx/AA macromonomers. It can, however, be observed that the intensities of the various signals change by simply changing the CIE employed. Macromonomers from MeOx/AA in both 1/1 and 1/2 feed ratios show significant signals that indicate homopolymerisation of the MeOx. In EtOx/AA 1/1 (Figure 2.8a) these signals are less abundant and almost disappear when the reaction is carried out in an excess of AA (Figure 2.8b). For EtOz/AA there is already negligible indication of homopropagation for an equimolar feed ratio (Figure 2.9a) and when the feed ratio is increased to EtOz/AA 1/2 no signals that suggest homopropagation can be observed (Figure 2.9b).

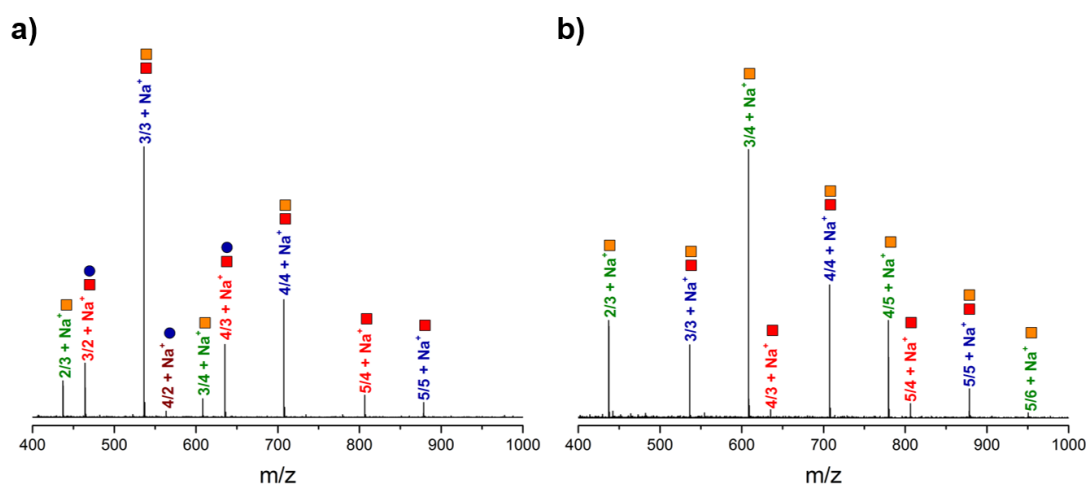


**Figure 2.8** MALDI-ToF spectra for EtOx/AA synthesised from (a) 1/1 and (b) 1/2 feed ratios. Rectangular symbols denote alternating compositions, circular symbols indicate distributions that deviate from an alternating composition.

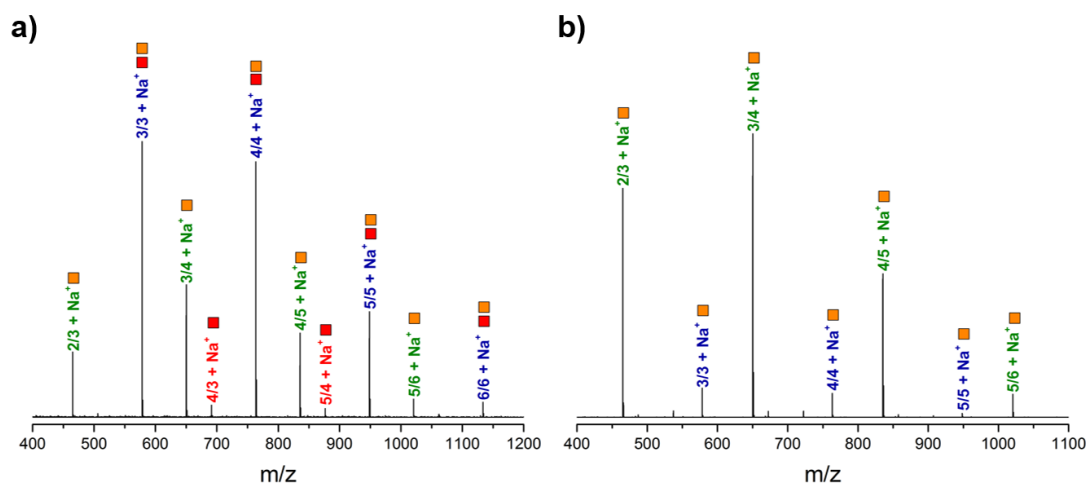


**Figure 2.9** MALDI-ToF spectra for EtOz/AA synthesised from (a) 1/1 and (b) 1/2 feed ratios. Rectangular symbols denote alternating compositions, circular symbols indicate distributions that deviate from an alternating composition.

## 2.2.6. Elemental analysis

The macromonomers were also analysed by elemental analysis, which follows a similar trend to the MALDI-ToF results. Considering MeOx/AA macromonomers as example, it can be seen in Table 2.4 that when the feed ratio of AA increases, the C/N ratio increases. This demonstrates a relatively larger incorporation of AA compared to MeOx. As AA should be unable to homopolymerise under the reaction conditions employed, this suggests a reduced homopropagation of MeOx and the macromonomers are therefore closer to an alternating structure. Similar results are observed for EtOx/AA macromonomers. Interestingly, changing the feed ratio for EtOz/AA macromonomers from equimolar to an excess of AA has a negligible effect on the C/N ratio. This result demonstrates that the relative incorporation of EtOz and AA is independent of the monomer feed ratio. Figure 2.10 provides a graphical representation of these results, which illustrates an effect of the monomer feed ratio on the relative incorporation of the CIE and AA during the SZWIP.

**Table 2.4** Elemental analysis results for NPAE macromonomers.

CIE/AA	Theoretical <sup>a</sup>				Experimental			
	C (%)	H (%)	N (%)	C/N	C (%)	H (%)	N (%)	C/N
<b>MeOx 1/1</b>	52.96	6.83	7.53	7.03	51.62	7.20	8.42	6.13
<b>MeOx 1/2</b>	53.04	6.86	7.73	6.86	49.08	7.15	7.28	6.74
<b>MeOx 2/1</b>	52.96	6.83	7.53	7.03	50.66	7.40	8.89	5.70
<b>EtOx 1/1</b>	55.25	7.36	7.00	7.89	53.51	7.91	7.85	6.82
<b>EtOx 1/2</b>	55.06	7.30	6.76	8.15	48.27	7.94	6.38	7.56
<b>EtOz 1/1</b>	57.42	7.87	6.70	8.57	49.26	6.98	5.42	9.09
<b>EtOz 1/2</b>	57.26	7.81	6.55	8.75	53.59	7.52	5.88	9.11

<sup>a</sup> Theoretical numbers calculated from the DP of the macromonomers as determined by <sup>1</sup>H NMR analysis, with the addition of the  $\alpha$ -acrylate end group.

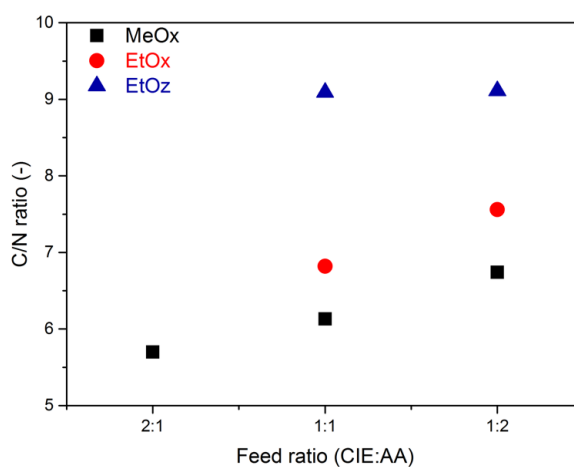


**Figure 2.10** Elemental analysis results for NPAE macromonomers.

### 2.2.7. Thermal analysis of NPAE macromonomers

In order to determine the thermal stability of these NPAE macromonomers, they were analysed by thermogravimetric analysis (TGA, Figure 2.11). No significant mass loss was observed for any of the macromonomers at temperatures up to 150 °C. Furthermore, it can be observed that the degradation profile depends on the monomers employed during the synthesis. For example, the AB<sub>2</sub>-type macromonomers obtained

from EtOx/CEA show a lower degradation onset compared to the macromonomers derived from AA, as well as an extra degradation step, which can be attributed to the presence of an extra ester in the macromonomer repeat unit.

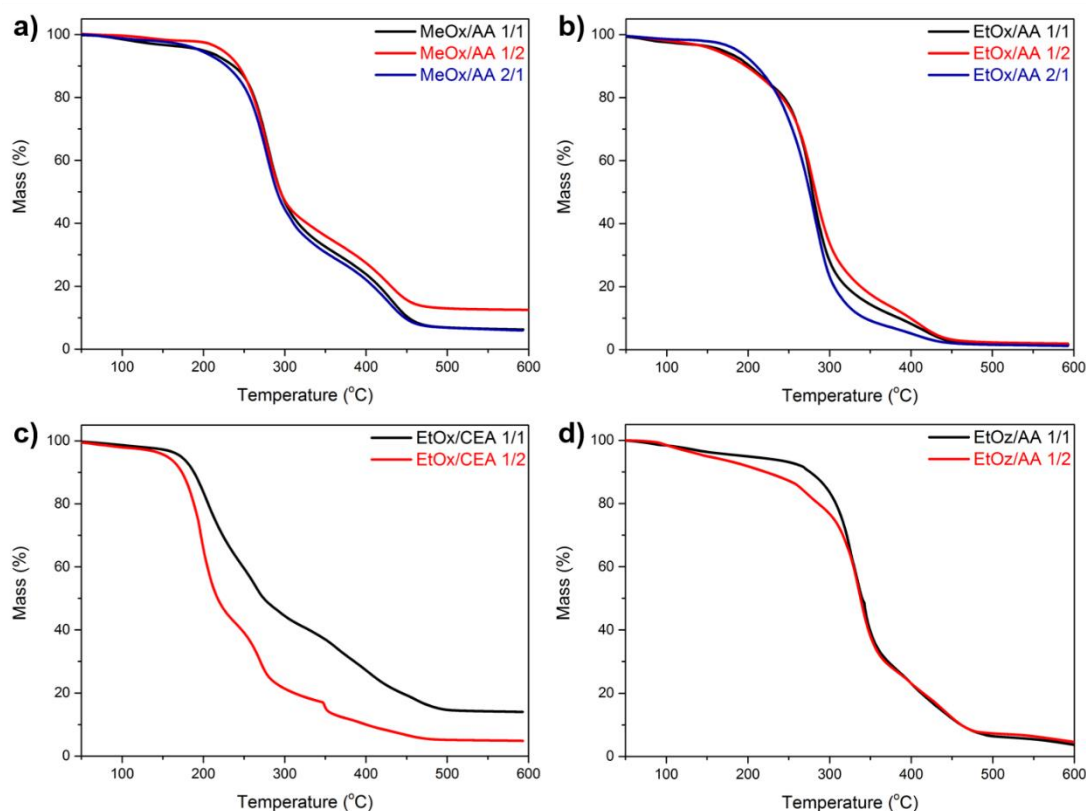


**Figure 2.11** Thermogravimetric analysis of NPAE macromonomers synthesised from MeOx/AA (a), EtOx/AA (b), EtOx/CEA (c) and EtOz/AA (d).

The thermal transitions were studied by differential scanning calorimetry (DSC, Figure 2.12 and Table 2.5). All macromonomers have glass transition temperatures ( $T_g$ s) below 0 °C, which correlates well to the observation that these macromonomers are viscous liquids at room temperature. It was observed that as the flexibility of the backbone increases, the  $T_g$  decreases, *e.g.* EtOx/CEA macromonomers show lower  $T_g$ s than EtOx/AA macromonomers.

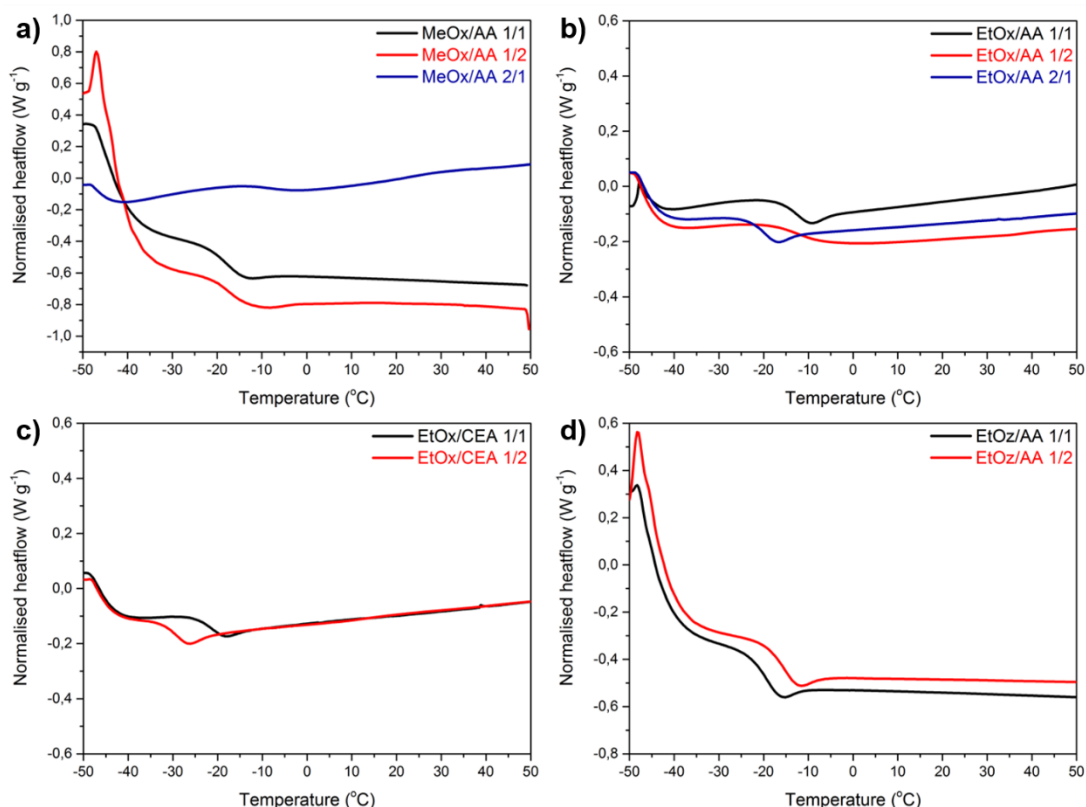


**Figure 2.12** DSC analysis (second heating curve) of NPAE macromonomers synthesised from MeOx/AA (a), EtOx/AA (b), EtOx/CEA (c) and EtOz/AA (d).

**Table 2.5** Glass transition temperatures for NPAE macromonomers.

Feed ratio	MeOx : AA	EtOx : AA	EtOx : CEA	EtOz : AA
2 : 1	- 6.6 °C	- 21.2 °C	n.d. <sup>a</sup>	n.d. <sup>a</sup>
1 : 1	- 17.0 °C	- 13.1 °C	- 21.8 °C	- 19.6 °C
1 : 2	- 14.9 °C	- 12.5 °C	- 30.0 °C	- 15.8 °C

Glass transition temperatures determined by DSC analysis on the second heating cycle.

<sup>a</sup> n.d. = not determined.

### 2.3. Conclusions

The spontaneous zwitterionic copolymerisation (SZWIP) of cyclic imino ethers with acidic acrylates is a relatively unknown, but interesting technique for the synthesis of *N*-acylated poly(aminoester) (NPAE) macromonomers. In this chapter the effect of the

reaction conditions on the resulting NPAE macromonomers was investigated. Even though the different reaction parameters generally have no significant effect on the DP of the resulting polymers and maintained quantitative introduction of the  $\alpha$ -acrylate group, it was demonstrated that the  $\omega$ -end group could be easily changed from 50 % carboxylic acid and 50 % amide end groups to quantitative introduction of the carboxylic acid functionality by employing an excess of AA during the SZWIP, thereby furnishing heterotelechelic materials. Furthermore, MALDI-ToF analysis demonstrated the presence of various distributions, both alternating and non-alternating species. This is further explored in Chapter 3. Elemental analysis confirmed an effect of the monomer feed ratio on the relative incorporation of the two monomers. Finally, it was shown that the NPAE macromonomers are thermally stable up to at least 150 °C and have glass transition temperatures between - 30 and 0 °C.

## 2.4. Experimental details

### 2.4.1. Materials

Acrylic acid (AA, 99 %, anhydrous, Sigma Aldrich), acetonitrile (MeCN, 99.8 %, anhydrous, Sigma Aldrich), 4-methoxyphenol (MEHQ, 99 %, Sigma Aldrich), diethyl ether (Et<sub>2</sub>O, > 98 %, Sigma Aldrich), *N,N*-dimethylformamide (DMF, 99.8 %, anhydrous, Sigma Aldrich), acetone (max. 0.0075 % H<sub>2</sub>O, anhydrous, Merck Millipore), sodium hydroxide standard solution (NaOH, 0.1001 M, Sigma Aldrich), hydrochloric acid (HCl, 37 %, Fisher Scientific), 2-carboxyethyl acrylate (CEA, 98 %, Sigma Aldrich), super-DHB (99 %, Sigma Aldrich), sodium iodide (NaI, > 99.5 %, Sigma Aldrich), poly(ethylene glycol) methyl ether methacrylate ( $M_w = 1100 \text{ g mol}^{-1}$ , > 99 %, Sigma Aldrich) and deuterated chloroform (CDCl<sub>3</sub>, 99.8 atom % D, Sigma Aldrich) were used as received. 2-Methyl-2-oxazoline (MeOx, 99 %, Acros Organics) and 2-ethyl-2-oxazoline (EtOx, > 99 %, Acros Organics) were distilled to dryness over barium oxide (BaO, 97 %, Sigma Aldrich) and stored under nitrogen. 2-Ethyl-2-oxazine

(EtOz) was synthesised according to literature procedure,<sup>52</sup> purified by distilling to dryness over BaO and stored under nitrogen.

## 2.4.2. Instruments and analysis

<sup>1</sup>H NMR spectra were recorded on a Bruker Avance III HD 400, Avance III HD 300 or Avance AV 300 spectrometer. Size exclusion chromatography (SEC) measurements were conducted using an Agilent 390-LC MDS fitted with differential refractive index (DRI), light scattering (LS) and viscometry (VS) detectors equipped with 2 x PLgel 5 mm mixed-D columns (300 x 7.5 mm), 1 x PLgel 5 mm guard column (50 x 7.5 mm) and autosampler. All samples were passed through 0.2 µm nylon filter before analysis. The mobile phase was DMF containing 5 mM NH<sub>4</sub>BF<sub>4</sub> with a flow rate of 1 mL min<sup>-1</sup> at 50 °C. SEC data was analysed using Agilent Technologies SEC software. Calibration curves were produced using Agilent Easi-Vials linear poly(methyl methacrylate) standards (200 – 4.7 x 10<sup>5</sup> g mol<sup>-1</sup>). MALDI-ToF spectra were recorded in reflection mode on a Bruker Daltonics Autoflex II MALDI-ToF mass spectrometer, equipped with a nitrogen laser delivering 2 ns pulses at 337 nm with positive ion ToF detection performed using an accelerating voltage of 25 kV. The matrix solution was prepared by dissolving super-DHB in MeOH (200 mg mL<sup>-1</sup>). Sodium iodide (NaI) was dissolved in MeOH (4 mg mL<sup>-1</sup>). Polymer samples were dissolved in MeOH (1 to 5 mg mL<sup>-1</sup>). The final MALDI solutions were prepared by mixing 20 µL of matrix solution with 5 µL of salt solution and 5 µL of polymer solution. Calibration was performed with a poly(ethylene glycol) methyl ether methacrylate (M<sub>w</sub> = 1100 g mol<sup>-1</sup>) standard. Acid-base titrations were performed on the macromonomers by dissolving them in water (9.5 mg mL<sup>-1</sup>). To protonate the carboxylic acid groups 0.1 M HCl was added. Subsequently, titration was run against 0.1001 M aqueous NaOH solution. Molecular weights determined by <sup>1</sup>H NMR spectroscopy were used to calculate the number of ω-carboxylic acid end groups. TGA spectra were recorded on a Mettler Toledo TGA/DSC1. Samples were analysed from 25 to 600 °C at a 10 °C min<sup>-1</sup> heating rate under a nitrogen atmosphere. DSC spectra were recorded on a Mettler Toledo DSC1. Samples were analysed from -50 to 50 °C at a 10 °C min<sup>-1</sup> heating rate under a nitrogen

atmosphere. Glass transition temperatures were determined on the second heating cycle. Elemental analysis was performed by Warwick Analytical Services.

### 2.4.3. Synthetic procedures

#### General procedure for the synthesis of macromonomers (example for M1)

In a dried Schlenk flask under nitrogen atmosphere equipped with a magnetic stirrer bar, MEHQ (1 mg,  $8.06 \times 10^{-6}$  mol) was dissolved in 7 mL of MeCN. To this were added MeOx (5.9 mL, 69.5 mmol) and AA (4.75 mL, 69.5 mmol) under nitrogen (see Table 2.6 for all macromonomers). The mixture was placed in a 70 °C oil bath for 24 h. Subsequently, the polymer solution was cooled down, precipitated in Et<sub>2</sub>O and isolated by centrifugation (three times) To remove the Et<sub>2</sub>O, the polymer was placed under vacuum to give the products as colourless-to-yellowish oils.

**Table 2.6** Quantities for the synthesis of the macromonomers.

Entry	CIE	Acrylate	CIE : acrylate	[CIE] [mol L <sup>-1</sup> ]	[acrylate] [mol L <sup>-1</sup> ]
1	MeOx	AA	1 : 1	9.92	9.92
2	MeOx	AA	1 : 2	4.48	9.92
3	MeOx	AA	2 : 1	6.32	3.16
4	EtOx	AA	1 : 1	9.92	9.92
5	EtOx	AA	1 : 2	6.60	13.2
6	EtOx	AA	2 : 1	2.48	1.24
7	EtOx	CEA	1 : 1	1.50	1.50
8	EtOx	CEA	1 : 2	4.00	8.00
9	EtOz	AA	1 : 1	3.32	3.32
10	EtOz	AA	1 : 2	2.21	4.42

Characterisation for MeOx/AA macromonomers.  $^1\text{H}$  NMR (400 MHz,  $\text{CDCl}_3$ ):  $\delta_{\text{H}}$  (ppm) 6.5-6.4 (d, 1H,  $\text{CH}_a\text{H}_b=\text{CH}$ ), 6.2-6.0 (t, 1H,  $\text{CH}_2=\text{CHCOO}$ ), 6.0-5.8 (d, 1H,  $\text{CH}_a\text{CH}_b=\text{CH}$ ), 4.4-4.2 (m, 6H,  $\text{COOCH}_2$ ), 3.8-3.4 (m, 12H,  $\text{CH}_2\text{N}(\text{COCH}_3)\text{CH}_2$ ), 2.7-2.5 (m, 6H,  $\text{CH}_2\text{COO}$ ), 2.2-2.0 (m, 9H,  $\text{NCOCH}_3$ ).  $\text{DP}_{\text{NMR}} = 3$ ,  $M_{n,\text{NMR}} = 543 \text{ g mol}^{-1}$ . SEC:  $M_n = 1500 \text{ g mol}^{-1}$ ,  $D_{\text{SEC}} = 1.27$ .

Characterisation for EtOx/AA macromonomers.  $^1\text{H}$  NMR (400 MHz,  $\text{CDCl}_3$ ):  $\delta_{\text{H}}$  (ppm) 6.5-6.4 (d, 1H,  $\text{CH}_a\text{H}_b=\text{CH}$ ), 6.2-6.0 (t, 1H,  $\text{CH}_2=\text{CHCOO}$ ), 6.0-5.8 (d, 1H,  $\text{CH}_a\text{CH}_b=\text{CH}$ ), 4.4-4.2 (m, 6H,  $\text{COOCH}_2$ ), 3.8-3.4 (m, 12H,  $\text{CH}_2\text{N}(\text{COCH}_3)\text{CH}_2$ ), 2.7-2.5 (m, 6H,  $\text{CH}_2\text{COO}$ ), 2.5-2.3 (m, 6H,  $\text{NCOCH}_2\text{CH}_3$ ), 1.3-1.0 (m, 9H,  $\text{NCOCH}_2\text{CH}_3$ ).  $\text{DP}_{\text{NMR}} = 3$ ,  $M_{n,\text{NMR}} = 585 \text{ g mol}^{-1}$ . SEC:  $M_{n,\text{SEC}} = 1600 \text{ g mol}^{-1}$ ,  $D_{\text{SEC}} = 1.22$ .

Characterisation for EtOx/CEA macromonomers.  $^1\text{H}$  NMR (400 MHz,  $\text{CDCl}_3$ ):  $\delta_{\text{H}}$  (ppm) 6.5-6.4 (d, 1H,  $\text{CH}_a\text{H}_b=\text{CH}$ ), 6.2-6.0 (t, 1H,  $\text{CH}_2=\text{CHCOO}$ ), 6.0-5.8 (d, 1H,  $\text{CH}_a\text{CH}_b=\text{CH}$ ), 4.4-4.2 (m, 14H,  $\text{COOCH}_2$ ), 3.8-3.4 (m, 12H,  $\text{CH}_2\text{N}(\text{COCH}_3)\text{CH}_2$ ), 2.7-2.5 (m, 14H,  $\text{CH}_2\text{COO}$ ), 2.5-2.3 (m, 6H,  $\text{NCOCH}_2\text{CH}_3$ ), 1.3-1.0 (m, 9H,  $\text{NCOCH}_2\text{CH}_3$ ).  $\text{DP}_{\text{NMR}} = 3$ ,  $M_{n,\text{NMR}} = 996 \text{ g mol}^{-1}$ . SEC:  $M_n = 1700 \text{ g mol}^{-1}$ ,  $D_{\text{SEC}} = 1.32$ .

Characterisation for EtOz/AA macromonomers.  $^1\text{H}$  NMR (400 MHz,  $\text{CDCl}_3$ ):  $\delta_{\text{H}}$  (ppm) 6.5-6.4 (d, 1H,  $\text{CH}_a\text{H}_b=\text{CH}$ ), 6.2-6.0 (t, 1H,  $\text{CH}_2=\text{CHCOO}$ ), 6.0-5.8 (d, 1H,  $\text{CH}_a\text{CH}_b=\text{CH}$ ), 4.4-4.2 (m, 6H,  $\text{COOCH}_2$ ), 3.8-3.4 (m, 12H,  $\text{CH}_2\text{N}(\text{COCH}_3)\text{CH}_2$ ), 2.7-2.5 (m, 6H,  $\text{CH}_2\text{COO}$ ), 2.5-2.3 (m, 6H,  $\text{NCOCH}_2\text{CH}_3$ ), 2.0-1.7 (m, 6H,  $\text{CH}_2\text{CH}_2\text{CH}_2$ ), 1.3-1.0 (m, 9H,  $\text{NCOCH}_2\text{CH}_3$ ).  $\text{DP}_{\text{NMR}} = 3$ ,  $M_{n,\text{NMR}} = 627 \text{ g mol}^{-1}$ . SEC:  $M_n = 2000 \text{ g mol}^{-1}$ ,  $D_{\text{SEC}} = 1.27$ .

## 2.5. References

- 1 L. S. Nair and C. T. Laurencin, *Prog. Polym. Sci.*, 2007, **32**, 762–798.
- 2 M. Winnacker and B. Rieger, *Polym. Chem.*, 2016, **7**, 7039–7046.
- 3 A. Rodriguez-Galan, L. Franco and J. Puiggali, *Polymers*, 2011, **3**, 65–99.
- 4 A. C. Fonseca, M. H. Gil and P. N. Simões, *Prog. Polym. Sci.*, 2014, **39**, 1291–1311.

- 5 H. Sun, F. Meng, A. A. Dias, M. Hendriks, J. Feijen and Z. Zhong, *Biomacromolecules*, 2011, **12**, 1937–1955.
- 6 M. Okada, *Prog. Polym. Sci.*, 2002, **27**, 87–133.
- 7 A. Díaz, R. Katsarava and J. Puiggali, *Int. J. Mol. Sci.*, 2014, **15**, 7064–7123.
- 8 A. Basu, K. R. Kunduru, J. Katzhendler and A. J. Domb, *Adv. Drug Deliv. Rev.*, 2016, **107**, 82–96.
- 9 Y. Feng, J. Lu, M. Behl and A. Lendlein, *Macromol. Biosci.*, 2010, **10**, 1008–1021.
- 10 W. Cheng, D. Wu and Y. Liu, *Biomacromolecules*, 2016, **17**, 3115–3126.
- 11 J. J. Green, R. Langer and D. G. Anderson, *Acc. Chem. Res.*, 2008, **41**, 749–759.
- 12 D. Wu, Y. Liu, X. Jiang, L. Chen, C. He, S. H. Goh and K. W. Leong, *Biomacromolecules*, 2005, **6**, 3166–3173.
- 13 A. Akinc, D. G. Anderson, D. M. Lynn and R. Langer, *Bioconjug. Chem.*, 2003, **14**, 979–88.
- 14 B. D. Mather, K. Viswanathan, K. M. Miller and T. E. Long, *Prog. Polym. Sci.*, 2006, **31**, 487–531.
- 15 S. Gokhale, Y. Xu and A. Joy, *Biomacromolecules*, 2013, **14**, 2489–2493.
- 16 J. P. Swanson, L. R. Monteleone, F. Haso, P. J. Costanzo, T. Liu and A. Joy, *Macromolecules*, 2015, **48**, 3834–3842.
- 17 J. P. Swanson, M. R. Martinez, M. A. Cruz, S. G. Mankoci, P. J. Costanzo and A. Joy, *Polym. Chem.*, 2016, **7**, 4693–4702.
- 18 Y. Wang, S. Gao, W.-H. Ye, H. S. Yoon and Y.-Y. Yang, *Nat. Mater.*, 2006, **5**, 791–796.
- 19 J. Zhou, J. Liu, C. J. Cheng, T. R. Patel, C. E. Weller, J. M. Piepmeier, Z. Jiang and W. M. Saltzman, *Nat. Mater.*, 2012, **11**, 82–90.
- 20 Y. B. Lim, S. M. Kim, Y. Lee, W. K. Lee, T. G. Yang, M. J. Lee, H. Suh and J. S. Park, *J. Am. Chem. Soc.*, 2001, **123**, 2460–2461.
- 21 T. R. Blake and R. M. Waymouth, *J. Am. Chem. Soc.*, 2014, **136**, 9252–9255.
- 22 B. M. Culbertson, *Prog. Polym. Sci.*, 2002, **27**, 579–626.
- 23 K. Kempe, *Macromol. Chem. Phys.*, 2017, **218**, 1700021.
- 24 K. Aoi and M. Okada, *Prog. Polym. Sci.*, 1996, **21**, 151–208.
- 25 S. Kobayashi and H. Uyama, *J. Polym. Sci. A Polym. Chem.*, 2002, **40**, 192–209.
- 26 A. Makino and S. Kobayashi, *J. Polym. Sci. A Polym. Chem.*, 2010, **48**, 1251–

- 1270.
- 27 B. Verbraeken, B. D. Monnery, K. Lava and R. Hoogenboom, *Eur. Polym. J.*, 2016, **88**, 451–469.
- 28 D. A. Tomalia and D. P. Sheetz, *J. Polym. Sci. A Polym. Chem.*, 1966, **4**, 2253–2265.
- 29 W. Seeliger, E. Aufderhaar, W. Diepers, R. Feinauer, R. Nehring, W. Thier and H. Hellmann, *Angew. Chem. Int. Ed.*, 1966, **5**, 875–888.
- 30 T. Kagiya, T. Maeda, K. Fukui and S. Narisawa, *Polym. Lett.*, 1966, **4**, 441–445.
- 31 B. Guillerm, S. Monge, V. Lapinte and J. J. Robin, *Macromol. Rapid Commun.*, 2012, **33**, 1600–1612.
- 32 K. Lava, B. Verbraeken and R. Hoogenboom, *Eur. Polym. J.*, 2015, **65**, 98–111.
- 33 E. Rossegger, V. Schenk and F. Wiesbrock, *Polymers*, 2013, **5**, 956–1011.
- 34 M. Bauer, S. Schroeder, L. Tauhardt, K. Kempe, U. S. Schubert and D. Fischer, *J. Polym. Sci. A Polym. Chem.*, 2013, **51**, 1816–1821.
- 35 M. Bauer, C. Lautenschlaeger, K. Kempe, L. Tauhardt, U. S. Schubert and D. Fischer, *Macromol. Biosci.*, 2012, **12**, 986–998.
- 36 R. Hoogenboom, *Angew. Chem. Int. Ed.*, 2009, **48**, 7978–7994.
- 37 K. Knop, R. Hoogenboom, D. Fischer and U. S. Schubert, *Angew. Chem. Int. Ed.*, 2010, **49**, 6288–6308.
- 38 O. Sedlacek, B. D. Monnery, S. K. Filippov, R. Hoogenboom and M. Hruby, *Macromol. Rapid Commun.*, 2012, **33**, 1648–1662.
- 39 N. Adams and U. S. Schubert, *Adv. Drug Deliv. Rev.*, 2007, **59**, 1504–1520.
- 40 H. Bludau, A. E. Czapar, A. S. Pitek, S. Shukla, R. Jordan and N. F. Steinmetz, *Eur. Polym. J.*, 2017, **88**, 679–688.
- 41 V. R. De La Rosa, *J. Mater. Sci. Mater. Med.*, 2014, **25**, 1211–1225.
- 42 M. Hartlieb, K. Kempe and U. S. Schubert, *J. Mater. Chem. B*, 2015, **3**, 526–538.
- 43 R. Luxenhofer, Y. Han, A. Schulz, J. Tong, Z. He, A. V Kabanov and R. Jordan, *Macromol. Rapid Commun.*, 2012, **33**, 1613–1631.
- 44 T. Saegusa, Y. Kimura and S. Kobayashi, *Macromolecules*, 1977, **10**, 236–239.
- 45 T. Saegusa, S. Kobayashi and Y. Kimura, *Macromolecules*, 1974, **7**, 139–140.
- 46 T. Saegusa, H. Ikeda and H. Fujii, *Macromolecules*, 1972, **5**, 354–359.
-

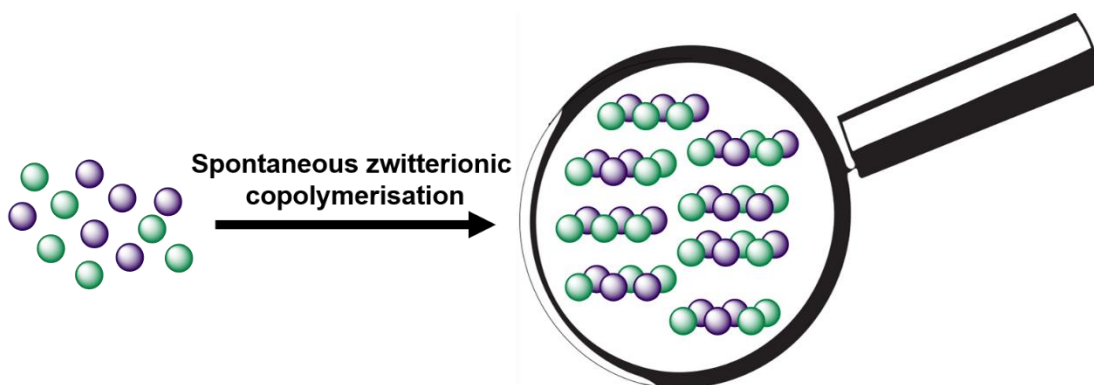
- 47 T. Saegusa, S. Kobayashi and Y. Kimura, *Macromolecules*, 1974, **7**, 1–4.
- 48 B. L. Rivas, G. S. Canessa and S. A. Pooley, *Eur. Polym. J.*, 1989, **25**, 225–230.
- 49 B. L. Rivas, G. S. Canessa and S. A. Pooley, *Makromol. Chem.*, 1987, **188**, 149–154.
- 50 B. L. Rivas, G. S. Canessa and S. A. Pooley, *Makromol. Chem.*, 1986, **187**, 71–79.
- 51 G. Odian and P. A. Gunatillake, *Macromolecules*, 1984, **17**, 1297–1307.
- 52 H. Witte and W. Seeliger, *Angew. Chem. Int. Ed.*, 1972, **11**, 287–288.

## Chapter 3

---

# Mechanistic studies on the spontaneous zwitterionic copolymerisation of cyclic imino ethers and acrylic acid

---



This chapter has been published:

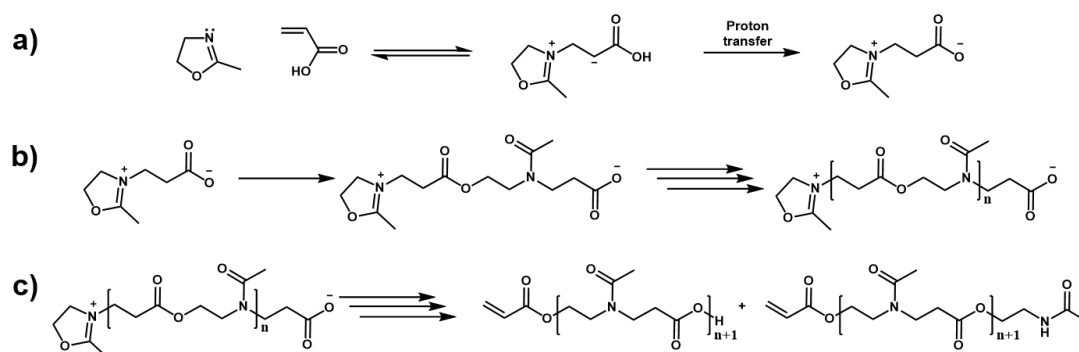
J. Steinkoenig, P.A.J.M. de Jongh, D.M. Haddleton, A.S. Goldmann, C. Barner-Kowollik, K. Kempe, *Macromolecules* **2018**, 51, 318-327

### 3.1. Introduction

The spontaneous zwitterionic copolymerisation (SZWIP) of nucleophilic ( $M_N$ ) and electrophilic monomers ( $M_E$ ) was introduced in the 1970s by Saegusa and co-workers when they reported its first example: the SZWIP of unsubstituted 2-oxazoline with  $\beta$ -propiolactone.<sup>1</sup> Since then, many other monomers capable of partaking in SZWIP have been investigated,<sup>2</sup> leading to a broad range of polymers that can be synthesised using this technique, including *N*-acylated poly(aminoester)s (NPAEs), poly(ester amide)s and poly(phosphoester)s. Despite the technique existing for over four decades, the analysis of the copolymers obtained by SZWIP and investigations into the SZWIP mechanism have been limited. In general, the copolymers have only been characterised by <sup>1</sup>H NMR analysis, vapour pressure osmometry and elemental analysis.

It is based on these limited analyses that Saegusa and co-workers proposed the mechanism for the SZWIP of 2-oxazolines with acrylic acid (AA).<sup>3</sup> Illustrated in Scheme 3.1 for the SZWIP of 2-methyl-2-oxazoline (MeOx) with AA, they postulated that upon mixing the monomers, an aza-Michael addition from MeOx to AA produces a carbocation that swiftly rearranges *via* a proton transfer into a zwitterionic species, termed the *genetic zwitterion* (a). This first step is considered to be reversible and depends on the equilibrium between the two monomers. Subsequently, two of these genetic zwitterions then propagate into a dimer by ring-opening of the oxazolinium ion by the carboxylate (b). Successive repeats of this ring-opening propagation then lead to higher degrees of polymerisation (DP). Odian and Gunatillake later investigated the polymer end groups.<sup>4</sup> An  $\alpha$ -acrylate end group is quantitatively introduced by ring-opening of an oxazolinium ion by AA. Two  $\omega$ -end groups can be introduced; a carboxylic acid is obtained by protonation of the carboxylate group, whereas an amide is formed if the carboxylate ring-opens a MeOx monomer.<sup>4</sup> In Chapter 2 it was shown that the  $\omega$ -end group can be easily tuned from 50 % carboxylic acids and 50 % amides for an equimolar feed ratio to (near-)quantitative introduction of an  $\omega$ -carboxylic acid group by changing the feed ratio to CIE:AA 1:2. Saegusa and co-workers previously isolated the genetic zwitterion formed by SZWIP of 2-phenyl-2-oxazoline with AA which supports this mechanism.<sup>5</sup>

Mechanistic studies on the spontaneous zwitterionic copolymerisation of cyclic imino ethers and acrylic acid



**Scheme 3.1** Mechanism for the SZWIP of MeOx and AA as proposed by Saegusa *et al.*<sup>3</sup>

In Chapter 2 the SZWIP between three different cyclic imino ethers, MeOx, 2-ethyl-2-oxazoline (EtOx) and 2-ethyl-2-oxazine (EtOz), and AA was investigated. The effect of various reaction conditions on the resulting copolymers was reported, revealing the formation of oligomers in these reactions. Interestingly, the results obtained from matrix-assisted laser desorption/ionisation-time of flight (MALDI-ToF) mass spectrometry analysis suggested the presence of several species. In addition to peaks that support an alternating structure, the spectra suggested the presence of homopropagation of the CIE, which is hypothesised to be the result of cationic ring-opening polymerisation (CROP) of the CIE taking place as a side reaction. It was observed that the extent of non-alternating species was dependant on the CIE, as well as the feed ratio of the two monomers. Furthermore, elemental analysis gave different results for different feed ratios of the same monomer combination, suggesting that the extent of incorporation of the two monomers can be influenced by the feed ratio of the CIE and AA.

Intrigued by these observations, it was decided to further investigate this behaviour in an attempt to further elucidate the SZWIP mechanism. There is a vast amount of literature investigating the mechanism of the CROP of 2-oxazolines into poly(2-oxazoline)s (POx),<sup>6-13</sup> which are structurally similar to the NPAEs investigated in this work.

In order to gain a better understanding of the SZWIP process, it was investigated using electrospray ionisation mass spectrometry (ESI MS). MS is a versatile technique that has been extensively used for the analysis of (co-)polymers, including the elucidation

of polymerisation mechanisms.<sup>11–14</sup> Collision-induced dissociation (CID)<sup>15</sup> – optionally in combination with higher energy collision dissociation (HCD)<sup>16</sup> – enables the detection of fragment ions from which structural information of the precursor ion can be deduced. By isolating a single isotope pattern in the HCD chamber, tandem MS can be used for quantitative comparison of isobaric species. However, this is only valid if the ionisation efficiency of the different species is not effected by chain termini, chain length, salt concentrations, hydrophobicity and surface activity of the analyte.<sup>17,18</sup> Quantification can be achieved through the molar fractions of the peaks within a single spectrum,<sup>19,20</sup> or by establishing a calibration curve to provide absolute quantities.<sup>17,18,21</sup> The first method can only be applied if the different species in an analyte have chain termini independent ionisation, efficient ion transmission<sup>19</sup> and the samples have identical molecular weights.<sup>22</sup> The latter is not typically the case for polymerisations as they produce molecular weight distributions. Moreover, the MALDI-ToF analysis in Chapter 2 strongly suggests different ionisation efficiencies for the two  $\omega$ -termini of the NPAE macromonomers.<sup>23</sup> It is for that reason that calibrating against a small molecule should provide more accurate results.

This Chapter discusses the post-mortem ESI MS and MS/MS investigation of NPAE macromonomers. After analysis by conventional ESI MS to obtain information about which species are present, analysis with MS/MS to evidence the presence of side reactions and semi-quantification of these side reactions and the chain termini are investigated.

## 3.2. Results and discussion

### 3.2.1. Macromonomer synthesis

A small library of seven macromonomers was synthesised by SZWIP of three CIEs with AA. Specifically, MeOx, EtOx and EtOz were copolymerised in 1:1 and 1:2 ratios with AA, while MeOx was also copolymerised in a 2:1 ratio with AA. Table 3.1 provides an overview of the macromonomers and their analysis results by <sup>1</sup>H NMR and

SEC. Their synthetic details, including  $^1\text{H}$  NMR and SEC analysis, can be found in the experimental details (Section 3.4.3, Figure 3.16).

**Table 3.1** Overview of the macromonomers studied in this work.

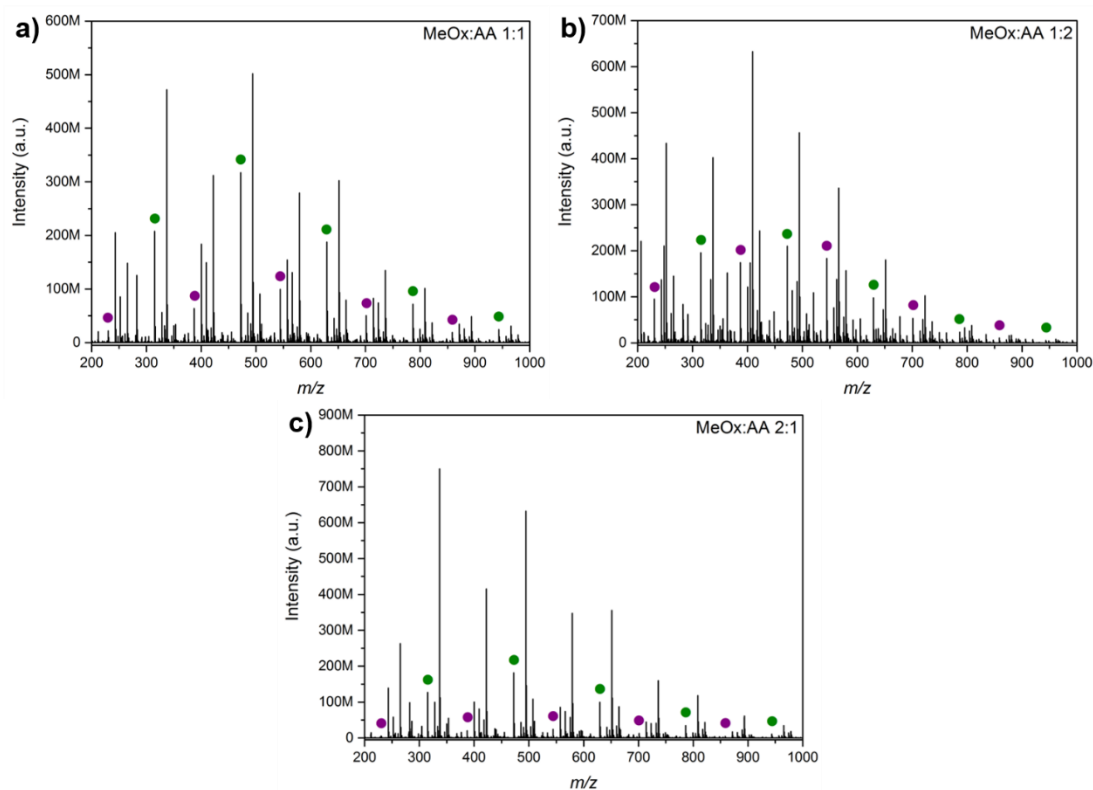
CIE	CIE:AA	DP <sup>a</sup>	M <sub>n,NMR</sub> <sup>a</sup>	M <sub>n,SEC</sub> <sup>b</sup>	Đ <sub>SEC</sub> <sup>b</sup>
		[CIE/AA]	[g mol <sup>-1</sup> ]	[g mol <sup>-1</sup> ]	
<b>MeOx</b>	2:1	2.5/2.5	465	1800	1.32
	1:1	2.5/2.5	465	1300	1.18
	1:2	3/3	543	1500	1.27
<b>EtOx</b>	1:1	2.5/2.5	500	1600	1.30
	1:2	2/2	414	1300	1.17
<b>EtOz</b>	1:1	3/3	627	2000	1.27
	1:2	2.5/2.5	535	1600	1.20

<sup>a</sup> Determined from  $^1\text{H}$  NMR analysis by integration of the  $\alpha$ -acrylate group against the repeat units of the CIE and AA. <sup>b</sup> Determined by SEC analysis.

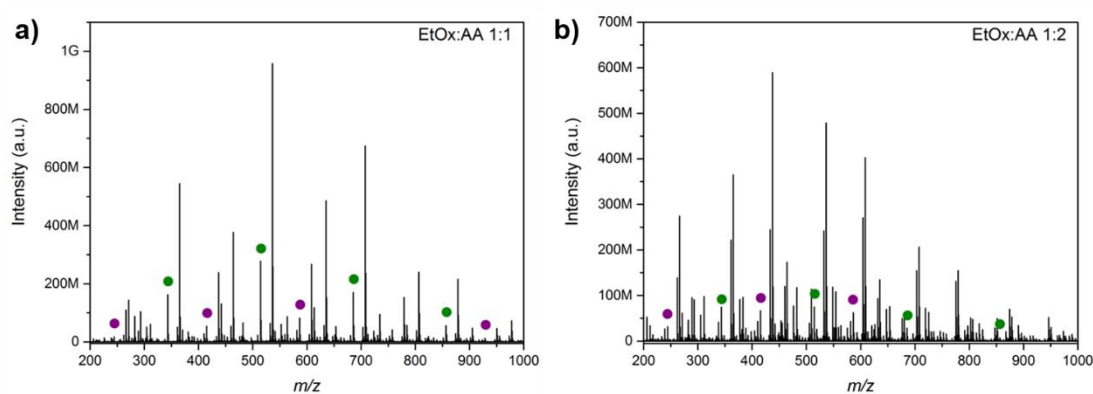
### 3.2.2. ESI MS analysis of macromonomers

The NPAE macromonomers were first analysed by conventional ESI MS to obtain a general impression of which species are present in each sample. Unlike the MALDI-ToF MS discussed in Chapter 2, ESI MS does not allow selective targeting of specific adducts and therefore the spectra contained a mixture of protonated and sodiated adducts. Figures 3.1 – 3.3 show the overview spectra of the seven macromonomers. For clarity, only the proton adducts are labelled. It can be clearly observed that changing the monomer feed ratio directly influences the  $\omega$ -end groups; an increase in AA in the monomer feed results in an increased amount of  $\omega$ -carboxylic acid end groups, based on the relative peak intensities, which is consistent with the MALDI-ToF MS results.

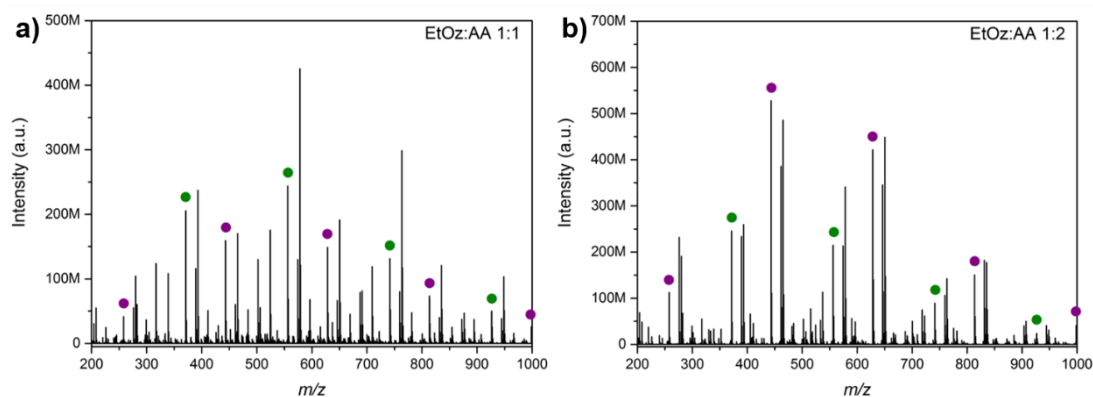
## Mechanistic studies on the spontaneous zwitterionic copolymerisation of cyclic imino ethers and acrylic acid



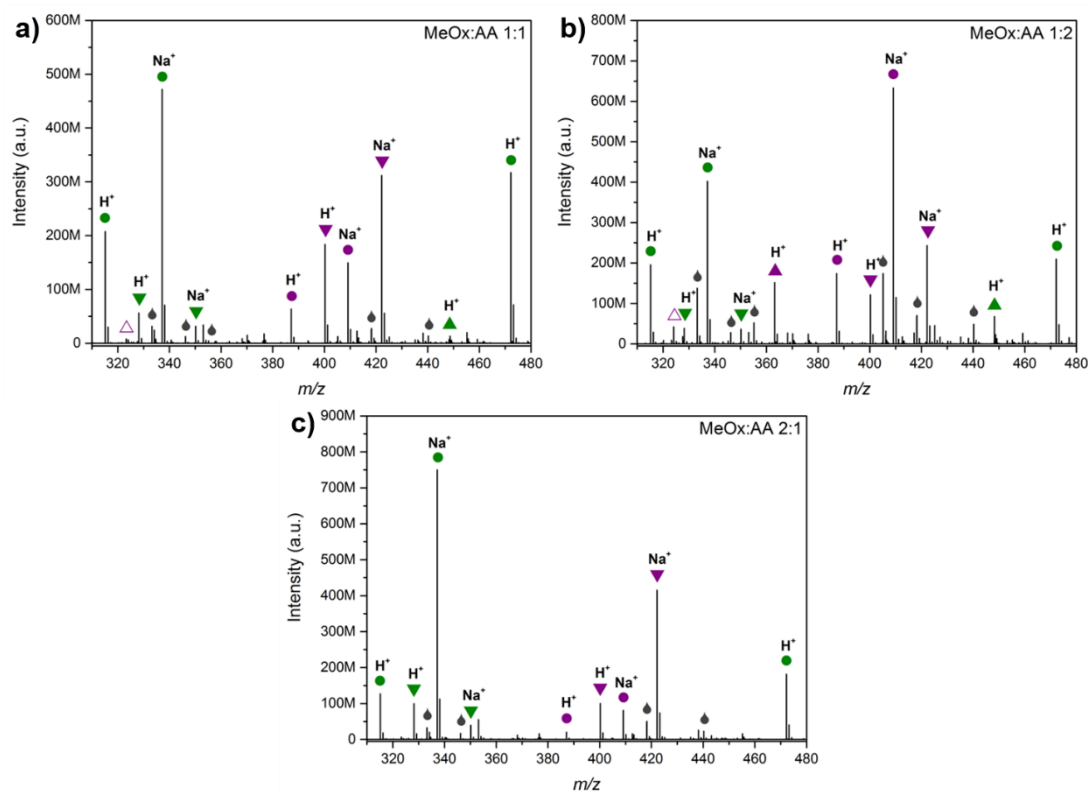
**Figure 3.1** Overview ESI MS spectra for oligo(MeOx-*alt*-AA)<sub>n</sub>A copolymers from MeOx:AA 1:1 (a), 1:2 (b) and 2:1 (c) feed ratios. Purple circles correspond to ω-carboxylic acid terminated H<sup>+</sup> ionised species, green circles correspond to ω-amide terminated H<sup>+</sup> ionised species.



**Figure 3.2** Overview ESI MS spectra for oligo(EtOx-*alt*-AA)<sub>n</sub>A copolymers from EtOx:AA 1:1 (a) and 1:2 (b) feed ratios. Purple circles correspond to ω-carboxylic acid terminated H<sup>+</sup> ionised species, green circles correspond to ω-amide terminated H<sup>+</sup> ionised species.



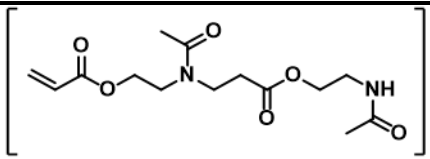
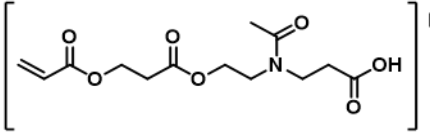
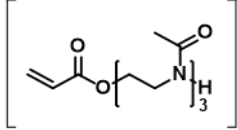
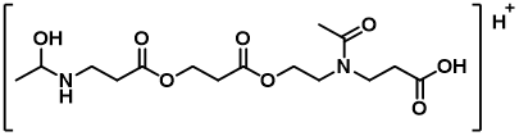
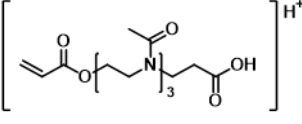
**Figure 3.3** Overview ESI MS spectra for oligo(EtOz-*alt*-AA)<sub>n</sub>A copolymers from EtOz:AA 1:1 (a) and 1:2 (b) feed ratios. Purple circles correspond to ω-carboxylic acid terminated H<sup>+</sup> ionised species, green circles correspond to ω-amide terminated H<sup>+</sup> ionised species.



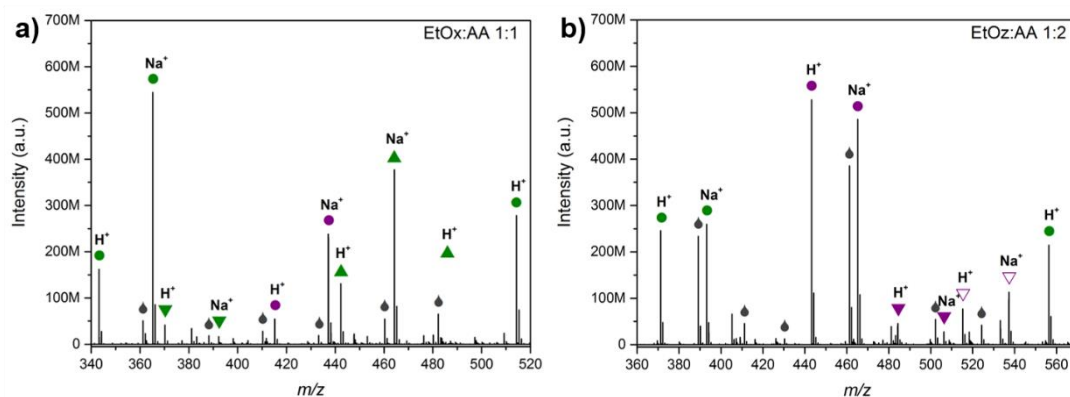
**Figure 3.4** Expanded ESI MS spectra for oligo(MeOx-*alt*-AA)<sub>n</sub>A macromonomers from MeOx:AA 1:1 (a), 1:2 (b) and 2:1 (c) feed ratios, showing all species within one repeat unit. A generalised peak assignment is shown in Table 3.2.

Figure 3.4 shows the ESI MS spectra within one repeat unit for oligo(MeOx-*alt*-AA)<sub>n</sub>A macromonomers in which all species are labelled. A complete assignment can be found in Table 3.2. The peak at  $m/z^{\text{exp}} = 315.1544$  corresponds to MeOx/AA 2/2 and supports an alternating microstructure. The peak at  $m/z^{\text{exp}} = 324.1047$  corresponds to MeOx/AA 1/3, suggesting homopropagation of AA *via* a Michael addition.<sup>24</sup> This peak is most prominent when an excess of AA is used during the SZWIP. A more prominent peak that can be observed in all spectra is at  $m/z^{\text{exp}} = 328.1859$ . This peak matches MeOx/AA 3/1 and is almost equally abundant in all spectra. Importantly, this peak supports the presence of homopropagation of the CIE as a side reaction during SZWIP. In similar fashion the ESI MS spectra within one repeat unit of the other two macromonomers were analysed (Figure 3.5/Table 3.3 and Figure 3.6/Table 3.4).

**Table 3.2** Peak assignment for the MeOx:AA ESI MS spectra (Figure 3.4).

Label	$m/z^{\text{exp}}$	$m/z^{\text{theo}}$	$\Delta m/z$	Structure <sup>a</sup>
●	315.1544	315.1552	0.0012	
△	324.1047	324.1054	0.0007	
▼	328.1859	328.1867	0.0008	
◆	363.1752	363.1762	0.0010	
▼	400.2067	400.2078	0.0011	

<sup>a</sup> One of various isobaric structures is shown.



**Figure 3.5** Expanded ESI MS spectra for oligo(EtOx-*alt*-AA)<sub>n</sub>A macromonomers from EtOx:AA 1:1 (a) and 1:2 (b) feed ratios, showing all species within one repeat unit. A generalised peak assignment is shown in Table 3.3.

**Table 3.3** Peak assignment for the EtOx:AA ESI MS spectra (Figure 3.5).

Label	$m/z^{\text{exp}}$	$m/z^{\text{theo}}$	$\Delta m/z$	Structure <sup>a</sup>
△	324.1047	324.1054	0.0007	
●	343.1859	343.1864	0.0005	
▼	370.2329	370.2336	0.0007	
●	415.2063	415.2075	0.0012	
▲	442.2535	442.2548	0.0013	

<sup>a</sup> One of various isobaric structures shown.

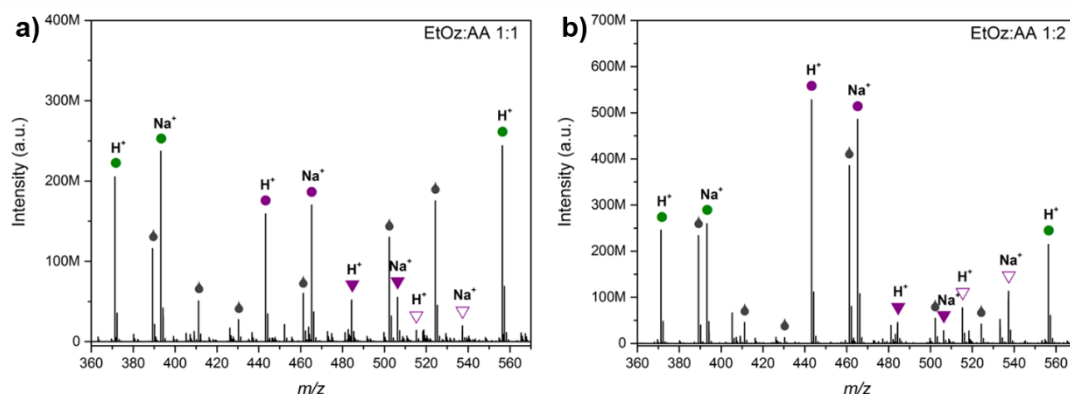


**Figure 3.6** Expanded ESI MS spectra for oligo(EtOz-*alt*-AA)<sub>n</sub>A macromonomers from EtOz:AA 1:1 (a) and 1:2 (b) feed ratios, showing all species within one repeat unit. A generalised peak assignment is shown in Table 3.4.

**Table 3.4** Peak assignment for the EtOz:AA ESI MS spectra (Figure 3.6).

Label	$m/z^{\text{exp}}$	$m/z^{\text{theo}}$	$\Delta m/z$	Structure <sup>a</sup>
●	371.2168	371.2177	0.0009	
●	443.2378	443.2382	0.0004	
▼	484.3006	484.3012	0.0006	
▽	515.2589	515.2594	0.0005	

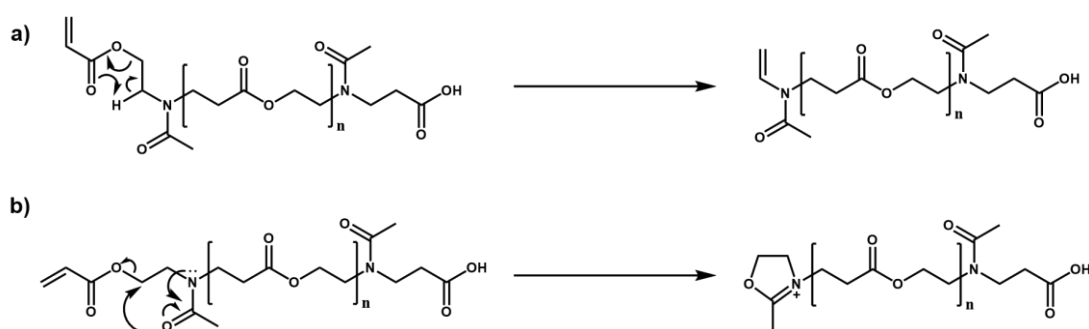
<sup>a</sup> One of various isobaric structures shown.

The species observed in the spectra for oligo(EtOx-*alt*-AA)<sub>n</sub>A and oligo(EtOz-*alt*-AA)<sub>n</sub>A are similar to those discussed for oligo(MeOx-*alt*-AA)<sub>n</sub>A. This suggests that the choice of CIE does not have a significant effect on the types of species produced. However, any given peak may harbour multiple isobaric structures and their (relative) presence may be directly influenced by the CIE employed. In order to further investigate this, as well as gain more insight about species that suggest homopropagation, tandem mass spectrometry (MS/MS) investigations were carried out.

### 3.2.3. Tandem mass spectrometry

The ESI MS analysis of the macromonomers demonstrated similar results as their MALDI-ToF analysis (Chapter 2). In an attempt to unambiguously identify the different microstructures formed during SZWIP of CIEs and AA, MS/MS analysis was employed. A benefit of the Orbitrap ESI MS used in this work is the ability to store a precursor ion in the HCD before fragmentation. This then enabled selective fragmentation of a single species from the original MS spectrum.

One of the key aspects of MS/MS is to develop a plausible fragmentation mechanism.<sup>25,26</sup> From the POx literature on MS/MS, two possible fragmentation mechanisms can be proposed, as shown in Scheme 3.2.<sup>11</sup>

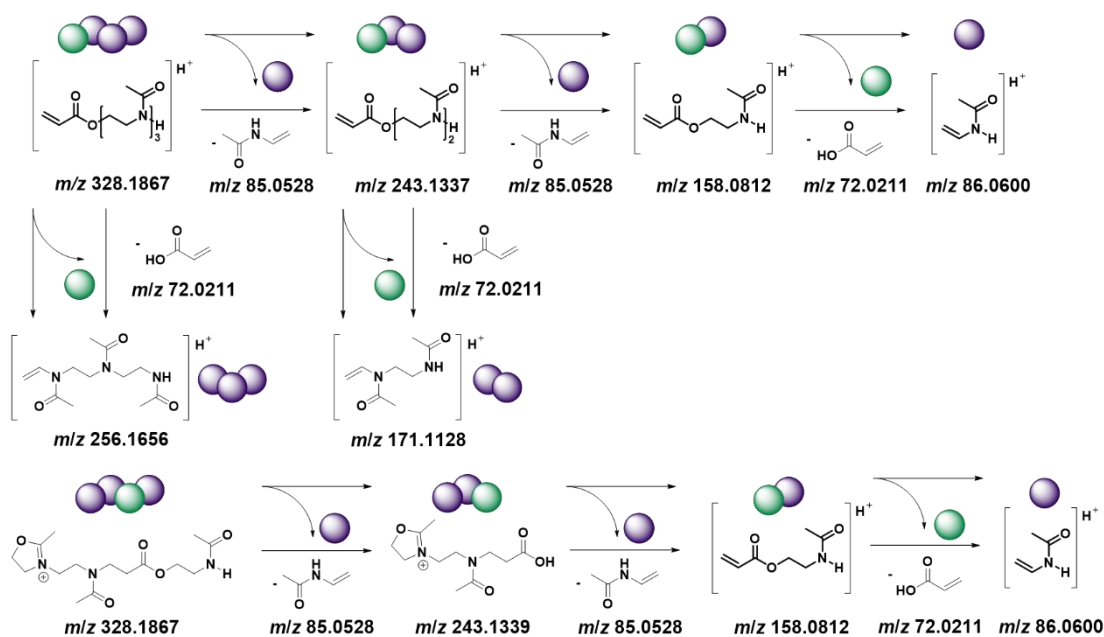


**Scheme 3.2** Fragmentation pathways for NPAE macromonomers in MS/MS *via* a concerted mechanism (a) and a ring-closure mechanism (b).

The first one is a concerted fragmentation *via* a six-membered transition state. This mechanism deliberates both chain termini and main chain fragments (Scheme 3.2a). The other mechanism proceeds *via* a ring closure depolymerisation and exclusively takes place in the  $\beta$ -position to the acetamide functionality (Scheme 3.2b). Based on the identified fragments in this work (*vide infra*) it was proposed that the concerted mechanism is favoured in the MS/MS fragmentation of NPAE macromonomers.

### 3.2.4. Evidencing microstructures

The primary objective of this MS/MS study was to prove the different microstructures suggested by the MALDI-ToF MS analysis in Chapter 2. This is discussed for selected species as examples. The signal at  $m/z^{\text{exp}} = 328.1867$  corresponds to MeOx/AA 3/1. Based on a concerted fragmentation mechanism, several species can be predicted to be found upon fragmentation of the parent peak (Scheme 3.3). The key fragments for homopropagation are  $m/z^{\text{theo}} = 171.1127$  (MeOx<sub>2</sub>) and  $m/z^{\text{theo}} = 256.1656$  (MeOx<sub>3</sub>), and  $m/z^{\text{exp}} = 158.0812$  for an alternating copolymerisation.



**Scheme 3.3** Fragmentation of two isobaric structures for MeOx/AA at  $m/z^{\text{exp}} = 328.1867$ .

The observed fragmentation with HCD = 25 eV for this species is shown in Figure 3.7. The predicted fragmentation products can be observed. Table 3.5 shows an overview of the peaks observed in the fragmentation spectrum and Scheme 3.4 the full fragmentation scheme based on the observed peaks.

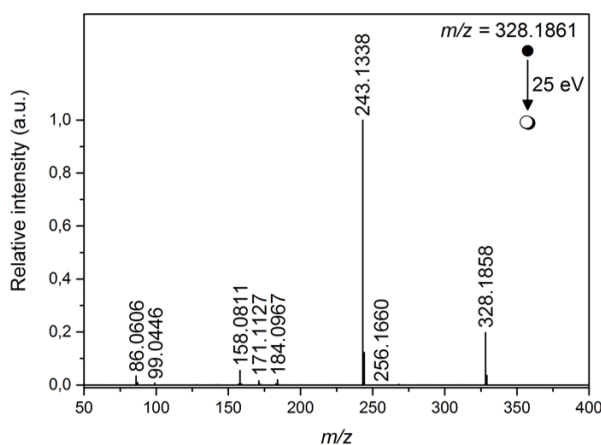
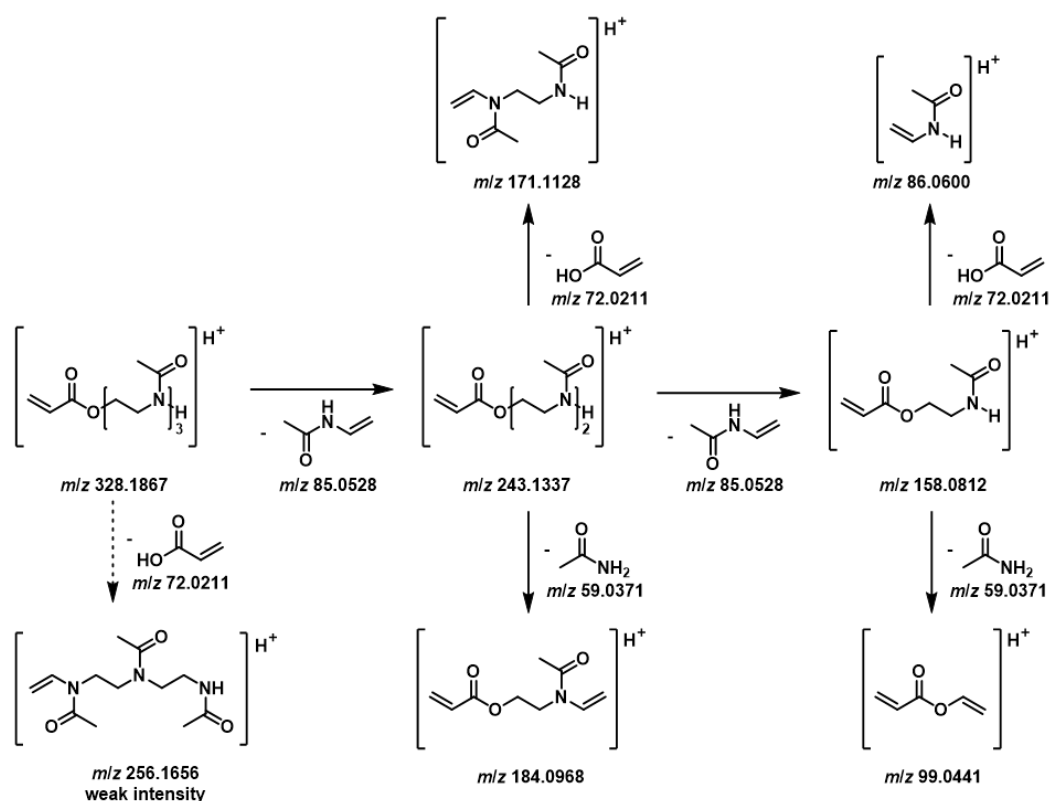


**Figure 3.7** ESI MS/MS spectrum for MeOx/AA of  $m/z^{\text{exp}} = 328.1861$  with an HCD of 25 eV. The corresponding peak assignments can be found in Table 3.5 and Scheme 3.4.

**Table 3.5** Overview of peaks observed upon fragmentation of MeOx/AA  $m/z^{\text{exp}}=328.1861$  (Figure 3.7). Structural assignment of the peaks are presented in Scheme 3.4.

$m/z^{\text{exp}}$	$m/z^{\text{theo}}$	$\Delta m/z$
328.1858	328.1867	0.0009
256.1660	256.1656	0.0004
243.1338	243.1337	0.0001
184.0967	184.0968	0.0001
171.1127	171.1128	0.0001
158.0811	158.0812	0.0001
99.0446	99.0441	0.0005
86.0606	86.0600	0.0006

The species at  $m/z^{\text{exp}} = 158.0812$  supports the alternating nature of the SZWIP oligomers. A small peak at  $m/z^{\text{exp}} = 256.1656$  can be observed. This corresponds to  $\text{MeOx}_3$ , the key fragment ion for a  $\text{MeOx}/\text{AA}$  3/1 parent peak, thereby confirming homopropagation of  $\text{MeOx}$  in the SZWIP with  $\text{AA}$ . It furthermore demonstrates that  $\text{AA}$  terminates the SZWIP in this reaction by ring-opening of  $\text{MeOx}$ . In addition to the weak  $m/z^{\text{exp}} = 256.1656$  peak indicating a  $\text{MeOx}_3$  fragment, a more significant signal at  $m/z^{\text{exp}} = 171.1128$  corresponding to  $\text{MeOx}_2$  provides clear evidence for  $\text{MeOx}$  dimerization. The observed species furthermore support the proposed concerted fragmentation mechanism (Scheme 3.2).



**Scheme 3.4** Fragmentation of  $\text{MeOx}/\text{AA}$   $m/z^{\text{exp}} = 328.1867$  as observed in Figure 3.7.

In addition to only fragment parent peaks that strongly suggest homopropagation, it is also interesting to analyse parent peaks that show an apparent alternating propagation and identify their possible isobaric structures. To illustrate this, the signal at  $m/z^{\text{exp}} =$

472.2295 corresponding to MeOx/AA 3/3 was selected, for which there are four possible isobaric structures, including an  $\omega$ -amide terminated alternating microstructure. Figure 3.8a shows these isobaric structures, along with the key fragment ion for each as determined from a concerted fragmentation mechanism. The observed fragmentation products are shown in Figure 3.8b. Two important fragmentation products can be observed. The signal at  $m/z^{\text{exp}} = 158.0814$  corresponds to MeOx/AA 1/1, which is the key fragment ion to support an alternating microstructure. The presence of a signal at  $m/z^{\text{exp}} = 171.1103$  matches MeOx<sub>2</sub>, the key fragment ion to support homopropagation of MeOx in this product. The key fragment ions for MeOx<sub>3</sub> and AA<sub>2</sub> were not observed. The fragmentation of this species importantly demonstrates that even oligomers that match an alternating structure in the overview ESI MS are a mixture of isobaric structures.

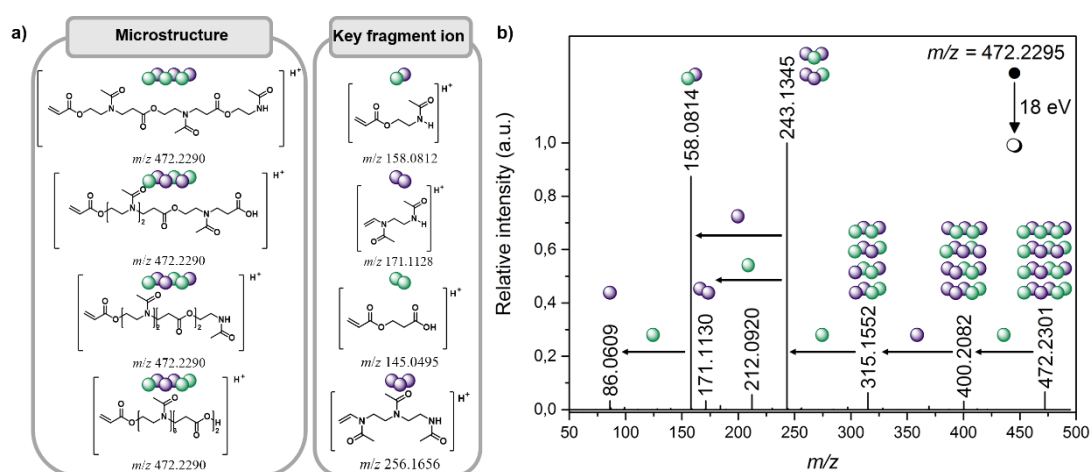


**Figure 3.8** Fragmentation of MeOx/AA  $m/z^{\text{exp}} = 472.2295$ . a) Possible microstructures and their key fragment ions. b) ESI MS/MS spectrum showing the fragmentation of various isobaric structures at an HCD of 18 eV and the presence of key fragment ions for two possible microstructures.

In addition to these two MeOx/AA species, several others have been analysed by ESI MS/MS. An overview of these species, their fragmentation spectra and the assignments for all relevant peaks can be found in the Appendix.

Using the same methodology as described for MeOx/AA oligomers, the oligomers from EtOx/AA and EtOz/AA were also analysed by ESI MS/MS to identify the various microstructures. Figure 3.9 shows an example for each type of oligomer, a full overview can be found in the Appendix.

Figure 3.9a shows the ESI MS/MS spectrum for the EtOx/AA species with  $m/z^{\text{exp}} = 365.1670$ , which corresponds to EtOx/AA 2/2 and has three possible isobaric structures, of which two can be found upon fragmentation. The presence of alternating microstructures is supported by the fragment at  $m/z^{\text{exp}} = 172.0964$  whereas the presence of the microstructure with EtOx homopropagation is confirmed by the  $m/z^{\text{exp}} = 199.1436$  fragment. In contrast to the MeOx/AA species, upon fragmentation both protonated and sodiated species are observed, giving double peaks for certain fragments. The fragmentation of EtOz/AA  $m/z^{\text{exp}} = 393.1995$  (EtOz/AA 2/2) is shown in Figure 3.9b. As for any CIE/AA 2/2, there are three possible isobaric structures, but upon fragmentation no peaks supporting homopropagation are observed. This is in sharp contrast to the MeOx/AA and EtOx/AA oligomers where homopropagation has been evidenced. This absence of homopropagation does not apply to all fragmented parent peaks in EtOz/AA oligomers, but where present it is significantly less than for MeOx/AA and EtOx/AA oligomers (see Section 3.2.5 for more details).

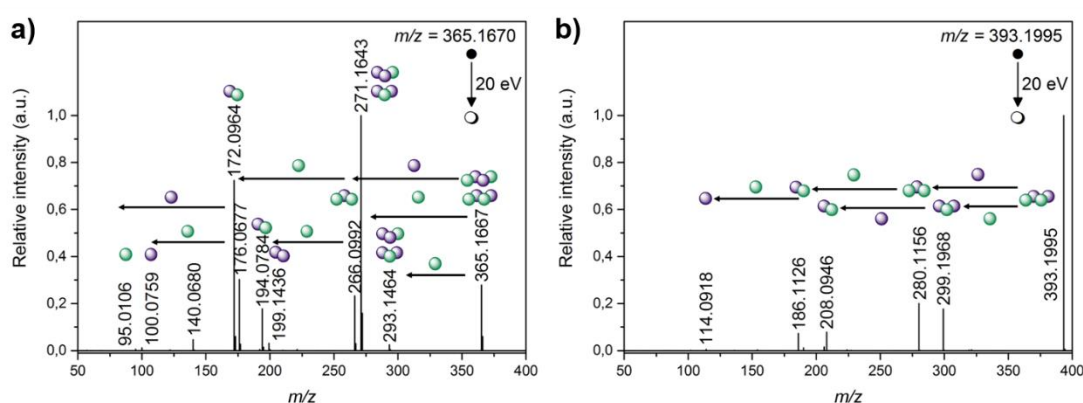
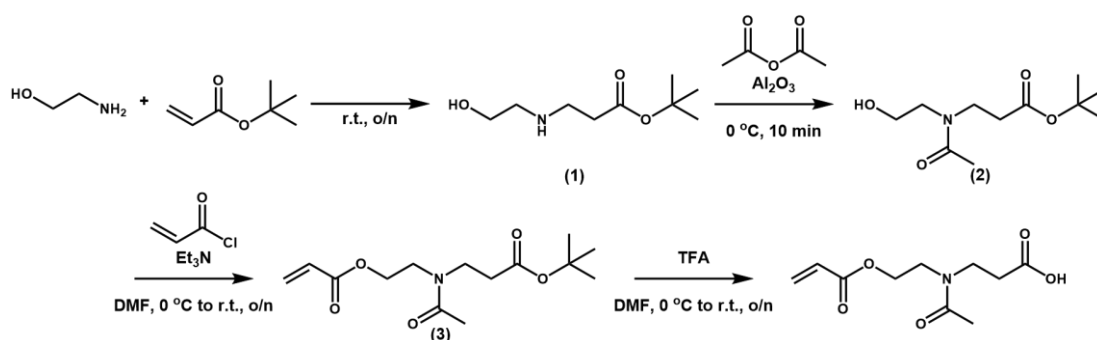


**Figure 3.9** ESI MS/MS spectra for EtOx/AA  $m/z^{\text{exp}} = 365.1670$  (a) and EtOz/AA  $m/z^{\text{exp}} = 393.1995$  (b).

### 3.2.5. Semi-quantification of homopropagation and $\omega$ -end groups

A look at the overview spectra (Figures 3.1 – 3.3) of the different NPAE macromonomers suggests that the CIE employed has an effect on the peaks observed in the MS spectra and their intensities, as does the monomer feed ratio. In order to semi-quantify this, a small molecule analogue was synthesised (Scheme 3.5). The full synthesis and analysis are described in the experimental details (Section 3.4.3). Briefly, *tert*-butyl acrylate and ethanolamine underwent an aza-Michael addition to produce (1).<sup>27</sup> Selective acylation of the amine in the presence of aluminium oxide produced the *N*-acylated intermediate (2).<sup>28</sup> Acylation of the hydroxyl group with acryloyl chloride introduced the  $\alpha$ -acrylate end group (3). Finally, the *tert*-butyl ester was hydrolysed to yield  $\omega$ -carboxylic acid terminated AA-MeOx-AA dimer ( $m/z^{\text{exp}} = 230.1019$ ).



**Scheme 3.5** Synthesis of the AA-MeOx-AA dimer for semi-quantification.

The peak corresponding to this dimer was present in all MeOx/AA MS spectra. Furthermore, it was assumed that the introduction of an additional methylene group in the side chain (EtOx) or in both the side chain and backbone (EtOz) has no significant effect on the ionisation of the macromonomers and hence, using the small molecule analogue, a calibration curve was established for both the protonated and sodiated species at a concentration range of 0.01 to 0.75 mg mL<sup>-1</sup> (Figure 3.10). Noteworthy is the observation that at a given concentration, the peak intensity for sodiated species is significantly higher, indicating a preferred ionisation with sodium.

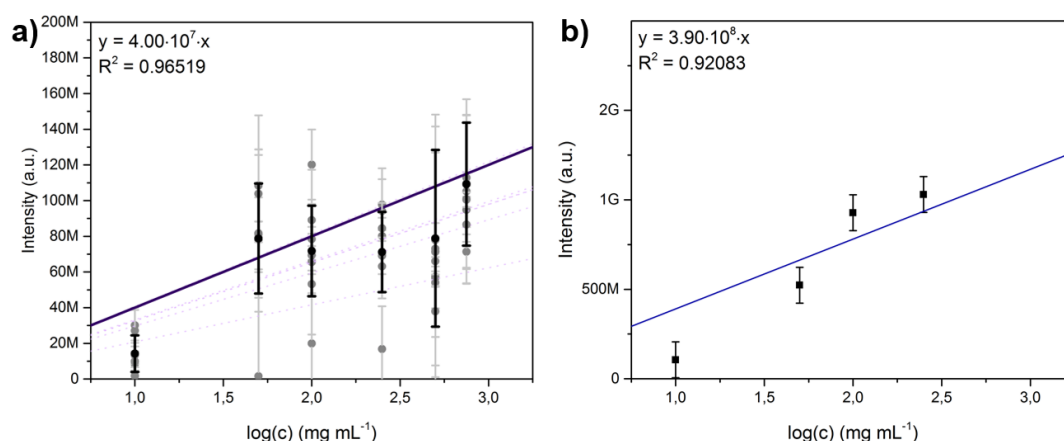


**Figure 3.10** Calibration curves for the AA-MeOx-AA small molecule analogue. a) Calibration based on protonated species ( $m/z^{\text{exp}} = 230.1019$ ). b) Calibration based on sodiated species ( $m/z^{\text{exp}} = 252.0835$ ).

The mole fraction of homopropagation was compared between the different feed ratios of a given monomer (MeOx : AA) combination, using Equation 3.1.<sup>19</sup> In this equation,  $\chi$  is the mole fraction of a species (■), *e.g.*  $m/z^{\text{exp}} = 328.1862$ , in a specific molar feed ratio (*e.g.* MeOx:AA 1:1) and calculated from the intensity of this species as a fraction of the total intensity of this species of all feed ratios combined. As a result of their different ionisation at a given concentration, the calculations are separate for  $\text{H}^+$  and  $\text{Na}^+$  ionised species, and their results should be compared separately.<sup>23</sup>

$$\chi^{\text{in sample}} = \frac{\text{Intensity}(\blacksquare)^{\text{in sample}}}{\sum \text{Intensity}(\blacksquare)^{\text{all feed ratios}}} \quad (3.1)$$

To quantify the extent of homopropagation in each macromonomer, species attributed to homopropagation were compared between macromonomers synthesised from the same monomers. Specifically, the species labelled with downward triangles (▼ and ▼) in the expanded ESI spectra (Figure 3.1 – 3.3), *e.g.*  $m/z(\text{MeOx}/\text{AA})^{\text{exp}} = 350.1681$ ,

were compared according to Equation 3.1. Table 3.6 provides an overview of the so-diated species associated with homopropagation within the MeOx/AA oligomers as an example for the semi-quantitative calculations.

**Table 3.6** Overview of species associated with homopropagation in MeOx/AA spectra and their respective mole fractions.

MeOx:AA feed	Repeat units [n]	$m/z^{\text{exp}}$	Intensity <sup>a</sup> [a.u.]	Mole fraction $\chi^b$
<b>1:1</b>	2	265.1154	$1.48 \cdot 10^8$	$0.27 \pm 0.04$
	3	350.1681	$3.16 \cdot 10^7$	$0.29 \pm 0.04$
	4	435.2206	$6.11 \cdot 10^6$	$0.30 \pm 0.05$
	5	520.2737	$7.91 \cdot 10^5$	$0.58 \pm 0.09$
<b>1:2</b>	2	265.1153	$1.48 \cdot 10^8$	$0.26 \pm 0.04$
	3	350.1681	$3.66 \cdot 10^7$	$0.34 \pm 0.05$
	4	435.2206	$7.64 \cdot 10^6$	$0.38 \pm 0.06$
	5	520.2752	$3.26 \cdot 10^4$	$0.02 \pm 0.01$
<b>2:1</b>	2	265.1153	$2.63 \cdot 10^8$	$0.47 \pm 0.07$
	3	350.1679	$3.95 \cdot 10^7$	$0.37 \pm 0.06$
	4	435.2203	$6.42 \cdot 10^6$	$0.32 \pm 0.05$
	5	520.2747	$5.49 \cdot 10^5$	$0.40 \pm 0.06$

<sup>a</sup> As determined from the ESI MS spectra. <sup>b</sup> Calculated according to Equation 3.1.

These numbers can then be plotted as in Figure 3.11a. An apparent dependency on the DP of the oligomers can be observed. For example, for  $n = 5$  for MeOx:AA 1:2,  $\chi$  is only 0.02, however, as an excess of AA in the monomer feed leads to slightly lower average molecular weights (Table 3.1), this is a biased result.

Instead, by considering the average mole fraction ( $\chi^{\text{avg}}$ ) over the whole range of DPs a better impression can be gained of the effect of monomer feed ratios on the extent of homopropagation. As such it can be observed that  $\chi^{\text{avg}} = 0.36$  for MeOx:AA 1:1 re-

duces to  $\chi^{\text{avg}} = 0.25$  for MeOx:AA 1:2, while increasing only slightly to  $\chi^{\text{avg}} = 0.39$  for MeOx:AA 2:1 (Figure 3.11a). Graphical representations for the other species can be found in the Appendix.

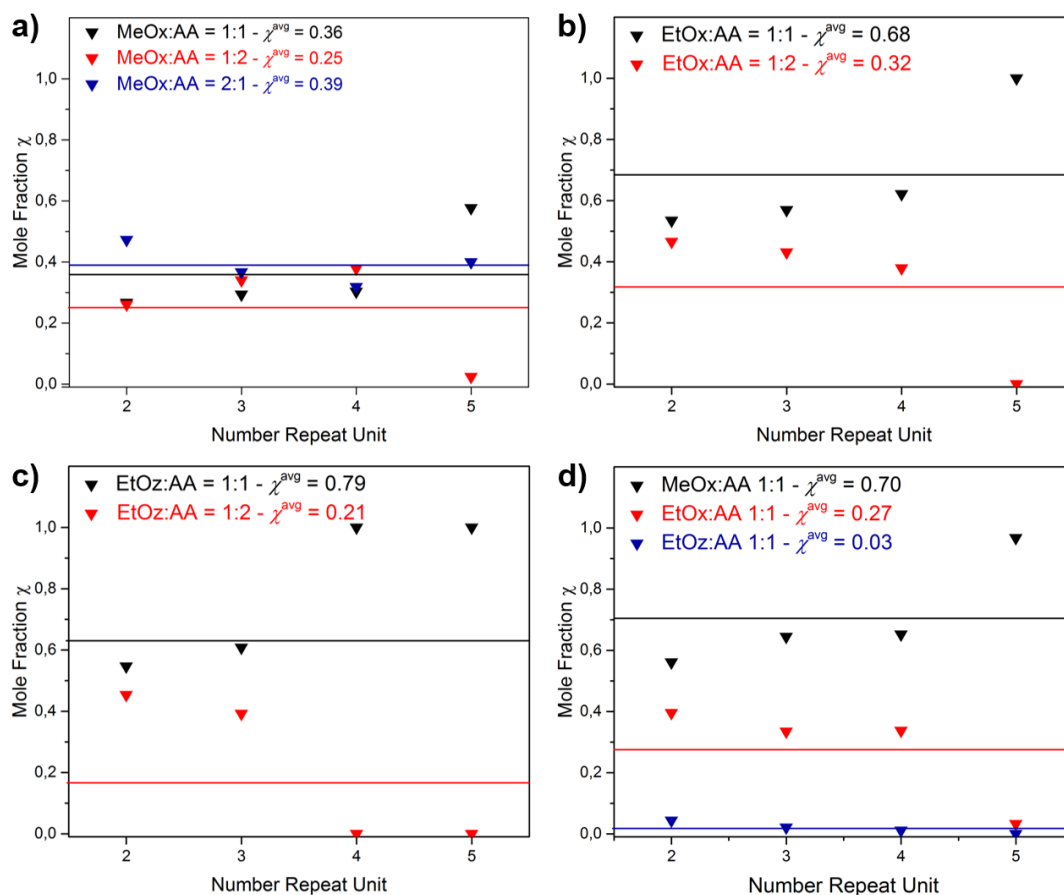


**Figure 3.11** Semi-quantitative results for the homopropagation. Comparison between MeOx/AA oligomers (a), EtOx/AA oligomers (b), EtOz/AA oligomers (c) and different oligomers from 1:1 feed ratios (d).

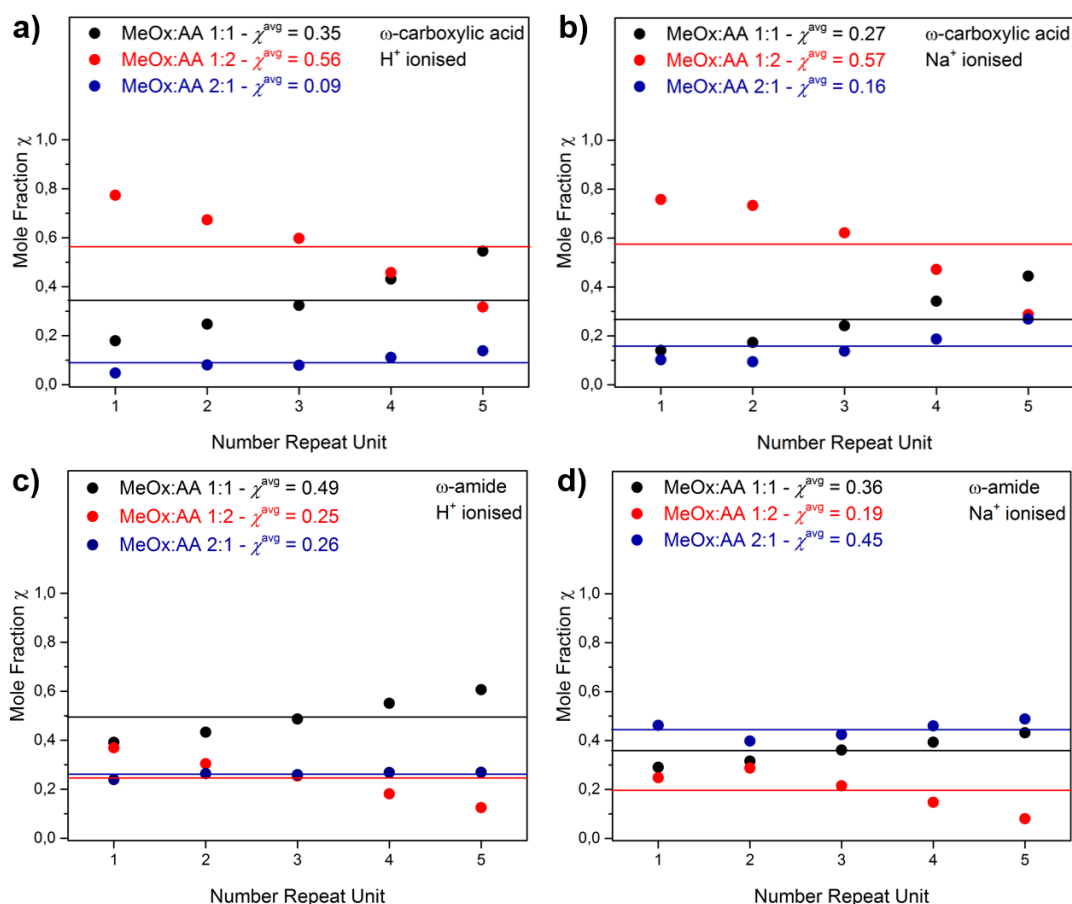
Semi-quantitative analysis of the homopropagation in EtOx/AA and EtOz/AA oligomers reveals the same trends, *i.e.* homopropagation is more pronounced at equimolar feed ratio than when an excess of AA is present during the SZWIP. Similar to MeOx/AA, the differences become more significant at higher DPs as the molecular weights for oligomers made in an excess of AA are slightly lower and consequently

there are less of these species present (Figure 3.11b-c). Figure 3.11d shows a comparison between the MeOx/AA, EtOx/AA and EtOz/AA oligomers synthesised from equimolar feed ratios, demonstrating striking differences between the three CIEs. MeOx demonstrates significant homopropagation ( $\chi^{\text{avg}} = 0.70$ ). This reduces to  $\chi^{\text{avg}} = 0.27$  for EtOx and almost diminishes for EtOz ( $\chi^{\text{avg}} = 0.03$ ).

Similarly, some semi-quantitative conclusions can also be made about the  $\omega$ -end groups. Considering the  $\omega$ -carboxylic acid terminated MeOx/AA oligomer at  $m/z^{\text{exp}} = 387.1756$  ( $\text{H}^+$  ionised) as example, the intensities between the different feed ratios can be compared. For this specific species, the molar ratios are  $\chi = 0.25$  (MeOx:AA 1:1),  $\chi = 0.67$  (MeOx:AA 1:2) and  $\chi = 0.08$  (MeOx:AA 2:1), respectively. Using Equation 3.1, the average molar ratio ( $\chi^{\text{avg}}$ ) can be determined. Figure 3.12a-b shows the molar ratios per repeat unit and a horizontal line indicating the  $\chi^{\text{avg}}$  for a given feed ratio.

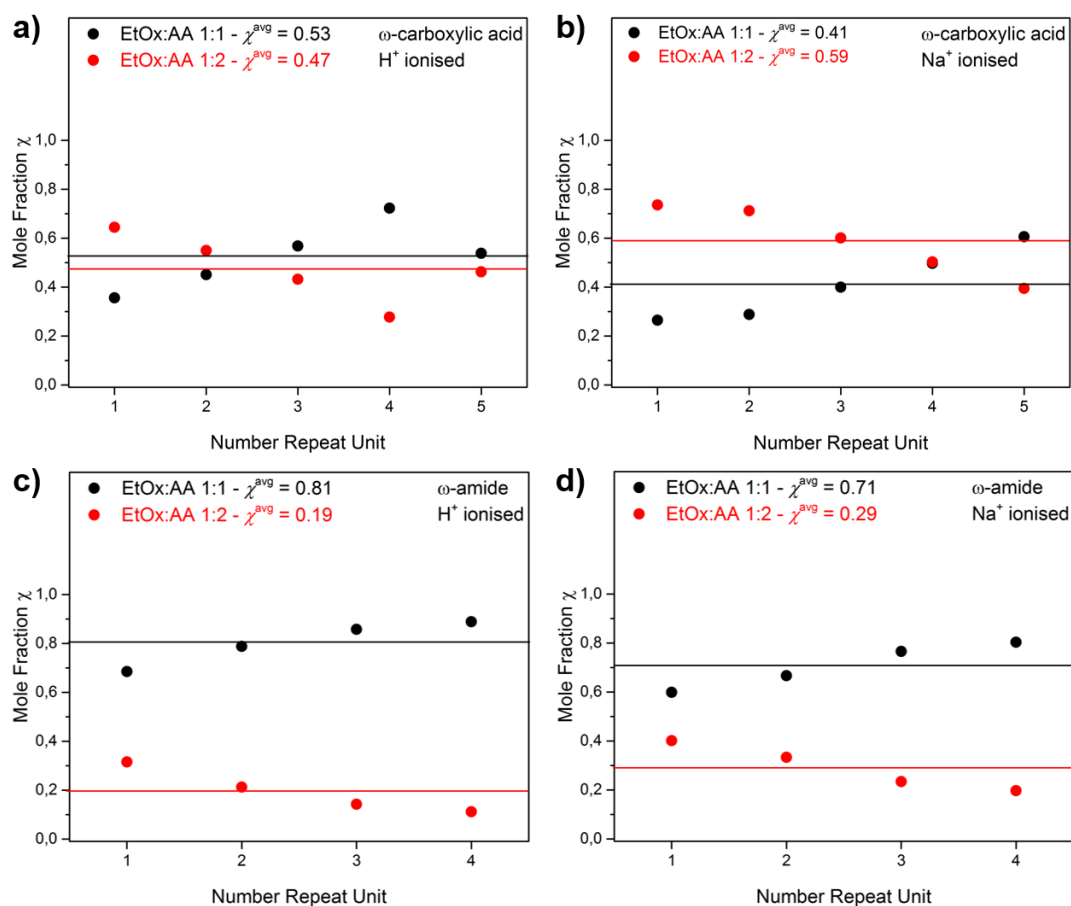
It was observed that for  $\text{H}^+$  ionised species, the  $\chi^{\text{avg}}$  for  $\omega$ -carboxylic acid groups decreases slightly from MeOx:AA 1:2 ( $\chi^{\text{avg}} = 0.56$ ) to MeOx:AA 1:1 ( $\chi^{\text{avg}} = 0.35$ ) and finally, more dramatically, reducing to MeOx:AA 2:1 ( $\chi^{\text{avg}} = 0.09$ ). Similarly, for sodiated species this is  $\chi^{\text{avg}} = 0.57$  (MeOx:AA 1:2),  $\chi^{\text{avg}} = 0.27$  (MeOx:AA 1:1) and  $\chi^{\text{avg}} = 0.16$  (MeOx:AA 2:1). These results can be directly linked to the amount of AA in the monomer feed; less AA in the monomer feed reduces its availability to terminate the  $\omega$ -chain end as a carboxylic acid.

Applying the same principle to the  $\omega$ -amide terminated species produces the graphs in Figure 3.12c-d. Somewhat surprisingly, for the  $\text{H}^+$  ionised species the  $\chi^{\text{avg}}$  is similar for the MeOx:AA 1:2 and 2:1 species, and only significantly higher for MeOx:AA 1:1, suggesting that an excess MeOx in the monomer feed does not promote the introduction of  $\omega$ -amide groups. A clearer trend that is more in line with expectation emerges when the  $\text{Na}^+$  ionised species are considered. In this case, oligomers from MeOx:AA 2:1 have  $\chi^{\text{avg}} = 0.45$ , which reduces to  $\chi^{\text{avg}} = 0.36$  for MeOx:AA 1:1 and  $\chi^{\text{avg}} = 0.19$  for MeOx:AA 1:2 as a result of the increasing AA concentration during the SZWIP.



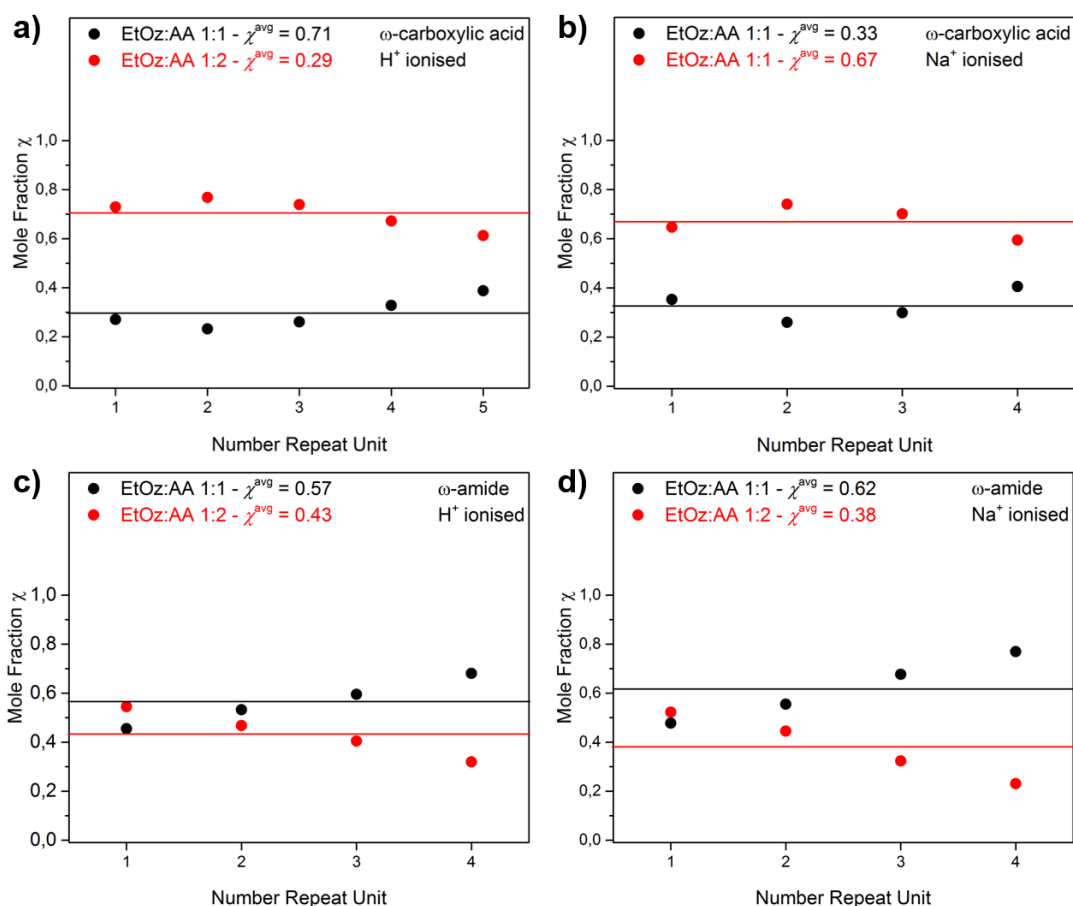
**Figure 3.12** Semi-quantitative  $\omega$ -end group analysis of MeOx/AA oligomers. a)  $\omega$ -carboxylic acid groups,  $H^+$  ionised. b)  $\omega$ -carboxylic acid groups,  $Na^+$  ionised. c)  $\omega$ -amide groups,  $H^+$  ionised. d)  $\omega$ -amide groups,  $Na^+$  ionised.

Figure 3.13 shows the semi-quantitative analysis for the EtOx/AA oligomers. The amount of  $\omega$ -carboxylic acid end groups is relatively similar for both feed ratios and both  $H^+$  and  $Na^+$  ionisation. For the  $\omega$ -amide end groups a more distinct trend was observed in which an equimolar feed ratio of EtOx/AA resulted in significantly more  $\omega$ -amide end groups than an excess of AA during the SZWIP. Similar to previously, mole ratios for EtOx:AA 1:2 at higher DPs become smaller as the average molecular weight of these oligomers is lower than for the average EtOx:AA 1:1 oligomers.



**Figure 3.13** Semi-quantitative  $\omega$ -end group analysis of EtOx/AA oligomers. a)  $\omega$ -carboxylic acid groups,  $H^+$  ionised. b)  $\omega$ -carboxylic acid groups,  $Na^+$  ionised. c)  $\omega$ -amide groups,  $H^+$  ionised. d)  $\omega$ -amide groups,  $Na^+$  ionised.

The same trend can be observed for the EtOz/AA oligomers. Compared to the EtOx/AA oligomers, a surplus of AA during the SZWIP lead to a relatively larger increase in  $\omega$ -carboxylic acid groups (Figure 3.14). Conversely, the relative number of  $\omega$ -amide groups was closer for both feed ratios, indicating a less pronounced effect of the EtOz:AA ratio on  $\omega$ -amide groups.



**Figure 3.14** Semi-quantitative ω-end group analysis of EtOz/AA oligomers. a) ω-carboxylic acid groups, H<sup>+</sup> ionised. b) ω-carboxylic acid groups, Na<sup>+</sup> ionised. c) ω-amide groups, H<sup>+</sup> ionised. d) ω-amide groups, Na<sup>+</sup> ionised.

Finally, Figure 3.15 compares the different end groups between the three CIEs. The different CIEs with the same ω-end group appear to prefer different ionisation adducts, *e.g.* EtOz-based oligomers with ω-carboxylic acid groups seem to prefer ionisation with H<sup>+</sup> whereas sodiated adducts are mainly observed for EtOx. Noteworthy are the significantly higher  $\chi^{avg}$  for EtOz-based oligomers with ω-carboxylic acids and H<sup>+</sup> ionisation, as well as EtOx-based oligomers with ω-amides and Na<sup>+</sup> ionisation compared to the other oligomers with the same end groups and ionisation adducts, suggesting an effect of the CIE on the end groups and ionisation adducts.

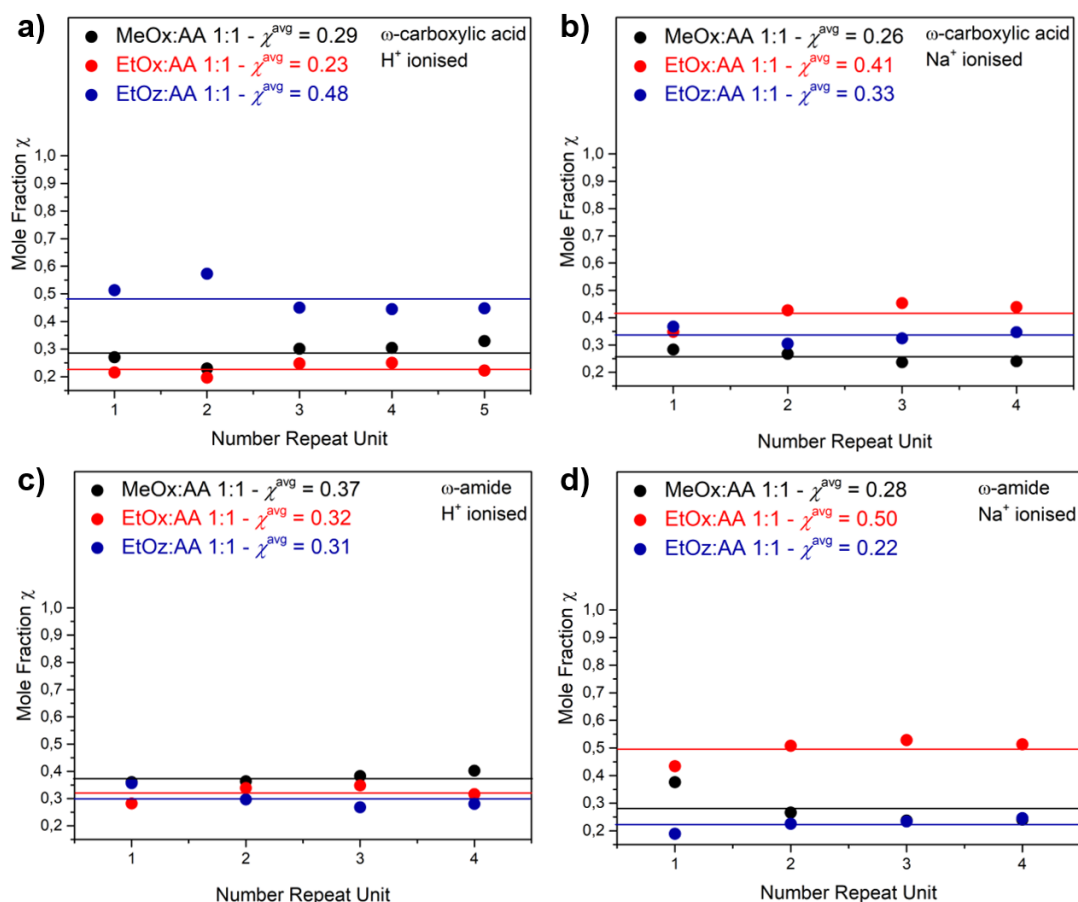


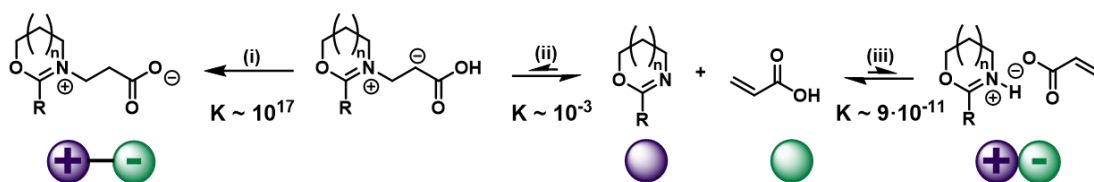
**Figure 3.15** Semi-quantitative comparison of ω-end group of CIE/AA oligomers. a) ω-carboxylic acid groups, H<sup>+</sup> ionised. b) ω-carboxylic acid groups, Na<sup>+</sup> ionised. c) ω-amide groups, H<sup>+</sup> ionised. d) ω-amide groups, Na<sup>+</sup> ionised.

### 3.2.6. Mechanism for SZWIP of cyclic imino ethers and acrylic acid

The qualitative and semi-quantitative information obtained by the post-mortem ESI MS/MS analysis of the seven NPAE macromonomers, provided new insights into the mechanism of the SZWIP between CIEs and AA and allowed to postulate an updated mechanism compared to that in Scheme 3.1 and is shown in Schemes 3.6 – 3.8.

The initiation step was previously identified as the aza-Michael addition of the CIE to AA, followed by a rapid proton transfer (Scheme 3.6). It is believed that this is still the major reaction taking place during initiation which provides the *genetic zwitterion*. This species has been previously isolated, thus supporting this reaction to take place.<sup>5</sup>

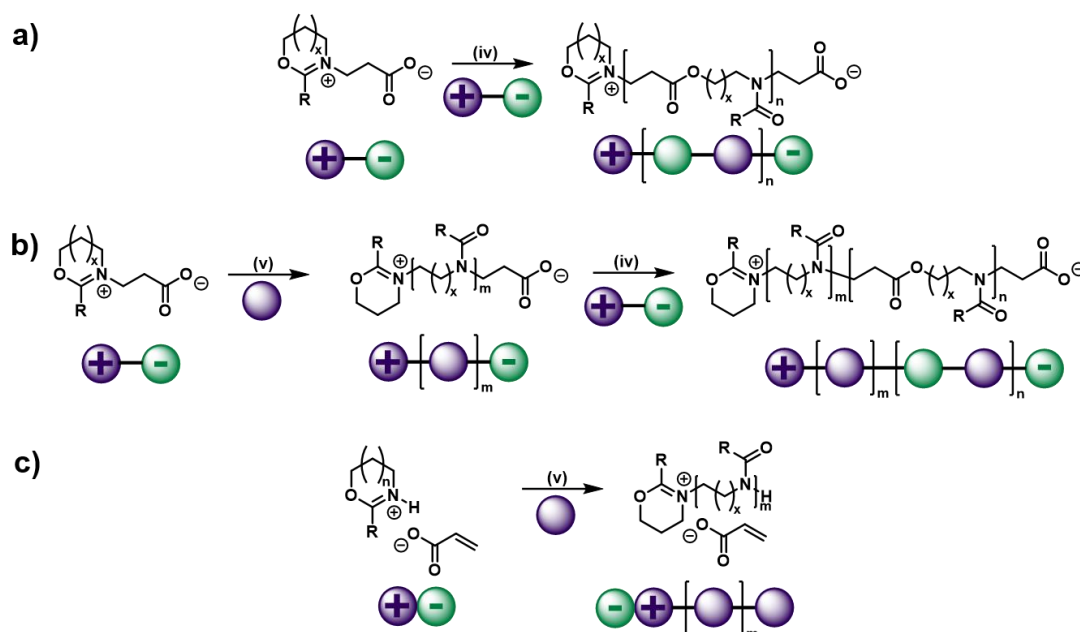
Supported by literature, the driving force for the formation of the genetic zwitterion appears to be the irreversible proton transfer.<sup>29</sup> In addition to that, it was postulated that an acid-base reaction between the CIE and AA takes place to form a [HCIE]<sup>+</sup>[AA]<sup>-</sup> ion pair. The acid-base reaction furthermore depends on the acidity of AA ( $pK_a = 4.26$ ) and the basicity of the CIEs (MeOx:  $pK_b = 5.77$ ; EtOx:  $pK_b = 5.65$ ; EtOz:  $pK_b = 6.49$ ).<sup>30</sup> Although these  $pK_a$  and  $pK_b$  values do not favour protonation of the CIE, the formation of the ion pair does seem to be crucial for the formation of  $\omega$ -amide groups. Based on these values and supported by the post-mortem ESI MS/MS analysis, EtOx is most likely to form its corresponding ion pair, [HEtOx]<sup>+</sup>[AA]<sup>-</sup>.



**Scheme 3.6** Initiation of SZWIP *via* an aza-Michael addition to form the genetic zwitterion (i, ii) or an acid-base reaction to form the [HCIE]<sup>+</sup>[AA]<sup>-</sup> ion pair (iii).

The ESI MS/MS results suggested three propagation pathways (Scheme 3.7). The primary propagation is *via* the addition reaction between zwitterions as originally proposed by Saegusa and co-workers and leads to the formation of alternating oligomers. Reaction of the oxazolinium group of a zwitterion with a CIE monomer or [HCIE]<sup>+</sup>[AA]<sup>-</sup> ion pair results in the introduction of homopropagation. Furthermore, the third propagation reaction involves a CIE homopolymerisation initiated by a [HCIE]<sup>+</sup>[AA]<sup>-</sup> ion pair. The mechanism for the last two propagation pathways is similar to that for cationic ring-opening polymerisation (CROP) of CIEs and their kinetics were estimated from the vast amount of literature on CIE homopolymerisation where MeOx is known to polymerise faster than EtOx,<sup>31</sup> whereas EtOz is approximately four times slower as a result of its six-membered ring structure.<sup>32</sup> This correlates well with

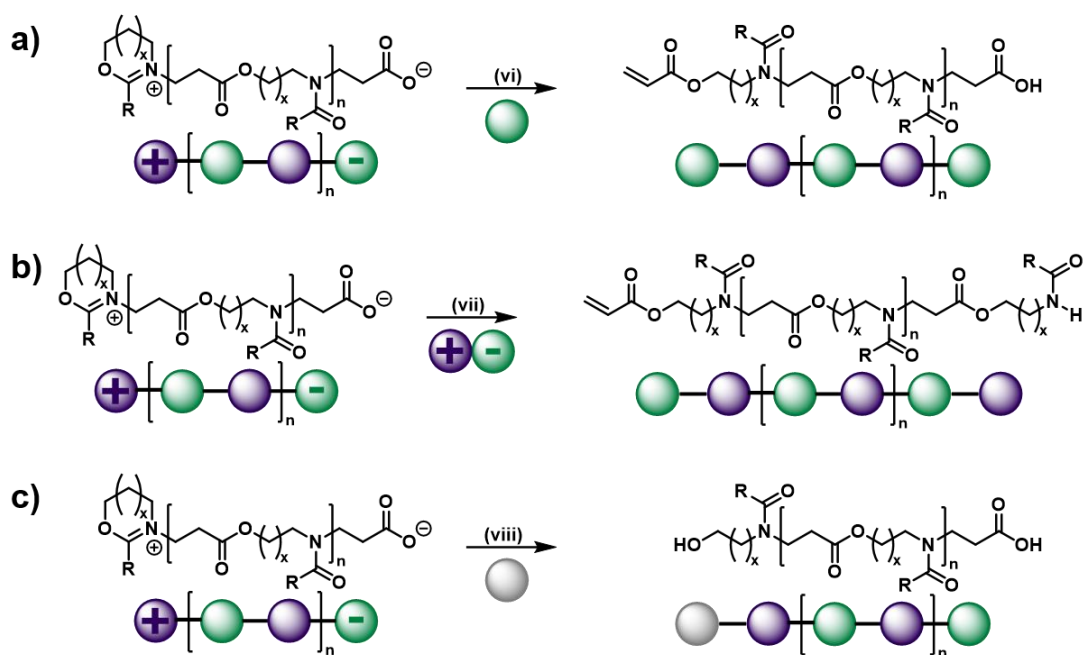
the observations made in the semi-quantification study: the homopropagation decreased from  $\chi^{\text{avg}} = 0.70$  for MeOx to  $\chi^{\text{avg}} = 0.27$  for EtOx to only  $\chi^{\text{avg}} = 0.03$  for EtOz in equimolar ratios with AA.



**Scheme 3.7** Propagation reactions for SZWIP. a) The addition reaction of two zwitterions leads to alternating structures. b) Reaction of a zwitterion with a CIE monomer introduces copolymers with defects from CIE homopropagation. c) The reaction of a [HCIE]<sup>+</sup>[AA]<sup>-</sup> ion pair with a CIE monomer produces poly(CIE) homopolymers.

Three termination pathways for the SZWIP of CIEs with AA were identified (Scheme 3.8). The first involves the termination by AA to introduce the  $\alpha$ -acrylate group by nucleophilic ring-opening of the oxazolinium ring and also introduces the  $\omega$ -carboxylic acid by protonation of the carboxylate group. Alternatively, a growing zwitterionic intermediate can be terminated by a [HCIE]<sup>+</sup>[AA]<sup>-</sup> ion pair. This pathway introduces the  $\alpha$ -acrylate group in the same way as the previous termination pathway, but also has an oxazolinium species from the ion pair, [HCIE]<sup>+</sup>, which can be ring-opened by the carboxylate group of the oligomer to introduce the  $\omega$ -amide group. This also highlighted why the formation of the ion pairs during initiation is important for termination

*via* this pathway. Finally, a third termination pathway involves ambient nucleophiles such as water, which can ring-open the oxazolinium ring and protonate the carboxylate group to produce an  $\alpha$ -hydroxy- $\omega$ -carboxylic acid-terminated NPAE.



**Scheme 3.8** Termination pathways for SZWIP. a) Reaction of a growing oligomer with AA introduces an  $\alpha$ -acrylate and  $\omega$ -carboxylic acid group. b) Reaction with a [HCIE]<sup>+</sup>[AA]<sup>-</sup> ion pair introduces an  $\alpha$ -acrylate and  $\omega$ -amide group. c) Reaction with ambient water introduces a  $\alpha$ -hydroxyl and  $\omega$ -carboxylic acid group.

### 3.3. Conclusions

This Chapter investigated the spontaneous zwitterionic copolymerisation (SZWIP) mechanism in detail *via* post-mortem analysis of a library of *N*-acylated poly(aminoester) (NPAE) oligomers by electrospray ionisation (tandem) mass spectrometry (ESI MS and MS/MS). Through evaluation of the overview spectra obtained from ESI MS and the fragmentation spectra from MS/MS analysis, in combination with semi-quantification using a model compound, several new aspects of the SZWIP mechanism were revealed. The amount of  $\omega$ -carboxylic acid groups can be directly influenced by

changing the monomer feed ratios ( $\chi^{\text{avg}} = 0.27$  for MeOx:AA 1:1;  $\chi^{\text{avg}} = 0.57$  for MeOx:AA;  $\chi^{\text{avg}} = 0.16$  for MeOx:AA 2:1). In contrast, an excess of the CIE has a less dramatic effect on the amount of  $\omega$ -amide group ( $\chi^{\text{avg}} = 0.36$  for MeOx:AA 1:1;  $\chi^{\text{avg}} = 0.49$  for MeOx:AA 2:1 and  $\chi^{\text{avg}} = 0.20$  for MeOx:AA 1:2). The formation of  $\omega$ -amide groups is dependent on the formation of a [HCIE]<sup>+</sup>[AA]<sup>-</sup> ion pair during initiation (as a competing event to the aza-Michael addition). The formation of this ion pair is in turn dependant on AA/CIE acid-base equilibrium which decreases from EtOx > MeOx > EtOz. Consequently, the highest  $\omega$ -amide group abundance is observed for EtOx ( $\chi^{\text{avg}} = 0.50$ ) and decreases to  $\chi^{\text{avg}} = 0.28$  and  $\chi^{\text{avg}} = 0.22$  for MeOx and EtOz, respectively. Finally, during the MS/MS studies, unambiguous evidence was found for the homopropagation of CIEs during SZWIP as a side reaction to the main SZWIP mechanism, which leads to defects in the alternating structure. The homopropagation is mainly observed in the SZWIP of the more reactive 5-membered 2-oxazolines (MeOx > EtOx) and is significantly less pronounced for the approximately four times less reactive six-membered 2-oxazine (EtOz). Based on these new insights, an updated mechanism for the SZWIP of CIEs with AA has been formulated.

## 3.4. Experimental

### 3.4.1. Materials

Acrylic acid (AA, 99 %, anhydrous, Sigma Aldrich), acetonitrile (MeCN, 99.8 %, Sigma Aldrich), 4-methoxyphenol (MEHQ, 99 %, Sigma Aldrich) and diethyl ether (Et<sub>2</sub>O, > 98 %, Sigma Aldrich), ethanolamine ( $\geq 99$  %, Sigma Aldrich), *tert*-butyl acrylate (98 %, Sigma Aldrich), acetic anhydride ( $\geq 99$  %, Sigma Aldrich), aluminium oxide (Al<sub>2</sub>O<sub>3</sub>,  $\geq 99.5$  % Sigma Aldrich), acryloyl chloride (97 %, Sigma Aldrich), triethylamine (Et<sub>3</sub>N,  $\geq 99$  %, Sigma Aldrich) and trifluoroacetic acid (TFA, 99 %, Sigma Aldrich) and deuterated chloroform (CDCl<sub>3</sub>, 99.8 atom % D, Sigma Aldrich) were used as received. 2-Methyl-2-oxazoline (MeOx, 99 %, Acros Organics) and 2-ethyl-2-oxazoline (EtOx, > 99 %, Acros Organics) were distilled to dryness over barium

oxide (BaO, 97 %, Sigma Aldrich) and stored under nitrogen. 2-Ethyl-2-oxazine (EtOz) was synthesised according to literature procedure,<sup>33</sup> purified by vacuum distilling over BaO and stored under nitrogen. *Tert*-butyl 3-((2-hydroxyethyl)amino)propanoate (1) was synthesised according to a literature procedure.<sup>27</sup> The ESI solvents were used without further purification: acetone (HPLC grade, Sigma Aldrich), acetic acid (analytical grade, Scharlau), acetonitrile (MeCN, LC-MS grade, Roth), dichloromethane (DCM, HPLC grade, Roth), methanol (MeOH, HPLC grade, Roth), H<sub>2</sub>O (Milli-Q) and tetrahydrofuran (THF, HPLC grade, Scharlau). Ammonium hexafluorophosphate ( $\geq 99.5$  %) was obtained from Thermo Scientific.

### 3.4.2. Instruments and analysis

<sup>1</sup>H NMR spectra were recorded on a Bruker Avance III HD 400, Avance III HD 300 or Avance AV 300 spectrometer. Size exclusion chromatography (SEC) measurements were conducted using an Agilent 390-LC MDS fitted with differential refractive index (DRI), light scattering (LS) and viscometry (VS) detectors equipped with 2 x PLgel 5  $\mu$ m mixed-D columns (300 x 7.5 mm), 1 x PLgel 5  $\mu$ m guard column (50 x 7.5 mm) and autosampler. All samples were passed through 0.2  $\mu$ m nylon filter before analysis. The mobile phase was DMF containing 5 mM NH<sub>4</sub>BF<sub>4</sub> with a flow rate of 1 mL min<sup>-1</sup> at 50 °C. SEC data was analysed using Agilent Technologies SEC software. Calibration curves were produced using Agilent EasiVial linear poly(methyl methacrylate) standards (200 – 4.7 x 10<sup>5</sup> g mol<sup>-1</sup>). ESI mass spectra were recorded on a Q Exactive Plus (BioPharma Option) (Orbitrap) mass spectrometer (Thermo Fisher Scientific) equipped with a HESI II probe. The instrument was calibrated in the *m/z* range 600 – 6000 g mol<sup>-1</sup> using ammonium hexafluorophosphate. All spectra were recorded in the positive ion mode. Samples were dissolved in water/acetonitrile/acetic acid 1:1:0.1 v/v (0.5 mg mL<sup>-1</sup>). The FT resolution was set to 140000 employing 3 microscans during an acquisition time between 2 min measuring with a capillary temperature of 320 °C. The aux gas flow was (dimensionless) 0.00, the sheath gas 5.00 and the spare gas 1.00. The flow rate was set to 5  $\mu$ L min<sup>-1</sup>. The spray voltage was set to 3.5 kV and kept constant while performing the experiments.

### 3.4.3. Synthetic procedures

#### General procedure for the synthesis of macromonomers (example for M1)

In a dried Schlenk flask under nitrogen atmosphere equipped with a magnetic stirrer bar, MEHQ (1 mg,  $8.06 \times 10^{-6}$  mol) was dissolved in 7 mL of MeCN. To this were added MeOx (5.9 mL, 69.5 mmol) and AA (4.75 mL, 69.5 mmol) under nitrogen (see Table 3.7 for all macromonomers). The mixture was placed in a 70 °C oil bath for 24 h. Subsequently, the polymer solution was cooled down, precipitated in Et<sub>2</sub>O, and isolated by centrifugation (three times). To remove the Et<sub>2</sub>O, the polymer was placed under vacuum to yield the products as colourless-to-yellowish oils. The <sup>1</sup>H NMR spectra and SEC molecular weight distribution are shown in Figure 3.16.

**Table 3.7** Quantities for the synthesis of the macromonomers.

Entry	CIE	Acrylate	CIE : acrylate	[CIE] [mol L <sup>-1</sup> ]	[acrylate] [mol L <sup>-1</sup> ]
1	MeOx	AA	1 : 1	9.92	9.92
2	MeOx	AA	1 : 2	4.48	9.92
3	MeOx	AA	2 : 1	6.32	3.16
4	EtOx	AA	1 : 1	9.92	9.92
5	EtOx	AA	1 : 2	6.60	13.2
6	EtOz	AA	1 : 1	3.32	3.32
7	EtOz	AA	1 : 2	2.21	4.42

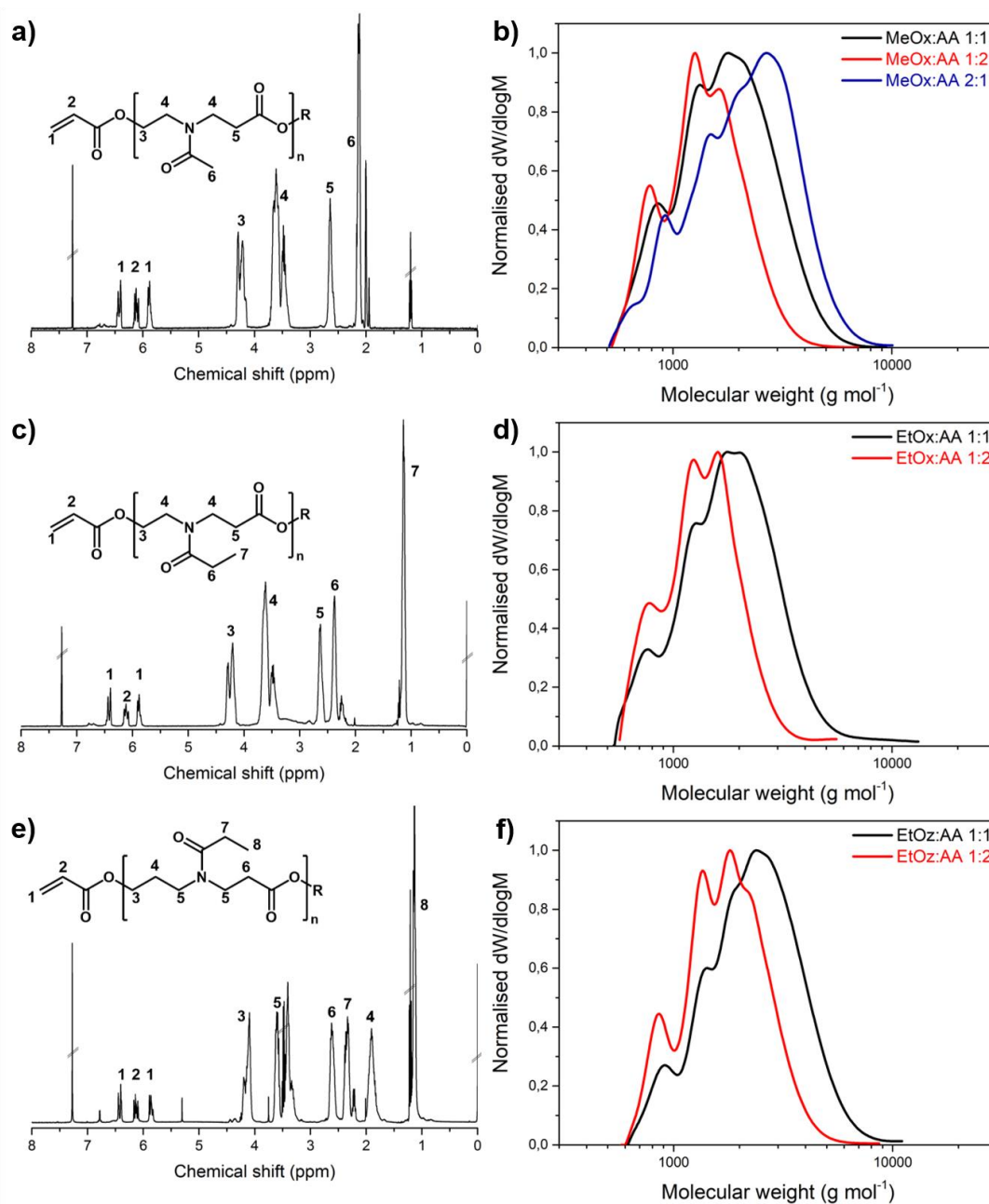


**Figure 3.16**  $^1\text{H}$  NMR spectra and SEC molecular weight distributions of the macromonomers.

Characterisation for MeOx/AA macromonomers.  $^1\text{H}$  NMR (400 MHz,  $\text{CDCl}_3$ ):  $\delta_{\text{H}}$  (ppm) 6.5-6.4 (d, 1H,  $\text{CH}_a\text{H}_b=\text{CH}$ ), 6.2-6.0 (t, 1H,  $\text{CH}_2=\text{CHCOO}$ ), 6.0-5.8 (d, 1H,  $\text{CH}_a\text{CH}_b=\text{CH}$ ), 4.4-4.2 (m, 6H,  $\text{COOCH}_2$ ), 3.8-3.4 (m, 12H,  $\text{CH}_2\text{N}(\text{COCH}_3)\text{CH}_2$ ), 2.7-2.5 (m, 6H,  $\text{CH}_2\text{COO}$ ), 2.2-2.0 (m, 9H,  $\text{NCOCH}_3$ ).  $\text{DP}_{\text{NMR}} = 2.5$ ,  $M_{\text{n,NMR}} = 465 \text{ g mol}^{-1}$ . SEC:  $M_{\text{n}} = 1800 \text{ g mol}^{-1}$ ,  $D_{\text{SEC}} = 1.32$ .

Characterisation for EtOx/AA macromonomers.  $^1\text{H}$  NMR (400 MHz,  $\text{CDCl}_3$ ):  $\delta_{\text{H}}$  (ppm) 6.5-6.4 (d, 1H,  $\text{CH}_a\text{H}_b=\text{CH}$ ), 6.2-6.0 (t, 1H,  $\text{CH}_2=\text{CHCOO}$ ), 6.0-5.8 (d, 1H,  $\text{CH}_a\text{CH}_b=\text{CH}$ ), 4.4-4.2 (m, 6H,  $\text{COOCH}_2$ ), 3.8-3.4 (m, 12H,  $\text{CH}_2\text{N}(\text{COCH}_3)\text{CH}_2$ ), 2.7-2.5 (m, 6H,  $\text{CH}_2\text{COO}$ ), 2.5-2.3 (m, 6H,  $\text{NCOCH}_2\text{CH}_3$ ), 1.3-1.0 (m, 9H,  $\text{NCOCH}_2\text{CH}_3$ ).  $\text{DP}_{\text{NMR}} = 2.5$ ,  $\text{M}_{\text{n,NMR}} = 500 \text{ g mol}^{-1}$ . SEC:  $\text{M}_{\text{n,SEC}} = 1600 \text{ g mol}^{-1}$ ,  $D_{\text{SEC}} = 1.30$ .

Characterisation for EtOz/AA macromonomers.  $^1\text{H}$  NMR (400 MHz,  $\text{CDCl}_3$ ):  $\delta_{\text{H}}$  (ppm) 6.5-6.4 (d, 1H,  $\text{CH}_a\text{H}_b=\text{CH}$ ), 6.2-6.0 (t, 1H,  $\text{CH}_2=\text{CHCOO}$ ), 6.0-5.8 (d, 1H,  $\text{CH}_a\text{CH}_b=\text{CH}$ ), 4.4-4.2 (m, 6H,  $\text{COOCH}_2$ ), 3.8-3.4 (m, 12H,  $\text{CH}_2\text{N}(\text{COCH}_3)\text{CH}_2$ ), 2.7-2.5 (m, 6H,  $\text{CH}_2\text{COO}$ ), 2.5-2.3 (m, 6H,  $\text{NCOCH}_2\text{CH}_3$ ), 2.0-1.7 (m, 6H,  $\text{CH}_2\text{CH}_2\text{CH}_2$ ), 1.3-1.0 (m, 9H,  $\text{NCOCH}_2\text{CH}_3$ ).  $\text{DP}_{\text{NMR}} = 3$ ,  $\text{M}_{\text{n,NMR}} = 627 \text{ g mol}^{-1}$ . SEC:  $\text{M}_{\text{n}} = 2000 \text{ g mol}^{-1}$ ,  $D_{\text{SEC}} = 1.27$ .

## Synthesis of the AA-MeOx-AA dimer

### *Synthesis of tert-butyl 3-(N-(2-hydroxyethyl)acetamido)propanoate (2)*

*Tert*-butyl 3-(*N*-(2-hydroxyethyl)acetamido)propanoate (**1**) was synthesised based on a literature procedure.<sup>28</sup> Compound **1** (1.00 g, 5.30 mmol) was transferred into a 20 mL vial filled with  $\text{Al}_2\text{O}_3$  (0.81 g, 7.90 mmol). Acetic anhydride ( $\text{Ac}_2\text{O}$ , 0.60 g, 5.80 mmol) was added under ice-cooling without stirring. After 3 min the ice-cooling was removed and the reaction was allowed to continue for another 7 min. Subsequently, 20 mL ethyl acetate was added and the mixture was filtered. The organic solvent and residual  $\text{Ac}_2\text{O}$  were removed under reduced pressure. Column chromatography ( $\text{SiO}_2$ , dichloromethane/methanol/hexane 8/1/1) yielded **2** as a colourless liquid in 80 % yield.  $^1\text{H}$  NMR (400 MHz,  $\text{CDCl}_3$ ):  $\delta_{\text{H}}$  (ppm) 3.69 (t, 2H,  $\text{HOCH}_2$ ), 3.57-3.50 (dt, 2H,  $\text{NCH}_2\text{CH}_2\text{COO}$ ), 3.46-3.40 (dt, 2H,  $\text{HOCH}_2\text{CH}_2\text{N}$ ), 2.50-2.44 (q, 2H,  $\text{CH}_2\text{COO}$ ), 2.10 (t, 3H,  $\text{NCOCH}_3$ ), 1.39 (s, 9H,  $\text{C}(\text{CH}_3)_3$ ).  $^{13}\text{C}$  NMR (100 MHz,  $\text{D}_2\text{O}$ ):  $\delta_{\text{C}}$  (ppm) 172.4+171.7 ( $\text{COO}$ ), 170.3 ( $\text{NCO}$ ), 81.5+81.8 ( $\text{C}(\text{CH}_3)_3$ ), 61.5+60.0 ( $\text{CH}_2\text{OH}$ ), 51.5+49.3 ( $\text{HOCH}_2\text{CH}_2\text{N}$ ), 46.0+42.4 ( $\text{NCH}_2\text{CH}_2\text{COO}$ ), 34.9+33.9 ( $\text{CH}_2\text{COO}$ ), 28.0 ( $\text{C}(\text{CH}_3)_3$ ), 21.8+21.4 ( $\text{NCOCH}_3$ ). HR ESI-MS:  $m/z^{\text{exp}} 254.1358$  ( $\text{M}+\text{Na}^+$ );  $m/z^{\text{theo}} 254.1363$  ( $\text{M}+\text{Na}^+$ );  $m/z^{\text{exp}} 232.1540$  ( $\text{M}+\text{H}^+$ );  $m/z^{\text{theo}} 232.1543$  ( $\text{M}+\text{H}^+$ ).

*Synthesis of 2-(N-(3-(tert-butoxy)-3-oxopropyl)acetamido)ethyl acrylate (3)*

Compound **2** (500.0 mg, 2.20 mmol) was dissolved in 3 mL dichloromethane. Under ice cooling, triethylamine (0.260 g, 2.60 mmol) was added and the solution was stirred for 5 min before adding acryloyl chloride (0.240 g, 2.60 mmol) over 5 min. The reaction was stirred for 18 h while allowing to warm up to room temperature. After filtration of the precipitate, the solvent and excess reagents were removed under reduced pressure. The product was used without further purification (yield: 60 %). <sup>1</sup>H NMR (400 MHz, CDCl<sub>3</sub>): δ<sub>H</sub> (ppm) 6.33 (d, 1H, CH<sub>a</sub>CH<sub>b</sub>=CH), 6.09-6.01 (m, 1H, CH<sub>2</sub>=CH), 5.80 (t, 1H, CH<sub>a</sub>CH<sub>b</sub>=CH), 4.23 (dt, 2H, COOCH<sub>2</sub>), 3.60-3.50 (m, 4H, CH<sub>2</sub>N(COCH<sub>3</sub>)CH<sub>2</sub>), 2.50-2.43 (quint, 2H, CH<sub>2</sub>COO), 2.08 (t, 3H, NCOCH<sub>3</sub>), 1.38 (s, 9H, C(CH<sub>3</sub>)<sub>3</sub>).

*Synthesis of 3-(N-(2-(acryloyloxy)ethyl)acetamido)propanoic acid (4)*

Compound **3** (0.33 g, 1.20 mmol) was dissolved in 2 mL dichloromethane. Under ice-cooling, trifluoroacetic acid (0.66 g, 5.80 mmol) in 2 mL dichloromethane was added dropwise. The solution was allowed to warm up to room temperature and stirred for 18 h. Subsequently, solvent and excess TFA were removed under reduced pressure. The crude product was purified by column chromatography (SiO<sub>2</sub>, hexane/acetone 1/1 to methanol) to yield the product as a colourless liquid (yield: 56 %). <sup>1</sup>H NMR (400 MHz, D<sub>2</sub>O): δ<sub>H</sub> (ppm) 6.34 (dd, 1H, CH<sub>a</sub>CH<sub>b</sub>=CH), 6.17-6.08 (m, 1H, CH<sub>2</sub>=CH), 5.92 (t, 1H, CH<sub>a</sub>CH<sub>b</sub>=CH), 4.34-4.27 (dt, 2H, COOCH<sub>2</sub>), 3.69-3.48 (tt, 4H, CH<sub>2</sub>N(COCH<sub>3</sub>)CH<sub>2</sub>), 2.44-2.34 (dt, 2H, CH<sub>2</sub>COOH), 2.07 (s, 3H, NCOCH<sub>3</sub>). <sup>13</sup>C NMR (100 MHz, D<sub>2</sub>O): δ<sub>C</sub> (ppm) 180.3+179.7 (COOH), 174.5+174.4 (NCOCH<sub>3</sub>), 168.4+168.2 (CHCOOCH<sub>2</sub>), 132.8+132.6 (CH<sub>2</sub>=CH), 127.4+127.3 (CH<sub>2</sub>=CH), 62.2+61.9 (COOCH<sub>2</sub>), 47.8+46.6 (COOCH<sub>2</sub>CH<sub>2</sub>N), 44.4+43.6 (NCH<sub>2</sub>CH<sub>2</sub>COOH), 36.2+35.2 (CH<sub>2</sub>COOH), 20.8+20.5 (NCOCH<sub>3</sub>). HR ESI MS: *m/z*<sup>exp</sup> 230.1019 (M+H<sup>+</sup>), *m/z*<sup>theo</sup> 230.1023 (M+H<sup>+</sup>).

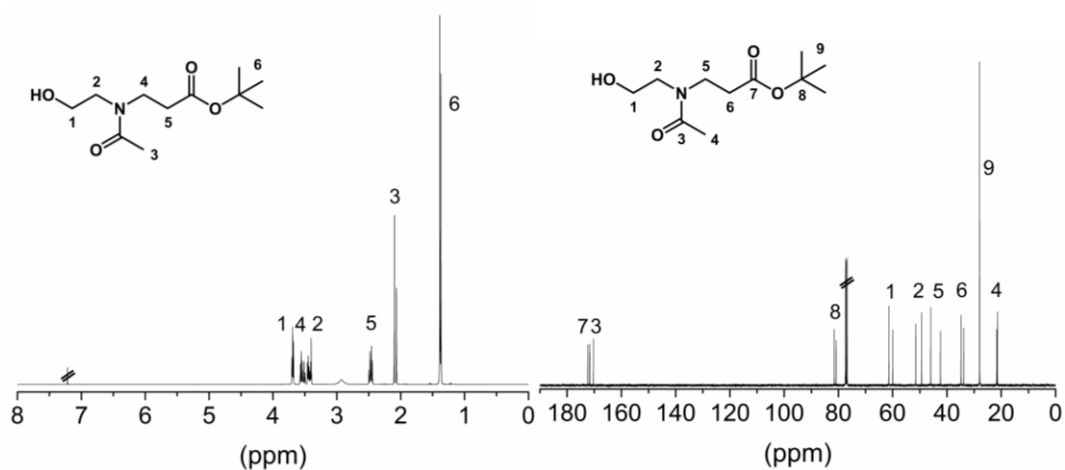


Figure 3.17 NMR analysis (CDCl<sub>3</sub>) of compound (2). Left: <sup>1</sup>H NMR. Right: <sup>13</sup>C NMR.

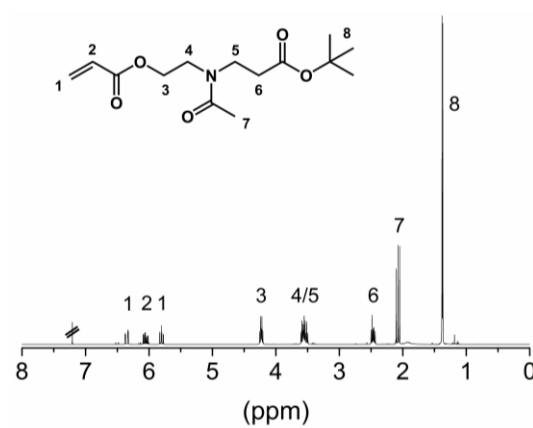


Figure 3.18 <sup>1</sup>H NMR analysis (CDCl<sub>3</sub>) of compound (3).

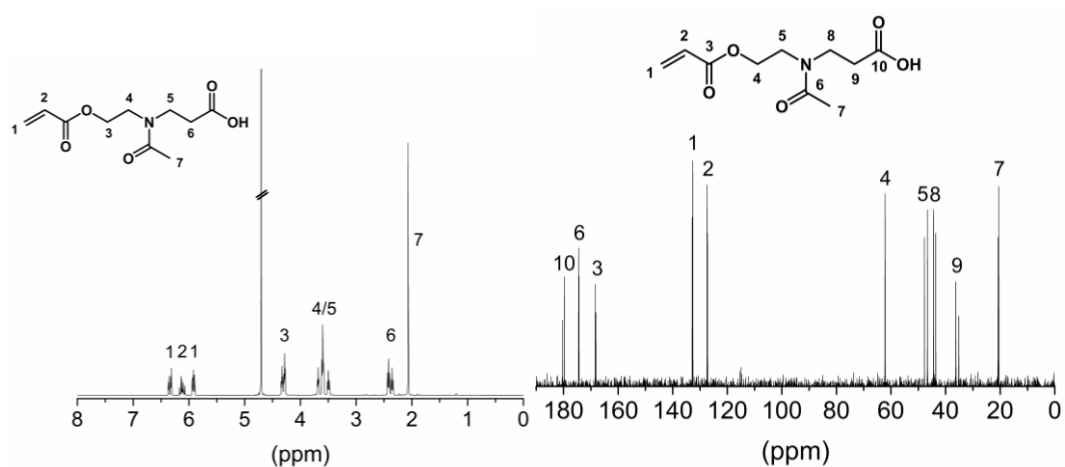


Figure 3.19 NMR analysis (D<sub>2</sub>O) of compound (4). Left: <sup>1</sup>H NMR. Right: <sup>13</sup>C NMR.

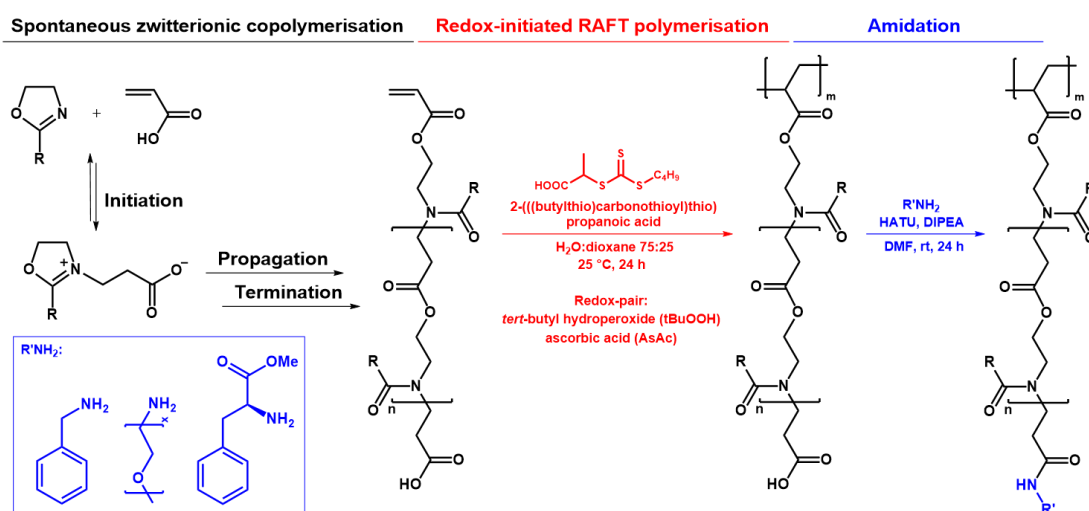
### 3.5. References

- 1 T. Saegusa, H. Ikeda and H. Fujii, *Macromolecules*, 1972, **5**, 354–359.
- 2 T. Saegusa, *Angew. Chem. Int. Ed.*, 1977, **16**, 826–835.
- 3 T. Saegusa, S. Kobayashi and Y. Kimura, *Macromolecules*, 1974, **7**, 139–140.
- 4 G. Odian and P. A. Gunatillake, *Macromolecules*, 1984, **17**, 1297–1307.
- 5 T. Saegusa, Y. Kimura and S. Kobayashi, *Macromolecules*, 1977, **10**, 236–239.
- 6 B. Verbraeken, B. D. Monnery, K. Lava and R. Hoogenboom, *Eur. Polym. J.*, 2017, **88**, 451–469.
- 7 W. Seeliger, E. Aufderhaar, W. Diepers, R. Feinauer, R. Nehring, W. Thier and H. Hellmann, *Angew. Chem. Int. Ed.*, 1966, **5**, 875–888.
- 8 T. Kagiya, T. Maeda, K. Fukui and S. Narisawa, *Polym. Lett.*, 1966, **4**, 441–445.
- 9 T. G. Bassiri, A. Levy and M. Litt, *Polym. Lett.*, 1967, **5**, 871–879.
- 10 D. A. Tomalia and D. P. Sheetz, *J. Polym. Sci. Part A Polym. Chem.*, 1966, **4**, 2253–2265.
- 11 E. Altuntaş, K. Kempe, A. Crecelius, R. Hoogenboom and U. S. Schubert, *Macromol. Chem. Phys.*, 2010, **211**, 2312–2322.
- 12 A. Baumgaertel, E. Altuntaş, K. Kempe, A. Crecelius and U. S. Schubert, *J. Polym. Sci. Part A Polym. Chem.*, 2010, **48**, 5533–5540.
- 13 A. Baumgaertel, C. Weber, K. Knop, A. Crecelius and U. S. Schubert, *Rapid Commun. Mass Spectrom.*, 2009, **23**, 756–762.
- 14 T. Gruending, S. Weidner, J. Falkenhagen and C. Barner-Kowollik, *Polym. Chem.*, 2010, **1**, 599.
- 15 G. Hart-Smith, *Anal. Chim. Acta*, 2014, **808**, 44–55.
- 16 J. V. Olsen, B. Macek, O. Lange, A. Makarov, S. Horning and M. Mann, *Nat. Methods*, 2007, **4**, 709–712.
- 17 P. Rizzarelli, D. Zampino, L. Ferreri and G. Impallomeni, *Anal. Chem.*, 2011, **83**, 654–660.
- 18 P. L. Urban, *Philos. Trans. R. Soc. A Math. Phys. Eng. Sci.*, 2016, **374**, 20150382.
- 19 D. Voll, T. Junkers and C. Barner-Kowollik, *J. Polym. Sci. Part A Polym. Chem.*, 2012, **50**, 2739–2757.
- 20 A. Lauer, D. E. Fast, A.-M. Kelterer, E. Frick, D. Neshchadin, D. Voll, G.

- Gescheidt and C. Barner-Kowollik, *Macromolecules*, 2015, **48**, 8451–8460.
- 21 B. Brügger, G. Erben, R. Sandhoff, F. T. Wieland and W. D. Lehmann, *Proc. Natl. Acad. Sci.*, 1997, **94**, 2339–2344.
- 22 B. T. Tuten, J. P. Menzel, K. Pahnke, J. P. Blinco and C. Barner-Kowollik, *Chem. Commun.*, 2017, **53**, 4501–4504.
- 23 K. Tang, J. S. Page and R. D. Smith, *J. Am. Soc. Mass Spectrom.*, 2004, **15**, 1416–1423.
- 24 M. Fujita, Y. Iizuka and A. Miyake, *J. Therm. Anal. Calorim.*, 2017, **128**, 1227–1233.
- 25 E. Altuntaş, C. Weber, K. Kempe and U. S. Schubert, *Eur. Polym. J.*, 2013, **49**, 2172–2185.
- 26 M. C. Bridoux and X. Machuron-Mandard, *Rapid Commun. Mass Spectrom.*, 2013, **27**, 2057–2070.
- 27 US2010016282, 2010.
- 28 V. K. Yadav and K. G. Babu, *J. Org. Chem.*, 2004, **69**, 577–580.
- 29 G. B. Desmet, R. D. Dagmar, P. S. Omurtag, P. Espeel, G. B. Marin and F. E. Du Prez, *J. Org. Chem.*, 2016, **81**, 12291–12302.
- 30 All pKa values are predicted values.
- 31 F. Wiesbrock, R. Hoogenboom, M. A. M. Leenen, M. A. R. Meier and U. S. Schubert, *Macromolecules*, 2005, **38**, 5025–5034.
- 32 M. M. Bloksma, R. M. Paulus, H. P. C. van Kuringen, F. van der Woerd, H. M. L. Lambermont-thijs and U. S. Schubert, *Macromol. Rapid Commun.*, 2012, **33**, 92–96.
- 33 H. Witte and W. Seeliger, *Angew. Chem. Int. Ed.*, 1972, **11**, 287–288.

## Chapter 4

# Dual stimuli-responsive comb polymer scaffolds from *N*-acylated poly(aminoester) macromonomers



Parts of this chapter have been published:

K. Kempe, P.A.J.M. de Jongh, A. Anastasaki, P. Wilson, D.M. Haddleton, *Chem. Commun.* **2015**, 51, 16213-16216; P.A.J.M. de Jongh, A. Mortiboy, G.S. Sulley, M.R. Bennett, A. Anastasaki, P. Wilson, D.M. Haddleton, K. Kempe, *ACS Macro Lett.* **2016**, 5, 321-325; P.A.J.M. de Jongh, M.R. Bennett, G.S. Sulley, P. Wilson, T.P. Davis, D.M. Haddleton, K. Kempe, *Polym. Chem.* **2016**, 7-6703-6707

## 4.1. Introduction

Stimuli-responsive polymers have become a major interest in polymer and material science over the last few decades for a wide range of applications, including drug delivery, tissue engineering, diagnostics and catalysis.<sup>1,2</sup> In general, the stimuli can be divided into three categories: physical, chemical and biological (Figure 4.1).<sup>3</sup> Dual- and multi-responsive materials are of particular interest as they are able to respond to complex environmental changes, such as in living organisms. For example, it has been demonstrated that tumour tissue generally has a lower pH compared to healthy tissue,<sup>4</sup> which has prompted the design of a wide range of pH-responsive drug delivery systems.<sup>5-7</sup> When combined with hyperthermia treatment, a common strategy against cancerous tissue,<sup>8</sup> an appropriately designed dual thermo- and pH-responsive material can be employed to specifically target tumour tissue by combining physical and chemical stimuli.<sup>9</sup>

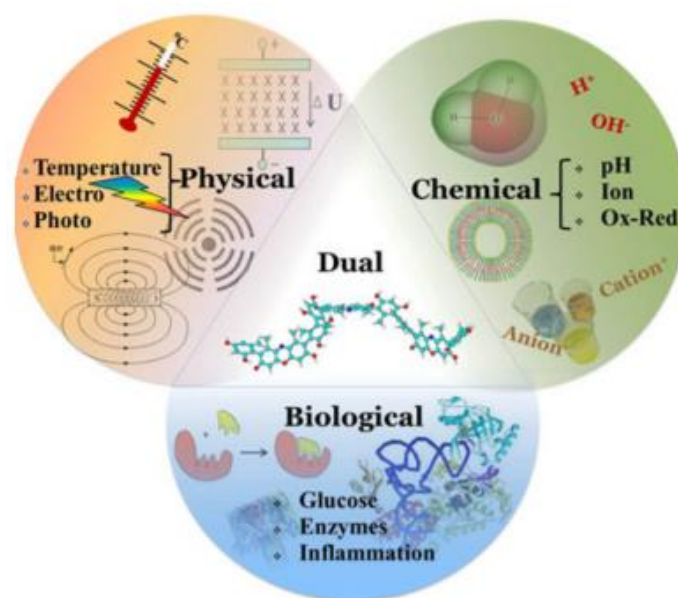


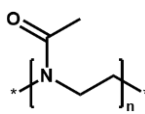
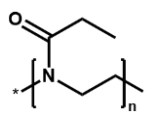
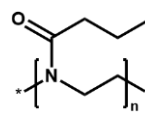
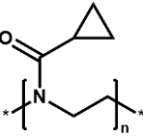
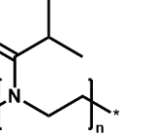
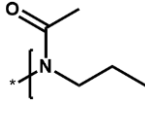
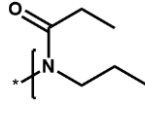
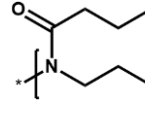
**Figure 4.1** Overview of physical, chemical and biological stimuli that can be implemented in polymer design. Adapted from ref. 3.

Amongst the various stimuli, pH- and thermo-responsiveness are the most widely investigated. Synthetically, pH-responsive polymers are typically obtained by (co-) polymerising monomers containing pendant pH-responsive groups.<sup>10</sup> The incorporation of pendant carboxylic acid groups, *e.g.* from (meth)acrylic acid, allows for hydrogen bonding below its  $pK_a$ . Similarly, the presence of amines in, for example, poly(ethyleneimine (PEI) and poly(amido amine) dendrimers allows pH-responsiveness in a different operational window and has been exploited in gene delivery applications.<sup>11</sup> There are only a few examples of dual-stimuli responsive homopolymers, of which tertiary amine-based methacrylates, in particular 2-(dimethylamino)ethyl methacrylate (DMAEMA), are the best-known examples.<sup>12–14</sup>

The class of thermo-responsive polymers mainly consists of materials that exhibit lower critical solution temperature (LCST) behaviour, which renders the polymer soluble below its cloud point ( $T_{CP}$ ), but insoluble when heated up above the  $T_{CP}$ . The temperature-induced insolubility results from broken hydrogen bonds between the polymers and the solvent as the  $T\Delta S$  term in  $\Delta G = \Delta H - T\Delta S$  becomes predominant, resulting in entropy-driven phase separation.<sup>15</sup> This selective solubility is particularly interesting when the  $T_{CP}$  is near body temperature, as it allows those polymers to be employed for drug delivery applications.

Most work on polymers with LCST behaviour has focussed on three main (classes of) polymers: poly(*N*-isopropylacrylamide) (PNIPAM), poly(oligo(ethylene glycol) monomethyl ether (meth)acrylate (PEG(M)A)), and poly(cyclic imino ether)s, specifically poly(2-oxazoline)s (POx) and poly(2-oxazine)s (POz). PNIPAM has received considerable interest as its LCST is close to body temperature (LCST = 32 °C).<sup>16</sup> POx have received significant attention over the last few decades as its facile synthesis of a wide range of monomers allows the synthesis of POx with tuneable LCST properties (Table 4.1), which, in combination with the biocompatibility of POx based on 2-methyl- (MeOx)<sup>17</sup> and 2-ethyl-2-oxazoline (EtOx),<sup>18</sup> has made it a highly attractive candidate for potential biomedical applications. POz are closely related to POx, but despite this have received far less attention.<sup>19,20</sup>

**Table 4.1** Structures and cloud points of water-soluble POx and POz.

<b>POx</b>					
	PMeOx	PEtOx	PnPrOx	PcPrOx	PiPrOx
<b><math>T_{CP}^a</math></b>	-	94 °C	27 °C	30 °C	44 °C
<b>POz</b>					
	PMeOz	PEtOz	PnPrOz		
<b><math>T_{CP}^a</math></b>	-	56 °C	11 °C		

<sup>a</sup> Cloud points for DPI100 homopolymers at 5 mg mL<sup>-1</sup> in water. Reproduced from ref. 21.

There are only a few examples of stimuli-responsive polymers based on poly(aminoester)s (PAEs). Joy and co-workers reported the synthesis of PAEs with similar structures to the NPAE macromonomers discussed in Chapters 2 and 3. A library of *N*-acylated diethanolamine monomers was synthesised by direct amidation of diethanolamine and the resulting monomers subsequently underwent polycondensation with succinic acid to form thermo-responsive NPAEs whereby the  $T_{CP}$  could be directly altered through modification of the polymer side chains.<sup>22–25</sup>

Zhou *et al.* synthesised hyperbranched PAEs through A<sub>2</sub> + B<sub>3</sub> Michael addition of 5-amino-1-pentanol with trimethylolpropane ethoxylate triacrylate. The resulting materials were not only thermoresponsive, but also pH responsive as a result of the introduction of tertiary amines. Interestingly, this dual-responsiveness leads to selective cell binding behaviour with HeLa cells as the collapse of the polymers above the pH-specific  $T_{CP}$  leads to shielding of the protonated polymers and thereby limits the interaction with the negatively charged cell membrane.<sup>26</sup>

Waymouth and co-workers developed a self-immolative cationic poly( $\alpha$ -aminoester). A Boc-protected 2-morpholinone monomer was synthesised in two-steps from diethanolamine and subsequently polymerised by organocatalytic ring-opening polymerisation (OROP).<sup>27</sup> Treatment with trifluoroacetic acid (TFA) efficiently removed the

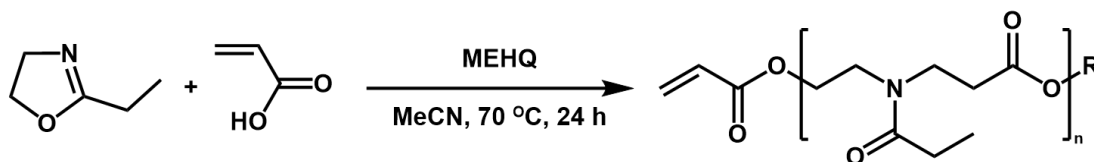
Boc protecting group to yield the PAE. When exposed to neutral (pH 7.4) or more alkaline conditions, the polymer rapidly degrades into *N,N'*-bis(2-hydroxyethyl)piperazine-2,5-dione. The cationic PAE enabled complexation with mRNA which is released upon pH-induced degradation of the polymer.<sup>28</sup> In a follow-up article they expanded this concept to lipid-modified versions for the delivery of plasmid DNA and obtained better results than the commercial standard Lipofectamine 2000.<sup>29</sup>

In this chapter the synthesis of well-defined dual stimuli-responsive comb polymers from *N*-acylated poly(aminoester) (NPAE) macromonomers by redox-initiated reversible addition-fragmentation chain transfer (RAFT) polymerisation is explored and their thermal properties in bulk and solution are studied. The efficient post-polymerisation functionalisation of these comb polymers is demonstrated with several model compounds.

## 4.2. Results and discussion

### 4.2.1. Macromonomer synthesis

A small library of NPAE macromonomers was synthesised by SZWIP, consisting of six macromonomers synthesised from three CIEs and two acrylates, and containing either 50 or 100 %  $\omega$ -carboxylic acid end groups using standard reaction conditions (Scheme 4.1).



**Scheme 4.1** Reaction conditions for the synthesis of macromonomers. SZWIP of EtOx with AA shown as example. R = H, CH<sub>2</sub>CH<sub>2</sub>NHCOEt.

<sup>1</sup>H NMR analysis (Figure 4.16, experimental details) revealed the degrees of polymerisation (DPs) of the various macromonomers by integrating the peaks of the  $\alpha$ -acrylate groups against the macromonomer backbone signals of the CIE and AA. The molecular weights were calculated from the DPs of the macromonomers. SEC analysis indicated relatively narrow molecular weight distributions (Figure 4.4), as summarised in Table 4.2.

**Table 4.2** Macromonomers employed for the synthesis of NPAE comb polymers.

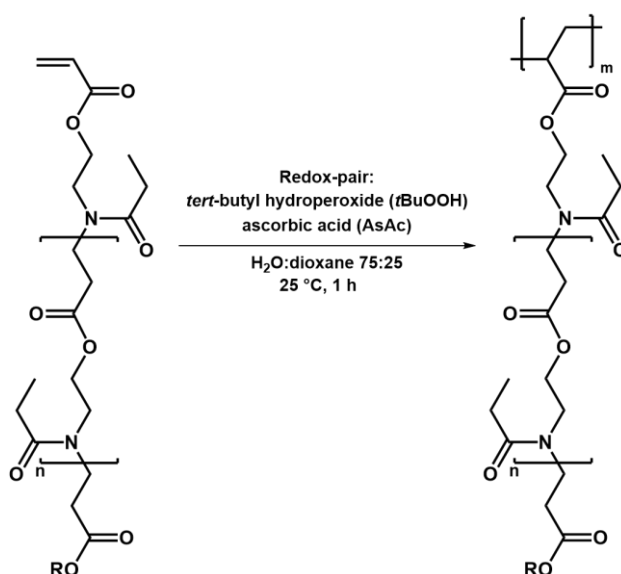
Entry <sup>a</sup>	CIE (M <sub>N</sub> )	Acrylate (M <sub>E</sub> )	Feed ratio	DP <sub>NMR</sub> [M <sub>N</sub> /M <sub>E</sub> ]	M <sub>n,NMR</sub> [g mol <sup>-1</sup> ]	M <sub>n,SEC</sub> [g mol <sup>-1</sup> ]	<i>D</i> <sub>SEC</sub>
<b>M1</b>	MeOx	AA	1 : 1	3/3	543	1500	1.27
<b>M2</b>	MeOx	AA	1 : 2	2.5/2.5	465	1300	1.18
<b>M3</b>	EtOx	AA	1 : 1	3/3	585	1600	1.22
<b>M4</b>	EtOx	AA	1 : 2	2/2	414	1300	1.16
<b>M5</b>	EtOx	CEA	1 : 1	3.5/3.5	996	1700	1.32
<b>M6</b>	EtOz	AA	1 : 1	3/3	627	2000	1.27

<sup>a</sup> All macromonomers synthesised using standard conditions: MeCN, 70 °C, 24 h.

## 4.2.2. Comb polymer synthesis

### 4.2.2.1. Free radical polymerisation

In order to evaluate the potential of the  $\alpha$ -acrylate end groups for polymerisation of the macromonomers into comb polymers, macromonomer M3 was subjected to a free radical polymerisation using the redox pair of ascorbic acid (AsAc) and *tert*-butylhydroperoxide (*t*BuOOH) as initiator at 25 °C (Scheme 4.2). <sup>1</sup>H NMR analysis of the crude reaction product revealed a complete disappearance of the acrylate signals ( $\delta = 5.5 - 6.5$  ppm, Figure 4.2b) and SEC analysis revealed the near-quantitative formation of a high molecular weight polymer ( $M_n = 245000$  g mol<sup>-1</sup>,  $D = 4.6$ , Figure 4.2c), thereby further demonstrating the quantitative introduction of the  $\alpha$ -acrylate end group.



**Scheme 4.2** Synthesis of comb polymers by redox-initiated free radical polymerisation of *N*-acylated poly(amino ester) macromonomer M3. R = H, CH<sub>2</sub>CH<sub>2</sub>NHCOEt.

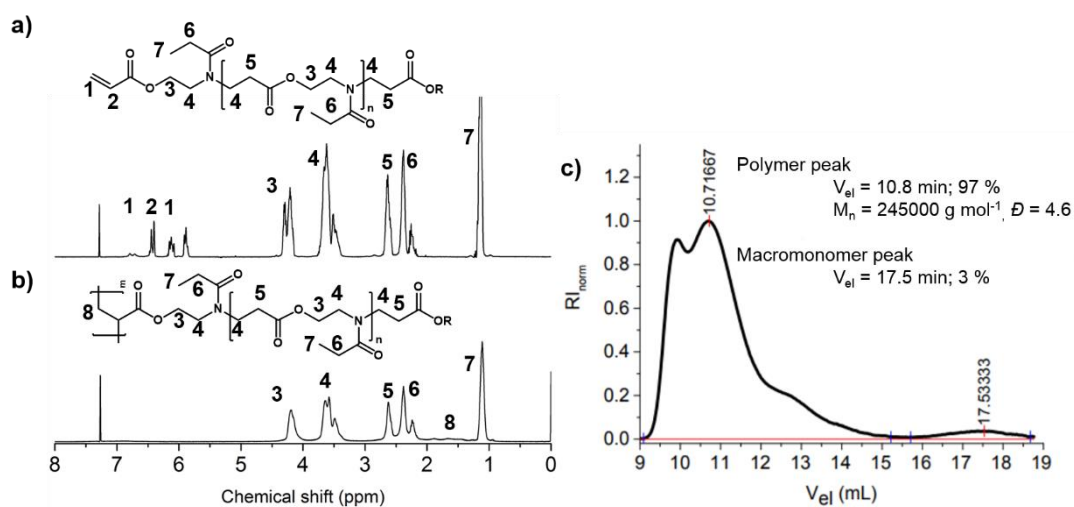


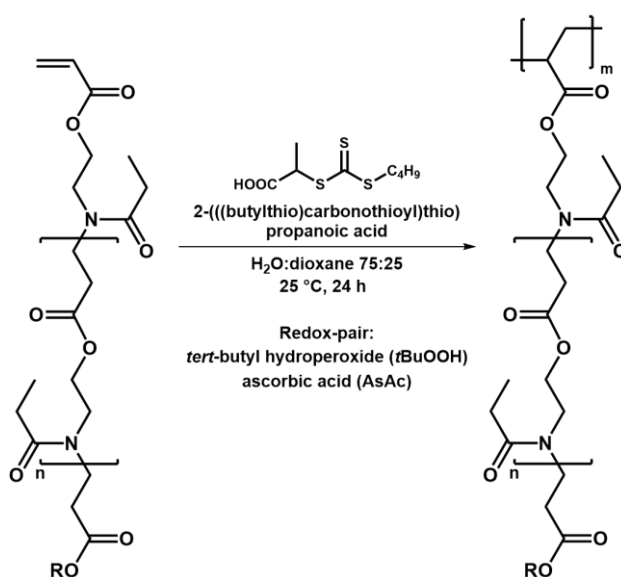
**Figure 4.2** <sup>1</sup>H NMR spectra (CDCl<sub>3</sub>) of macromonomer M3 (a) and the corresponding comb polymer (b) and SEC analysis of the comb polymer (c). R = H, CH<sub>2</sub>CH<sub>2</sub>NHCOEt.

#### 4.2.2.2. Redox-initiated RAFT polymerisation

In order to achieve more control over radical polymerisations, several controlled polymerisation techniques have been developed,<sup>30</sup> such as nitroxide mediated

polymerisation (NMP),<sup>31–33</sup> transition metal-mediated polymerisation<sup>34,35</sup> (including atom transfer radical polymerisation (ATRP)<sup>36–39</sup> and Cu(0)-mediated reversible deactivation radical polymerisation<sup>40–45</sup>), as well as reversible addition-fragmentation chain-transfer (RAFT) polymerisation (including macromolecular design *via* the interchange of xanthates (MADIX)),<sup>46–55</sup> and, most recently, sulphur-free RAFT.<sup>56–58</sup>

As a result of the general incompatibility of transition metal-mediated techniques with acidic monomers,<sup>35,38,39,44,45</sup> RAFT polymerisation technique was employed instead. Since it was first reported in 1998,<sup>46</sup> RAFT polymerisation has emerged as a popular polymerisation technique as it allows for the polymerisation of a broad range of monomers into polymers with predictable molecular weights, narrow molecular weight distributions (*D*) and high end-group fidelity.<sup>55</sup> A wide range of stimuli-responsive polymers has previously been synthesised by RAFT polymerisation and have been discussed in recent reviews by McCormick,<sup>59</sup> Sumerlin,<sup>60–62</sup> Dworak,<sup>63</sup> Bütün<sup>10</sup> and Moad.<sup>64</sup>



**Scheme 4.3** Synthesis of comb polymers by redox-initiated RAFT (RRAFT) polymerisation of *N*-acylated poly(aminoester) macromonomer M3. R = H, CH<sub>2</sub>CH<sub>2</sub>NHCOEt.

In this work an aqueous redox-initiated RAFT (RRAFT) polymerisation method that was recently developed by Perrier and co-workers was employed, which was demonstrated to facilitate the synthesis of polyacrylate and polyacrylamide multiblock copolymers at ambient temperatures below the LCST of the final polymers.<sup>65</sup>

Using 2-(((butylthio)carbonothioyl)thio)propanoic acid as a chain transfer agent (CTA) and the *AsAc*/*t*BuOOH redox pair as initiator (Scheme 4.3), a library of comb polymers was prepared (Figure 4.3, Table 4.3).

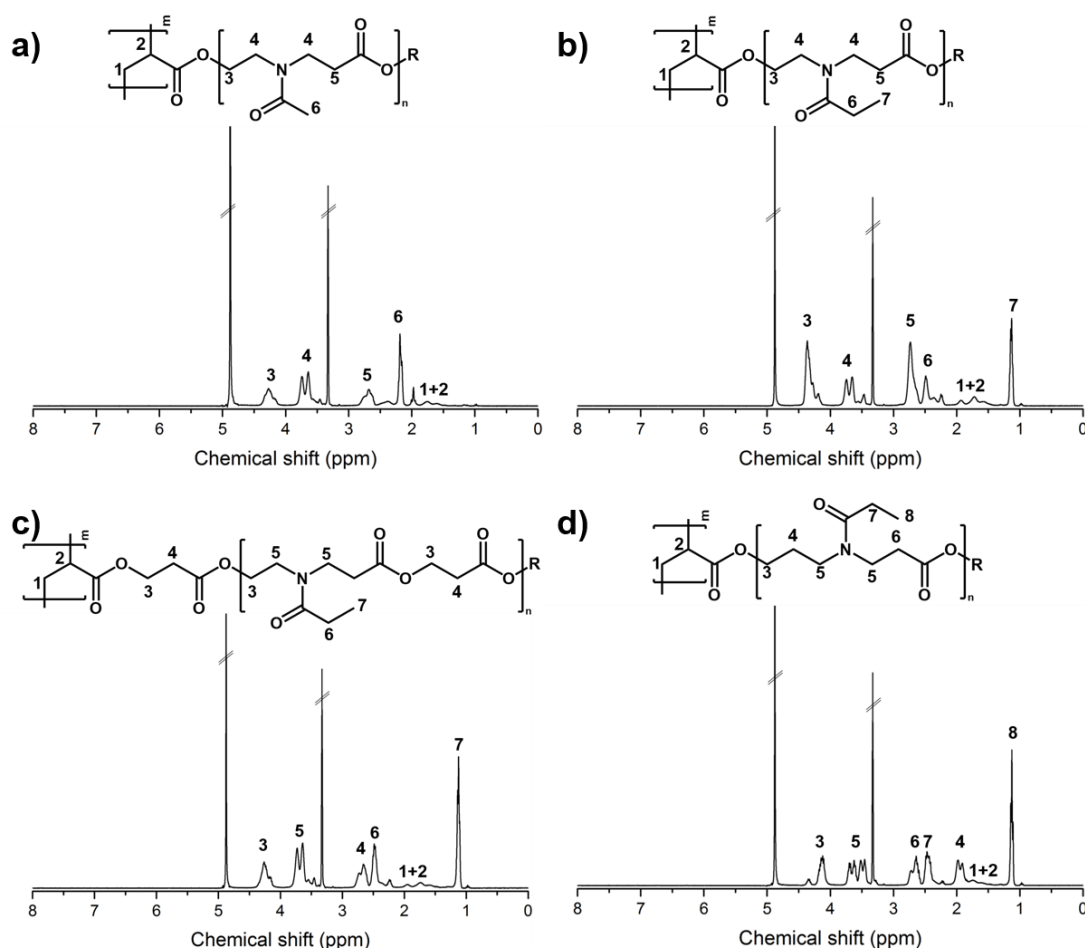


**Figure 4.3** <sup>1</sup>H NMR spectra (MeOD) for the comb polymers synthesised from NPAE macromonomers MeOx/AA (a), EtOx/AA (b), EtOx/CEA (c) and EtOz/AA (d). R = H or CH<sub>2</sub>CH<sub>2</sub>NHCOMe (MeOx), H or CH<sub>2</sub>CH<sub>2</sub>NHCOEt (EtOx), H or CH<sub>2</sub>CH<sub>2</sub>CH<sub>2</sub>NHCOEt (EtOz).

In all cases near-quantitative conversions ( $\geq 97\%$ ) were obtained after 24 h as determined by  $^1\text{H}$  NMR analysis of the crude sample. Any unreacted macromonomer was easily removed by dialysis against deionised water, followed by freeze-drying to yield the pure products (Figure 4.3). By changing the macromonomer-to-CTA ratio the DP of the comb polymers was adjusted from 10 to 100.

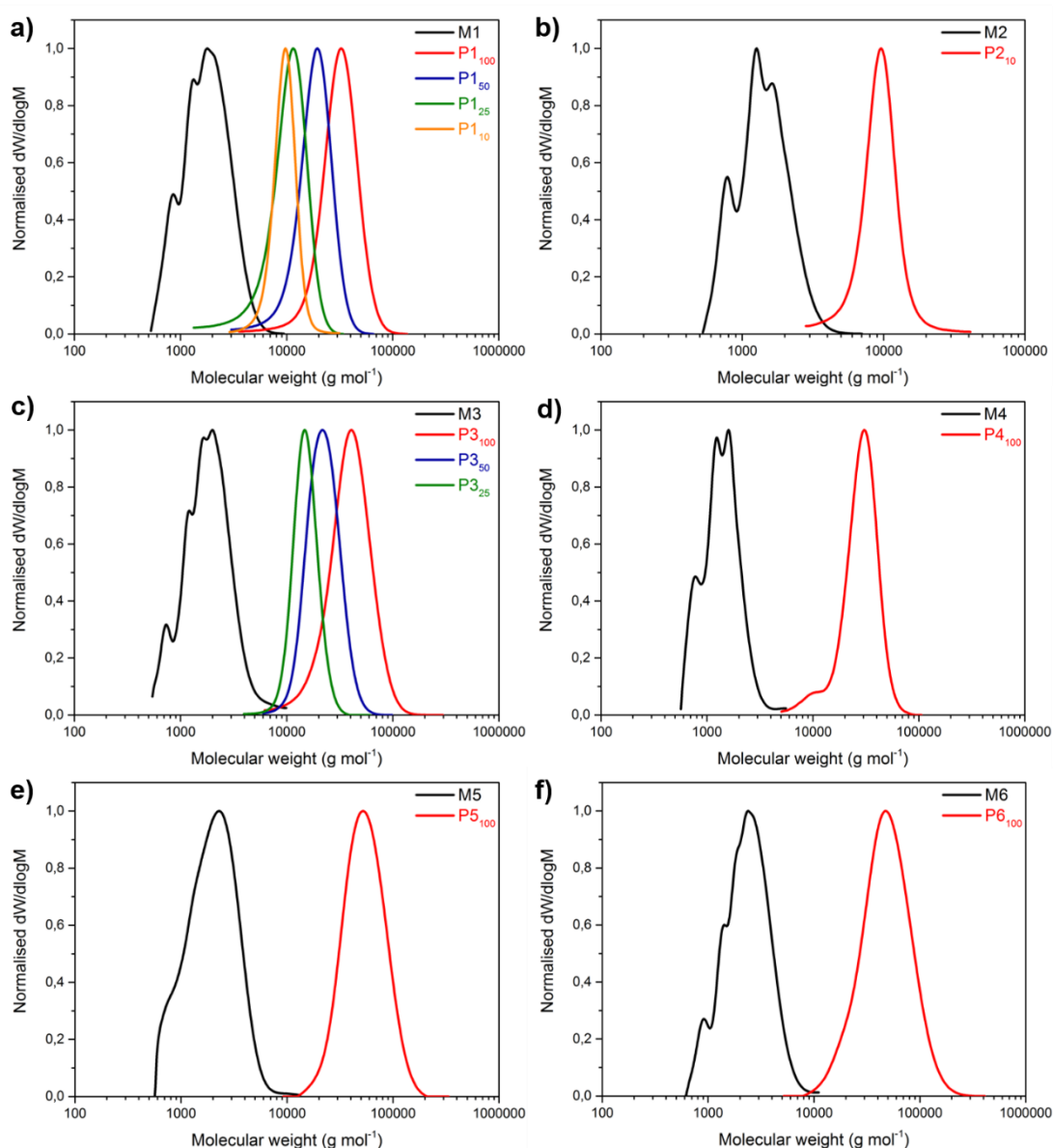


**Figure 4.4** Conventional SEC analysis of the macromonomers and comb polymers. Molecular weights and dispersity values are summarised in Tables 4.2 and 4.3.

SEC analysis revealed narrow molecular weight distributions ( $D_{SEC} \leq 1.35$ ) for all comb polymers. The molecular weights determined by SEC analysis for most comb polymers were significantly lower than those obtained from  $^1\text{H}$  NMR analysis as a result of the differences in solvodynamic volume between the linear PMMA calibrants and the comb polymers.<sup>66</sup>

Table 4.3 shows a complete overview of the comb polymers prepared by RRAFT, along with their molecular weights as determined by  $^1\text{H}$  NMR and conventional SEC analysis against PMMA calibrants.

**Table 4.3** Overview of comb polymers prepared by redox-initiated RAFT polymerisation.

Entry <sup>a</sup>	Macro- monomer	DP <sub>NMR</sub> <sup>b</sup>	M <sub>n,NMR</sub> <sup>b</sup> [g mol <sup>-1</sup> ]	M <sub>n,SEC</sub> <sup>c</sup> [g mol <sup>-1</sup> ]	M <sub>w,SEC</sub> <sup>c</sup> [g mol <sup>-1</sup> ]	D <sub>SEC</sub> <sup>c</sup>
P1 <sub>100</sub>	M1	100	54500	27600	33400	1.21
P1 <sub>50</sub>	M1	50	27300	16300	19400	1.19
P1 <sub>25</sub>	M1	25	13800	8700	10900	1.25
P1 <sub>10</sub>	M1	10	5670	9100	9800	1.07
P2 <sub>10</sub>	M2	10	4890	8800	9900	1.12
P3 <sub>100</sub>	M3	100	58740	36500	45300	1.24
P3 <sub>50</sub>	M3	50	29500	20600	24100	1.17
P3 <sub>25</sub>	M3	25	14870	14400	15600	1.08
P4 <sub>100</sub>	M4	100	41600	24900	29600	1.19
P5 <sub>100</sub>	M5	100	87550	48300	58400	1.21
P6 <sub>100</sub>	M6	100	63300	40400	54500	1.35

<sup>a</sup> Synthesised under standard conditions as shown in Scheme 4.3. <sup>b</sup> Calculated from crude  $^1\text{H}$  NMR sample. <sup>c</sup> Determined by SEC analysis in DMF against PMMA calibration.

#### 4.2.2.3. Triple detection SEC analysis

The molecular weights observed by SEC analysis are significantly lower than those determined by  $^1\text{H}$  NMR, which is a result of the significant difference in solvodynamic

volume of the linear PMMA used for calibration compared to the NPAE comb polymers studied in this work. In order to obtain molecular weights closer to their actual values, triple detection (TD) SEC analysis was employed for a selection of comb polymers (Figure 4.5, Table 4.4). The molecular weights obtained by TD SEC analysis are significantly closer to those calculated by  $^1\text{H}$  NMR analysis. The Mark-Houwink constant,  $\alpha$ , indicates all polymers behave as linear random coils.<sup>66</sup>

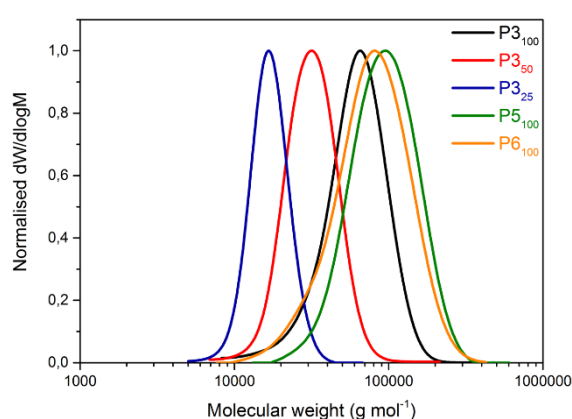


**Figure 4.5** Triple detection SEC analysis results for selected comb polymers.

**Table 4.4** Triple detection SEC analysis results for selected comb polymers.

Entry	$M_{n,NMR}^a$ [g mol <sup>-1</sup> ]	$M_{n,TD SEC}^b$ [g mol <sup>-1</sup> ]	$M_{w,TD SEC}^b$ [g mol <sup>-1</sup> ]	$\bar{D}_{TD}$ SEC <sup>b</sup>	$\alpha^{bc}$	$R_g^{bd}$	$R_h^{be}$	IV <sup>bf</sup>
<b>P3<sub>100</sub></b>	58740	52400	67100	1.28	0.47	5.27	4.53	0.103
<b>P3<sub>50</sub></b>	29500	28600	33500	1.17	0.41	3.85	3.35	0.080
<b>P3<sub>25</sub></b>	14870	16000	17600	1.10	0.42	3.15	2.61	0.064
<b>P5<sub>100</sub></b>	87550	81500	102700	1.26	0.46	6.75	5.77	0.118
<b>P6<sub>100</sub></b>	63300	64400	87600	1.36	0.51	6.28	5.53	0.120

<sup>a</sup> Calculated from the crude  $^1\text{H}$  NMR sample. <sup>b</sup> Determined by TD SEC in DMF using differential refractive index (dRI), light scattering (LS, 90 ° and 15 °) and viscometry (VS) detectors. <sup>c</sup> Mark-Houwink constant. <sup>d</sup> Radius of gyration. <sup>e</sup> Solvodynamic radius. <sup>f</sup> Intrinsic viscosity.

### 4.2.3. Thermal analysis

The bulk thermal properties of the comb polymers were determined by TGA and DSC analysis (Figure 4.6). All comb polymers exhibit thermal stability up to a temperature of 200 °C, after which a structure-dependant degradation can be observed.

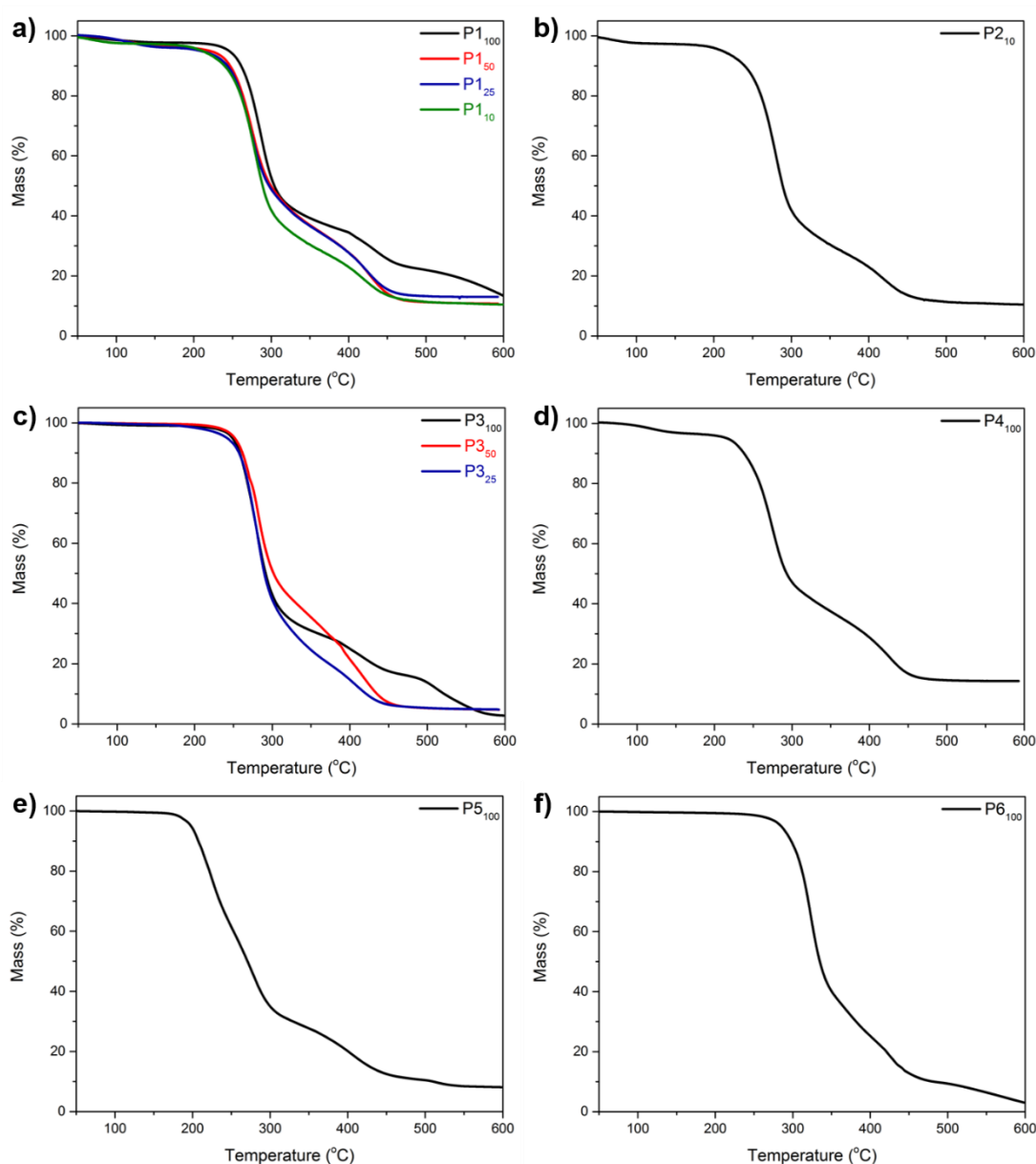


**Figure 4.6** Thermogravimetric analysis of comb polymers P1<sub>x</sub> (a), P2<sub>10</sub> (b), P3<sub>x</sub> (c), P4<sub>100</sub> (d), P5<sub>100</sub> (e) and P6<sub>100</sub> (f).

DSC analysis (Figure 4.7, Table 4.5) revealed two main trends. Comb polymers with a higher number of  $\omega$ -carboxylic acid side chains have higher  $T_g$ s, which results from increased hydrogen bonding between the side chain end groups and polymer backbone.<sup>67–69</sup> Furthermore, the  $T_g$  decreases as the comb polymer side chain size increases (e.g. P1<sub>100</sub> cf. P6<sub>100</sub>) as a result of disrupted packing of the polymer chains.<sup>70</sup>

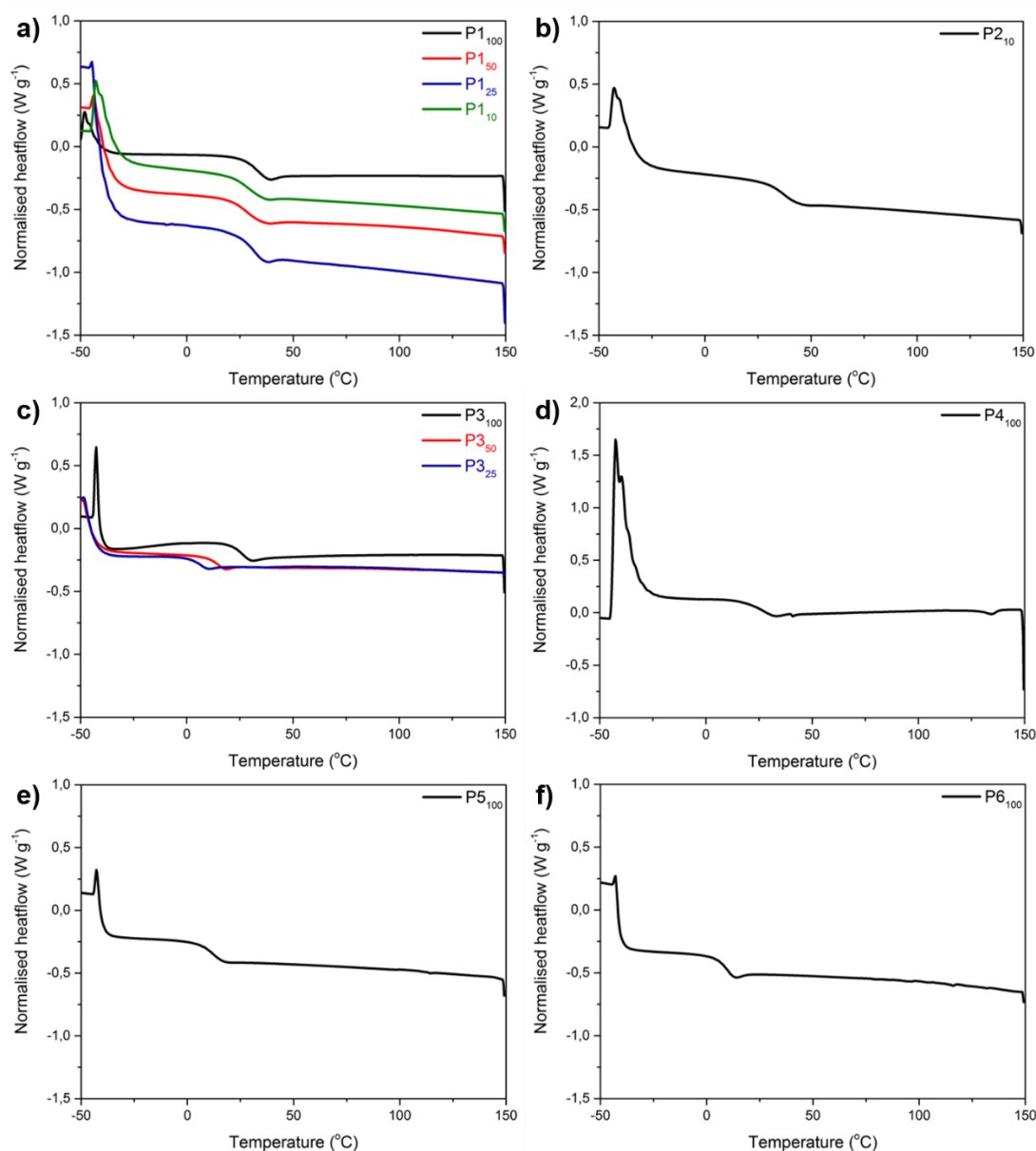


**Figure 4.7** DSC analysis (second heating curve) of comb polymers P1<sub>x</sub> (a), P2<sub>10</sub> (b), P3<sub>x</sub> (c), P4<sub>100</sub> (d), P5<sub>100</sub> (e) and P6<sub>100</sub> (f).

**Table 4.5** Glass transition temperatures for comb polymers from NPAE macromonomers.

<b>Comb polymer</b>	<b>P1<sub>100</sub></b>	<b>P1<sub>50</sub></b>	<b>P1<sub>25</sub></b>	<b>P1<sub>10</sub></b>
<b><i>T<sub>g</sub></i> (°C)</b>	33.8	31.0	31.9	31.0
<b>Comb polymer</b>	<b>P2<sub>10</sub></b>	<b>P3<sub>100</sub></b>	<b>P3<sub>50</sub></b>	<b>P3<sub>25</sub></b>
<b><i>T<sub>g</sub></i> (°C)</b>	38.7	25.6	13.5	5.4
<b>Comb polymer</b>	<b>P4<sub>100</sub></b>	<b>P5<sub>100</sub></b>	<b>P6<sub>100</sub></b>	
<b><i>T<sub>g</sub></i> (°C)</b>	27.0	12.2	8.7	

Glass transition temperatures determined by DSC analysis on the second heating run.

#### 4.2.4. LCST studies

Poly(2-oxazoline)s (POx) are well known for their LCST behaviour, which has made them interesting candidates for drug delivery applications.<sup>21,71–74</sup> The NPAE macromonomers studied in this work are structurally similar to POx and it was therefore hypothesised that they could exhibit similar aqueous solubility properties. The macromonomers are completely soluble in aqueous solutions between 10 and 90 °C, as determined by turbidity studies using UV-Vis spectroscopy at  $\lambda = 500$  nm. Comb polymers based on MeOx/AA macromonomers also remained soluble at concentrations up to 20 mg mL<sup>-1</sup>, similar to poly(2-methyl-2-oxazoline)s,<sup>21</sup> however, comb polymers synthesised from the other macromonomers did show temperature-dependant solubility in aqueous solutions (5 mg mL<sup>-1</sup> in HPLC grade H<sub>2</sub>O, unless otherwise stated).

Figure 4.8a illustrates a typical third heating and cooling cycle for P3<sub>100</sub>, measured at pristine pH (~ 4.2). A  $T_{CP}$  of 37.3 °C was observed on the heating cycle and a slightly lower  $T_{CP}$  of 33.5 °C on the cooling cycle as a result of thermal hysteresis. To illustrate the reproducibility of these results, five batches of macromonomer M3 were synthesised and polymerised into five batches of P3<sub>100</sub>.  $T_{CP}$  measurements at pH 4.0 revealed an average  $T_{CP}$  of  $34.85 \pm 1.35$  °C, demonstrating good reproducibility of the results (Figure 4.8b). A  $T_{CP}$  study at different concentrations revealed a  $T_{CP}$  of 37.5 °C for P3<sub>100</sub> at 0.25 mg mL<sup>-1</sup> decreasing to 29.2 °C at 20 mg mL<sup>-1</sup> (Figure 4.8c), which is an expected trend at this concentration range.<sup>15</sup> Moreover, the  $T_{CP}$  is often dependant on

the molecular weight of the polymer, with higher molecular weights leading to lower  $T_{CP}$ ,<sup>74</sup> and thus the effect of the DP of P3 on the  $T_{CP}$  was studied by comparing P3<sub>100</sub>, P3<sub>50</sub> and P3<sub>25</sub>. As the DP and thus the molecular weight decreases, the  $T_{CP}$  increases from 34.5 °C to 38.2 °C (Figure 4.8d).

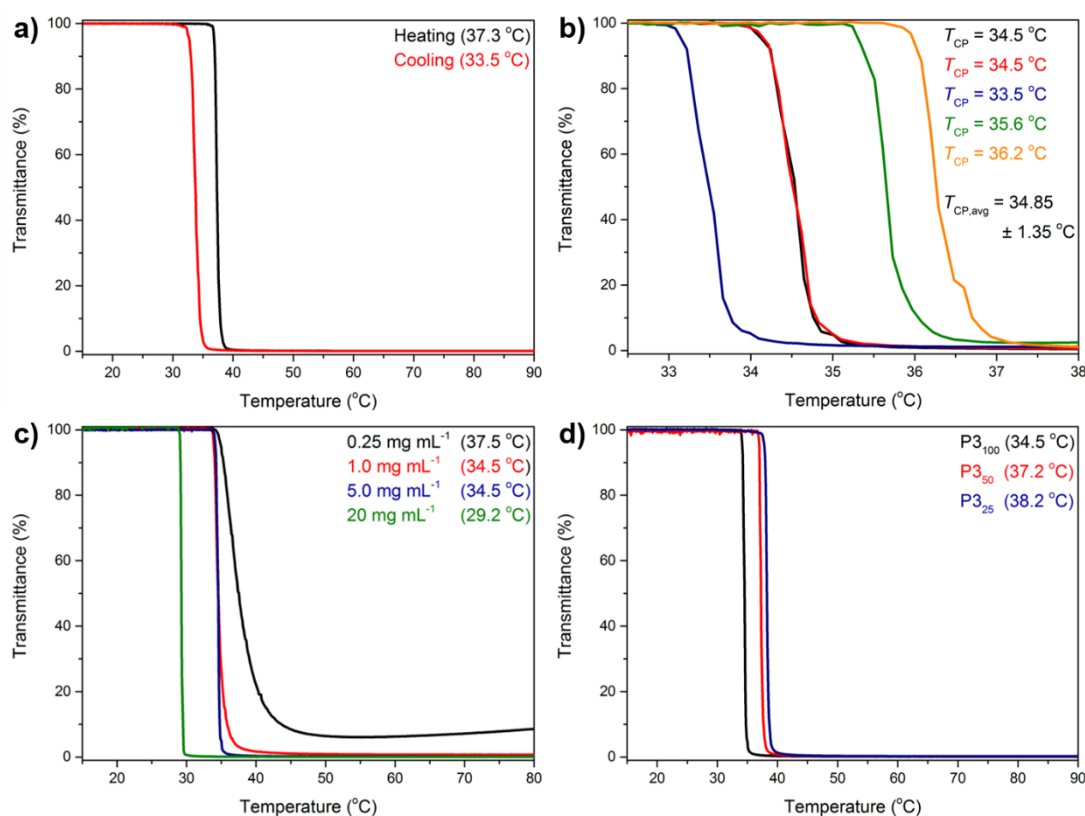


**Figure 4.8** Cloud point studies on comb polymer P3 at pH 4.0, 5 mg mL<sup>-1</sup> in HPLC grade H<sub>2</sub>O, unless otherwise stated. a) Heating and cooling cycle of P3<sub>100</sub> at pristine pH. b) Reproducibility studies on P3<sub>100</sub>. c) Effect of concentration of P3<sub>100</sub> on the cloud point. d). Effect of DP of P3 on the cloud point.

The  $T_{CP}$  of P3<sub>100</sub> was then studied at different pH values, to evaluate the effect of different degrees of protonation of the  $\omega$ -carboxylic acid end groups on the comb polymer side chains on the  $T_{CP}$  of the comb polymer. It was observed that lower pH, and thus more protonation, leads to a decrease in  $T_{CP}$ , with a  $T_{CP}$  as low as 15 °C observed at pH 2.91. Conversely, an increase in pH by addition of aqueous NaOH increases the

$T_{CP}$  up to 76 °C at pH 4.81. At higher pH the comb polymer remains completely soluble within the evaluated temperature range (Figure 4.9a). Increased protonation at lower pH increases the hydrogen bonding of the  $\omega$ -carboxylic acid end groups to the macromonomer backbone and thereby reduces hydrogen bonding with surrounding water molecules. This demonstrates that these NPAE comb polymers are not only thermoresponsive, but also pH-responsive materials, making them even more interesting for various applications. It was hypothesised that increasing the amount of  $\omega$ -carboxylic acid end groups on the comb polymer side chains from 50 % to 100 %, would have an additional effect on the  $T_{CP}$ . Indeed, comparing P3<sub>100</sub> with P4<sub>100</sub> revealed a significant decrease in  $T_{CP}$  from 34.9 °C to 19.3 °C at pH 4.0 (Figure 4.9b). The higher  $\omega$ -carboxylic acid content of the side chains allows for more hydrogen bonding with the macromonomer backbone and thereby influences the solubility of the comb polymer as the available hydrogen bonds with the surrounding water molecules decreases.

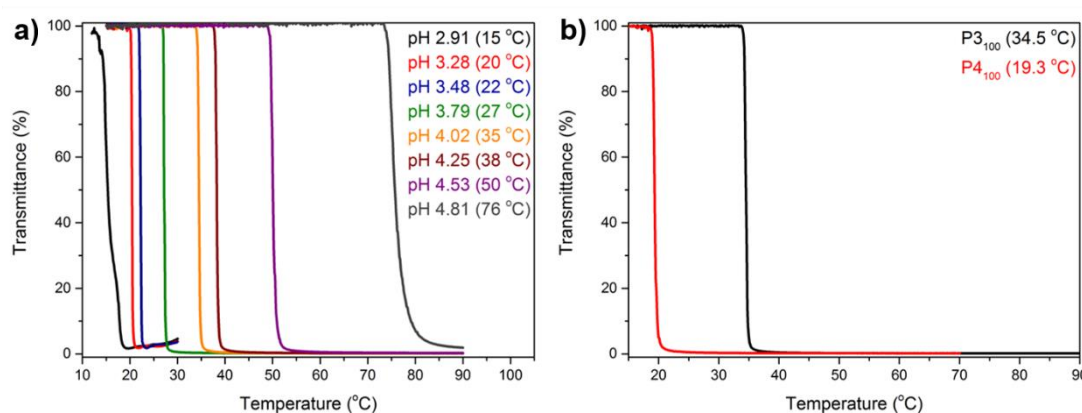


**Figure 4.9** Dual-responsive aqueous solubility of NPAE comb polymers. a) The cloud point of P3<sub>100</sub> is dependent on the pH of the solution and decreases with decreasing pH. b) Decrease of cloud point with increase  $\omega$ -carboxylic acid end groups on the comb polymer side chain.

To investigate the effect of different comb polymer structures, P3<sub>100</sub> (from EtOx/AA), and P6<sub>100</sub> (EtOz/AA) were compared. Similar to P3<sub>100</sub> discussed before, the solubility of P6<sub>100</sub> at different pH was evaluated. As a result of the more hydrophobic nature of

EtOz compared to EtOx units, the  $T_{CP}$  for P6<sub>100</sub> at a given pH is lower than for P3<sub>100</sub> (Figure 4.10).

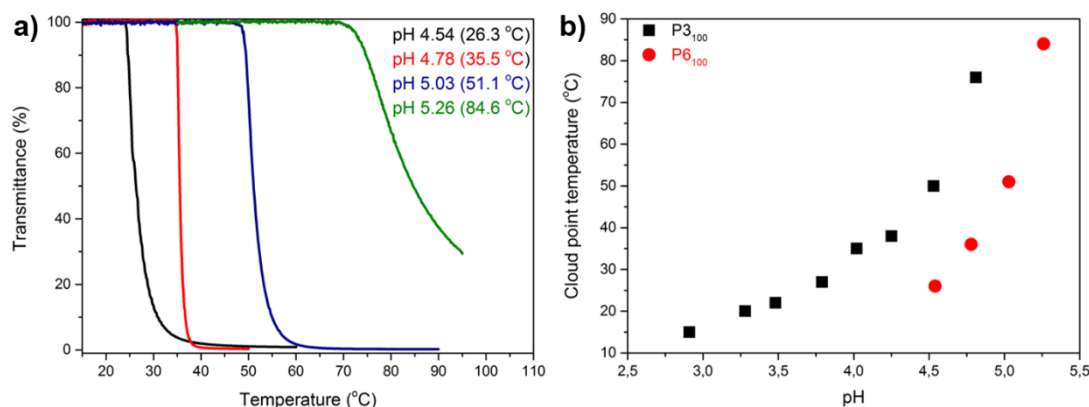


**Figure 4.10** Cloud point measurements of P6<sub>100</sub> at varying pH (a) and compared to P3<sub>100</sub> (b) in HPLC grade H<sub>2</sub>O (5 mg mL<sup>-1</sup>).

It is known that the addition of salts to the medium in which  $T_{CP}$  measurements are conducted can have a significant effect on the  $T_{CP}$ , either through salting-in or salting-out effects. In order to establish if such effects also apply to these NPAE comb polymers, the solubility of P3<sub>100</sub> and P6<sub>100</sub> in HPLC grade H<sub>2</sub>O was compared to that in PBS buffer. Two different pH values were tested for each comb polymer. For both comb polymers as well as at both pH, the  $T_{CP}$  in PBS buffer is lower than in HPLC grade H<sub>2</sub>O (Figure 4.11). This salting-out effect can be mainly attributed to the presence of kosmotropic Cl<sup>-</sup> (from NaCl) in the PBS buffer, which destabilises hydrogen bonds between the polymers and water.<sup>75</sup> Further coagulation of the polymer aggregates can be observed in PBS, leading to phase segregation and increased transmittance.

Finally, the solubility of P3<sub>100</sub>, P5<sub>100</sub> (EtOx/CEA) and P6<sub>100</sub> were compared at different pH in HPLC grade H<sub>2</sub>O and PBS buffer at a constant temperature of 25 °C. As shown in Figure 4.12, P5<sub>100</sub> is the most hydrophobic of these three comb polymers. Whereas solutions of P3<sub>100</sub> are soluble at pH 3.5 and above, P6<sub>100</sub> becomes insoluble below pH

4.5 and P5<sub>100</sub> is insoluble below pH 5.3. This further illustrates the dependency of the solubility behaviour on the comb polymer composition as well as the medium.

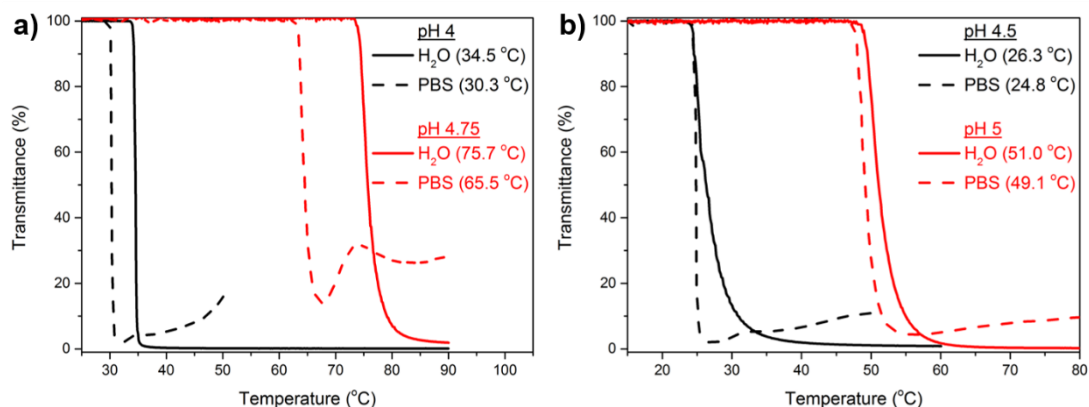


**Figure 4.11** Cloud point measurements of P3<sub>100</sub> (a) and P6<sub>100</sub> (b) in HPLC grade H<sub>2</sub>O and PBS buffer, demonstrating a salting out effect.

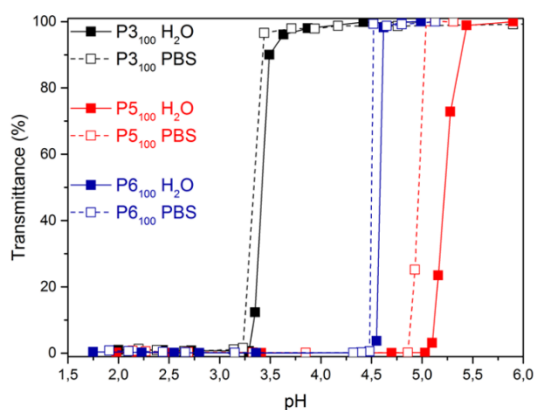


**Figure 4.12** pH-dependent aqueous solubility of P3<sub>100</sub>, P5<sub>100</sub> and P6<sub>100</sub> in HPLC grade H<sub>2</sub>O and PBS buffer at 25 °C.

#### 4.2.5. Comb polymer functionalisation

Post-polymerisation functionalisation has become an interesting route for the synthesis of functional materials.<sup>76,77</sup> Rather than polymerising pre-functionalised monomers,

post-polymerisation functionalisation allows the synthesis of a common precursor polymer which can then be conveniently modified. This is not only a more efficient strategy to obtain a library of polymers with different functionalities, but is also particularly useful for functional groups that interfere with the polymerisation itself. Common post-polymerisation methods, which are preferably highly selective, quantitative and enable facile purification, include the copper-catalysed alkyne-azide cycloaddition (CuAAC), activated ester coupling, thiol-X reactions (*e.g.* thiol-ene), Diels-Alder cycloaddition, isocyanate modifications, ring-opening reactions, nucleophilic substitution reactions and multicomponent reactions.<sup>76-80</sup>

The comb polymers studied in this work have pendant carboxylic acid groups and thus amidation is a logical choice to functionalise the comb polymers. Specifically, the modification of comb polymers P1<sub>10</sub> and P2<sub>10</sub> with a small molecule (benzylamine), a polymer (PEG-amine) and an amino acid (phenylalanine methylester (PME)) as a peptide mimic were investigated, employing 1-[bis(dimethylamino)methylene]-1*H*-1,2,3-triazolo[4,5-*b*]pyridinium 3-oxid hexafluorophosphate (HATU) and *N,N*-diisopropylethylamine (DIPEA) as the coupling agent and base, respectively.

Reactions were carried out for 24 h in DMF at room temperature, after which the polymers were purified by dialysis. <sup>1</sup>H NMR analysis allowed quantification of the degree of functionalisation (DF). By integration of the relevant peaks, it was determined that for P1<sub>10</sub> approximately 50 % of the comb polymer side chains are functionalised. This is in good agreement with the results discussed in Chapter 2 that approximately 50 % of the macromonomers prepared from an equimolar CIE:AA feed (*i.e.* M1 used for P1<sub>10</sub>) bear ω-carboxylic acid end groups. For the functionalisation of P2<sub>10</sub> with benzylamine and PME (near-)quantitative functionalisation was observed, again in good agreement with the ω-carboxylic acid end group titration results. Only P2<sub>10</sub> with PEG-amine did not show full functionalisation, which is most likely the result of steric hindrance of the comb polymer side chains after partial functionalisation.

SEC analysis of the functionalised comb polymers showed a small shift in molecular weight for the functionalisation with benzylamine and PME, whereas functionalisation with PEG-amine resulted in more significant shifts in the SEC spectra (Figure 4.13).

For all examples narrow distributions were retained, indicative of the absence of side reactions.

**Table 4.6** Results for the functionalisation of DP10 comb polymers with selected amines.

Comb polymer	Amine	DF <sup>a</sup> [%]	M <sub>n,SEC</sub> [g mol <sup>-1</sup> ]	<i>D</i> <sub>SEC</sub>	T <sub>g</sub> <sup>b</sup> [°C]
<b>P1<sub>10</sub></b>	-	-	9100	1.07	31.0
	Benzylamine	54	8200	1.14	32.4
	PEG-amine	45	12600	1.14	33.0
	PME <sup>c</sup>	51	9100	1.10	34.7
<b>P2<sub>10</sub></b>	-	-	8800	1.07	38.7
	Benzylamine	Quant.	9200	1.22	36.8
	PEG-amine	80	17200	1.16	- <sup>d</sup>
	PME <sup>c</sup>	95	9900	1.09	42.7

<sup>a</sup> Degree of functionalisation as determined by <sup>1</sup>H NMR based on DP10 comb polymers and one RRAFT CTA carboxylic end group. <sup>b</sup> Determined by DSC analysis on the second heating cycle. <sup>c</sup> Phenylalanine methylester hydrochloride. <sup>d</sup> No T<sub>g</sub> observed.

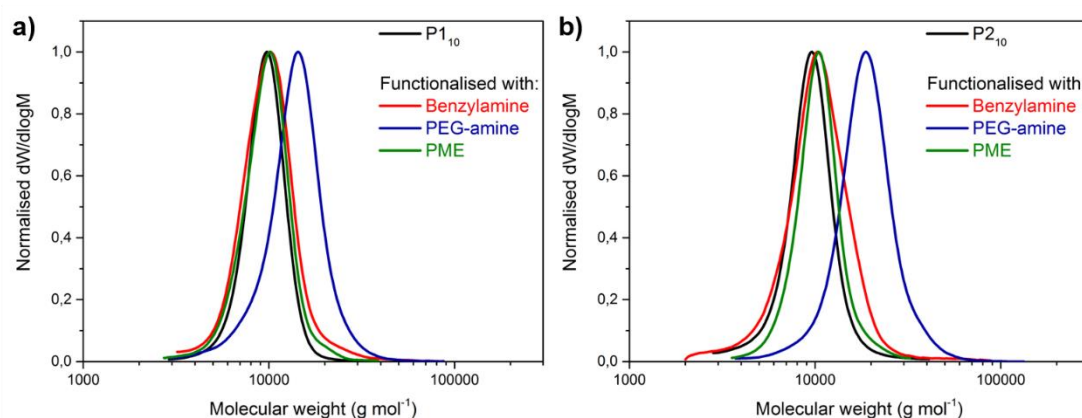


**Figure 4.13** SEC analysis for the functionalisation of P1<sub>10</sub> and P2<sub>10</sub> with selected amines. PME = phenylalanine methyl ester.

The introduction of new side chain end groups lead to small changes in the glass transition temperatures ( $T_g$ ) of the comb polymers, except for the PEG-amine functionalisation of P2<sub>10</sub> where a  $T_g$  was no longer observed (Figure 4.14). Thermogravimetric analysis showed similar degradation profiles for the benzylamine and PME functionalised comb polymers compared to the for the non-functionalised comb polymers. An additional degradation step can be observed for the comb polymers with PEG-amine functionalisation, which provides additional evidence for the successful functionalisation (Figure 4.15).

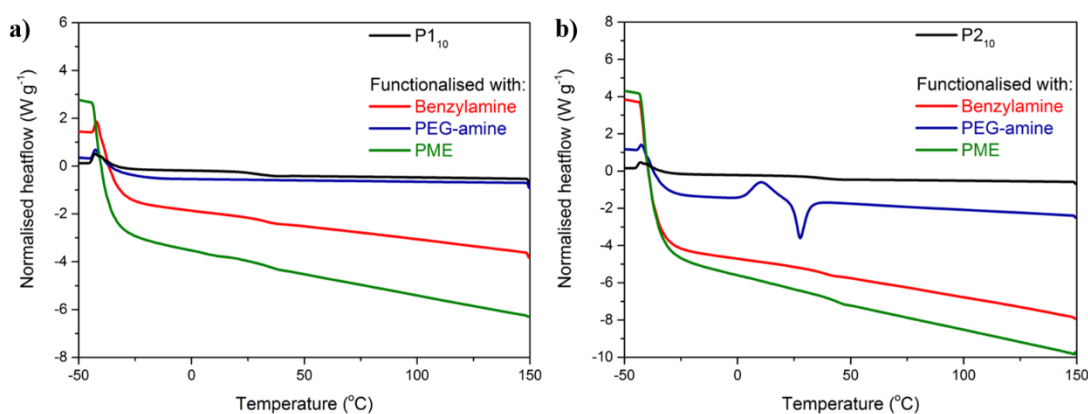


**Figure 4.14** DSC analysis of the functionalisation of P1<sub>10</sub> and P2<sub>10</sub> with selected amines. PME = phenylalanine methyl ester.

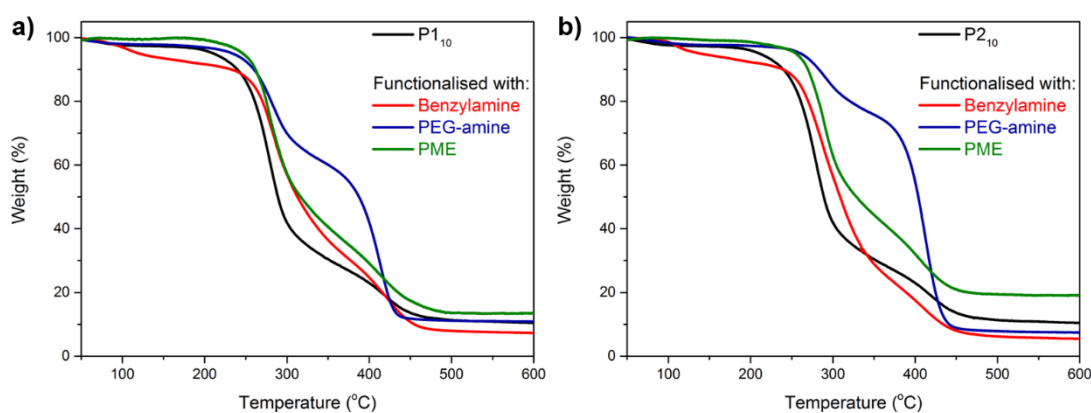


**Figure 4.15** Thermogravimetric analysis of the functionalisation of P1<sub>10</sub> and P2<sub>10</sub> with selected amines. PME = phenylalanine methyl ester.

### 4.3. Conclusions

In this Chapter the synthesis of well-defined comb polymers from *N*-acylated poly(aminoester) macromonomers by aqueous redox-initiated RAFT polymerisation was investigated. The degree of polymerisation could be easily tuned from 10 to 100 while retaining narrow molecular weight distributions. The comb polymers have good thermal stability and structure-dependant glass transition temperatures. Studies on the aqueous solubility of these NPAE comb polymers revealed a dual-stimuli responsive nature for comb polymers synthesised from EtOx/AA, EtOx/CEA and EtOz/AA macromonomers. These comb polymers have cloud points that can be further changed by alteration of the pH. It was observed that the  $T_{CP}$  could be influenced by the hydrophobicity and amount of  $\omega$ -carboxylic acid groups of the macromonomers, as well as the DP of the comb polymers, facilitating a broad operational window. Finally, the facile functionalisation of the pendant carboxylic acid groups with three model amines was demonstrated, thereby further emphasising the potential of these comb polymers.

### 4.4. Experimental details

#### 4.4.1. Materials

Acrylic acid (AA, 99 %, anhydrous, Sigma Aldrich), acetonitrile (MeCN, 99.8 %, Sigma Aldrich), 4-methoxyphenol (MEHQ, 99 %, Sigma Aldrich), diethyl ether (Et<sub>2</sub>O, > 98 %, Sigma Aldrich), 2-carboxyethyl acrylate (CEA, 98 %, Sigma Aldrich), Luperox® TBH70X *tert*-butylhydroperoxide solution (*t*BuOOH, 70 wt. % in H<sub>2</sub>O, Sigma Aldrich) and L-ascorbic acid (AsAc, > 99.5 %, Sigma Aldrich), 1,4-dioxane (> 98 %, Sigma Aldrich), benzylamine (99 %, Sigma Aldrich),  $\alpha$ -methoxy- $\omega$ -aminopoly(ethylene glycol) (PEG-amine,  $M_w = 750 \text{ g mol}^{-1}$ , > 99 %, Rapp Polymere), phenylalanine methylester hydrochloride (PME, 98 %, Sigma Aldrich), 1-[bis(dimethylamino)methylene]-1*H*-1,2,3-triazolo[4,5-*b*]pyridinium 3-oxid hexafluorophosphate (HATU, 98

%, Alfa Aesar), *N,N*-diisopropylethylamine (DIPEA, 99 %, Sigma Aldrich), *N,N*-dimethylformamide (DMF, 99 %, Fisher Scientific), phosphate buffered saline (PBS, 10x concentrate, Bioperformance Certified, Sigma Aldrich), deuterated chloroform ( $\text{CDCl}_3$ , 99.8 atom % D, Sigma Aldrich) and deuterated methanol (MeOH, 99.8 atom % D, Sigma Aldrich) were used as received. 2-Methyl-2-oxazoline (MeOx, 99 %, Acros Organics) and 2-ethyl-2-oxazoline (EtOx, > 99 %, Acros Organics) were distilled to dryness over barium oxide (BaO, 97 %, Sigma Aldrich) and stored under nitrogen. 2-Ethyl-2-oxazine (EtOz) was synthesised according to literature procedure,<sup>81</sup> purified by vacuum distilling over BaO and stored under nitrogen. The 2-(((butylthio)carbonothioyl)thio)propionic acid chain transfer agent (CTA) was prepared according to literature procedure.<sup>82</sup> Dialysis membrane (MWCO 500, 1000 and 3500  $\text{g mol}^{-1}$ ) was obtained from Spectrum Labs.

#### 4.4.2. Instruments and analysis

$^1\text{H}$  NMR spectra were recorded on a Bruker Avance III HD 400, Avance III HD 300 or Avance AV 300 spectrometer. Size exclusion chromatography (SEC) measurements were conducted using an Agilent 390-LC MDS fitted with differential refractive index (DRI), light scattering (LS) and viscometry (VS) detectors equipped with 2 x Agilent PLgel 5  $\mu\text{m}$  mixed-D columns (300 x 7.5 mm), 1 x Agilent PLgel 5 mm guard column (50 x 7.5 mm) and autosampler. All samples were passed through a 0.2  $\mu\text{m}$  nylon filter before analysis. The mobile phase was DMF containing 5 mM  $\text{NH}_4\text{BF}_4$  with a flow rate of 1  $\text{mL min}^{-1}$  at 50  $^\circ\text{C}$ . SEC data was analysed using Agilent Technologies SEC software. Calibration curves were produced using Agilent EasiVials linear poly(methyl methacrylate) standards (200 – 4.7 x 10<sup>5</sup>  $\text{g mol}^{-1}$ ). For multi-detector analysis, the  $\text{dn/dc}$  values were calculated online by the software based on a known concentration. TGA spectra were recorded on a Mettler Toledo TGA/DSC1. Samples were analysed from 25 to 600  $^\circ\text{C}$  at a 10  $^\circ\text{C min}^{-1}$  heating rate under a nitrogen atmosphere. DSC spectra were recorded on a Mettler Toledo DSC1. Samples were analysed from -50 to 50  $^\circ\text{C}$  at a 10  $^\circ\text{C min}^{-1}$  heating rate under a nitrogen atmosphere. Glass transition temperatures were determined on the second heating cycle. Cloud point

measurements were recorded on an Agilent Technologies Cary 60 UV-Vis spectrometer at a wavelength of 500 nm using a cuvette with a 1 cm path length. The solutions (5 mg mL<sup>-1</sup>, pH 4, unless otherwise stated) were heated and cooled (temperature range: 10 – 90 °C) at a rate of 1 °C min<sup>-1</sup> while stirring at 1200 rpm. The cloud point was determined as the temperature where the transmittance decreased to 50 % in the third heating run.

#### 4.4.3. Synthetic procedures

##### General procedure for the synthesis of macromonomers (example for M1)

In a dried Schlenk flask under nitrogen atmosphere equipped with a magnetic stirrer bar, MEHQ (1 mg, 8.06 x 10<sup>-6</sup> mol) was dissolved in 7 mL of MeCN. To this were added MeOx (5.9 mL, 69.5 mmol) and AA (4.75 mL, 69.5 mmol) under nitrogen (see Table 4.7 for exact quantities). The mixture was placed in a 70 °C oil bath for 24 h. Subsequently, the polymer solution was cooled down, precipitated in Et<sub>2</sub>O and isolated by centrifugation (three times). To remove the Et<sub>2</sub>O, the polymer was placed under vacuum to give the products as colourless-to-yellowish oils.

**Table 4.7** Quantities for the synthesis of the macromonomers.

Entry	CIE	Acrylate	CIE : acrylate	[CIE] [mol L <sup>-1</sup> ]	[AA] [mol L <sup>-1</sup> ]
M1	MeOx	AA	1 : 1	9.92	9.92
M2	MeOx	AA	1 : 2	4.48	9.92
M3	EtOx	AA	1 : 1	9.92	9.92
M4	EtOx	AA	1 : 2	6.60	13.2
M5	EtOx	CEA	1 : 1	1.50	1.50
M6	EtOz	AA	1 : 1	3.32	3.32

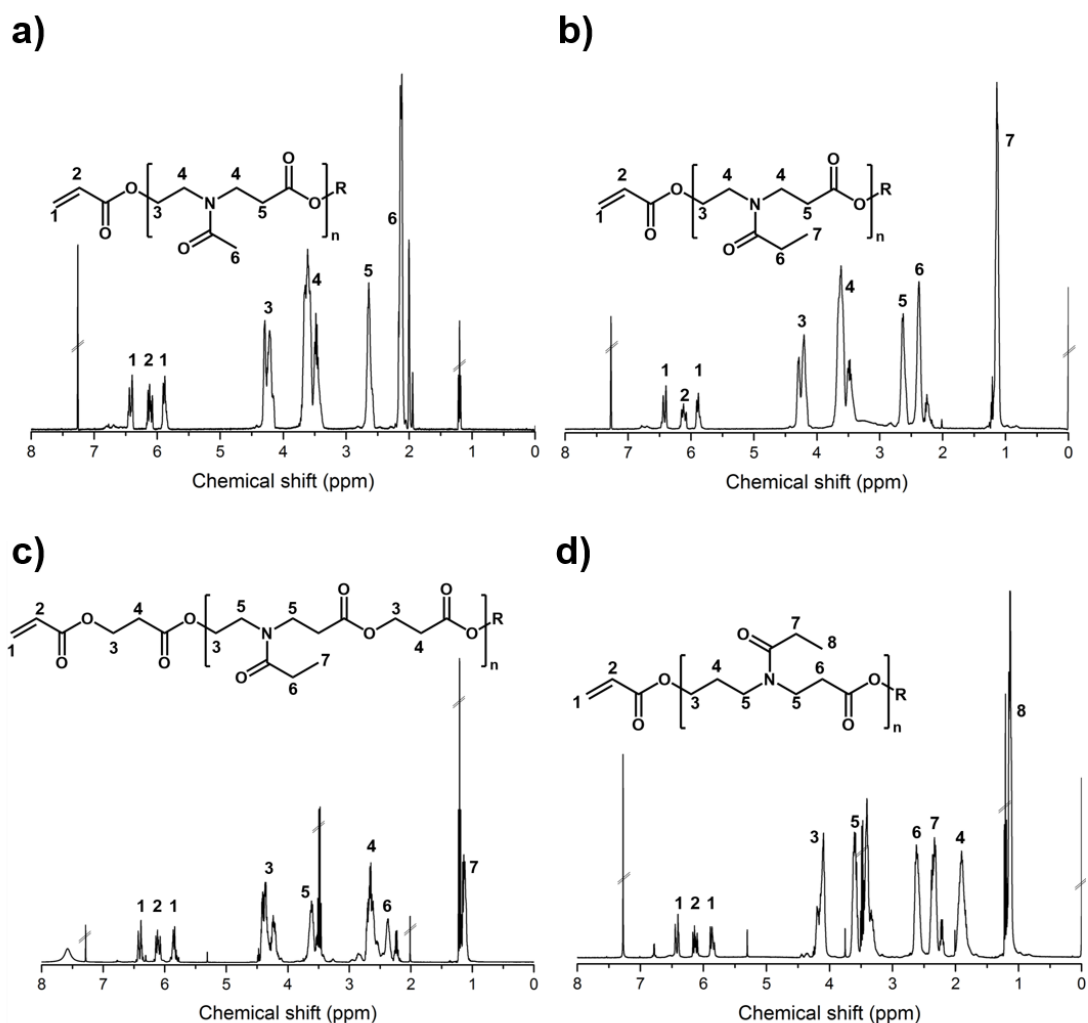


**Figure 4.16**  $^1\text{H}$  NMR spectra ( $\text{CDCl}_3$ ) of the macromonomers: a) MeOx/AA, b) EtOx/AA, c) EtOx/CEA, and d) EtOz/AA. R = H or  $\text{CH}_2\text{CH}_2\text{NHCOMe}$  (MeOx), H or  $\text{CH}_2\text{CH}_2\text{NHCOEt}$  (EtOx), H or  $\text{CH}_2\text{CH}_2\text{CH}_2\text{NHCOEt}$  (EtOz).

Characterisation for MeOx/AA macromonomers.  $^1\text{H}$  NMR (400 MHz,  $\text{CDCl}_3$ ):  $\delta_{\text{H}}$  (ppm) 6.5-6.4 (d, 1H,  $\text{CH}_a\text{H}_b=\text{CH}$ ), 6.2-6.0 (t, 1H,  $\text{CH}_2=\text{CHCOO}$ ), 6.0-5.8 (d, 1H,  $\text{CH}_a\text{CH}_b=\text{CH}$ ), 4.4-4.2 (br, 6H,  $\text{COOCH}_2$ ), 3.8-3.4 (br, 12H,  $\text{CH}_2\text{N}(\text{COCH}_3)\text{CH}_2$ ), 2.7-2.5 (br, 6H,  $\text{CH}_2\text{COO}$ ), 2.2-2.0 (br, 9H,  $\text{NCOCH}_3$ ).  $\text{DP}_{\text{NMR}} = 3$ ,  $M_{\text{n,NMR}} = 543 \text{ g mol}^{-1}$ . SEC:  $M_{\text{n}} = 1500 \text{ g mol}^{-1}$ ,  $D_{\text{SEC}} = 1.27$ .

Characterisation for EtOx/AA macromonomers.  $^1\text{H}$  NMR (400 MHz,  $\text{CDCl}_3$ ):  $\delta_{\text{H}}$  (ppm) 6.5-6.4 (d, 1H,  $\text{CH}_a\text{H}_b=\text{CH}$ ), 6.2-6.0 (t, 1H,  $\text{CH}_2=\text{CHCOO}$ ), 6.0-5.8 (d, 1H,  $\text{CH}_a\text{CH}_b=\text{CH}$ ), 4.4-4.2 (br, 6H,  $\text{COOCH}_2$ ), 3.8-3.4 (br, 12H,  $\text{CH}_2\text{N}(\text{COCH}_3)\text{CH}_2$ ), 2.7-2.5 (br, 6H,  $\text{CH}_2\text{COO}$ ), 2.5-2.3 (br, 6H,  $\text{NCOCH}_2\text{CH}_3$ ), 1.3-1.0 (br, 9H,  $\text{NCOCH}_2\text{CH}_3$ ).  $\text{DP}_{\text{NMR}} = 3$ ,  $M_{\text{n,NMR}} = 585 \text{ g mol}^{-1}$ . SEC:  $M_{\text{n,SEC}} = 1600 \text{ g mol}^{-1}$ ,  $D_{\text{SEC}} = 1.22$ .

Characterisation for EtOx/CEA macromonomers.  $^1\text{H}$  NMR (400 MHz,  $\text{CDCl}_3$ ):  $\delta_{\text{H}}$  (ppm) 6.5-6.4 (d, 1H,  $\text{CH}_a\text{H}_b=\text{CH}$ ), 6.2-6.0 (t, 1H,  $\text{CH}_2=\text{CHCOO}$ ), 6.0-5.8 (d, 1H,  $\text{CH}_a\text{CH}_b=\text{CH}$ ), 4.4-4.2 (br, 14H,  $\text{COOCH}_2$ ), 3.8-3.4 (br, 12H,  $\text{CH}_2\text{N}(\text{COCH}_3)\text{CH}_2$ ), 2.7-2.5 (br, 14H,  $\text{CH}_2\text{COO}$ ), 2.5-2.3 (br, 6H,  $\text{NCOCH}_2\text{CH}_3$ ), 1.3-1.0 (br, 9H,  $\text{NCOCH}_2\text{CH}_3$ ).  $\text{DP}_{\text{NMR}} = 3$ ,  $M_{\text{n,NMR}} = 996 \text{ g mol}^{-1}$ . SEC:  $M_{\text{n}} = 1700 \text{ g mol}^{-1}$ ,  $D_{\text{SEC}} = 1.32$ .

Characterisation for EtOz/AA macromonomers.  $^1\text{H}$  NMR (400 MHz,  $\text{CDCl}_3$ ):  $\delta_{\text{H}}$  (ppm) 6.5-6.4 (d, 1H,  $\text{CH}_a\text{H}_b=\text{CH}$ ), 6.2-6.0 (t, 1H,  $\text{CH}_2=\text{CHCOO}$ ), 6.0-5.8 (d, 1H,  $\text{CH}_a\text{CH}_b=\text{CH}$ ), 4.4-4.2 (br, 6H,  $\text{COOCH}_2$ ), 3.8-3.4 (br, 12H,  $\text{CH}_2\text{N}(\text{COCH}_3)\text{CH}_2$ ), 2.7-2.5 (br, 6H,  $\text{CH}_2\text{COO}$ ), 2.5-2.3 (br, 6H,  $\text{NCOCH}_2\text{CH}_3$ ), 2.0-1.7 (br, 6H,  $\text{CH}_2\text{CH}_2\text{CH}_2$ ), 1.3-1.0 (br, 9H,  $\text{NCOCH}_2\text{CH}_3$ ).  $\text{DP}_{\text{NMR}} = 3$ ,  $M_{\text{n,NMR}} = 627 \text{ g mol}^{-1}$ . SEC:  $M_{\text{n}} = 2000 \text{ g mol}^{-1}$ ,  $D_{\text{SEC}} = 1.27$ .

### Procedure for the free radical polymerisation of M3

120 mg (0.21 mmol) of M3 was dissolved in 65  $\mu\text{L}$   $\text{H}_2\text{O}$  and 48  $\mu\text{L}$  1,4-dioxane in a sample vial equipped with a magnetic stirrer bar. Ascorbic acid (54  $\mu\text{g}$ , 0.3  $\mu\text{mol}$ ) in 50  $\mu\text{L}$  of  $\text{H}_2\text{O}$  was added and the solution deoxygenated for 10 min. Subsequently, a deoxygenated solution of *t*BuOOH (54  $\mu\text{g}$ , 0.6  $\mu\text{mol}$ ) in 15  $\mu\text{L}$   $\text{H}_2\text{O}$  was added *via* a deoxygenated syringe. The vial was placed in a thermostated water bath set at 25  $^\circ\text{C}$  for 1 h after which the reaction was terminated and the product analysed.  $^1\text{H}$  NMR (400 MHz,  $\text{CDCl}_3$ ):  $\delta_{\text{H}}$  (ppm) 4.4-4.2 (br,  $\text{COOCH}_2$ ), 3.8-3.4 (br,  $\text{CH}_2\text{N}(\text{COCH}_3)\text{CH}_2$ ), 2.7-2.5 (br,  $\text{CH}_2\text{COO}$ ), 2.5-2.3 (br,  $\text{NCOCH}_2\text{CH}_3$ ), 1.8-1.5 (br, acrylate backbone), 1.3-1.0 (br,  $\text{NCOCH}_2\text{CH}_3$ ). SEC:  $M_{\text{n,SEC}} = 245000 \text{ g mol}^{-1}$ ,  $D_{\text{SEC}} = 4.6$ .

### General procedure for the synthesis of comb polymers by RRAFT

CTA, macromonomer and ascorbic acid were added to a sample vial equipped with a magnetic stirrer and dissolved in HPLC grade H<sub>2</sub>O and 1,4-dioxane. The mixture was deoxygenated for 15 min. In parallel, an aqueous stock solution of *t*BuOOH was deoxygenated. An aliquot of the latter was added to the sample vial *via* a nitrogen-purged syringe (final solvent: 25 % dioxane, 75 % water). The sample vial was placed in a thermostated bath set at 25 °C for 24 h. Subsequently, <sup>1</sup>H NMR and SEC samples were taken to determine the conversion. The comb polymers were purified by dialysis (MWCO = 1000 g mol<sup>-1</sup> for DP10, MWCO = 3500 g mol<sup>-1</sup> for others) against deionised water for two days and freeze dried to isolate the product. Amounts and concentrations of the individual RRAFT polymerisations are provided in Table 4.8.

**Table 4.8** Quantities for the synthesis of comb polymers by redox-initiated RAFT.

Entry	Macromonomer	DP	[M <sub>0</sub> ] [mol L <sup>-1</sup> ]	[CTA] [mmol L <sup>-1</sup> ]	[AsAc] [mmol L <sup>-1</sup> ]	[ <i>t</i> BuOOH] [mmol L <sup>-1</sup> ]
<b>P1<sub>100</sub></b>	M1	100	0.87	8.7	1.09	2.18
<b>P1<sub>50</sub></b>	M1	50	1.75	34.8	4.35	8.70
<b>P1<sub>25</sub></b>	M1	25	1.75	69.6	5.8	11.6
<b>P1<sub>10</sub></b>	M1	10	1.01	100	9.30	18.4
<b>P2<sub>10</sub></b>	M2	10	1.13	110	13.9	27.5
<b>P3<sub>100</sub></b>	M3	100	0.8	8.1	1.01	2.02
<b>P3<sub>50</sub></b>	M3	50	1.6	32.4	4.05	8.10
<b>P3<sub>25</sub></b>	M3	25	1.6	64.8	5.40	10.8
<b>P4<sub>100</sub></b>	M4	100	0.86	8.60	1.10	2.10
<b>P5<sub>100</sub></b>	M5	100	0.64	6.40	0.80	1.60
<b>P6<sub>100</sub></b>	M6	100	0.65	6.50	0.81	1.62

Characterisation for MeOx/AA comb polymers. <sup>1</sup>H NMR (400 MHz, MeOD): δ<sub>H</sub> (ppm) 4.4-4.2 (br, 600H, COOCH<sub>2</sub>), 3.8-3.4 (br, 1200H, CH<sub>2</sub>N(COCH<sub>3</sub>)CH<sub>2</sub>), 2.7-2.5

(br, 600H,  $\underline{\text{CH}_2\text{COO}}$ ), 2.2-2.0 (br, 900H,  $\text{NCO}\underline{\text{CH}_3}$ ), 1.8-1.5 (br, 300H, acrylate backbone).  $\text{DP}_{\text{NMR}} = 100$ ,  $\text{M}_{\text{n,NMR}} = 54500 \text{ g mol}^{-1}$ . SEC:  $\text{M}_{\text{n}} = 27600 \text{ g mol}^{-1}$ ,  $D_{\text{SEC}} = 1.21$ .

Characterisation for EtOx/AA comb polymers.  $^1\text{H}$  NMR (400 MHz, MeOD):  $\delta_{\text{H}}$  (ppm) 4.4-4.2 (br, 600H,  $\text{COO}\underline{\text{CH}_2}$ ), 3.8-3.4 (br, 1200H,  $\underline{\text{CH}_2\text{N}(\text{COCH}_3)\underline{\text{CH}_2}}$ ), 2.7-2.5 (br, 600H,  $\underline{\text{CH}_2\text{COO}}$ ), 2.5-2.3 (br, 600H,  $\text{NCO}\underline{\text{CH}_2\text{CH}_3}$ ), 1.8-1.5 (br, 300H, acrylate backbone), 1.3-1.0 (br, 900H,  $\text{NCO}\underline{\text{CH}_2\text{CH}_3}$ ).  $\text{DP}_{\text{NMR}} = 100$ ,  $\text{M}_{\text{n,NMR}} = 58740 \text{ g mol}^{-1}$ . SEC:  $\text{M}_{\text{n,SEC}} = 36500 \text{ g mol}^{-1}$ ,  $D_{\text{SEC}} = 1.24$ .

Characterisation for EtOx/CEA comb polymers.  $^1\text{H}$  NMR (400 MHz, MeOD):  $\delta_{\text{H}}$  (ppm) 4.4-4.2 (br, 1400H,  $\text{COO}\underline{\text{CH}_2}$ ), 3.8-3.4 (br, 1200H,  $\underline{\text{CH}_2\text{N}(\text{COCH}_3)\underline{\text{CH}_2}}$ ), 2.7-2.5 (br, 1400H,  $\underline{\text{CH}_2\text{COO}}$ ), 2.5-2.3 (br, 600H,  $\text{NCO}\underline{\text{CH}_2\text{CH}_3}$ ), 1.8-1.5 (br, 300H, acrylate backbone), 1.3-1.0 (br, 900H,  $\text{NCO}\underline{\text{CH}_2\text{CH}_3}$ ).  $\text{DP}_{\text{NMR}} = 100$ ,  $\text{M}_{\text{n,NMR}} = 87550 \text{ g mol}^{-1}$ . SEC:  $\text{M}_{\text{n}} = 48300 \text{ g mol}^{-1}$ ,  $D_{\text{SEC}} = 1.21$ .

Characterisation for EtOz/AA comb polymers.  $^1\text{H}$  NMR (400 MHz, MeOD):  $\delta_{\text{H}}$  (ppm) 4.4-4.2 (br, 600H,  $\text{COO}\underline{\text{CH}_2}$ ), 3.8-3.4 (br, 1200H,  $\underline{\text{CH}_2\text{N}(\text{COCH}_3)\underline{\text{CH}_2}}$ ), 2.7-2.5 (br, 600H,  $\underline{\text{CH}_2\text{COO}}$ ), 2.5-2.3 (br, 600H,  $\text{NCO}\underline{\text{CH}_2\text{CH}_3}$ ), 2.0-1.8 (br, 600H,  $\text{CH}_2\underline{\text{CH}_2\text{CH}_2}$ ), 1.8-1.5 (br, 300H, acrylate backbone), 1.3-1.0 (br, 900H,  $\text{NCO}\underline{\text{CH}_2\text{CH}_3}$ ).  $\text{DP}_{\text{NMR}} = 100$ ,  $\text{M}_{\text{n,NMR}} = 63300 \text{ g mol}^{-1}$ . SEC:  $\text{M}_{\text{n}} = 40400 \text{ g mol}^{-1}$ ,  $D_{\text{SEC}} = 1.35$ .

### General procedure for the amidation of comb polymers P1<sub>10</sub> and P2<sub>10</sub>

Approximately 30 mg of comb polymer was dissolved in 400  $\mu\text{L}$  DMF. 1-[bis(dimethylamino)methylene]-1*H*-1,2,3-triazolo[4,5-*b*]pyridinium 3-oxid hexafluorophosphate (HATU, 12.1 equiv.) and *N,N*-diisopropylethylamine (DIPEA, 24.2 equiv.\*) were added and the mixture was stirred for 15 min to activate the carboxylic acid groups. Next, the amine (16.5 equiv.) was added and the reaction mixture stirred at room temperature for 24 h. The product was purified by dialysis against deionised water (MWCO = 1000  $\text{g mol}^{-1}$ , for PEG-amine) or MeOH (MWCO = 500  $\text{g mol}^{-1}$ , for others) for two days and freeze dried to isolate the product. Exact quantities for each functionalisation are provided in Table 4.9.

\* For phenylalanine methylester hydrochloride 40 equiv. of DIPEA were used.

**Table 4.9** Quantities for the functionalisation of P1<sub>10</sub> and P2<sub>10</sub> with selected amines.

Entry	Comb polymer	Amine	Comb polymer [mg]	HATU [mg]	DIPEA [ $\mu$ L]	Amine
<b>P1<sub>10a</sub></b>	P1 <sub>10</sub>	Benzylamine	29.4	24.6	22	10 $\mu$ L
<b>P1<sub>10b</sub></b>	P1 <sub>10</sub>	PEG-amine	20.1	18.4	15	47.8 mg
<b>P1<sub>10c</sub></b>	P1 <sub>10</sub>	PME <sup>a</sup>	32.6	26.4	37	21.3 mg
<b>P2<sub>10a</sub></b>	P2 <sub>10</sub>	Benzylamine	30.5	30.5	26	11 $\mu$ L
<b>P2<sub>10b</sub></b>	P2 <sub>10</sub>	PEG-amine	31.5	29.6	26	76.1 mg
<b>P2<sub>10c</sub></b>	P2 <sub>10</sub>	PME <sup>a</sup>	32.1	32.9	43	27.8 mg

<sup>a</sup> PME = Phenylalanine methylester hydrochloride

Characterisation for P1a. <sup>1</sup>H NMR (400 MHz, MeOD):  $\delta_{\text{H}}$  (ppm) 7.4-7.2 (br, 25H, Ar), 4.8-4.7 (br, 10H, ArCH<sub>2</sub>), 4.4-4.2 (br, 60H, COOCH<sub>2</sub>), 3.8-3.4 (br, 120H, CH<sub>2</sub>N(COCH<sub>3</sub>)CH<sub>2</sub>), 2.7-2.5 (br, 60H, CH<sub>2</sub>COO), 2.2-2.0 (br, 90H, NCOCH<sub>3</sub>), 1.8-1.5 (br, 30H, acrylate backbone). DF = 54 %,  $M_{\text{n,NMR}} = 6200 \text{ g mol}^{-1}$ . SEC:  $M_{\text{n}} = 8200 \text{ g mol}^{-1}$ ,  $D_{\text{SEC}} = 1.14$ .

Characterisation for P1b. <sup>1</sup>H NMR (400 MHz, MeOD):  $\delta_{\text{H}}$  (ppm) 4.4-4.2 (br, 60H, COOCH<sub>2</sub>), 3.8-3.6 (br, 280H, PEG backbone), 3.6-3.4 (br, 120H, CH<sub>2</sub>N(COCH<sub>3</sub>)CH<sub>2</sub>), 3.4-3.2 (br, 15, PEG-OCH<sub>3</sub>), 2.7-2.5 (br, 60H, CH<sub>2</sub>COO), 2.2-2.0 (br, 90H, NCOCH<sub>3</sub>), 1.8-1.5 (br, 30H, acrylate backbone). DF = 45 %,  $M_{\text{n,NMR}} = 9400 \text{ g mol}^{-1}$ . SEC:  $M_{\text{n}} = 12600 \text{ g mol}^{-1}$ ,  $D_{\text{SEC}} = 1.14$ .

Characterisation for P1c. <sup>1</sup>H NMR (400 MHz, MeOD):  $\delta_{\text{H}}$  (ppm) 7.4-7.2 (br, 25H, Ar), 4.8-4.7 (br, 5H, CONHCHCOOCH<sub>3</sub>), 4.4-4.2 (br, 60H, COOCH<sub>2</sub>), 3.8-3.4 (br, 135H, CH<sub>2</sub>N(COCH<sub>3</sub>)CH<sub>2</sub>, COOCH<sub>3</sub> from PME), 3.0-2.8 (br, 10H, ArCH<sub>2</sub>), 2.7-2.5 (br, 60H, CH<sub>2</sub>COO), 2.2-2.0 (br, 90H, NCOCH<sub>3</sub>), 1.8-1.5 (br, 30H, acrylate backbone). DF = 51 %,  $M_{\text{n,NMR}} = 6560 \text{ g mol}^{-1}$ . SEC:  $M_{\text{n}} = 9100 \text{ g mol}^{-1}$ ,  $D_{\text{SEC}} = 1.10$ .

## 4.5. References

- 1 T. M. Reineke, *ACS Macro Lett.*, 2016, **5**, 14–18.
- 2 M. A. Cohen Stuart, W. T. S. Huck, J. Genzer, M. Müller, C. Ober, M. Stamm, G. B. Sukhorukov, I. Szleifer, V. V Tsukruk, M. Urban, F. Winnik, S. Zauscher, I. Luzinov and S. Minko, *Nat. Mater.*, 2010, **9**, 101–113.
- 3 E. Cabane, X. Zhang, K. Langowska, C. G. Palivan and W. Meier, *Biointerphases*, 2012, **7**, 9.
- 4 P. Vaupel, F. Rallino and P. Okunieff, *Cancer Res.*, 1989, **49**, 6449–6465.
- 5 M. Kanamala, W. R. Wilson, M. Yang, B. D. Palmer and Z. Wu, *Biomaterials*, 2016, **85**, 152–167.
- 6 X. Pang, Y. Jiang, Q. Xiao, A. W. Leung, H. Hua and C. Xu, *J. Control. Release*, 2016, **222**, 116–129.
- 7 J. Liu, Y. Huang, A. Kumar, A. Tan, S. Jin, A. Mozhi and X. J. Liang, *Biotechnol. Adv.*, 2014, **32**, 693–710.
- 8 A. Chicheł, J. Skowronek, M. Kubaszewska and M. Kanikowski, *Reports Pract. Oncol. Radiother.*, 2007, **12**, 267–275.
- 9 C. Y. Chen, T. H. Kim, W. C. Wu, C. M. Huang, H. Wei, C. W. Mount, Y. Tian, S. H. Jang, S. H. Pun and A. K. Y. Jen, *Biomaterials*, 2013, **34**, 4501–4509.
- 10 G. Kocak, C. Tuncer and V. Bütün, *Polym. Chem.*, 2017, **8**, 144–176.
- 11 X. Zhao, X. Li, Y. Zhao, Y. Cheng, Y. Yang, Z. Fang, Y. Xie, Y. Liu, Y. Chen, Y. Ouyang and W. Yuan, *Front. Pharmacol.*, 2017, **8**, 1–8.
- 12 V. Bütün, S. P. Armes and N. C. Billingham, *Polymer*, 2001, **42**, 5993–6008.
- 13 P. Cotanda, D. B. Wright, M. Tyler and R. K. O'Reilly, *J. Polym. Sci. A Polym. Chem.*, 2013, **51**, 3333–3338.
- 14 J. Hu, G. Zhang, Z. Ge and S. Liu, *Prog. Polym. Sci.*, 2014, **39**, 1096–1143.
- 15 Q. Zhang, C. Weber, U. S. Schubert and R. Hoogenboom, *Mater. Horiz.*, 2017, **4**, 109–116.
- 16 S. Fujishige, K. Kubota and I. Ando, *J. Phys. Chem.*, 1989, **93**, 3311–3313.
- 17 M. Bauer, S. Schroeder, L. Tauhardt, K. Kempe, U. S. Schubert and D. Fischer, *J. Polym. Sci. A Polym. Chem.*, 2013, **51**, 1816–1821.
- 18 M. Bauer, C. Lautenschlaeger, K. Kempe, L. Tauhardt, U. S. Schubert and D. Fischer, *Macromol. Biosci.*, 2012, **12**, 986–998.
- 19 M. M. Bloksma, U. S. Schubert and R. Hoogenboom, *Macromol. Rapid Commun.*, 2011, **32**, 1419–1441.

- 20 M. M. Bloksma, R. M. Paulus, H. P. C. van Kuringen, F. van der Woerd, H. M. L. Lambermont-thijs and U. S. Schubert, *Macromol. Rapid Commun.*, 2012, **33**, 92–96.
- 21 K. Kempe, *Macromol. Chem. Phys.*, 2017, **218**, 1700021.
- 22 S. Gokhale, Y. Xu and A. Joy, *Biomacromolecules*, 2013, **14**, 2489–2493.
- 23 J. P. Swanson, L. R. Monteleone, F. Haso, P. J. Costanzo, T. Liu and A. Joy, *Macromolecules*, 2015, **48**, 3834–3842.
- 24 J. P. Swanson, M. R. Martinez, M. A. Cruz, S. G. Mankoci, P. J. Costanzo and A. Joy, *Polym. Chem.*, 2016, **7**, 4693–4702.
- 25 J. P. Swanson, M. A. Cruz, L. R. Monteleone, M. R. Martinez, P. J. Costanzo and A. Joy, *Polym. Chem.*, 2017, **8**, 7195–7206.
- 26 D. Zhou, L. Pierucci, Y. Gao, J. O’Keeffe Ahern, X. Huang, A. Sigen and W. Wang, *ACS Appl. Mater. Interfaces*, 2017, **9**, 5793–5802.
- 27 T. R. Blake and R. M. Waymouth, *J. Am. Chem. Soc.*, 2014, **136**, 9252–9255.
- 28 C. J. McKinlay, J. R. Vargas, T. R. Blake, J. W. Hardy, M. Kanada, C. H. Contag, P. A. Wender and R. M. Waymouth, *Proc. Natl. Acad. Sci.*, 2017, **114**, E448–E456.
- 29 N. L. Benner, K. E. Near, M. H. Bachmann, C. H. Contag, R. M. Waymouth and P. A. Wender, *Biomacromolecules*, 2018, DOI: 10.1021/acs.biomac.8b00401.
- 30 W. A. Braunecker and K. Matyjaszewski, *Prog. Polym. Sci.*, 2007, **32**, 93–146.
- 31 M. K. Georges, R. P. N. Veregin, P. M. Kazmaier and G. K. Hamer, *Macromolecules*, 1993, **26**, 2987–2988.
- 32 C. J. Hawker, A. W. Bosman and E. Harth, *Chem. Rev.*, 2011, **101**, 3661–3688.
- 33 J. Nicolas, Y. Guillaneuf, D. Bertin, D. Gigmes and B. Charleux, *Prog. Polym. Sci.*, 2013, **38**, 63–235.
- 34 M. Kamigaito, T. Ando and M. Sawamoto, *Metal-catalyzed living radical polymerization.*, 2001, vol. 101.
- 35 M. Ouchi and M. Sawamoto, *Macromolecules*, 2017, **50**, 2603–2614.
- 36 M. Kato, M. Kamigaito, M. Sawamoto and T. Higashimuras, *Macromolecules*, 1996, **28**, 1721–1723.
- 37 J. S. Wang and K. Matyjaszewski, *J. Am. Chem. Soc.*, 1995, **117**, 5614–5615.
- 38 K. Matyjaszewski and J. Xia, *Chem. Rev.*, 2001, **101**, 2921–2990.
- 39 K. Matyjaszewski, *Macromolecules*, 2012, **45**, 4015–4039.

- 40 V. Percec, A. V. Popov, E. Ramirez-Castillo, M. Monteiro, B. Barboiu, O. Weichold, A. D. Asandei and C. M. Mitchell, *J. Am. Chem. Soc.*, 2002, **124**, 4940–4941.
- 41 V. Percec, T. Guliashvili, J. S. Ladislaw, A. Wistrand, A. Stjerndahl, M. J. Sienkowska, M. J. Monteiro and S. Sahoo, *J. Am. Chem. Soc.*, 2006, **128**, 14156–14165.
- 42 B. M. Rosen and V. Percec, *Chem. Rev.*, 2009, **109**, 5069–5119.
- 43 Q. Zhang, P. Wilson, Z. Li, R. McHale, J. Godfrey, A. Anastasaki, C. Waldron and D. M. Haddleton, *J. Am. Chem. Soc.*, 2013, **135**, 7355–7363.
- 44 A. Anastasaki, V. Nikolaou, G. Nurumbetov, P. Wilson, K. Kempe, J. F. Quinn, T. P. Davis, M. R. Whittaker and D. M. Haddleton, *Chem. Rev.*, 2016, **116**, 835–877.
- 45 A. Anastasaki, V. Nikolaou and D. M. Haddleton, *Polym. Chem.*, 2016, **7**, 1002–1026.
- 46 J. Chiefari, Y. K. B. Chong, F. Ercole, J. Krstina, J. Jeffery, T. P. T. Le, R. T. A. Mayadunne, G. F. Meijs, C. L. Moad, G. Moad, E. Rizzardo and S. H. Thang, *Macromolecules*, 1998, **31**, 5559–5562.
- 47 G. Moad, E. Rizzardo and S. H. Thang, *Aust. J. Chem.*, 2005, **58**, 379–410.
- 48 G. Moad, E. Rizzardo and S. H. Thang, *Aust. J. Chem.*, 2006, **59**, 669–692.
- 49 G. Moad, E. Rizzardo and S. H. Thang, *Aust. J. Chem.*, 2009, **62**, 1402–1472.
- 50 G. Moad, E. Rizzardo and S. H. Thang, *Aust. J. Chem.*, 2012, **65**, 985–1076.
- 51 S. Perrier and P. Takolpuckdee, *J. Polym. Sci. A Polym. Chem.*, 2005, **43**, 5347–5393.
- 52 C. Boyer, V. Bulmus, T. P. Davis, V. Ladmiral, J. Liu and S. Perrier, *Chem. Rev.*, 2009, **109**, 5402–5436.
- 53 A. Gregory and M. H. Stenzel, *Prog. Polym. Sci.*, 2012, **37**, 38–105.
- 54 M. R. Hill, R. N. Carmean and B. S. Sumerlin, *Macromolecules*, 2015, **48**, 5459–5469.
- 55 S. Perrier, *Macromolecules*, 2017, **50**, 7433–7447.
- 56 N. G. Engelis, A. Anastasaki, G. Nurumbetov, N. P. Truong, V. Nikolaou, A. Shegiwal, M. R. Whittaker, T. P. Davis and D. M. Haddleton, *Nat. Chem.*, 2017, **9**, 171–178.
- 57 G. Nurumbetov, N. Engelis, J. Godfrey, R. Hand, A. Anastasaki, A. Simula, V. Nikolaou and D. M. Haddleton, *Polym. Chem.*, 2017, **8**, 1084–1094.
- 58 N. G. Engelis, A. Anastasaki, R. Whit, G. R. Jones, E. Liarou, V. Nikolaou, G. Nurumbetov and D. M. Haddleton, *Macromolecules*, 2018, **51**, 336–342.

- 59 A. E. Smith, X. Xu and C. L. McCormick, *Prog. Polym. Sci.*, 2010, **35**, 45–93.
- 60 D. Roy, J. N. Cambre and B. S. Sumerlin, *Prog. Polym. Sci.*, 2010, **35**, 278–301.
- 61 D. Roy, W. L. Brooks and B. S. Sumerlin, *Chem. Soc. Rev.*, 2013, **42**, 7214–7243.
- 62 I. Cobo, M. Li, B. S. Sumerlin and S. Perrier, *Nat. Mater.*, 2015, **14**, 143–149.
- 63 B. Trzebicka, R. Szweda, D. Kosowski, D. Szweda, Ł. Otulakowski, E. Haladjova and A. Dworak, *Prog. Polym. Sci.*, 2017, **68**, 35–76.
- 64 G. Moad, *Polym. Chem.*, 2017, **8**, 177–219.
- 65 L. Martin, G. Gody and S. Perrier, *Polym. Chem.*, 2015, **6**, 4875–4886.
- 66 A. M. Striegel, W. W. Yau, J. J. Kirkland and D. D. Bly, in *Modern Size-Exclusion Liquid Chromatography: Practice of Gel Permeation and Gel Filtration Chromatography*, Wiley & Sons, Inc., Second edi., 2009.
- 67 R. G. M. van der Sman, *J. Phys. Chem. B*, 2013, **117**, 16303–16313.
- 68 M. M. Feldstein, A. Roos, C. Chevallier, C. Creton and E. E. Dormidontova, *Polymer*, 2003, **44**, 1819–1834.
- 69 S. W. Kuo, H. Xu, C. F. Huang and F. C. Chang, *J. Polym. Sci. B Polym. Phys.*, 2002, **40**, 2313–2323.
- 70 H. K. Reimschuessel, *J. Polym. Sci. Part A-polymer Chem.*, 1979, **17**, 2447–2457.
- 71 R. Hoogenboom and H. Schlaad, *Polym. Chem.*, 2017, **8**, 24–40.
- 72 R. Hoogenboom, *Angew. Chem. Int. Ed.*, 2009, **48**, 7978–7994.
- 73 M. Glassner, M. Vergaelen and R. Hoogenboom, *Polym. Int.*, 2018, **67**, 32–45.
- 74 C. Weber, R. Hoogenboom and U. S. Schubert, *Prog. Polym. Sci.*, 2012, **37**, 686–714.
- 75 M. M. Bloksma, D. J. Bakker, C. Weber, R. Hoogenboom and U. S. Schubert, *Macromol. Rapid Commun.*, 2010, **31**, 724–728.
- 76 E. Blasco, M. B. Sims, A. S. Goldmann, B. S. Sumerlin and C. Barner-Kowollik, *Macromolecules*, 2017, **50**, 5215–5252.
- 77 D. J. Lunn, E. H. Discekici, J. Read de Alaniz, W. R. Gutekunst and C. J. Hawker, *J. Polym. Sci. A Polym. Chem.*, 2017, **55**, 2903–2914.
- 78 H. C. Kolb, M. G. Finn and K. B. Sharpless, *Angew. Chem. Int. Ed.*, 2001, **40**, 2004–2021.
- 79 A. Llevot, A. C. Boukis, S. Oelmann, K. Wetzal and M. A. R. Meier, *Top.*
-

*Curr. Chem.*, 2017, **375**, 1–29.

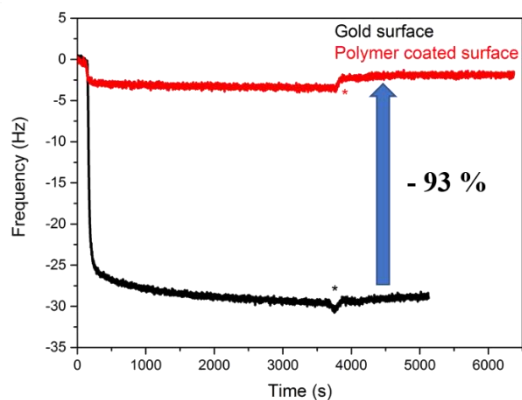
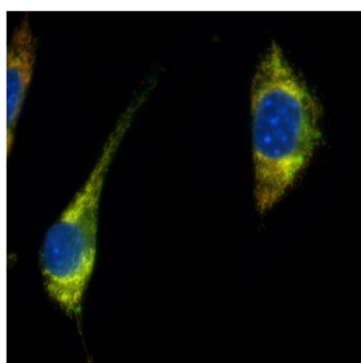
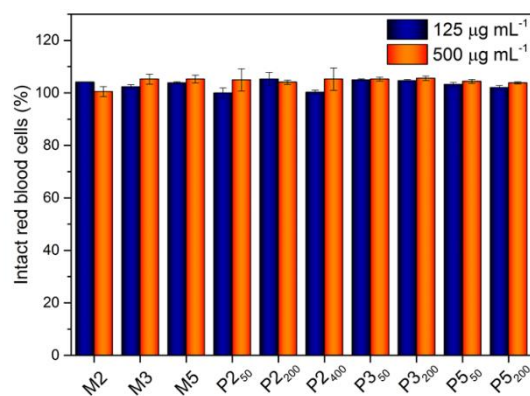
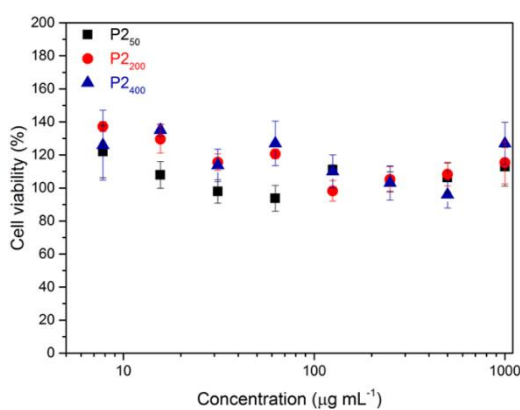
80 A. Das and P. Theato, *Chem. Rev.*, 2016, **116**, 1434–1495.

81 H. Witte and W. Seeliger, *Angew. Chem. Int. Ed.*, 1972, **11**, 287–288.

82 C. J. Ferguson, R. J. Hughes, D. Nguyen, B. T. T. Pham, R. G. Gilbert, A. K. Serelis, C. H. Such and B. S. Hawkett, *Macromolecules*, 2005, **38**, 2191–2204.

## Chapter 5

# Evaluating the potential of *N*-acylated poly(aminoester)s-based comb polymers for biological applications



## 5.1. Introduction

Polymers have received immense interest from the scientific community for use in biomedical applications. Compared to other macromolecular therapeutics, such as proteins, polymers benefit from their synthetic versatility, allowing for precise tuning of their properties and enabling the option to include bio-responsive elements. Within the field of so-called polymer therapeutics, poly(ethylene glycol) (PEG) is often considered the gold standard, which is attributed to its non-toxicity and stealth behaviour. Its use for conjugating to enzymes (also known as PEGylation) dates back to 1977 when Abuchowski *et al.* conjugated PEG to bovine serum albumin (BSA)<sup>1</sup> and bovine liver catalase.<sup>2</sup> Following the first market approved PEG-based drug conjugates, PEG-adenosine deaminase and PEG-L-asparaginase, in the 1990s, several more PEG-based polymer therapeutics followed in the next two decades.<sup>3</sup>

However, in more recent research it has come to light that PEG is not the perfect polymer once believed to be.<sup>4,5</sup> Despite an excellent aqueous solubility, PEG undergoes oxidative degradation in aqueous solution. Furthermore, hypersensitivity, liver toxicity and PEG antibodies have been observed.<sup>6-8</sup> From a chemical point of view, PEG is limited in terms of possible functionalisation as it only has two end groups that can be modified.

This has prompted researchers to evaluate other polymers as alternatives to PEG.<sup>8-10</sup> Several natural polymers have been investigated for this, including heparin, dextran and chitosan. Poly(amino acid)s, in particular poly(L-glutamic acid) (PLGA) derivatives, have received attention as they can be degraded into individual amino acids and metabolised *via* physiological pathways. Some other prominent synthetic polymers that have been investigated for biological applications are poly(glycerol)s, poly(acrylamide) (PAAm), poly(*N*-vinylpyrrolidone) (PVP), poly(*N*-(2-hydroxypropyl)methacrylamide) (PHPMA) and poly(2-oxazoline)s (POx). In particular POx have received significant interest over the last few years for their synthetic versatility and the lower critical solution temperature (LCST) behaviour of most hydrophilic POx.<sup>11-20</sup> Furthermore, Bauer *et al.* demonstrated the absence of cell toxicity and erythrocyte membrane

damage of POx synthesised from 2-methyl- (MeOx)<sup>21</sup> and 2-ethyl-2-oxazoline (EtOx).<sup>22</sup> No immune-response or antibodies against POx have been observed either.<sup>23</sup>

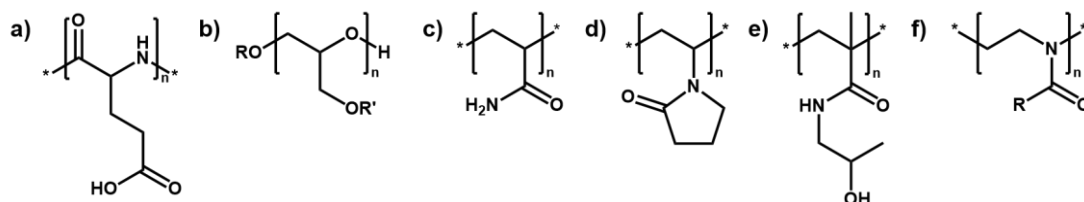


**Figure 5.1** Polymers investigated as alternative to poly(ethylene glycol) in biomedical applications. a) Poly(*L*-glutamic acid). b) Poly(glycerol). c) Poly(acrylamide). d) Poly(*N*-vinylpyrrolidone). e) Poly(*N*-(2-hydroxypropyl)methacrylamide). f) Poly(2-oxazoline)s.

Despite the extensive research on novel polymer-drug conjugates and their promising potential,<sup>24</sup> only a small selection has made it past proof-of-concept studies and into clinical trials. Apart from polymer therapeutics based on PEG, this mostly includes systems designed from PLGA and PHPMA.<sup>25</sup> Moreadith *et al.* recently published a PEtOx functionalised with rotigotine, a therapeutic used against Parkinson's disease that has made it to clinical trials (Figure 5.2). In brief, they synthesised a PEtOx scaffold with pendant alkyne groups and reacted this with azide-functionalised rotigotine. Hydrolysis of the ester enabled release of the drug to deliver a sustained dose of rotigotine over a period of seven days.<sup>23</sup>

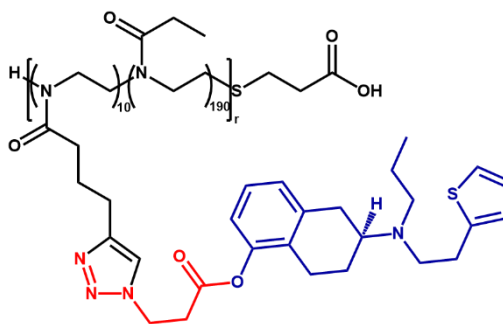


**Figure 5.2** Structure of a poly(2-oxazoline) functionalised with rotigotine, a drug used in treatment of Parkinson's disease. Reproduced from ref. 23.

The *N*-acylated poly(aminoester)s (NPAEs)-based comb polymers studied in the previous chapter have side chains structurally similar to POx. It was therefore hypothesised that they might exhibit similar properties that make them potential candidates for biomedical applications. This chapter therefore investigates some of these aspects. Specifically, the degradability, cell toxicity, cellular uptake behaviour and their application as anti-fouling materials are studied.

## 5.2. Results and discussion

The comb polymers studied in this chapter are shown in Figure 5.3. In order to investigate the effect of different NPAE-based comb polymers, five different macromonomers (M1 – M5) were synthesised by SZWIP and polymerised into a library of comb polymers by RRAFT. An overview of their analytical data is presented in Table 5.1.

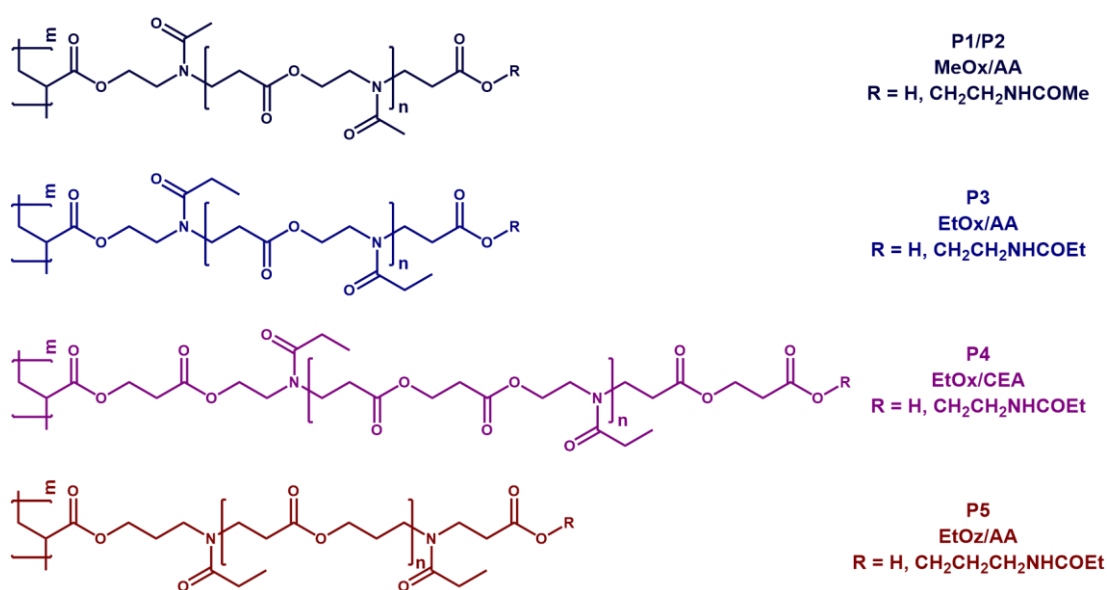


**Figure 5.3** Overview of the comb polymers studied in this chapter.

**Table 5.1** Overview of the macromonomers and comb polymers studied in this chapter.

Name <sup>a</sup>	DP comb polymer <sup>b</sup>	$\omega$ -carboxylic acid group <sup>c</sup> (%)	$M_{n,NMR}$ <sup>b</sup> [g mol <sup>-1</sup> ]	$M_{n,TD SEC}$ <sup>d</sup> [g mol <sup>-1</sup> ]	$D_{TD SEC}$ <sup>d</sup>
<b>M1</b>	-	48	546	1500 <sup>f</sup>	1.27 <sup>f</sup>
<b>P1<sub>25</sub></b>	25	48	13800	18900	1.06
<b>P1<sub>50</sub></b>	50	48	27400	42500	1.09
<b>P1<sub>100</sub></b>	100	48	54600	61500	1.11
<b>P1<sub>200</sub></b>	200	48	108900	132400	1.18
<b>M2</b>	-	99	467	1300 <sup>f</sup>	1.18 <sup>f</sup>
<b>P2<sub>50</sub></b>	50	99	19300	22500	1.03
<b>P2<sub>100</sub></b>	100	99	46700	60500	1.12
<b>P2<sub>200</sub></b>	200	99	93200	128400	1.10
<b>P2<sub>400</sub></b>	400	99	154400	138200	1.14
<b>M3</b>	-	98	500	1200 <sup>f</sup>	1.19 <sup>f</sup>
<b>P3<sub>50</sub></b>	50	98	25000	25700	1.32
<b>P3<sub>200</sub></b>	200	98	100000	61600	1.44
<b>M4</b>	-	n.d. <sup>e</sup>	631	780 <sup>f</sup>	1.21 <sup>f</sup>
<b>P4<sub>50</sub></b>	50	n.d. <sup>e</sup>	31550	12300 <sup>f</sup>	1.13 <sup>f</sup>
<b>M5</b>	-	99	630	1400 <sup>f</sup>	1.26 <sup>f</sup>
<b>P5<sub>50</sub></b>	50	99	31500	31800	1.44
<b>P5<sub>200</sub></b>	200	99	126000	113600	1.40

<sup>a</sup> Experimental details in Section 5.4.3. <sup>b</sup> Determined by <sup>1</sup>H NMR analysis of the crude product. <sup>c</sup> Determined by acid-base titration of the macromonomers. <sup>d</sup> Determined by TD SEC in DMF using differential refractive index (dRI), light scattering (LS, 90 °) and viscometry (VS) detectors. <sup>e</sup> n.d. = not determined. <sup>f</sup> Determined by conventional SEC in DMF against PMMA calibration.

Comb polymers P1<sub>x</sub> and P2<sub>x</sub> were synthesised from MeO<sub>x</sub>/AA macromonomers with 50 and 100 %  $\omega$ -carboxylic acid end groups, respectively, using the standard RRAFT polymerisation protocol as discussed in Chapter 4. This procedure was not applicable to the RRAFT polymerisation of the other macromonomers as a result of the LCST

behaviour of the resulting comb polymers. Therefore, the solvent system was changed from 25 % dioxane in water to 20 % water in dioxane. The presence of at least 20 % water is essential for the redox reaction between ascorbic acid and *tert*-butylhydroperoxide to take place. A drawback of switching to a more organic reaction medium was a reduction in the rate of propagation and therefore an increase in reaction time from 24 h to 48 h in order to attain complete conversion of the macromonomers. A full description of their synthesis and analysis is provided in Section 5.4.3.

### 5.2.1. Degradation studies

One of the main drawbacks of PEG and POx in biomedical applications is that they are not degradable. The comb polymers studied in this work contain poly(aminoester) side chains and should therefore be able to degrade, leaving low molecular weight degradation products that can be excreted by the body, along with poly(acrylic acid) (PAA) from the polymer backbone, a polymer which has been explored for biomedical applications itself.<sup>26</sup> The degradability of P2<sub>50</sub>, P3<sub>50</sub>, P4<sub>50</sub> and P5<sub>50</sub> was studied by HPLC analysis, using a calibration curve of the ratios between the peak areas of the comb polymers and an internal standard (Figure 5.4).

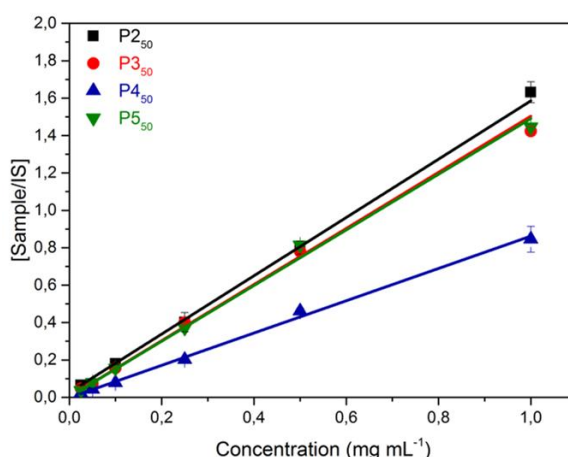


**Figure 5.4** HPLC calibration for comb polymers P2<sub>50</sub>, P3<sub>50</sub>, P4<sub>50</sub> and P5<sub>50</sub>.

Their degradability was first studied in an accelerated degradation test. The comb polymers were dissolved at  $2 \text{ mg mL}^{-1}$  in  $0.1 \text{ M KOH}$  in  $\text{H}_2\text{O}$  and incubated for 24 h at  $80 \text{ }^\circ\text{C}$ . Figure 5.5 shows the HPLC traces before and after degradation. A complete disappearance of the comb polymer peaks can be observed, thereby demonstrating the degradability of these comb polymers. The appearance of a PAA peak cannot be clearly observed as a result of the low UV absorbance of PAA at the concentrations employed in these studies.

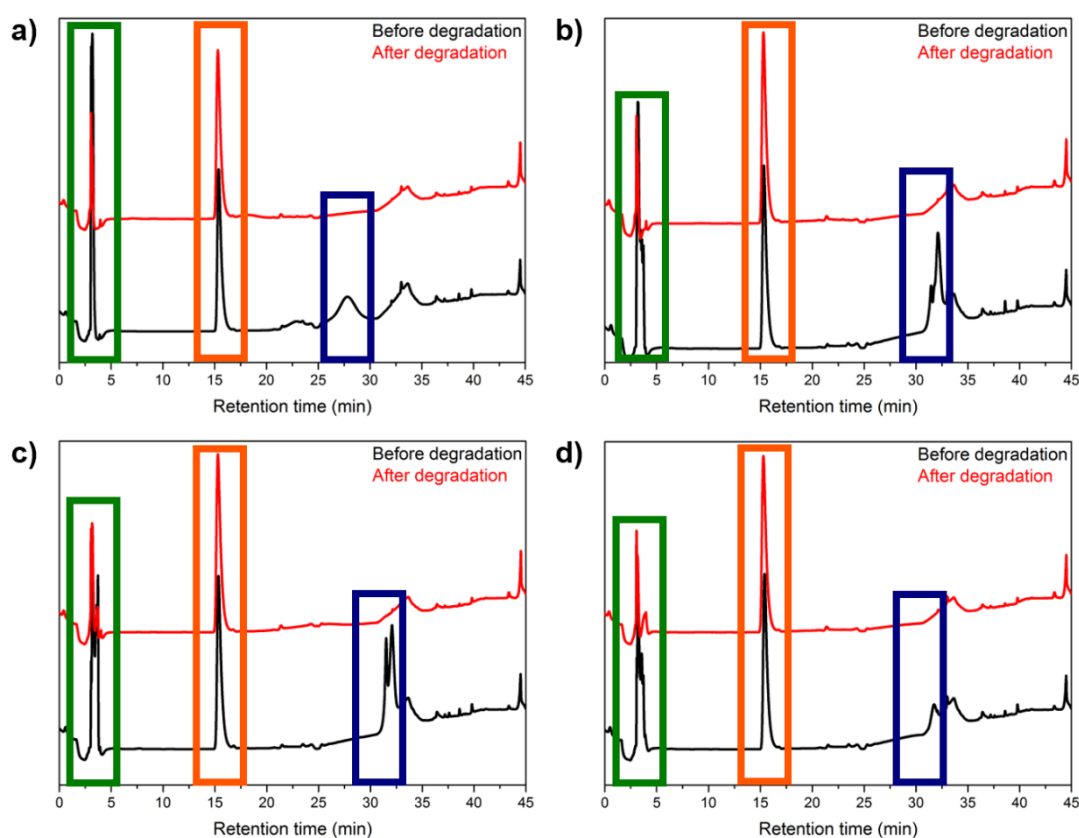


**Figure 5.5** HPLC traces illustrating the degradation of P2<sub>50</sub> (a), P3<sub>50</sub> (b), P4<sub>50</sub> (c) and P5<sub>50</sub> (d) in  $0.1 \text{ M KOH}$  at  $80 \text{ }^\circ\text{C}$ . The boxes highlight the comb polymer (blue), internal standard (orange) and solvent elution (green) peaks.

Subsequently, their degradation under biologically relevant conditions was studied. The comb polymers were dissolved in PBS and the pH adjusted to 7.4 or 5.0. The

samples were incubated at 37 °C and samples withdrawn regularly for HPLC analysis (Figure 5.6). Surprisingly, prolonged incubation at 37 °C does not lead to hydrolysis of the comb polymers, instead they remain stable over a period of a month under both neutral and mild acidic conditions.

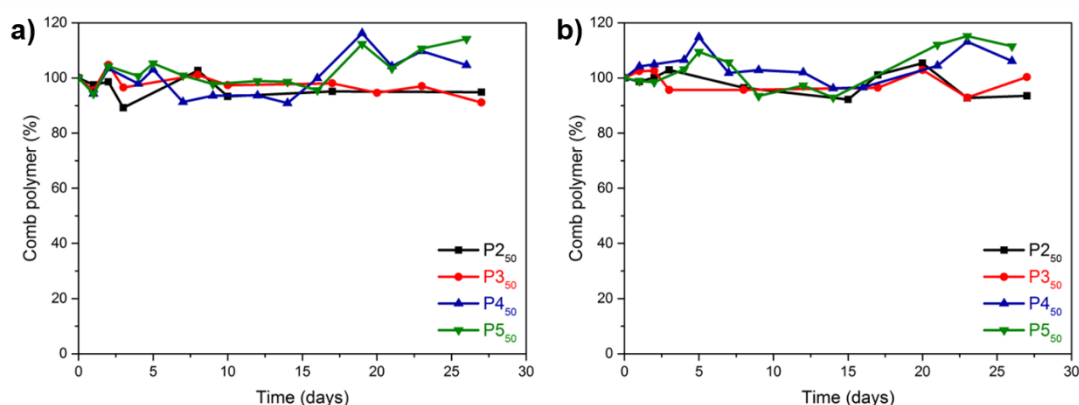


**Figure 5.6** Degradation of comb polymers P2<sub>50</sub>, P3<sub>50</sub>, P4<sub>50</sub> and P5<sub>50</sub> in PBS at pH 7.4 (a) and pH 5.0 (b).

Their degradation in the presence of an enzyme was also investigated. Most studies involving enzymatic degradation of polyesters employ non-human enzymes as they are less expensive and more readily available, but there is a limited number of reports using human enzymes capable of hydrolysing polyesters, which include Cathepsin B (lysosomes),<sup>27,28</sup> human carboxylesterase I (liver, gastrointestinal tract),<sup>29</sup> lipoprotein lipase (endothelial cells),<sup>30,31</sup> human pancreatic lipase (pancreas)<sup>32,33</sup> and amylase (saliva, pancreas).<sup>34–36</sup> Whereas most of these enzymes are rather expensive, amylase is more affordable and therefore chosen for enzymatic degradation studies. The enzyme activity was determined according to a modified method reported by Dangkulwanich *et al.*<sup>37</sup> at 9.0 units mg<sup>-1</sup> enzyme. The ability of amylase to degrade the NPAE comb polymers was assessed at three enzyme concentrations: 10, 1.0 and 0.1 µg mL<sup>-1</sup> and followed for two weeks (Figure 5.7). However, similar to the results in the absence of an enzyme, the comb polymers appear remarkably stable at all evaluated amylase concentrations.

Although the HPLC studies indicate good aqueous stability of the NPAE comb polymers, the method used may not have been suitable to study the degradability of these materials. Therefore, the method should be re-evaluated and other options, such as SEC, explored as alternative methods to study the degradability.

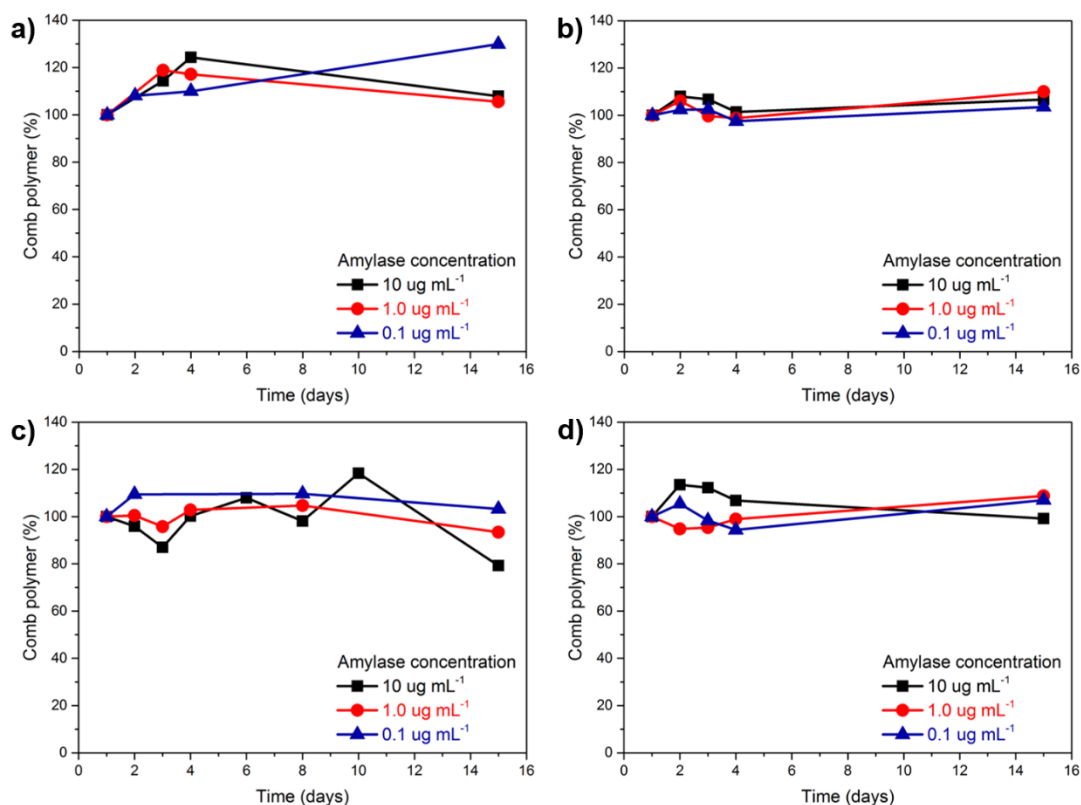


**Figure 5.7** Degradation of comb polymers P2<sub>50</sub> (a), P3<sub>50</sub> (b), P4<sub>50</sub> (c) and P5<sub>50</sub> (d) in the presence of amylase.

### 5.2.2. Cell toxicity studies

The cell toxicity of these materials was tested on two cells lines, a mouse fibroblast cell line (NIH 3T3) and a human lung carcinoma cell line (A549), and evaluated using the Alamar Blue assay. The polymer samples (P2<sub>x</sub>, P3<sub>x</sub> and P5<sub>x</sub>, dissolved in Dulbecco's modified Eagle's medium (DMEM)) were incubated with the cells for 24 h at

concentrations ranging from 7.8 to 1000  $\mu\text{g mL}^{-1}$ . After incubation, the polymer-containing DMEM was replaced with a solution of the Alamar Blue reagent in DMEM and incubated for an additional 4 h, after which the cells were analysed by UV-Vis spectroscopy.

Macromonomers M3 and M5 induced some cell toxicity in the NIH 3T3 and A549 cells, which is expected as a result of their pendant, reactive  $\alpha$ -acrylate groups. Surprisingly, macromonomer M2 does not display any cell toxicity, despite having the same  $\alpha$ -acrylate group available for reaction with intracellular functionalities.

Incubation of comb polymers P2<sub>x</sub>, P3<sub>x</sub> and P5<sub>x</sub> does not show any significant negative effects on the cell viability of NIH 3T3 mouse fibroblast cells (Figure 5.8b-d). The same results are observed for A549 human lung carcinoma cells (Figure 5.9b-d).

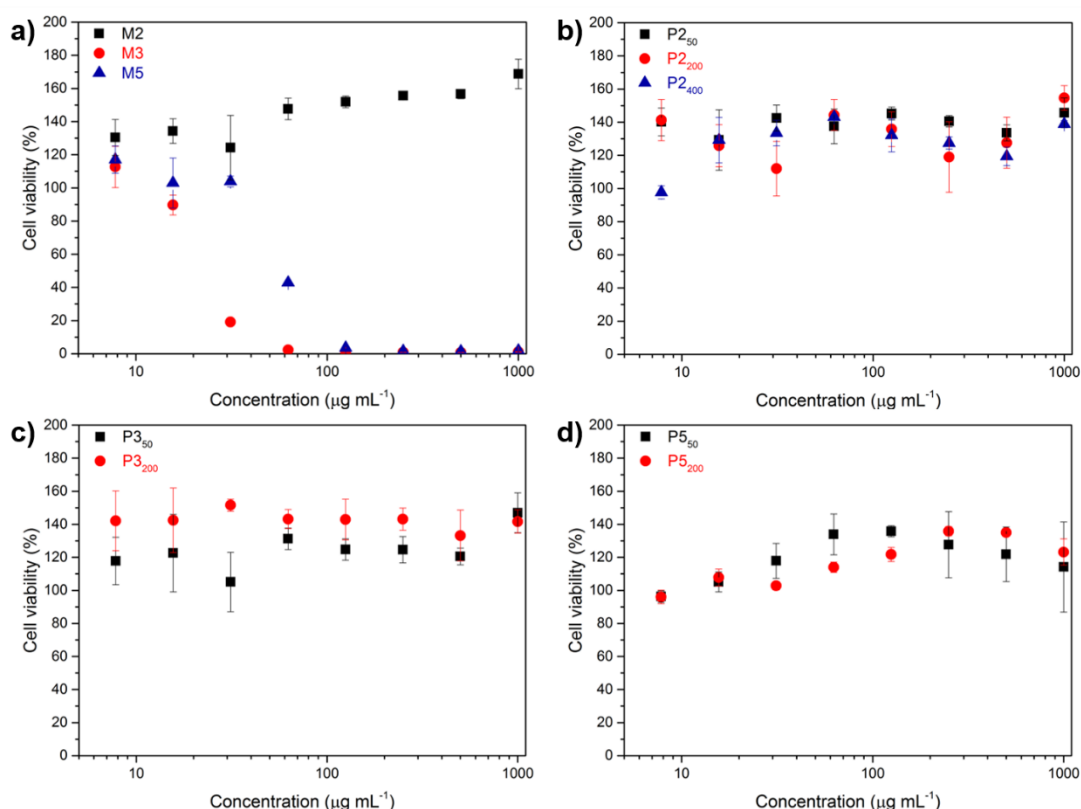


**Figure 5.8** Cell viability results for macromonomers M2, M3 and M5 and their corresponding comb polymers for NIH 3T3 cells. All values are averaged from triplicates.

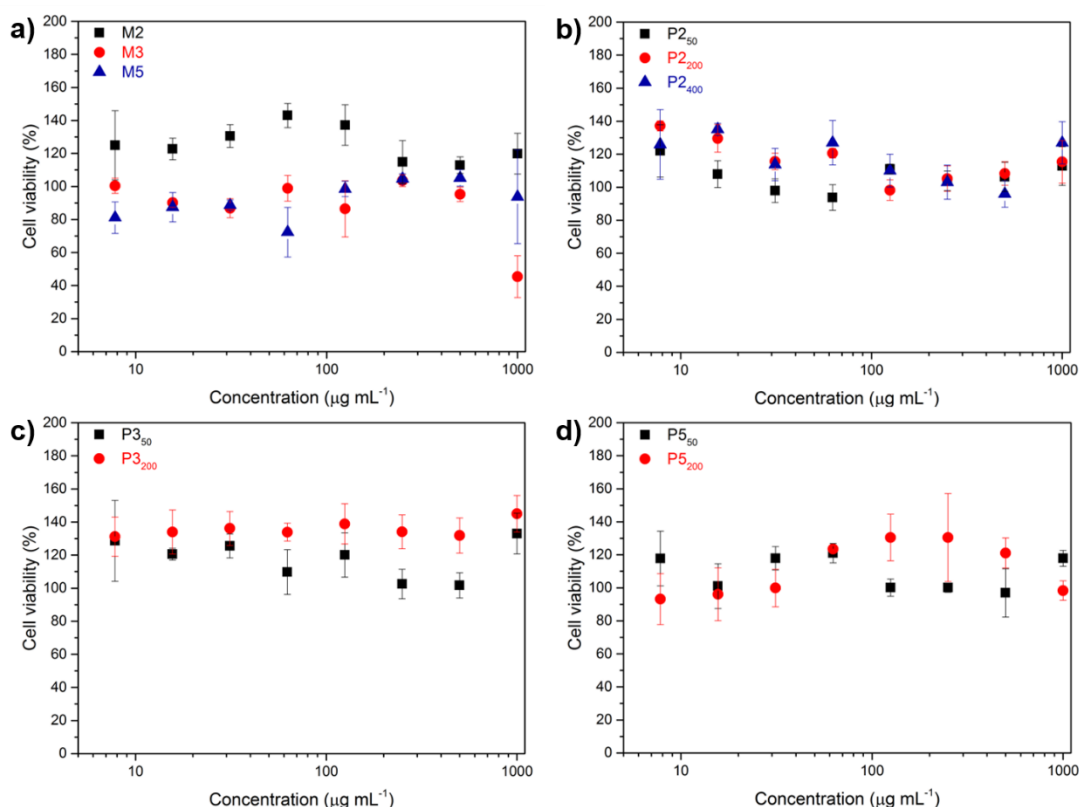


**Figure 5.9** Cell viability results for macromonomers M2, M3 and M5 and their corresponding comb polymers for A549 cells. All values are averaged from triplicates.

### 5.2.3. Haemolysis studies

The compatibility of these polymers with erythrocyte membranes was assessed by incubating the polymers with red blood cells obtained from a rat for 1 h at pH 5.0 and 7.4. Although pH-selective haemolysis can be of interest for certain applications,<sup>38,39</sup> the focus in this work was on demonstrating the absence of erythrocyte membrane damage at various pH. Indeed, when incubated at pH 5.0 and 7.4 at concentrations of 125 or 500  $\mu\text{g mL}^{-1}$  no significant haemolysis can be observed as determined by the release of haemoglobin, with exception of macromonomer M2 which shows approximately 50 % haemolysis at pH 5.0 at a concentration of 500  $\mu\text{g mL}^{-1}$  (Figure 5.10). However, for any applications the comb polymers would be used, rather than the macromonomers, so the haemolysis caused by M2 is no problem for any future applications.

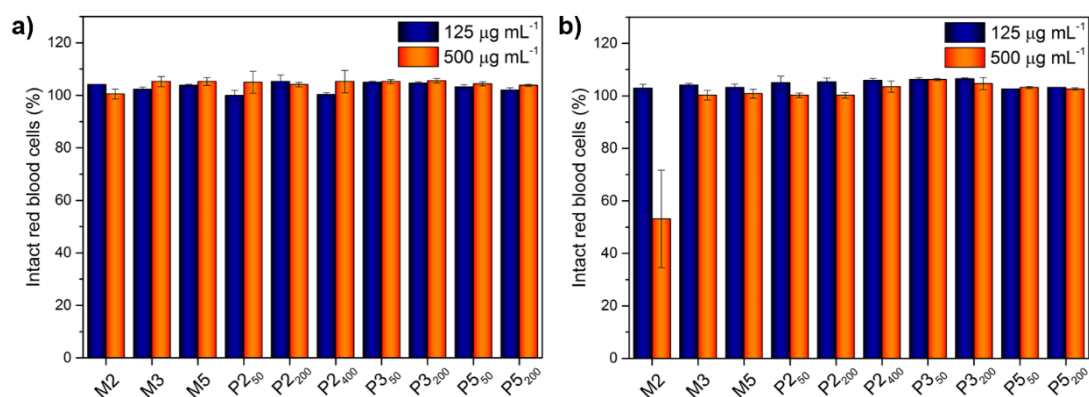


**Figure 5.10** Haemolysis results at pH 7.4 (a) and pH 5.0 (b). All values are averaged from triplicates.

#### 5.2.4. Comb polymers for cell association and uptake studies

Four comb polymers were selected to study their cell association and uptake behaviour. Comb polymers P2<sub>50</sub>, P2<sub>400</sub>, P3<sub>50</sub> and P5<sub>50</sub> were chosen to study the effect of different hydrophobicity and different DPs on their association with NIH 3T3 cells. In this context selected physical properties of the comb polymers in solution were analysed, specifically their viscosity, size and zeta-potential were determined. The viscosity measurements show that the comb polymers in HPLC grade water have similar viscosities as pure water (Table 5.2). This suggest there will be a minimal influence of the solution viscosity on the cell association and uptake studies, especially as the concentration will be significantly lower after the polymer concentration will further decrease upon mixing with cell medium. Size measurements by dynamic light scattering (DLS) show sizes below 10 nm in HPLC grade water and PBS buffer pH 7.4, with the exception of P2<sub>400</sub> which is just above 10 nm (Figure 5.11). This suggests that the comb polymers do not aggregate in solution and remain unimers, which could be relevant for their ability to be taken up by cells. Finally, as expected for the carboxylic acid decorated comb polymers, negative zeta-potentials were found by zeta-potential measurements (Table 5.2).

**Table 5.2** Viscosity, size and zeta potential analysis of comb polymers.

Comb polymer	Solvent <sup>a</sup>	Viscosity <sup>b</sup>	Size <sup>c</sup>	Zeta potential <sup>c</sup>
		[mPa·s]	[nm]	[mV]
P2 <sub>50</sub>	H <sub>2</sub> O	1.08	1.67 ± 0.35	- 21.6 ± 1.69
	PBS	n.d. <sup>d</sup>	4.63 ± 0.99	- 10.3 ± 0.81
P2 <sub>400</sub>	H <sub>2</sub> O	1.21	1.61 ± 0.35	- 32.4 ± 2.54
	PBS	n.d. <sup>d</sup>	15.8 ± 3.87	- 9.98 ± 0.79
P3 <sub>50</sub>	H <sub>2</sub> O	1.32 <sup>d</sup>	3.40 ± 0.56	- 31.9 ± 3.07
	PBS	n.d.	4.57 ± 0.93	- 9.30 ± 0.73
P5 <sub>50</sub>	H <sub>2</sub> O	1.09	1.31 ± 0.25	- 50.3 ± 3.94
	PBS	n.d. <sup>d</sup>	4.57 ± 0.90	- 13.2 ± 1.04

<sup>a</sup> All solutions are 1 mg mL<sup>-1</sup>, pristine pH in H<sub>2</sub>O, pH 7.4 in PBS. <sup>b</sup> Determined by viscometry from the average of four measurements (pure water = 1.07). <sup>c</sup> Determined by DLS from three runs of ≥ 11 measurements. <sup>d</sup> n.d. = not determined.

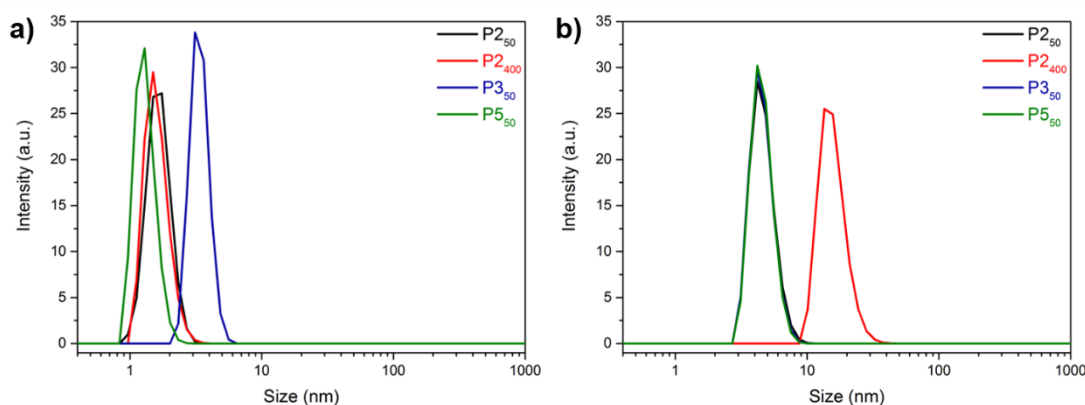
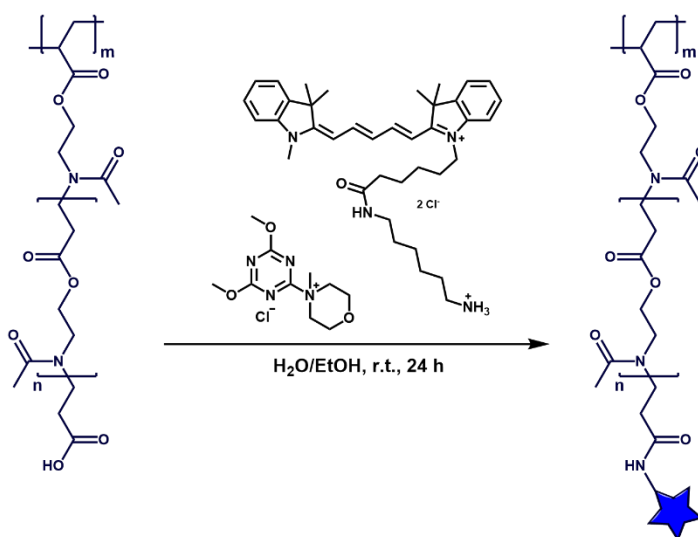


**Figure 5.11** DLS size analysis of comb polymers P2<sub>50</sub>, P2<sub>400</sub>, P3<sub>50</sub> and P5<sub>50</sub> in water (a) and PBS (b) at 1 mg mL<sup>-1</sup>.

In order to enable analysis by flow cytometry and visualisation by microscopy, the comb polymers were labelled with a cyanine 5 dye (Cy5), using 4-(4,6-dimethoxy-1,3,5-triazin-2-yl)-4-methyl-morpholinium chloride (DMTMM) as activating agent

for the carboxylic acid groups (Scheme 5.1). The emission maxima of the functionalised comb polymers were determined using fluorescence spectroscopy ( $\lambda_{\text{ex}} = 600 \text{ nm}$ ), which were nearly identical to that of pure Cy5 ( $\lambda_{\text{em, max}} = 656 \text{ nm}$ ; Figure 5.12), thus allowing the use of Cy5 spectral filters on the flow cytometer. By determining the fluorescence maxima for all comb polymers at the same concentration, their relative fluorescence can be used to extract semi-quantitative data from the flow cytometry experiments.



**Scheme 5.1** Labelling of comb polymers with cyanine 5 dye.

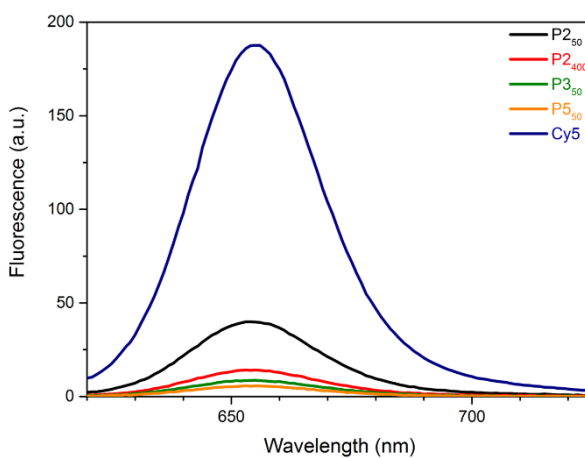


**Figure 5.12** Fluorescence spectroscopy spectra for Cy5-functionalised comb polymers.

As shown in Table 5.3, P2<sub>50</sub> has the relative highest fluorescence and this decreases going to P3<sub>50</sub> and P5<sub>50</sub>, *i.e.* the fluorescence appears to decrease with increasing hydrophobicity of the comb polymers.

**Table 5.3** Fluorescence spectroscopy analysis results for Cy5-functionalised comb polymers.

Comb polymer	$\lambda_{em,max}$ (nm)	Relative fluorescence
P2 <sub>50</sub>	653	1
P2 <sub>400</sub>	655	0.335
P3 <sub>50</sub>	655	0.217
P5 <sub>50</sub>	653	0.144

### 5.2.5. Cell association studies

Firstly, the effect of the polymer concentration on the cell association was studied. The four comb polymers were incubated at three different concentrations (2.5, 0.25 and 0.025  $\mu\text{g mL}^{-1}$ ) for 4 h. After removing non-associated polymer and addition of propidium iodide (PI) to stain dead cells, the cell association was analysed by flow cytometry. After processing the raw data by subtracting the blank cells and correcting for the relative fluorescence intensity of the different comb polymers, the mean fluorescence intensity of the comb polymers at different concentrations can be compared.

The mean fluorescence intensity of the comb polymers at the three different concentrations were evaluated (Figure 5.13a). It can be observed that the cell association increases with increasing polymer concentrations and with increasing hydrophobicity of the comb polymers ( $P2_{400} \approx P2_{50} < P3_{50} < P5_{50}$ ). The latter could be explained by increased interactions between the more hydrophobic comb polymers and the hydrophobic cell membrane. When these results are plotted on a logarithmic scale, a clearer overview is obtained, demonstrating how the cell association scales directly with concentration and how the relative cell association between the comb polymers is similar at each concentration (Figure 5.13b). It should be noted that these results are no quantification of the cell uptake, as flow cytometry does not discriminate between polymers

taken up by the cells and polymers associated to the outside of the cells that were not removed during the preparation of the cells for flow cytometry analysis. Nevertheless, it does provide an indication of the relative interaction of the comb polymers with the cells.

Following this, kinetic studies were carried out. The comb polymers ( $1 \mu\text{g mL}^{-1}$ ) were incubated with NIH 3T3 cells for 15 min to 4 h at temperatures of 4 and 37 °C. The kinetic study at 37 °C (Figure 5.14a) shows similar trends as the concentration studies.

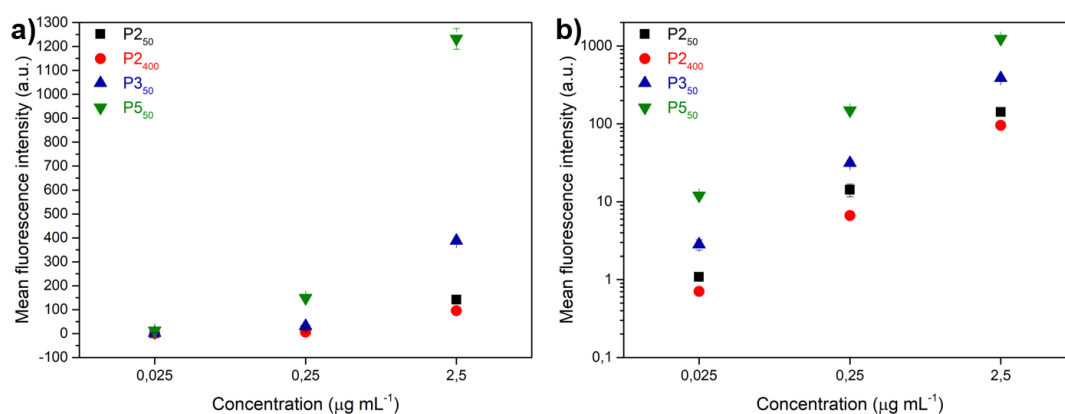


**Figure 5.13** Concentration dependant cell association results for comb polymers P<sub>250</sub>, P<sub>2400</sub>, P<sub>350</sub> and P<sub>550</sub>, shown on a linear (a) and logarithmic scale (b).

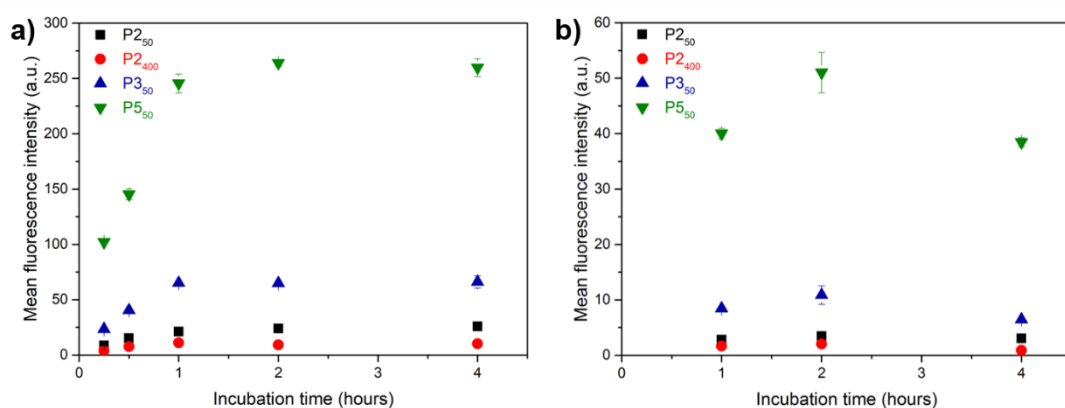


**Figure 5.14** Kinetic study of the cell association of comb polymers P<sub>250</sub>, P<sub>2400</sub>, P<sub>450</sub> and P<sub>550</sub> at 37 °C (a) and 4 °C (b).

It can be observed that the level of cell association increases up to 1 h of incubation, after which it remains virtually constant. Similarly, when incubated at 4 °C, it can be seen that there is no increase of cell association after incubating for 1 h. Compared to 37 °C, the cell association at 4 °C is approximately five times lower. This reduced cell association at 4 °C is expected and could be a preliminary indication of the temperature dependent cell uptake mechanism for these comb polymers.

### 5.2.6. Cell uptake studies

In order to evaluate the potential of these comb polymers for drug delivery into cells, their cell uptake behaviour was studied on NIH 3T3 cells containing lysosome associated modified protein 1 (LAMP1) to enable visualisation as it was hypothesised that the comb polymers would most likely end up in the lysosomes. The Cy5-functionalised polymers ( $10 \mu\text{g mL}^{-1}$ ) were incubated with the cells for 4 h at 37 °C, washed and incubated with PI and Hoechst stains, followed by imaging the cells (Figure 5.15).

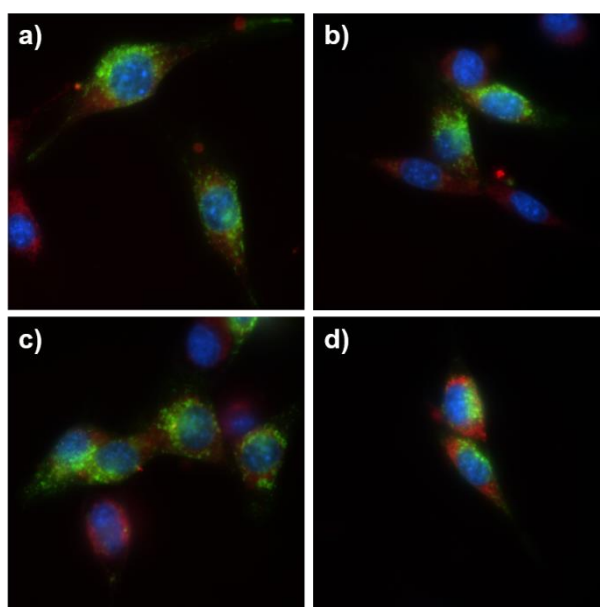


**Figure 5.15** Cell uptake experiments with lysosomal staining for comb polymers P2<sub>50</sub> (a), P2<sub>400</sub> (b), P3<sub>50</sub> (c) and P5<sub>50</sub> (d). Polymers, cell nuclei and lysosomes are labelled red, blue and green, respectively.

Surprisingly, it was found that the polymers did not co-localise with the lysosomes. Instead, it appeared they localised within the mitochondria. In order to investigate this, the experiment was repeated using NIH 3T3 COX8A cells, a modification which enables visualisation of the mitochondria. As shown in Figure 5.16, the comb polymers do indeed colocalise with the mitochondria. This observation is surprising as polymers co-localising with the mitochondria are usually cationic,<sup>40</sup> which these polymers are not, although there are some examples of non-toxic nanomaterials that localise in the mitochondria.<sup>40,41</sup>

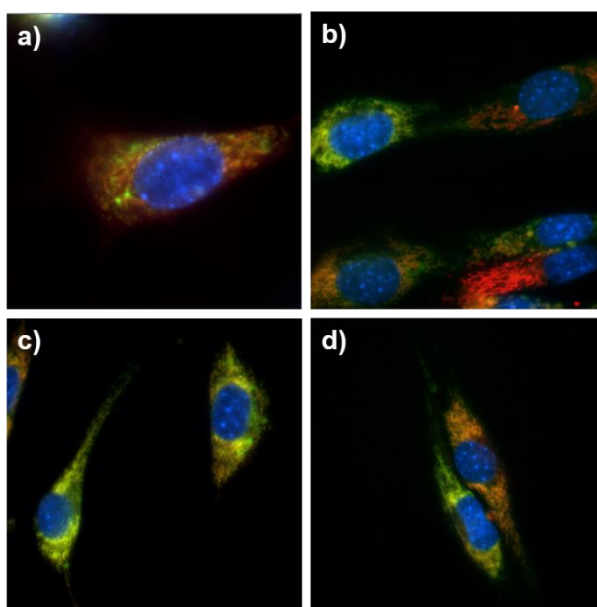


**Figure 5.16** Cell uptake experiments with mitochondrial staining for comb polymers P2<sub>50</sub> (a), P2<sub>400</sub> (b), P3<sub>50</sub> (c) and P5<sub>50</sub> (d). Polymers, cell nuclei and mitochondria are labelled red, blue and green, respectively.

### 5.2.7. Film formation and anti-fouling properties

One of the many biological applications for which polymers are used is the field of anti-fouling materials, for example for the coating for medical devices (*e.g.* stents, catheters) or nanoparticles (*e.g.* extended blood circulation, specific cell targeting). The key material property for such application is their surface hydration and for this

reason many polymers used in anti-fouling applications are hydrophilic. Typical examples include PEG, PHPMA, PAAm and POx. Other factors that influence the anti-fouling properties include the film thickness, grafting density and uniformity.<sup>42–44</sup>

In this work, the anti-fouling properties of comb polymers P1<sub>x</sub> and P2<sub>x</sub> were investigated using a quartz crystal microbalance with dissipation monitoring (QCM-D). Comb polymers from MeOx/AA were chosen as they do not have an LCST behaviour and allow to compare the effect of 50 or 100 % ω-carboxylic acid end groups, while also studying various comb polymer chain lengths. The RRAFT CTA trithiocarbonate group allows for grafting the comb polymers onto gold surfaces as a result of the high affinity between gold and sulphur.<sup>45,46</sup> The resulting bottle brush films have an increased hydration layer compared to linear polymers onto gold surfaces, an aspect that has been shown to be important for the anti-fouling properties of polymer films.<sup>44</sup>

First the optimal conditions for film formation were studied. Comb polymer P1<sub>100</sub> was used as a model and dissolved (2 mg mL<sup>-1</sup>, pH 7.2) in HPLC grade H<sub>2</sub>O, 0.5 M NaCl and 0.165 M CaCl<sub>2</sub>. The comb polymers were passed over the gold QCM chips at 0.2 μL min<sup>-1</sup> and incubated for 1 h, after which any non-bound material was washed off, recording the changes in frequency (Δ*f*) and dissipation (Δ*D*) (Figure 5.17).

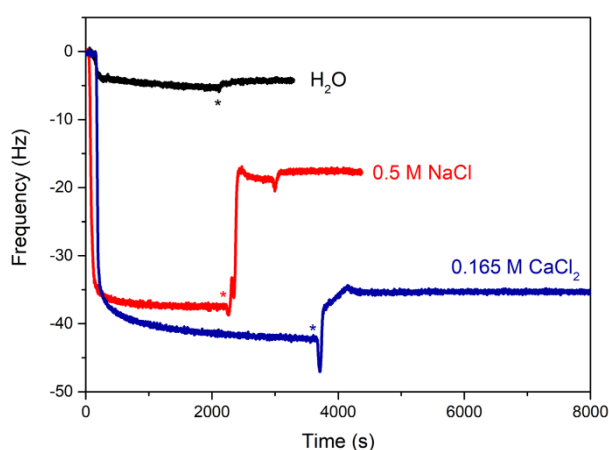


**Figure 5.17** QCM-D traces for the film formation optimisation results with P1<sub>100</sub>. The polymer solutions were added at  $t = 0$  s and unbound material was washed away at the time point marked with an asterisk.

It can be seen in Figure 5.17 that  $\Delta f$  increases going from pure H<sub>2</sub>O to 0.5 M NaCl, which is attributed to the sodium cation limiting the repulsion between the carboxylate end groups on the comb polymer side chains, thereby allowing a more densely packed film to be formed. When 0.165 M CaCl<sub>2</sub> is used as medium, the  $\Delta f$  becomes even larger. This is most likely the result of the divalent nature of Ca<sup>2+</sup> compared to the monovalent Na<sup>+</sup>. For the remainder of the QCM-D studies, 0.165 M CaCl<sub>2</sub> was used for all polymer solutions.

The formation of films with different comb polymers or P1<sub>x</sub> (x = 25, 50, 100 and 200) and P2<sub>x</sub> (x = 100 and 200) was studied using the optimised conditions (2 mg mL<sup>-1</sup>, 0.165 M CaCl<sub>2</sub>, pH 7.2) discussed above. The observed  $\Delta f$  and  $\Delta D$  values are summarised in Table 5.4.

**Table 5.4** Overview of the QCM-D results for comb polymers P1<sub>x</sub> and P2<sub>x</sub>.

Comb polymer	$\Delta f$ [Hz]	$\Delta D$	$\Delta f / \Delta D$ [Hz <sup>-1</sup> ]	$\Delta m$ <sup>a</sup> [ng cm <sup>-2</sup> ]	$\Delta m$ mol <sup>b</sup> [mmol cm <sup>-2</sup> ]
<b>P1<sub>25</sub></b>	17.4 ± 1.6	0.6 ± 0.3	31.8 ± 11.9	307.7 ± 28.5	22.3 ± 2.1
<b>P1<sub>50</sub></b>	23.1 ± 2.6	1.3 ± 0.1	15.9 ± 3.8	349.4 ± 81.2	12.8 ± 3.0
<b>P1<sub>100</sub></b>	37.5 ± 3.3	3.8 ± 0.7	10.2 ± 1.9	663.1 ± 58.1	12.2 ± 1.07
<b>P1<sub>200</sub></b>	52.7 ± 6.2	9.4 ± 0.8	5.6 ± 0.6	932.3 ± 109.9	8.6 ± 1.0
<b>P2<sub>100</sub></b>	47.4 ± 6.6	5.0 ± 1.2	10.2 ± 2.0	834.3 ± 107.2	17.9 ± 2.3
<b>P2<sub>200</sub></b>	36.2 ± 4.2	6.6 ± 0.9	5.5 ± 0.4	640.3 ± 74.4	6.8 ± 0.8

All results are the average of four measurements. <sup>a</sup> Calculated using the Sauerbrey equation. <sup>b</sup> Calculated using the molecular weights determined by <sup>1</sup>H NMR (see Table 5.1)

Through the Sauerbrey equation (Equation 5.1) it is possible to correlate the observed frequency changes to the deposited mass ( $\Delta m$ ).<sup>47</sup> In this equation,  $C$  is the Sauerbrey constant (-17.7 ng cm<sup>-1</sup> Hz<sup>-1</sup> for a 5 MHz crystal)<sup>48</sup> and  $n$  the overtone ( $n = 5$  in these studies). It should be noted that this equation is only valid for rigid films ( $\Delta f / \Delta D \geq 10$ ).<sup>47</sup> For non-rigid, viscoelastic films more complex models have been developed.<sup>49–53</sup> When the Sauerbrey equation is used for viscoelastic films, the calculated masses

are underestimations as the mass of the material is not fully coupled to the oscillator.<sup>48</sup> Comb polymers up to DP 100 are rigid films, however, the DP 200 comb polymers are viscoelastic films, but were still analysed using the Sauerbrey equation to enable facile comparison with the other comb polymers.

$$\Delta m = \frac{C \cdot \Delta f}{n} \quad (5.1)$$

It can be observed that the deposited mass of polymer ( $\Delta m$ ) increases as the DP of the comb polymers increases. To obtain a better insight into how many comb polymers are bound to the gold surface, the deposited masses were converted to moles using the molecular weights determined from <sup>1</sup>H NMR analysis (Table 5.1). The number of moles bound to the gold surfaces decreases with increasing DPs, which can be explained by increased crowding of the polymers on the gold surface. A comparison of the results for P1<sub>100</sub> and P2<sub>100</sub> suggest that a higher amount of carboxylate groups on the comb polymer side chains leads to more bound polymers through the previously discussed binding with divalent calcium ions. Although the results for P1<sub>200</sub> and P2<sub>200</sub> suggest the opposite, it should be noted that the difference in deposited moles of comb polymer is significantly smaller and those calculations are less accurate as they are not rigid films.

Finally, the anti-fouling properties of these polymer films against two model proteins, bovine serum albumin (BSA) and lysozyme, were studied. BSA has an isoelectric point (pI) of 4.7 – 5.0, which means it is negatively charged, whereas lysozyme is positively charged (pI = 11.3). After grafting the polymers onto the gold surface as described above, they were washed with PBS before addition of a solution of protein in PBS (4 mg mL<sup>-1</sup>). After 1 h incubation the unbound enzyme was washed off and the reduction in binding of the enzymes to the surface compared to non-coated gold surfaces calculated using the Sauerbrey equation. Figure 5.18a shows the result for P1<sub>100</sub> as an example, demonstrating a 93 % reduction in the amount of BSA bound to the

surface compared to a non-coated gold surface. Table 5.5 shows the results for the anti-fouling studies of P1<sub>x</sub> and P2<sub>x</sub> against BSA.

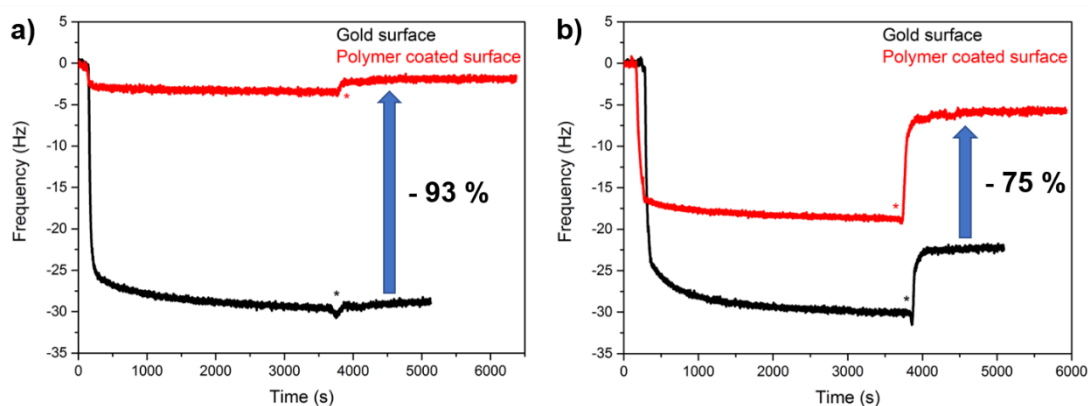


**Figure 5.18** QCM-D traces for the anti-fouling behaviour of P1<sub>100</sub> against BSA (a) and lysozyme (b). The protein solutions were added at  $t = 0$  s and unbound enzyme was washed away at the time point marked with an asterisk.

**Table 5.5** Anti-fouling behaviour of comb polymers P1<sub>x</sub> and P2<sub>x</sub> against BSA.

Comb polymer	$\Delta f^a$ [Hz]	$\Delta D$	$\Delta m^b$ [ng cm <sup>-2</sup> ]	$\Delta \text{mmol}^c$ [mmol cm <sup>-2</sup> ]	Reduction <sup>d</sup> [%]
None	$26.0 \pm 3.81$	$0.93 \pm 0.17$	$459.3 \pm 67.5$	$6.96 \pm 1.02$	n/a
P1 <sub>25</sub>	$4.85 \pm 1.47$	$0.36 \pm 0.10$	$85.8 \pm 26.0$	$1.30 \pm 0.39$	81.3
P1 <sub>50</sub>	$3.95 \pm 0.43$	$0.32 \pm 0.09$	$69.8 \pm 7.5$	$1.10 \pm 0.11$	84.8
P1 <sub>100</sub>	$1.73 \pm 0.98$	$0.19 \pm 0.05$	$30.7 \pm 17.4$	$0.47 \pm 0.26$	93.3
P1 <sub>200</sub>	$2.64 \pm 1.28$	$0.06 \pm 0.04$	$46.7 \pm 22.7$	$0.71 \pm 0.34$	89.8
P2 <sub>100</sub>	$1.08 \pm 0.84$	$0.43 \pm 0.07$	$19.1 \pm 12.2$	$0.29 \pm 0.19$	95.8
P2 <sub>200</sub>	$36.2 \pm 4.20$	$6.58 \pm 0.86$	$95.1 \pm 7.7$	$1.40 \pm 0.12$	79.3

All results are the average of four measurements. <sup>a</sup> Frequency changes are compared to the polymer coated gold surfaces (except in the absence of polymer coating). <sup>b</sup> Calculated using the Sauerbrey equation. <sup>c</sup> Calculated using the molecular weight of BSA (66 kg mol<sup>-1</sup>). <sup>d</sup> Reduction compared to deposited mass in the absence of polymer coating.

The presence of a polymer film on the gold surfaces significantly reduces the amount of bound BSA with numbers ranging from 79 to 96 % reduction. When comparing P1<sub>25</sub>, P1<sub>50</sub> and P1<sub>100</sub> a trend can be observed. With increasing chain lengths, an increased reduction in surface bound BSA is observed. This can most likely be explained by the film thickness and the presence of an increased amount of carboxylate groups, creating a larger hydration layer. This hypothesis is strengthened by comparison of P1<sub>100</sub> and P2<sub>100</sub>. The results for P2<sub>100</sub> and P2<sub>200</sub> are underestimates as these films do not meet the requirements for the Sauerbrey equations, but nevertheless demonstrate a significant reduction of BSA on the surfaces.

Similar results were observed for anti-fouling experiments using lysozyme (Figure 5.18b, Table 5.6). A lower anti-fouling behaviour can be observed, with the reduction of surface bound lysozyme between 72 and 77 %, compared to 79 to 96 % for BSA. Lysozyme has a pI of 11.3, therefore will be cationic under these conditions, and it is therefore hypothesised that electrostatic interactions between lysozyme and the anionic comb polymers is the most likely explanation for the differences observed.

**Table 5.6** Anti-fouling behaviour of comb polymers P1<sub>x</sub> and P2<sub>x</sub> against lysozyme.

Comb polymer	$\Delta f^a$ [Hz]	$\Delta D$	$\Delta m^b$ [ng cm <sup>-2</sup> ]	$\Delta mmol^c$ [mmol cm <sup>-2</sup> ]	Reduction <sup>d</sup> [%]
None	22.7 ± 1.46	0.20 ± 0.14	402.5 ± 25.8	28.2 ± 1.80	n/a
P1 <sub>25</sub>	5.55 ± 1.00	0.18 ± 0.09	98.3 ± 18.3	6.9 ± 1.28	75.6
P1 <sub>50</sub>	6.11 ± 0.76	0.42 ± 0.12	108.2 ± 13.5	7.6 ± 0.95	73.1
P1 <sub>100</sub>	5.69 ± 0.93	0.45 ± 0.14	100.7 ± 16.5	7.0 ± 1.20	75.0
P1 <sub>200</sub>	5.72 ± 0.43	0.36 ± 0.13	101.2 ± 7.7	7.1 ± 0.54	74.9
P2 <sub>100</sub>	6.20 ± 0.07	0.68 ± 0.30	109.7 ± 5.2	7.7 ± 0.37	72.7
P2 <sub>200</sub>	6.60 ± 1.14	0.44 ± 0.11	116.9 ± 20.2	8.2 ± 1.41	77.0

All results are the average of four measurements. <sup>a</sup> Frequency changes are compared to the polymer coated gold surfaces (except in the absence of polymer coating). <sup>b</sup> Calculated using the Sauerbrey equation. <sup>c</sup> Calculated using the molecular weight of lysozyme (14.3 kg mol<sup>-1</sup>). <sup>d</sup> Reduction compared to deposited mass in the absence of polymer coating.

Furthermore, it can be observed that there is no pronounced effect of the DP of the comb polymers or the amount of carboxylic acid groups on the side chains on the anti-fouling properties against lysozyme. Although the comb polymers display a lower anti-fouling behaviour against lysozyme than BSA, the observed reductions of 72 to 79 % are still very significant results that clearly demonstrate the potential of these comb polymers for anti-fouling applications.

### **5.3. Conclusions**

Polymeric materials have great potential for biological applications. This Chapter focussed on proof-of-concept experiments evaluating the potential of comb polymers from *N*-acylated poly(aminoester)s (NPAEs) in this context. Degradation studies suggested a remarkable aqueous stability of these comb polymers, although more research is required to confirm this. Cell toxicity on NIH 3T3 and A549 cells, as well as haemolysis tests showed negligible cell death and erythrocyte membrane damage. Flow cytometry demonstrated clear trends and correlations between the concentrations, incubation times and hydrophobicity of these comb polymers on their cell association. Surprisingly, cell uptake studies revealed these comb polymers to localise in the mitochondria. Finally, moving on to potential applications of these materials, gold surfaces coated with NPAE comb polymers demonstrated good anti-fouling properties against BSA and lysozyme. Even though this is only a first step towards biological applications, the results discussed in this Chapter clearly show the potential of these materials.

### **5.4. Experimental details**

#### **5.4.1. Materials**

Acrylic acid (AA, 99 %, anhydrous, Sigma Aldrich), acetonitrile (MeCN, 99.8 %, Sigma Aldrich), 4-methoxyphenol (MEHQ, 99 %, Sigma Aldrich), diethyl ether (Et<sub>2</sub>O,

> 98 %, Sigma Aldrich), 2-carboxyethyl acrylate (CEA, 98 %, Sigma Aldrich), Luperox<sup>®</sup> TBH70X *tert*-butylhydroperoxide solution (*t*BuOOH, 70 wt. % in H<sub>2</sub>O, Sigma Aldrich) and L-ascorbic acid (AsAc, > 99.5 %, Sigma Aldrich), HPLC grade H<sub>2</sub>O (Fisher Scientific), 1,4-dioxane (> 98 %, Sigma Aldrich), phosphate buffered saline (PBS, 10x concentrate, Bioperformance Certified, Sigma Aldrich), potassium hydroxide (KOH, > 85 %, Fisher Scientific), deuterated chloroform (CDCl<sub>3</sub>, 99.8 atom % D, Sigma Aldrich), deuterated methanol (MeOH, 99.8 atom % D, Sigma Aldrich), HPLC grade acetonitrile (MeCN, Fisher Scientific), HPLC grade methanol (MeOH, Fisher Scientific), glucose (ACS reagent, Sigma Aldrich), 3,5-dinitrosalicylic acid (DNS, ≥ 98 %, Sigma Aldrich), sodium potassium tartrate tetrahydrate (≥ 98 %, Sigma Aldrich), starch (≤ 0.01 % insolubles, Alfa Aesar), sodium chloride (NaCl, > 98 %, Fisher Scientific), calcium chloride (CaCl<sub>2</sub>, > 98 %, Fisher Scientific), bovine serum albumin (BSA, > 96 %, Sigma Aldrich), lysozyme from chicken egg white (90 %, Sigma Aldrich), 4-(4,6-dimethoxy-1,3,5-triazin-2-yl)-4-methylmorpholinium chloride (DMTMM, ≥ 96 %, Sigma Aldrich) and cyanine 5-amine (Cy5-amine, 95 %, Lumi-probe) were used as received. 2-Methyl-2-oxazoline (MeOx, 99 %, Acros Organics) and 2-ethyl-2-oxazoline (EtOx, > 99 %, Acros Organics) were distilled to dryness over barium oxide (BaO, 97 %, Sigma Aldrich) and stored under nitrogen. 2-Ethyl-2-oxazine (EtOz) was synthesised according to literature procedure,<sup>54</sup> purified by vacuum distilling over BaO and stored under nitrogen. The 2-(((butylthio)carbonothioyl)thio)propionic acid chain transfer agent (CTA) was prepared according to literature procedure.<sup>55</sup> Dialysis membrane (MWCO = 1000 and 3500 g mol<sup>-1</sup>) was obtained from Spectrum Labs. Dulbecco's modified Eagles medium (DMEM) Glutamax<sup>™</sup> supplemented with 1 mM sodium pyruvate and 10 % v/v or 20 % v/v foetal bovine serum (FBS), FluoroBrite and trypsin solution were obtained from Gibco and used as received. Alamar Blue, Trypan Blue, Hoechst stain and propidium iodide (PI) solutions were obtained from ThermoFisher Scientific. NIH 3T3 and A549 cell lines were obtained from ATCC. Triton X-100 was obtained from Sigma Aldrich. Snap Cell 505 was obtained from New England Biolabs.

### 5.4.2. Instruments and analysis

<sup>1</sup>H NMR spectra were recorded on a Bruker Avance III HD 400, Avance III HD 300 or Avance AV 300 spectrometer. Size exclusion chromatography (SEC) measurements were conducted using an Agilent 390-LC MDS fitted with differential refractive index (DRI), light scattering (LS) and viscometry (VS) detectors equipped with 2 x PLgel 5 mm mixed-D columns (300 x 7.5 mm), 1 x PLgel 5 mm guard column (50 x 7.5 mm) and autosampler. All samples were passed through 0.2 µm nylon filter before analysis. The mobile phase was DMF containing 5 mM NH<sub>4</sub>BF<sub>4</sub> with a flow rate of 1 mL min<sup>-1</sup> at 50 °C. SEC data was analysed using Agilent Technologies SEC software. Calibration curves were produced using Agilent EasiVials linear poly(methyl methacrylate) standards (200 – 4.7 x 10<sup>5</sup> g mol<sup>-1</sup>). For universal calibration, the dn/dc values were calculated by the software based on a known concentration. Viscometry measurements were conducted on an Anton Paar Lovis 2000 M/ME viscometer calibrated against water. Samples were analysed at 1 mg mL<sup>-1</sup> in HPLC grade water or PBS at 25 °C. Dynamic light scattering (DLS) measurements (size and zeta potential) were carried out on a Malvern Zetasizer equipped with a 633 nm He-Ne laser. Samples (1 mg mL<sup>-1</sup> in HPLC grade water or PBS) were analysed at 25 °C at an 173 ° scattering angle (back scattering) over three runs of ≥ 11 measurements against a poly(*n*-butyl acrylate) refractive index calibration. Samples were equilibrated for 60 seconds before measurement. Automatic attenuation and measurement position selected were applied. The zeta potential measurements were modelled against the Smoluchowski theory. Single sample fluorescence spectra were recorded on a Shimadzu RF-5301-PC. Samples (2.5 µg mL<sup>-1</sup> in PBS) were excited at 600 nm and their emission recorded at 620-750 nm. For the cell viability studies, fluorescence spectra of 96 well plates were recorded on a BMG Labtech FLUOstar OPTIMA microplate reader. Cell association analysis was recorded on a Stratadigm S1000EXi and the data analysed using FlowJo (version 8.7). Cell uptake studies were analysed using an Olympus IX83 equipped with a DAPI/FITC/CY3/CY5 filter set and processed with Slidebook 6.0 software. QCM-D experiments were conducted on a Q-Sense E4 System containing four sensor chambers, equipped with a QE 401 Electronics Unit, a QCP 401 Chamber Platform and a QFM401 Flow Module with Ismatec IPC-N Pump. Films were grafted on a gold coated

quartz sensor (frequency: 4.95 MHz  $\pm$  50 kHz; cut: AT; diameter: 14 mm, thickness: 0.3 mm; finish: optically polished, surface roughness of electrode < 3 nm; electrode layer: 10 – 300 nm).

### 5.4.3. Synthetic procedures

#### General procedure for the synthesis of macromonomers (example for M1)

In a dried Schlenk flask under nitrogen atmosphere equipped with a magnetic stirrer bar, MEHQ (1 mg,  $8.06 \times 10^{-6}$  mol) was dissolved in 7 mL of MeCN. To this were added MeOx (5.9 mL, 69.5 mmol) and AA (4.75 mL, 69.5 mmol) under nitrogen (see Table 5.7 for exact quantities). The mixture was placed in a 70 °C oil bath for 24 h. Subsequently, the polymer solution was cooled down, precipitated in Et<sub>2</sub>O and isolated by centrifugation (three times). To remove the Et<sub>2</sub>O, the polymer was placed under vacuum to give the products as colourless-to-yellowish oils.

**Table 5.7** Quantities for the synthesis of the macromonomers.

Entry	CIE	Acrylate	CIE : acrylate	[CIE] [mol L <sup>-1</sup> ]	[AA] [mol L <sup>-1</sup> ]
<b>M1</b>	MeOx	AA	1 : 1	9.92	9.92
<b>M2</b>	MeOx	AA	1 : 2	4.48	9.92
<b>M3</b>	EtOx	AA	1 : 2	6.60	13.2
<b>M4</b>	EtOx	CEA	1 : 2	4.00	8.00
<b>M5</b>	EtOz	AA	1 : 2	2.21	4.42

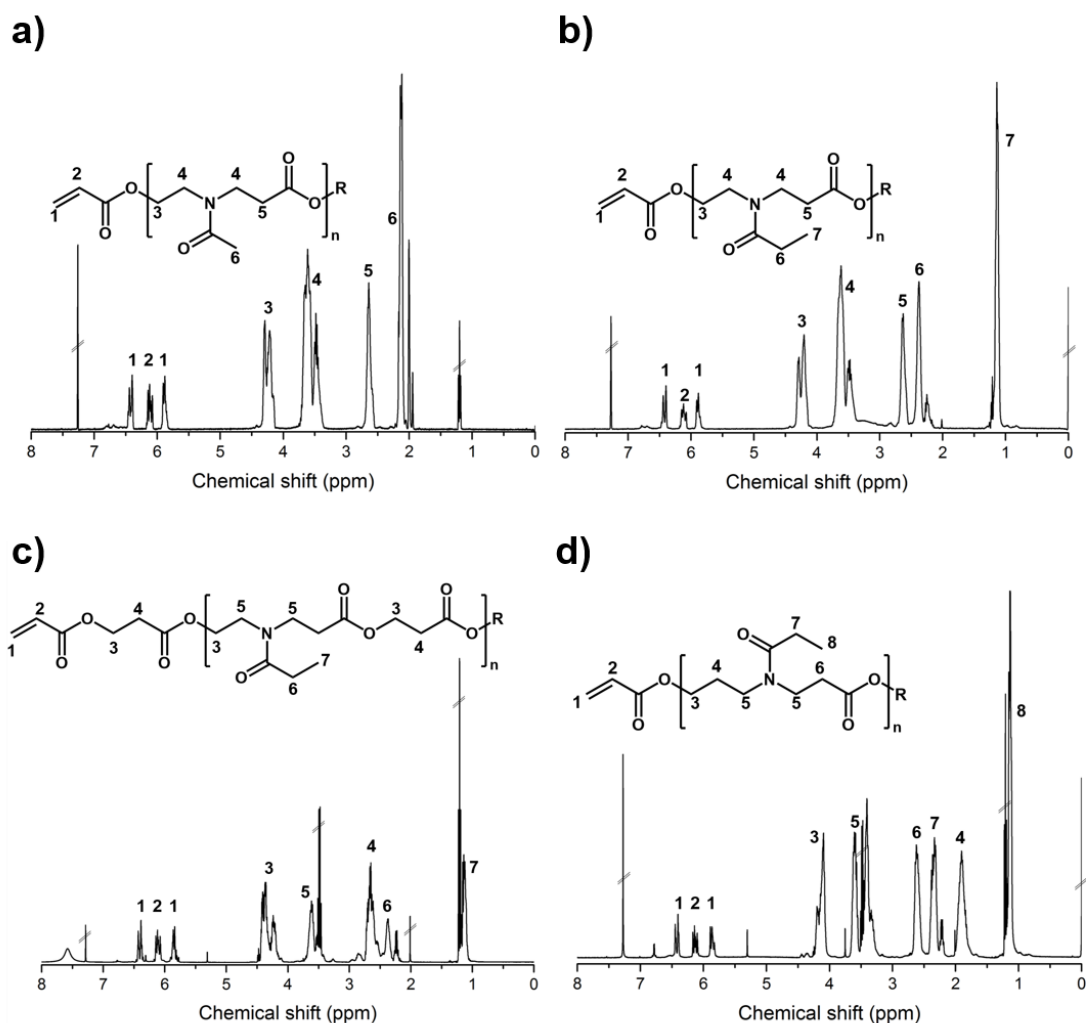


**Figure 5.19**  $^1\text{H}$  NMR spectra ( $\text{CDCl}_3$ ) of the macromonomers: a) MeOx/AA, b) EtOx/AA, c) EtOx/CEA and d) EtOz/AA. R = H or  $\text{CH}_2\text{CH}_2\text{NHCOMe}$  (MeOx), H or  $\text{CH}_2\text{CH}_2\text{NHCOEt}$  (EtOx), H or  $\text{CH}_2\text{CH}_2\text{CH}_2\text{NHCOEt}$  (EtOz).

Characterisation for MeOx/AA macromonomers.  $^1\text{H}$  NMR (400 MHz,  $\text{CDCl}_3$ ):  $\delta_{\text{H}}$  (ppm) 6.5-6.4 (d, 1H,  $\text{CH}_a\text{H}_b=\text{CH}$ ), 6.2-6.0 (t, 1H,  $\text{CH}_2=\text{CHCOO}$ ), 6.0-5.8 (d, 1H,  $\text{CH}_a\text{CH}_b=\text{CH}$ ), 4.4-4.2 (br, 6H,  $\text{COOCH}_2$ ), 3.8-3.4 (br, 12H,  $\text{CH}_2\text{N}(\text{COCH}_3)\text{CH}_2$ ), 2.7-2.5 (br, 6H,  $\text{CH}_2\text{COO}$ ), 2.2-2.0 (br, 9H,  $\text{NCOCH}_3$ ).  $\text{DP}_{\text{NMR}} = 3$ ,  $M_{\text{n,NMR}} = 543 \text{ g mol}^{-1}$ . SEC:  $M_{\text{n}} = 1500 \text{ g mol}^{-1}$ ,  $D_{\text{SEC}} = 1.27$ .

Characterisation for EtOx/AA macromonomers.  $^1\text{H}$  NMR (400 MHz,  $\text{CDCl}_3$ ):  $\delta_{\text{H}}$  (ppm) 6.5-6.4 (d, 1H,  $\text{CH}_a\text{H}_b=\text{CH}$ ), 6.2-6.0 (t, 1H,  $\text{CH}_2=\text{CHCOO}$ ), 6.0-5.8 (d, 1H,

$\text{CH}_a\text{CH}_b=\text{CH}$ ), 4.4-4.2 (br, 6H,  $\text{COOCH}_2$ ), 3.8-3.4 (br, 12H,  $\text{CH}_2\text{N}(\text{COCH}_3)\text{CH}_2$ ), 2.7-2.5 (br, 6H,  $\text{CH}_2\text{COO}$ ), 2.5-2.3 (br, 6H,  $\text{NCOCH}_2\text{CH}_3$ ), 1.3-1.0 (br, 9H,  $\text{NCOCH}_2\text{CH}_3$ ).  $\text{DP}_{\text{NMR}} = 3$ ,  $M_{n,\text{NMR}} = 585 \text{ g mol}^{-1}$ . SEC:  $M_{n,\text{SEC}} = 1600 \text{ g mol}^{-1}$ ,  $D_{\text{SEC}} = 1.22$ .

Characterisation for EtOx/CEA macromonomers.  $^1\text{H}$  NMR (400 MHz,  $\text{CDCl}_3$ ):  $\delta_{\text{H}}$  (ppm) 6.5-6.4 (d, 1H,  $\text{CH}_a\text{H}_b=\text{CH}$ ), 6.2-6.0 (t, 1H,  $\text{CH}_2=\text{CHCOO}$ ), 6.0-5.8 (d, 1H,  $\text{CH}_a\text{CH}_b=\text{CH}$ ), 4.4-4.2 (br, 14H,  $\text{COOCH}_2$ ), 3.8-3.4 (br, 12H,  $\text{CH}_2\text{N}(\text{COCH}_3)\text{CH}_2$ ), 2.7-2.5 (br, 14H,  $\text{CH}_2\text{COO}$ ), 2.5-2.3 (br, 6H,  $\text{NCOCH}_2\text{CH}_3$ ), 1.3-1.0 (br, 9H,  $\text{NCOCH}_2\text{CH}_3$ ).  $\text{DP}_{\text{NMR}} = 3$ ,  $M_{n,\text{NMR}} = 996 \text{ g mol}^{-1}$ . SEC:  $M_n = 1700 \text{ g mol}^{-1}$ ,  $D_{\text{SEC}} = 1.32$ .

Characterisation for EtOz/AA macromonomers.  $^1\text{H}$  NMR (400 MHz,  $\text{CDCl}_3$ ):  $\delta_{\text{H}}$  (ppm) 6.5-6.4 (d, 1H,  $\text{CH}_a\text{H}_b=\text{CH}$ ), 6.2-6.0 (t, 1H,  $\text{CH}_2=\text{CHCOO}$ ), 6.0-5.8 (d, 1H,  $\text{CH}_a\text{CH}_b=\text{CH}$ ), 4.4-4.2 (br, 6H,  $\text{COOCH}_2$ ), 3.8-3.4 (br, 12H,  $\text{CH}_2\text{N}(\text{COCH}_3)\text{CH}_2$ ), 2.7-2.5 (br, 6H,  $\text{CH}_2\text{COO}$ ), 2.5-2.3 (br, 6H,  $\text{NCOCH}_2\text{CH}_3$ ), 2.0-1.7 (br, 6H,  $\text{CH}_2\text{CH}_2\text{CH}_2$ ), 1.3-1.0 (br, 9H,  $\text{NCOCH}_2\text{CH}_3$ ).  $\text{DP}_{\text{NMR}} = 3$ ,  $M_{n,\text{NMR}} = 627 \text{ g mol}^{-1}$ . SEC:  $M_n = 2000 \text{ g mol}^{-1}$ ,  $D_{\text{SEC}} = 1.27$ .

### General procedure for the synthesis of comb polymers by RRAFT

CTA, macromonomer and ascorbic acid were added to a sample vial equipped with a magnetic stirrer and dissolved in HPLC grade  $\text{H}_2\text{O}$  and 1,4-dioxane. The mixture was deoxygenated for 15 min. In parallel, an aqueous stock solution of *t*BuOOH was deoxygenated. An aliquot of the latter was added to the sample vial via a nitrogen-purged syringe (final solvent: 25 % dioxane, 75 % water). The sample vial was placed in a thermostated bath set at 25 °C for 24 h. Subsequently,  $^1\text{H}$  NMR and SEC samples were taken to determine the conversion. The comb polymers were purified by dialysis ( $\text{MWCO} = 3500 \text{ g mol}^{-1}$ ) against deionised water for two days and freeze dried to isolate the product. Amounts and concentrations of the individual RRAFT polymerisations are provided in Table 5.8.

**Table 5.8** Quantities for the synthesis of comb polymers by RRAFT.

Entry	Macromonomer	DP	[M <sub>0</sub> ] [mol L <sup>-1</sup> ]	[CTA] [mmol L <sup>-1</sup> ]	[AsAc] [mmol L <sup>-1</sup> ]	[ <i>t</i> BuOOH] [mmol L <sup>-1</sup> ]
<b>P1<sub>25</sub></b>	M1	25	0.99	39.3	2.32	4.59
<b>P1<sub>50</sub></b>	M1	50	0.99	19.7	2.32	4.59
<b>P1<sub>100</sub></b>	M1	100	1.00	9.15	1.16	2.31
<b>P1<sub>200</sub></b>	M1	200	1.02	4.72	0.59	1.18
<b>P2<sub>50</sub></b>	M2	50	0.74	13.9	1.74	3.45
<b>P2<sub>100</sub></b>	M2	100	1.22	12.2	1.15	2.29
<b>P2<sub>200</sub></b>	M2	200	1.18	5.91	0.74	1.14
<b>P2<sub>400</sub></b>	M2	400	0.83	1.73	0.21	0.42

#### General procedure for the synthesis of comb polymers by organic RRAFT

CTA, macromonomer and ascorbic acid were added to a sample vial equipped with a magnetic stirrer and dissolved in HPLC grade H<sub>2</sub>O and 1,4-dioxane. The mixture was deoxygenated for 15 min. In parallel, an aqueous stock solution of *t*BuOOH was deoxygenated. An aliquot of the latter was added to the sample vial via a nitrogen-purged syringe (final solvent: 80 % dioxane, 20 % water). The sample vial was placed in a thermostated bath set at 25 °C. Conversions were checked every 24 h and if necessary new initiator was added until complete conversion of the macromonomer was observed. Subsequently, <sup>1</sup>H NMR and SEC samples were taken to determine the conversion. The comb polymers were purified by dialysis (MWCO = 3500 g mol<sup>-1</sup>) against deionised water for two days and freeze dried to isolate the product. Amounts and concentrations of the individual RRAFT polymerisations are shown in Table 5.9.

**Table 5.9** Quantities for the synthesis of comb polymers by organic RRAFT.

Entry	Macromonomer	DP	[M <sub>0</sub> ] [mol L <sup>-1</sup> ]	[CTA] [mmol L <sup>-1</sup> ]	[AsAc] [mmol L <sup>-1</sup> ]	[ <i>t</i> BuOOH] [mmol L <sup>-1</sup> ]
<b>P3<sub>50</sub></b>	M3	50	0.61	10.8	1.22	2.38
<b>P3<sub>200</sub></b>	M3	200	0.60	2.70	0.30	0.60
<b>P4<sub>50</sub></b>	M4	50	0.46	8.55	1.07	2.14
<b>P5<sub>50</sub></b>	M4	50	0.45	8.55	1.07	2.09
<b>P5<sub>200</sub></b>	M5	200	0.48	2.14	0.27	0.54

Characterisation for MeOx/AA comb polymers. <sup>1</sup>H NMR (400 MHz, MeOD): δ<sub>H</sub> (ppm) 4.4-4.2 (br, 300H, COOCH<sub>2</sub>), 3.8-3.4 (br, 600H, CH<sub>2</sub>N(COCH<sub>3</sub>)CH<sub>2</sub>), 2.7-2.5 (br, 300H, CH<sub>2</sub>COO), 2.2-2.0 (br, 450H, NCOCH<sub>3</sub>), 1.8-1.5 (br, 150H, acrylate backbone). DP<sub>NMR</sub> = 50, M<sub>n,NMR</sub> = 27400 g mol<sup>-1</sup>. TD SEC: M<sub>n</sub> = 42500 g mol<sup>-1</sup>, D<sub>SEC</sub> = 1.09.

Characterisation for EtOx/AA comb polymers. <sup>1</sup>H NMR (400 MHz, MeOD): δ<sub>H</sub> (ppm) 4.4-4.2 (br, 300H, COOCH<sub>2</sub>), 3.8-3.4 (br, 600H, CH<sub>2</sub>N(COCH<sub>3</sub>)CH<sub>2</sub>), 2.7-2.5 (br, 300H, CH<sub>2</sub>COO), 2.5-2.3 (br, 300H, NCOCH<sub>2</sub>CH<sub>3</sub>), 1.8-1.5 (br, 150H, acrylate backbone), 1.3-1.0 (br, 450H, NCOCH<sub>2</sub>CH<sub>3</sub>). DP<sub>NMR</sub> = 50, M<sub>n,NMR</sub> = 25000 g mol<sup>-1</sup>. TD SEC: M<sub>n,SEC</sub> = 25700 g mol<sup>-1</sup>, D<sub>SEC</sub> = 1.32.

Characterisation for EtOx/CEA comb polymers. <sup>1</sup>H NMR (400 MHz, MeOD): δ<sub>H</sub> (ppm) 4.4-4.2 (br, 700H, COOCH<sub>2</sub>), 3.8-3.4 (br, 600H, CH<sub>2</sub>N(COCH<sub>3</sub>)CH<sub>2</sub>), 2.7-2.5 (br, 700H, CH<sub>2</sub>COO), 2.5-2.3 (br, 300H, NCOCH<sub>2</sub>CH<sub>3</sub>), 1.8-1.5 (br, 150H, acrylate backbone), 1.3-1.0 (br, 450H, NCOCH<sub>2</sub>CH<sub>3</sub>). DP<sub>NMR</sub> = 50, M<sub>n,NMR</sub> = 31550 g mol<sup>-1</sup>. SEC: M<sub>n</sub> = 12300 g mol<sup>-1</sup>, D<sub>SEC</sub> = 1.44.

Characterisation for EtOz/AA comb polymers. <sup>1</sup>H NMR (400 MHz, MeOD): δ<sub>H</sub> (ppm) 4.4-4.2 (br, 300H, COOCH<sub>2</sub>), 3.8-3.4 (br, 600H, CH<sub>2</sub>N(COCH<sub>3</sub>)CH<sub>2</sub>), 2.7-2.5 (br, 300H, CH<sub>2</sub>COO), 2.5-2.3 (br, 300H, NCOCH<sub>2</sub>CH<sub>3</sub>), 2.0-1.8 (br, 300H, CH<sub>2</sub>CH<sub>2</sub>CH<sub>2</sub>), 1.8-1.5 (br, 150H, acrylate backbone), 1.3-1.0 (br, 450H, NCOCH<sub>2</sub>CH<sub>3</sub>). DP<sub>NMR</sub> = 50, M<sub>n,NMR</sub> = 31500 g mol<sup>-1</sup>. TD SEC: M<sub>n</sub> = 31800 g mol<sup>-1</sup>, D<sub>SEC</sub> = 1.40.

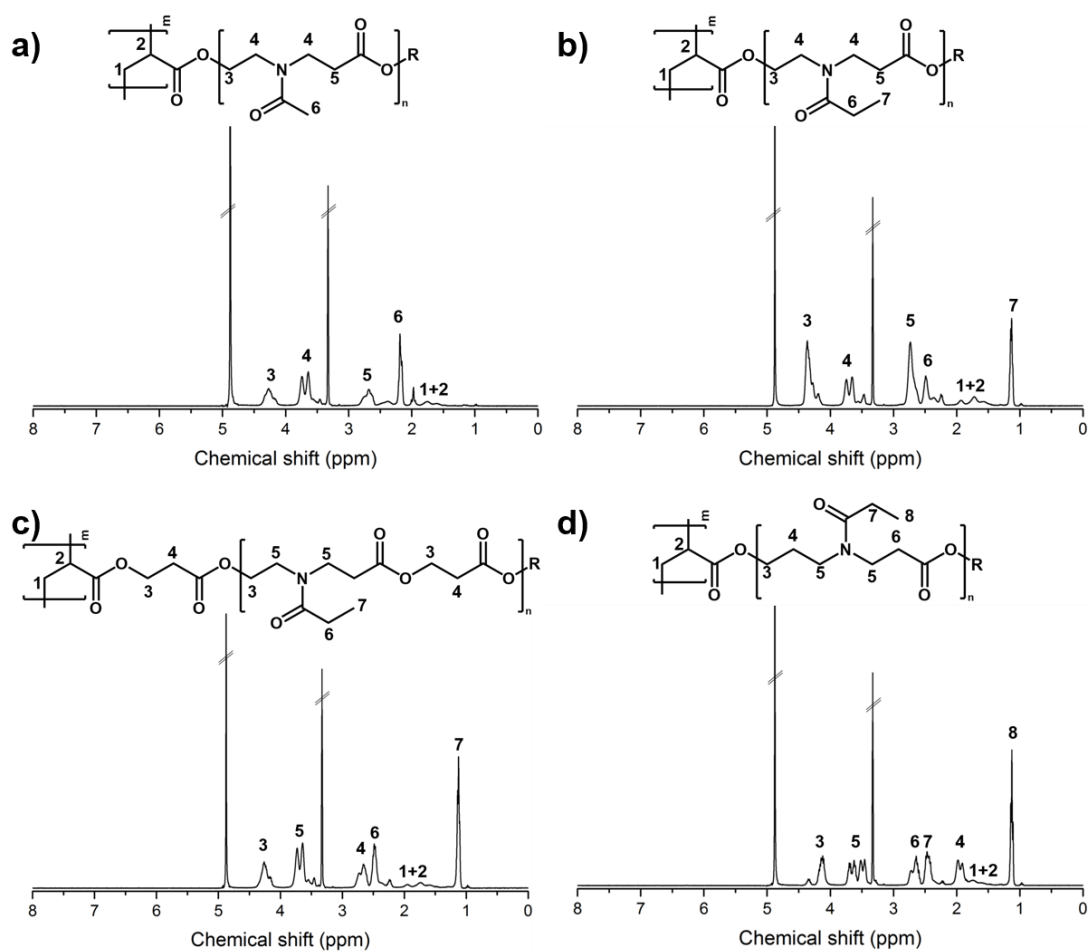


**Figure 5.20**  $^1\text{H}$  NMR spectra (MeOD) of the comb polymers: a)  $\text{P1}_x/\text{P2}_x$ , b)  $\text{P3}_x$ , c)  $\text{P4}_{50}$  and d)  $\text{P5}_x$ .  $\text{R} = \text{H}$  or  $\text{CH}_2\text{CH}_2\text{NHCOMe}$  ( $\text{P1}_x/\text{P2}_x$ ),  $\text{H}$  or  $\text{CH}_2\text{CH}_2\text{NHCOEt}$  ( $\text{P3}_x$ ,  $\text{P4}_{50}$ ),  $\text{H}$  or  $\text{CH}_2\text{CH}_2\text{CH}_2\text{NHCOEt}$  ( $\text{P5}_x$ ).

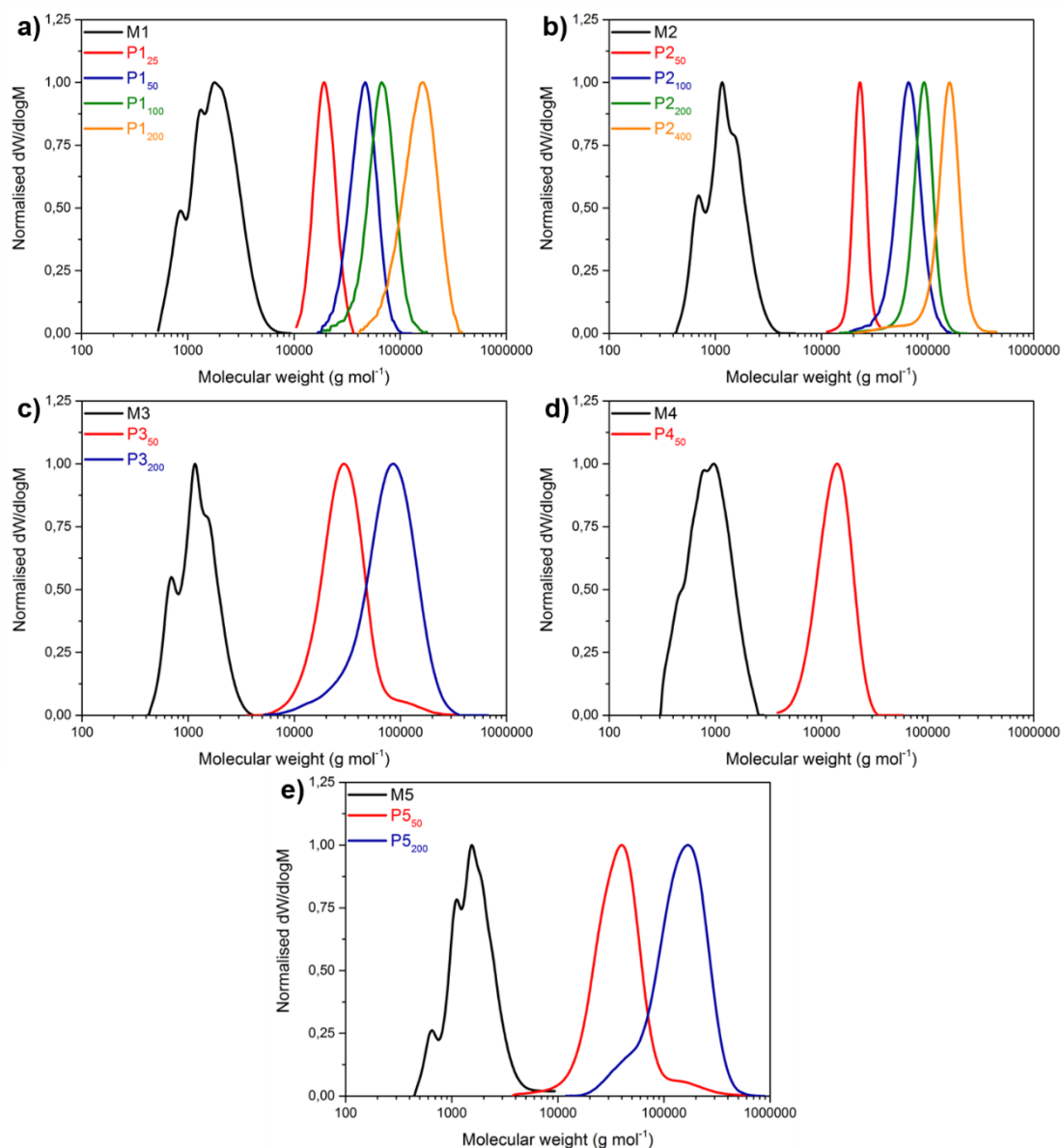


**Figure 5.21** SEC analysis of macromonomers M1 - M5 and their corresponding comb polymers P1<sub>x</sub> – P5<sub>x</sub>.

### General procedure for the labelling of comb polymers with Cy5-dye

In a small vial, 20 mg of comb polymer was dissolved in HPLC grade H<sub>2</sub>O or a mixture of H<sub>2</sub>O/MeOH. 1.3 equiv. of (4-(4,6-dimethoxy-1,3,5-triazin-2-yl)-4-methyl-morpholinium chloride (DMTMM, from a 20 mg mL<sup>-1</sup> stock solution) was added and the resulting mixture stirred for 10 min at room temperature. 2 equiv. of Cy5-amine in H<sub>2</sub>O was added. the resulting mixture was stirred for 24 h in the absence of light. The

product was purified by dialysis against deionised water ( $MWCO = 1000 \text{ g mol}^{-1}$ ) and freeze dried to isolate the product. Exact quantities for each functionalisation are shown in Table 5.10.

**Table 5.10** Quantities for the functionalisation of comb polymers with Cy5-amine.

<b>Entry</b>	<b>Comb polymer</b>	<b>Comb polymer [mg]</b>	<b>DMTMM [mg]</b>	<b>Cy5-amine [mg]</b>
<b>P2<sub>50</sub>L</b>	P2 <sub>50</sub>	20.16	0.37	1.35
<b>P2<sub>400</sub>L</b>	P2 <sub>400</sub>	19.62	0.47	0.31
<b>P3<sub>50</sub>L</b>	P3 <sub>50</sub>	20.78	0.29	1.05
<b>P5<sub>50</sub>L</b>	P5 <sub>50</sub>	19.98	0.23	3.15

#### **5.4.4. Degradation studies**

##### **HPLC conditions**

HPLC analysis was performed on an Agilent 1260 Infinity series stack equipped with an Agilent 1260 binary pump and degasser. 100  $\mu\text{L}$  samples were injected using an Agilent 1260 auto sampler with a  $1 \text{ ml min}^{-1}$  flow rate. The HPLC was fitted with a Phenomenex Luna C18 column (250 x 4.6 mm) with 5 micron packing (100  $\text{\AA}$ ). Detection was achieved using an Agilent 1260 variable wavelength detector monitoring at 220 nm. Mobile phase A consisted of 100 % HPLC grade  $\text{H}_2\text{O}$  containing 0.04 % trifluoroacetic acid (TFA). Mobile phase B consisted of 20 % HPLC grade MeOH and 80 % HPLC grade MeCN, containing 0.04 % TFA. A blank run was carried out the first sample in a series. The gradient method used for all samples is as follows:

<u>Time (min)</u>	<u>Mobile phase A (%)</u>	<u>Mobile phase B (%)</u>
0	90	10
27	55	45
30	25	75
36	0	100
40	0	100
50	90	10

### **Comb polymer calibration curves**

A stock solution for each polymer was made at 2 mg mL<sup>-1</sup> in 25 % MeCN in HPLC grade H<sub>2</sub>O and serially diluted to 0.05 mg mL<sup>-1</sup>. To 1.0 mL of each comb polymer solution, 1.0 mL of 1 mg mL<sup>-1</sup> benzyl alcohol (internal standard) in 25 % MeCN in HPLC grade H<sub>2</sub>O was added to give the final solutions. Calibration curves made from the ratio between the polymer peak area and the internal standard peak.

### **Accelerated degradation in 0.1 M KOH at 80 °C**

Comb polymers were dissolved in 0.1 M KOH in water (2 mg mL<sup>-1</sup>) containing 1 mg mL<sup>-1</sup> benzyl alcohol and placed in an 80 °C oven for 24 h. After incubation, 0.5 mL of polymer solution was diluted with 0.5 mL MeCN/H<sub>2</sub>O 1/1 and analysed by HPLC.

### **Degradation in PBS pH 7.4 and 5.0 at 37 °C**

Comb polymers were dissolved in PBS (2 mg mL<sup>-1</sup>) containing 1 mg mL<sup>-1</sup> benzyl alcohol and the pH adjusted to 7.4 or 5.0. The solutions were placed in a 37 °C incubator. Aliquots of 0.5 mL were taken, diluted with 0.5 mL MeCN/H<sub>2</sub>O 1/1 and analysed by HPLC.

### **Determination of the enzyme activity of amylase**

The enzymatic activity was determined using a modified version of the amylase activity assay reported by Dangkulwanich *et al.*<sup>37</sup> A calibration curve was prepared for glucose at a range of concentrations (0 – 1 mg mL<sup>-1</sup>), by reacting it with an aqueous solution of 3,5-dinitrosalicylic acid (DNS) solution (1 g of DNS in 25 mL of HPLC grade H<sub>2</sub>O, 15 g sodium potassium tartrate tetrahydrate and 20 mL of 2 M NaOH and HPLC grade water to a final volume of 50 mL). After mixing the glucose solutions (1 mL) and DNS solution (1 mL), the resulting mixture was placed in boiling water for 5 min, cooled in an ice bath and its absorbance measured by UV-Vis spectroscopy at 540 nm. The enzyme activity was determined by adding 0.5 mL of a 0.5 mg mL<sup>-1</sup> amylase in PBS pH 7.4 to a vial containing 1.5 mL of 2 % w/v starch in PBS pH 7.4 and 1 mL of PBS pH 7.4 and placed in a 37 °C incubator for 10 min. After incubation for 10 min, 0.5 mL of the DNS reagent solution was added, the mixture placed in boiling water for 5 min and subsequently cooled in ice. The absorbance was analysed by UV-Vis spectroscopy, giving an enzymatic activity of 8.98 units mg<sup>-1</sup>.

### **Enzymatic degradation in PBS pH 7.4 at 37 °C**

Comb polymers were dissolved in PBS containing 1 mg mL<sup>-1</sup> benzyl alcohol and the pH adjusted to 7.4. A solution of amylase in PBS was subsequently added. The final polymer concentration was 2 mg mL<sup>-1</sup> and final amylase concentrations were 10, 1.0 or 0.1 µg mL<sup>-1</sup>. The solutions were placed in an incubator at 37 °C. Aliquots of 0.5 mL were taken, diluted with 0.5 mL MeCN/H<sub>2</sub>O 1/1 and analysed by HPLC.

## **5.4.5. Cell viability studies**

### **Cell culture**

NIH 3T3 cells and A549 cells were used and tested and cleared for mycoplasma. The cells were maintained in Dulbecco's modified Eagle's medium (DMEM) Glutamax™

supplemented with 1 mM sodium pyruvate and 10 % v/v (A549) and 20 % v/v (NIH 3T3) foetal bovine serum (FBS). Cells were cultured at 37 °C in a humidified incubator with 5 % atmospheric CO<sub>2</sub>. Cell counting for passaging was achieved by adding 0.4 % Trypan Blue solution to the cells in medium and counting on a haemocytometer.

### Cell viability

Cells were seeded on 96 well plates at a density of 10<sup>4</sup> cells per well and incubated for 24 h. The cells were then incubated with polymer samples (0.06 to 1 mg mL<sup>-1</sup> in PBS, prepared through serial dilution) and incubated at 37 °C for 24 h in a humidified incubator with 5 % atmospheric CO<sub>2</sub>. Samples were run in triplicate. After incubation the medium was removed and a 10 % v/v solution of Alamar Blue in DMEM was added. The cells were incubated for a further 4 h at 37 °C. Cell viability was determined by measuring the fluorescence (excitation: 540 nm, emission: 590 nm). Wells incubated without cells were used as blank. Control samples were cells incubated with PBS (without polymer). The viability was calculated using Equation 5.2.

$$\text{Cell viability} = \frac{\text{Fluorescence polymer} - \text{fluorescence blank}}{\text{Fluorescence control} - \text{fluorescence blank}} \times 100 \% \quad (5.2)$$

### 5.4.6. Haemolysis studies

Red blood cells (RBCs) from rat blood were purified and isolated by repeated centrifuging and washing with PBS. The purified RBCs were then dissolved in PBS pH 5.0 and 7.4 at a concentration of 0.05 % w/v. The RBC solutions were transferred to 96 well plates (140 µL per well) and 10 µL of polymer solution (125 or 500 µg mL<sup>-1</sup> final concentration) was added. Triton X-100 was used as positive control, no additives were used for the negative control. The RBCs were incubated for 1 h at 37 °C in a humidified incubator with 5 % atmospheric CO<sub>2</sub>. After incubation, the 96 well plates were centrifuged at 3000 rpm to spin down non-lysed cells. 100 µL of the supernatant (containing any lysed haemoglobin) was transferred into new 96 well plates. The haemolysis was analysed by UV absorbance at 540 nm and calculated using Equation 5.3.

$$\text{Haemolysis} = \frac{\text{UV abs. polymer} - \text{UV abs. blank}}{\text{UV abs. control} - \text{UV abs. blank}} \times 100 \% \quad (5.3)$$

#### 5.4.7. Cell association studies

NIH 3T3 cells were seeded on a 24 well plate at  $10^5$  cells per well and incubated for 24 h at 37 °C in a humidified incubator with 5 % atmospheric CO<sub>2</sub>. A solution of polymer in PBS was added and the cells were incubated for the specific time at 37 °C in a humidified incubator with 5 % atmospheric CO<sub>2</sub> or in a 4 °C cold room. Following incubation, the old cell medium was removed and the cells were washed three times with 300 μL 1 % BSA in PBS solution and once with PBS. The cells were detached by addition of 200 μL trypsin solution and incubating for 5 min. 100 μL of 1 % BSA in PBS was added and the cell suspensions transferred to V-shaped 96 well plates. The plates were centrifuged at 400 g for 5 min, after which the supernatant was removed. Cells used for calibrating the flow cytometer were re-suspended in PBS only. All other cells, including viability controls, were re-suspended in a solution of PBS containing 1 % BSA and 0.5 μg mL<sup>-1</sup> propidium iodide (PI). The flow cytometer was calibrated against blank cells and the required filters were set-up for cyanine 5 (excitation 642 nm, emission bandpass 676/29 nm), PI (excitation 488 nm, emission bandpass 615/30 nm) and Alexa Fluor (excitation 640 nm, emission bandpass 710/40 nm).

#### 5.4.8. Cell uptake studies

##### Cell uptake studies with lysosomal staining

NIH 3T3 LAMP1 cells were seeded on an 8-chamber plate at a density of 4.000 cells per chamber and incubated for 24 h at 37 °C in a humidified incubator with 5 % atmospheric CO<sub>2</sub>. After addition of the polymer solutions, the cells were incubated for 1 h at 37 °C in a humidified incubator with 5 % atmospheric CO<sub>2</sub>. After incubation, the old cell medium was removed and the cells were washed thrice with FluoroBrite (phenol red-free medium). 400 μL of FluoroBrite was added, followed by 100 μL of

0.1 % propidium iodide in FluoroBrite ( $0.5 \mu\text{g mL}^{-1}$ ) and 100  $\mu\text{L}$  of Hoechst stain in FluoroBrite ( $2.5 \mu\text{g mL}^{-1}$ ). After 5 min the FluoroBrite solution was removed and a fresh 100  $\mu\text{L}$  FluoroBrite was added. The cell uptake was analysed by optical microscopy. Images were recorded on an Olympus IX83 equipped with a DAPI/FITC/CY3/CY5 filter set and processed with Slidebook 6.0 software.

### **Cell uptake studies with mitochondrial staining**

NIH 3T3 COX8A cells were seeded on an 8-chamber plate at a density of 4.000 cells per chamber and incubated for 24 h at 37 °C in a humidified incubator with 5 % atmospheric CO<sub>2</sub>. After addition of the polymer solutions, the cells were incubated for 1 h at 37 °C in a humidified incubator with 5 % atmospheric CO<sub>2</sub>. After incubation, the old cell medium was removed and the cells were washed trice with FluoroBrite. 100  $\mu\text{L}$  of a 0.5 % v/v Snap Cell 505 (mitochondrial stain) in FluoroBrite was added and the cells were incubated for 30 min at 37 °C in a humidified incubator with 5 % atmospheric CO<sub>2</sub>. The FluoroBrite was removed and the cells were washed trice with FluoroBrite. After 30 min, 100  $\mu\text{L}$  of propidium iodide in FluoroBrite ( $0.5 \mu\text{g mL}^{-1}$ ) and 100  $\mu\text{L}$  of Hoechst stain in FluoroBrite ( $2.5 \mu\text{g mL}^{-1}$ ) were added. After 5 min the FluoroBrite solutions were removed and a fresh 100  $\mu\text{L}$  of FluoroBrite was added. The cell uptake was analysed by optical microscopy. Images were recorded on an Olympus IX83 equipped with a DAPI/FITC/CY3/CY5 filter set and processed with Slidebook 6.0 software.

### **5.4.9. Anti-fouling properties**

#### **General comments**

The gold coated quartz sensors were cleaned with piranha solution, rinsed with water and dried under nitrogen gas prior to use. The QCM-D chambers were rinsed with

HPLC grade H<sub>2</sub>O prior to use to achieve a steady baseline before the addition of polymer or protein solutions.

### Optimisation studies

Comb polymer P1<sub>100</sub> was dissolved in HPLC grade H<sub>2</sub>O, 0.5 M NaCl or 0.165 M CaCl<sub>2</sub> (2 mg ml<sup>-1</sup>, pH 7.2). 0.3 μL of polymer solution was then pumped through the chambers (0.2 μL min<sup>-1</sup>) and incubated for 1 h until the signal stabilised, before rinsing the system with HPLC grade H<sub>2</sub>O (0.5 μL, 0.2 μL min<sup>-1</sup>) to remove unbound material.

### Film formation studies

Comb polymers were dissolved in 0.165 M CaCl<sub>2</sub> (2 mg mL<sup>-1</sup>, pH 7.2). 0.3 μL of polymer solution was then pumped through the chambers (0.2 μL min<sup>-1</sup>) and incubated for 1 h until the signal stabilised, before rinsing the system with HPLC grade H<sub>2</sub>O (0.5 μL min<sup>-1</sup>) to remove unbound material.

### Anti-fouling studies

The polymer coated surfaces were washed with PBS buffer solution (0.5 μL, 0.2 μL min<sup>-1</sup>) until a steady baseline was obtained. BSA or lysozyme in PBS solution (4 mg mL<sup>-1</sup>, pH 7.2) was pumped through the chambers (0.3 μL, 0.2 μL min<sup>-1</sup>) and incubated for 1 h, before washing with PBS buffer (0.5 μL, 0.2 μL min<sup>-1</sup>) to remove unbound material. Control experiments were carried out in the same way, using non-coated gold coated quartz sensors instead of the polymer film-coated sensors.

## 5.5. References

- 1 A. Abuchowski, T. van Es, N. C. Palczuk and F. F. Davis, *J. Biol. Chem.*, 1977, **252**, 3578–3581.
- 2 A. Abuchowski, J. R. McCoy, N. C. Palczuk, T. V. A. N. Es and F. F. Davis, *J.*

- Biol. Chem.*, 1976, **252**, 3582–3586.
- 3 S. N. S. Alconcel, A. S. Baas and H. D. Maynard, *Polym. Chem.*, 2011, **2**, 1442.
- 4 H. Schellekens, W. E. Hennink and V. Brinks, *Pharm. Res.*, 2013, **30**, 1729–1734.
- 5 J. J. F. Verhoef, J. F. Carpenter, T. J. Anchordoquy and H. Schellekens, *Drug Discov. Today*, 2014, **19**, 1945–1952.
- 6 P. Zhang, F. Sun, S. Liu and S. Jiang, *J. Control. Release*, 2016, **244**, 184–193.
- 7 M. Chen, F. Sun, W. Xu, L. Zhou and F. Zhang, *J. Mater. Sci.*, 2016, **51**, 5113–5121.
- 8 K. Knop, R. Hoogenboom, D. Fischer and U. S. Schubert, *Angew. Chem. Int. Ed.*, 2010, **49**, 6288–6308.
- 9 E. M. Pelegri-O’Day, E.-W. Lin and H. D. Maynard, *J. Am. Chem. Soc.*, 2014, **136**, 14323–14332.
- 10 Y. Qi and A. Chilkoti, *Curr. Opin. Chem. Biol.*, 2015, **28**, 181–193.
- 11 K. Aoi and M. Okada, *Prog. Polym. Sci.*, 1996, **21**, 151–208.
- 12 M. Glassner, M. Vergaelen and R. Hoogenboom, *Polym. Int.*, 2018, **67**, 32–45.
- 13 B. Guillermin, S. Monge, V. Lapinte and J. J. Robin, *Macromol. Rapid Commun.*, 2012, **33**, 1600–1612.
- 14 R. Hoogenboom, *Macromol. Chem. Phys.*, 2007, **208**, 18–25.
- 15 R. Hoogenboom, *Angew. Chem. Int. Ed.*, 2009, **48**, 7978–7994.
- 16 K. Kempe, M. Lobert, R. Hoogenboom and U. S. Schubert, *J. Polym. Sci. A Polym. Chem.*, 2009, **47**, 3829–3838.
- 17 S. Kobayashi and H. Uyama, *J. Polym. Sci. A Polym. Chem.*, 2002, **40**, 192–209.
- 18 A. Makino and S. Kobayashi, *J. Polym. Sci. A Polym. Chem.*, 2010, **48**, 1251–1270.
- 19 E. Rossegger, V. Schenk and F. Wiesbrock, *Polymers*, 2013, **5**, 956–1011.
- 20 B. Verbraeken, B. D. Monnery, K. Lava and R. Hoogenboom, *Eur. Polym. J.*, 2017, **88**, 451–469.
- 21 M. Bauer, S. Schroeder, L. Tauhardt, K. Kempe, U. S. Schubert and D. Fischer, *J. Polym. Sci. A Polym. Chem.*, 2013, **51**, 1816–1821.
- 22 M. Bauer, C. Lautenschlaeger, K. Kempe, L. Tauhardt, U. S. Schubert and D.
-

- Fischer, *Macromol. Biosci.*, 2012, **12**, 986–998.
- 23 R. W. Moreadith, T. X. Viegas, M. D. Bentley, J. M. Harris, Z. Fang, K. Yoon, B. Dizman, R. Weimer, B. P. Rae, X. Li, C. Rader, D. Standaert and W. Olanow, *Eur. Polym. J.*, 2017, **88**, 524–552.
- 24 R. Duncan, *Nat. Rev. Drug Discov.*, 2003, **2**, 347–360.
- 25 R. Duncan, *Nat. Rev. Cancer*, 2006, **6**, 688–701.
- 26 Z. Qu, H. Xu and H. Gu, *ACS Appl. Mater. Interfaces*, 2015, **7**, 14537–14551.
- 27 V. Turk, V. Stoka, O. Vasiljeva, M. Renko, T. Sun, B. Turk and D. Turk, *Biochim. Biophys. Acta - Proteins Proteomics*, 2012, **1824**, 68–88.
- 28 S. S. Cotrin, L. Puzer, W. A. De Souza Judice, L. Juliano, A. K. Carmona and M. A. Juliano, *Anal. Biochem.*, 2004, **335**, 244–252.
- 29 T. Imai, M. Taketani, M. Shii, M. Hosokawa and K. Chiba, *Drug Metab. Dispos.*, 2006, **34**, 1734–1741.
- 30 H. Shirahama, A. Kanetani and H. Yasuda, *Polym. J.*, 2000, **32**, 280–286.
- 31 C. Tsutsumi, K. Nakagawa, H. Shirahama and H. Yasuda, *Macromol. Biosci.*, 2002, **2**, 223–232.
- 32 M. V. Volokitina, V. A. Korzhikov-Vlakh, T. B. Tennikova and E. G. Korzhikova-Vlakh, *J. Pharm. Biomed. Anal.*, 2017, **145**, 169–177.
- 33 H. Peng, J. Ling, J. Liu, N. Zhu, X. Ni and Z. Shen, *Polym. Degrad. Stab.*, 2010, **95**, 643–650.
- 34 R. Belibel, N. Marival, H. Hlawaty and C. Barbaud, *Polym. Degrad. Stab.*, 2016, **130**, 288–299.
- 35 S.-M. Lai, W.-W. Sun and T.-M. Don, *Polym. Eng. Sci.*, 2015, **55**, 1321–1329.
- 36 A. Buzarovska and A. Grozdanov, *J. Appl. Polym. Sci.*, 2012, **123**, 2187–2193.
- 37 M. Dangkulwanich, K. Kongnithigarn and N. Aurnoppakhun, *J. Chem. Educ.*, 2018, **95**, 141–145.
- 38 N. Murthy, J. R. Robichaud, D. A. Tirrell, P. S. Stayton and A. S. Hoffman, *J. Control. Release*, 1999, **61**, 137–143.
- 39 C. A. Lackey, N. Murthy, O. W. Press, D. A. Tirrell, A. S. Hoffman and P. S. Stayton, *Bioconjug. Chem.*, 1999, **10**, 401–405.
- 40 S. Marrache and S. Dhar, *Proc. Natl. Acad. Sci.*, 2012, **109**, 16288–16293.
- 41 J. M. Noy, H. Lu, P. J. Hogg, J. L. Yang and M. Stenzel, *Bioconjug. Chem.*, 2018, **29**, 546–558.
- 42 L. Liu, W. Li and Q. Liu, *Wiley Interdiscip. Rev. Nanomedicine*
-

- Nanobiotechnology*, 2014, **6**, 599–614.
- 43 M. Charnley, M. Textor and C. Acikgoz, *React. Funct. Polym.*, 2011, **71**, 329–334.
- 44 S. Krishnan, C. J. Weinman and C. K. Ober, *J. Mater. Chem.*, 2008, **18**, 3405.
- 45 A. S. Duwez, P. Guillet, C. Colard, J. F. Gohy and C. A. Fustin, *Macromolecules*, 2006, **39**, 2729–2731.
- 46 S. Slavin, A. H. Soeriyadi, L. Voorhaar, M. R. Whittaker, C. R. Becer, C. Boyer, T. P. Davis and D. M. Haddleton, *Soft Matter*, 2012, **8**, 118–128.
- 47 G. Sauerbrey, *Z. Phys.*, 1959, **155**, 206–222.
- 48 T. Mohan, K. Niegelhell, C. S. P. Zarth, R. Kargl, S. Köstler, V. Ribitsch, T. Heinze, S. Spirk and K. Stana-Kleinschek, *Biomacromolecules*, 2014, **15**, 3931–3941.
- 49 M. V. Voinova, M. Rodahl, M. Jonson and B. Kasemo, *Phys. Scr.*, 1999, **59**, 391–396.
- 50 M. V. Voinova, M. Jonson and B. Kasemo, *Biosens. Bioelectron.*, 2002, **17**, 835–841.
- 51 D. Johannsmann, *Macromol. Chem. Phys.*, 1999, **516**, 501–516.
- 52 D. Johannsmann, *Phys. Chem. Chem. Phys.*, 2008, **10**, 4516–4534.
- 53 Y. Zhang, B. Du, X. Chen, H. Ma, Y. Zhang, B. Du, X. Chen and H. Ma, *Anal. Chem.*, 2009, **81**, 642–648.
- 54 H. Witte and W. Seeliger, *Angew. Chem. Int. Ed.*, 1972, **11**, 287–288.
- 55 C. J. Ferguson, R. J. Hughes, D. Nguyen, B. T. T. Pham, R. G. Gilbert, A. K. Serelis, C. H. Such and B. S. Hawkett, *Macromolecules*, 2005, **38**, 2191–2204.

## Chapter 6

---

# Thermal study on polyester networks based on the renewable monomers citric acid and gluconolactone

---

*“Paper or plastic? Polylactic acid (PLA) or polyethylene terephthalate (PET)? London or Paris? Which of these decisions impacts your sustainability index the most? An airline flight from Atlanta to Athens could include a layover in London or Paris. Paris lies closer to the Atlanta/Athens great circle and thus is the better option, resulting in a flight path of 5682 miles. Flying through London, however, would add 18 miles to your trip. This may seem inconsequential, but at 77 miles/gallon per passenger (typical for a Boeing 767), this amounts to about 1.5 pounds of hydrocarbon fuel (per passenger), a mass equivalent to about 70 PET water bottles, a significant fraction of the 200 consumed annually per American. Now, what if you skip the journey to Athens altogether? That could save 500 pounds of fuel, or the mass equivalent of 23000 water bottles, just for one passenger! The foregoing scenario paints a fairly bleak picture. When the average American consumes 21000 bottles of fossil fuel per year, does it really matter if we save a few ounces or pounds by using biorenewable PLA instead of PET? The answer is complicated, but yes.”*

Stephen Miller, *ACS Macro Lett.* **2013**, 2, 550-554

Parts of this chapter have been published:

P.A.J.M. de Jongh, P.K.C. Paul, E. Khoshdel, P. Wilson, K. Kempe, D.M. Haddleton, *Polym. Int.* **2017**, 66, 59-63

## 6.1. Introduction

The majority of polyesters used commercially today are made from non-renewable fossil sources. As a result of fluctuating oil prices and their ultimate depletion,<sup>1</sup> polyesters derived from renewable resources have attracted significant attention in recent years.<sup>2</sup> In particular, their biodegradability, potential biocompatibility and the relatively easy access to bio-based/biomass monomers makes them highly interesting next generation sustainable materials. Of all the polymers available from renewable resources polyesters stand out as the most available and versatile class. However, limiting this at the moment are the costs of bio-based polyesters which are significantly higher than for petrochemical-based polyesters – this will inevitably change in the future.<sup>3</sup>

In recent years an ever increasing list of monomers that can be obtained from biomass has been reported.<sup>4-6</sup> An important subclass are oxygen-rich monomers such as carboxylic acids, polyols, dianhydroalditols and furans.<sup>2</sup> In a recent review, Vilela *et al.* highlighted succinic acid, fumaric acid, itaconic acid and furandicarboxylic acid as promising diacids, and isosorbide, isomannide, isoidide, 1,3-propanediol and 1,4-butanediol as diol monomers for the synthesis of polyesters.<sup>2</sup>

A further interesting monomer is citric acid (CA), a tricarboxylic acid with a sterically hindered tertiary hydroxyl group. CA is a common metabolite of plants and animals and produced industrially by fermentation with *Aspergillus Niger* strains.<sup>7</sup> Substrates for the production of CA include rapeseed oil, corncobs, and brewery wastes.<sup>8,9</sup> CA is the most commonly used polyacid monomer for the production of polyesters by melt polycondensation. In this context, it has been co-polymerised with various aliphatic diols,<sup>10-14</sup> D-sorbitol<sup>15</sup> and glycerol,<sup>16-19</sup> amongst others. The polyester networks resulting from those reactions have found applications in, for example, tissue engineering<sup>20,21</sup> and drug delivery.<sup>16,17</sup>

Apart from easy access to monomers, the safety of use of monomers is important to many applications. The US Food and Drug Administration has a database of 379 compounds that are *generally recognised as safe* (GRAS) as ingredients, for packaging and labelling.<sup>22</sup> Some of these compounds have been used in the synthesis of polyesters,

including citric acid,<sup>10–19</sup> glycerol,<sup>16–19</sup> lactic acid,<sup>23</sup> malic acid,<sup>24–27</sup> sorbitol<sup>15</sup> and sucrose.<sup>28</sup>

In the context of using GRAS starting materials, Tsutsumi *et al.* investigated the polycondensation between CA and D-glucono- $\delta$ -lactone (GL) in detail (Figure 6.1).<sup>29</sup> Pre-polymers in molar ratios from CA/GL 4/1 to 1/4 were prepared by melt polycondensation at 165 °C, cast from a tetrahydrofuran solution, and subsequently post-polymerised at 180 °C. The resulting films were analysed for their thermal, mechanical, and physiochemical properties, as well as enzymatic degradation by *Rhizopus delemar*, which increased with increasing CA concentrations.

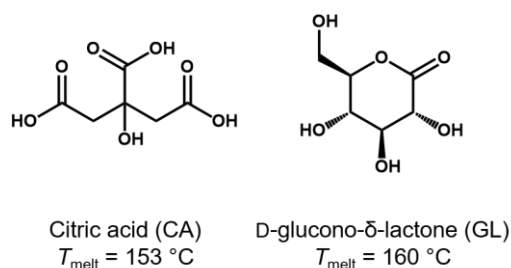


**Figure 6.1** Structures of citric acid and D-glucono- $\delta$ -lactone.

In this present study, we have further investigated the melt polycondensation between CA ( $T_{\text{melt}} = 153\text{ °C}$ ) and GL ( $T_{\text{melt}} = 160\text{ °C}$ ) and the thermal properties of the resulting polyester networks. A “green”, minimalistic approach was used in which reactions took place in the absence of solvent at temperatures just above the melting point of CA ( $T_{\text{react}} = 160\text{ °C}$ ). The influence of reaction temperature and time was evaluated and a systematic study of different GRAS and relatively safe co-monomers was performed to provide more insight into this reaction and the factors that influence the reaction and material properties. Finally, the effect of some catalysts was studied.

## 6.2. Results and discussion

Melt polycondensations between bi- and multifunctional monomers were studied by differential scanning calorimetry (DSC), analysing the melting and reaction characteristics on the first heating cycle and the thermal properties of the polyesters formed on

the second heating cycle. By studying the reactions by DSC, insight could be gained about both the reaction and the thermal properties of the resulting polyester networks simultaneously.

### 6.2.1. Citric acid and D-glucono- $\delta$ -lactone

At first, the standard system in this study, CA ( $T_{\text{melt}} = 153\text{ }^{\circ}\text{C}$ ) and GL ( $T_{\text{melt}} = 160\text{ }^{\circ}\text{C}$ ) in a 1/1 molar ratio was investigated. It was observed within the first heating cycle that the monomer mixture melts at a lower temperature than the individual monomers (Figure 6.2a). The broad endothermic peak results from an impure mixture (both monomers act as an impurity to the other), as well as the reaction that takes place in the melt state.

Within the second thermal cycle a glass transition at  $17\text{ }^{\circ}\text{C}$  was observed. By introducing an isothermal segment (ITS) on the first cycle, between heating and cooling, the reaction time of the polycondensation could be changed. As expected for a polycondensation reaction, an increase in reaction time resulted in polymer networks with higher glass transition temperatures, increasing the  $T_g$  up to  $43\text{ }^{\circ}\text{C}$  for a 20 min ITS (Figure 6.2b). Similarly, when the reaction was performed at different temperatures the glass transition temperature increased with increasing reaction temperatures. A minimum reaction temperature of  $130\text{ }^{\circ}\text{C}$  was required to observe polyesters with a glass transition in the measurement range ( $T_g = 15\text{ }^{\circ}\text{C}$ , Figure 6.2c).

In order to further investigate the lower melting temperature observed for the CA and GL mixture, a series of CA/GL monomer mixtures was prepared with monomer ratios varying from 10 to 90 mol% GL in CA. Melt onset temperatures for all mixtures were found to be between  $129$  and  $132\text{ }^{\circ}\text{C}$ , with the exception of the equimolar mixture which was found to be  $125\text{ }^{\circ}\text{C}$ . This shows that the CA and GL system has a eutectic melting behaviour, but with a small window to tune the melting temperature as they are close to each other (Figure 6.2d). No relation was found between the monomer ratios or functional group ratios and the glass transition temperatures observed. This demonstrates that a temperature of only  $125\text{ }^{\circ}\text{C}$  is required to melt the monomers at their eutectic composition, and a 10 min reaction at  $130\text{ }^{\circ}\text{C}$  already produces polyester networks with a glass transition temperature in the measurement window ( $15\text{ }^{\circ}\text{C}$ ).

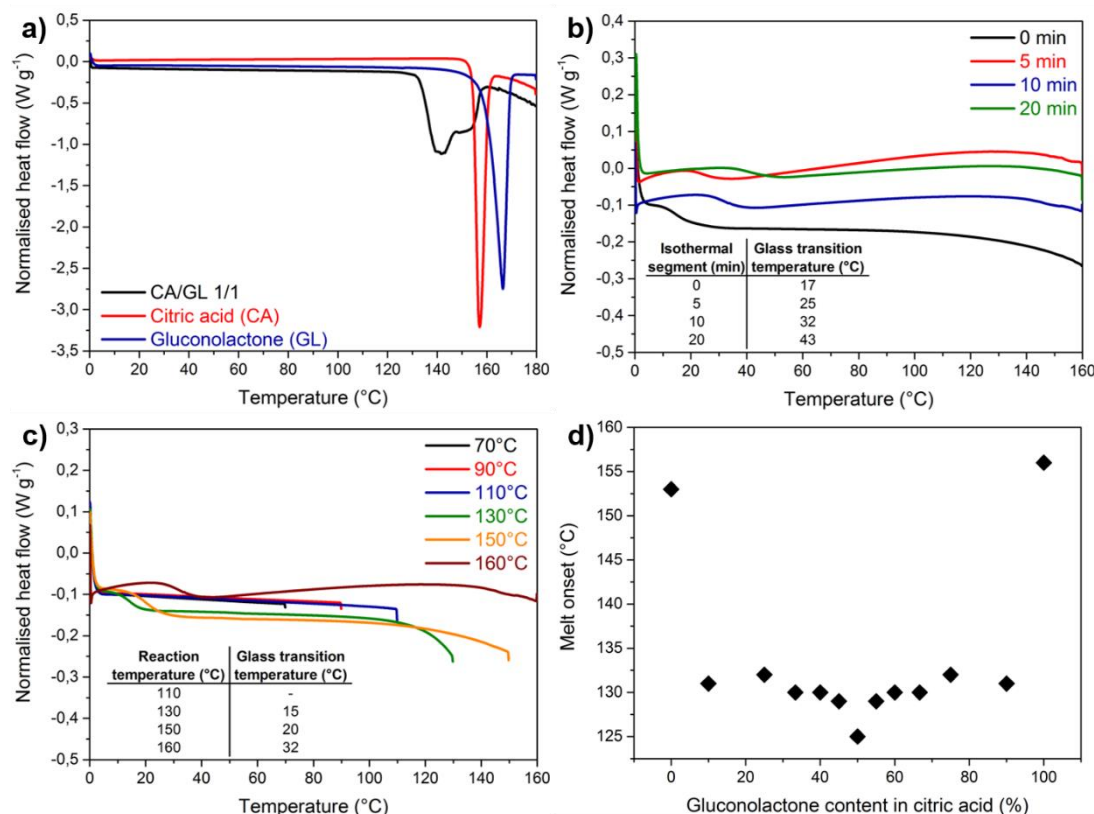


**Figure 6.2** Polycondensation of CA and GL followed by DSC. a) The reaction mixture of CA and GL (1/1) melts and reacts at a lower temperature than the individual monomers. b) On the second heating cycle a glass transition temperature can be observed, which increases with increasing reaction time ( $T_{\text{react}} = 160$  °C). c) The glass transition temperature increases with increasing reaction temperatures, with a minimum of 130 °C required (10 min ITS). d) The melt onset temperature of CA and GL mixtures revealed a eutectic melt behaviour.

### 6.2.2. Aliphatic bifunctional co-monomers

A range of aliphatic, bifunctional co-monomers were studied with the objective of reducing the melting temperature of the monomer mixture while increasing the glass transition temperature of the polyester networks (Figure 6.3).

For all multi-monomer systems, the molar ratios of monomers were chosen to keep the functional group stoichiometry approximately 1/1 (acid/hydroxyl). Glycolic acid (GA,  $T_{\text{melt}} = 75 - 80$  °C) mixed in an equimolar ratio with CA and GL shows a sharp melting peak at the melting temperature of GA (Figure 6.4a). The CA and GL monomers do not completely dissolve in GA at this point, but start to dissolve into, and react with,

GA just below 100 °C. Within the second a cycle a glass transition is observed, but at lower a temperature than the pure CA/GL system at the same reaction temperature and time (Figure 6.4b). Higher glass transition temperatures could be obtained by further increasing the reaction time.

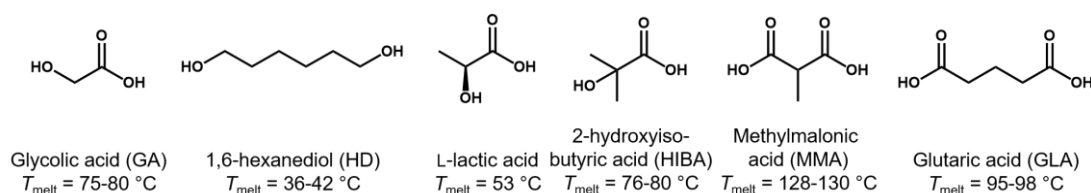


**Figure 6.3** Structures of aliphatic bifunctional co-monomers.

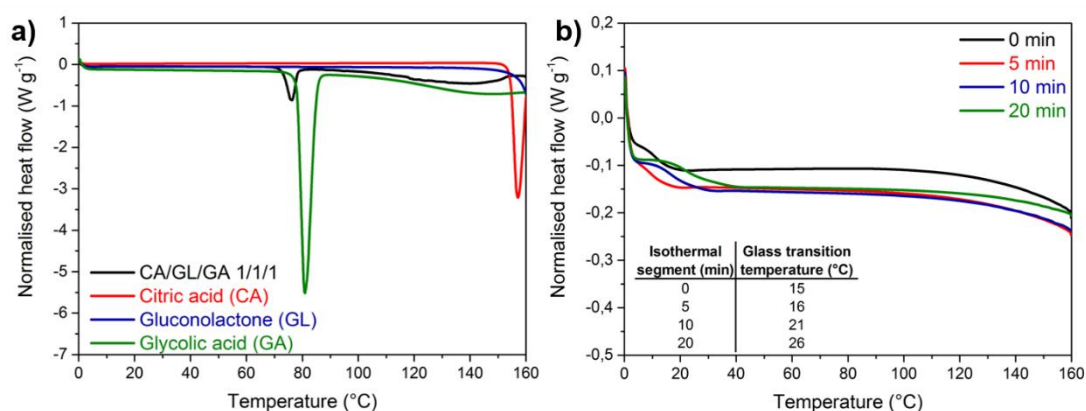


**Figure 6.4** DSC polymerisation of CA and GL with glycolic acid. a) First heating cycle. b) Second heating cycle.

It was hypothesised that these observations result from the introduction of linear segments through GA. In order to investigate this, 1,6-hexanediol (HD,  $T_{\text{melt}} = 38 - 42\text{ }^{\circ}\text{C}$ ) was subsequently evaluated. The first heating cycle looks similar, but now the co-monomer melts at 38 - 42 °C reacting with CA/GL at 90 °C (Figure 6.5a). Only for the 10 and 20 min reactions glass transition temperatures were observed (Figure 6.5b). This finding suggests that linear segments lower the glass transition temperature, as well as that a long flexible chain between the functional groups has a significant effect on the resulting material properties.

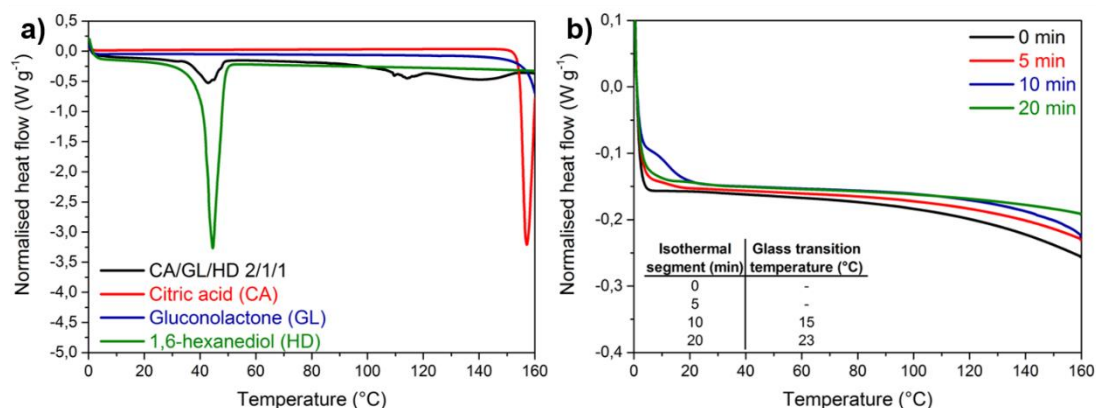


**Figure 6.5** DSC polymerisation of CA and GL with 1,6-hexanediol. a) First heating cycle. b) Second heating cycle.

This hypothesis is further confirmed by other bifunctional monomers: L-lactic acid (LA,  $T_{\text{melt}} = 53\text{ }^{\circ}\text{C}$ ), 2-hydroxyisobutyric acid (HIBA,  $T_{\text{melt}} = 76 - 80\text{ }^{\circ}\text{C}$ ), methylmalonic acid (MMA,  $T_{\text{melt}} = 128 - 130\text{ }^{\circ}\text{C}$ ) and glutaric acid (GLA,  $T_{\text{melt}} = 95 - 98\text{ }^{\circ}\text{C}$ ), which all show lower glass transition temperatures, or no glass transition at all in case of GLA, within the measured temperature range (Figures 6.6 – 6.9). Figure 6.10 provides a comparison for the copolymerisation of CA and GL with aliphatic bifunctional co-monomers and demonstrates that only the co-polymerisation of MMA leads to  $T_{\text{gs}}$  comparable to the pure CA/GL system, whereas all other aliphatic bifunctional co-monomers lead to lower  $T_{\text{gs}}$ .

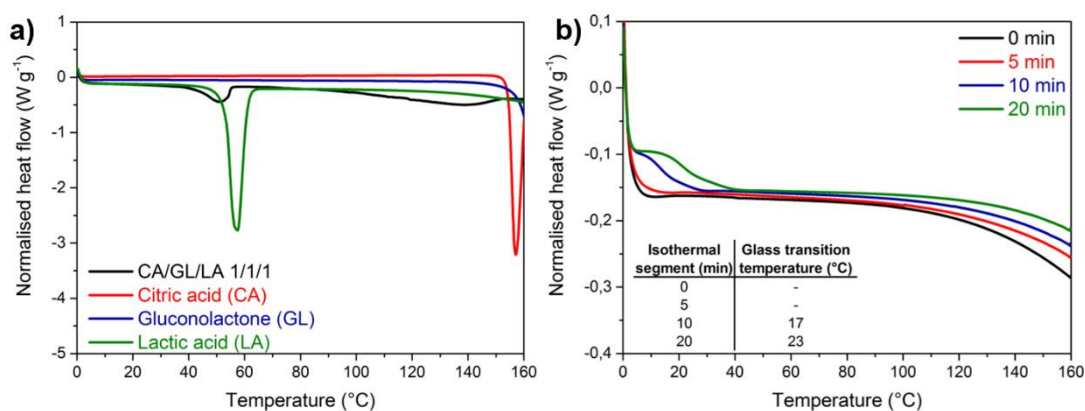


**Figure 6.6** DSC polymerisation of CA and GL with L-lactic acid. a) First heating cycle. b) Second heating cycle.

Thermal study on polyester networks based on the renewable monomers citric acid and gluconolactone

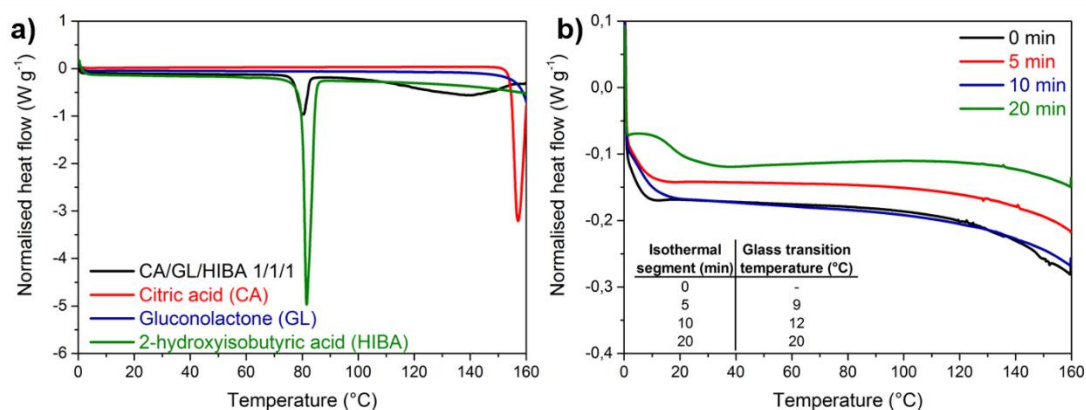


**Figure 6.7** DSC polymerisation of CA and GL with 2-hydroxyisobutyric acid. a) First heating cycle. b) Second heating cycle.

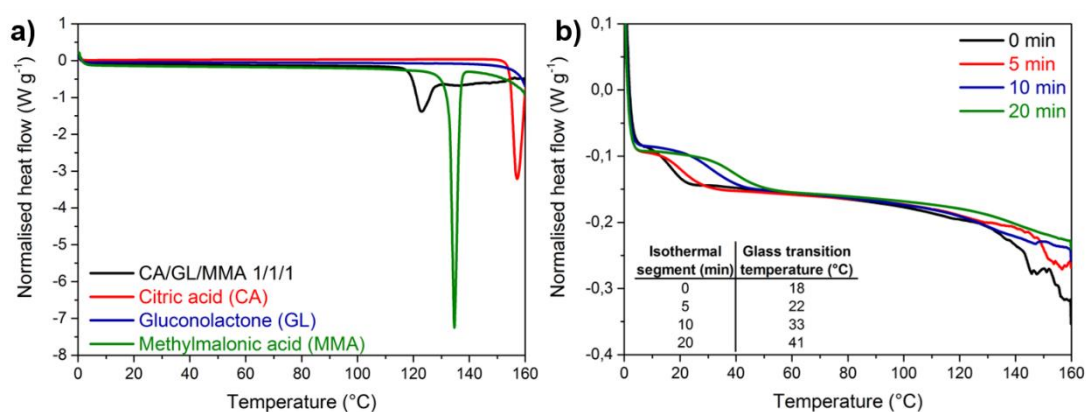


**Figure 6.8** DSC polymerisation of CA and GL with methylmalonic acid. a) First heating cycle. b) Second heating cycle.

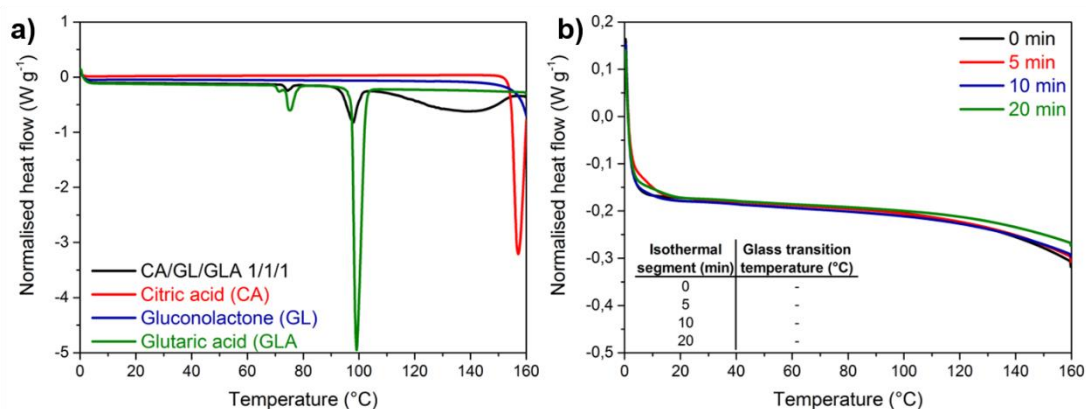


**Figure 6.9** DSC polymerisation of CA and GL with glutaric acid. a) First heating cycle. b) Second heating cycle.

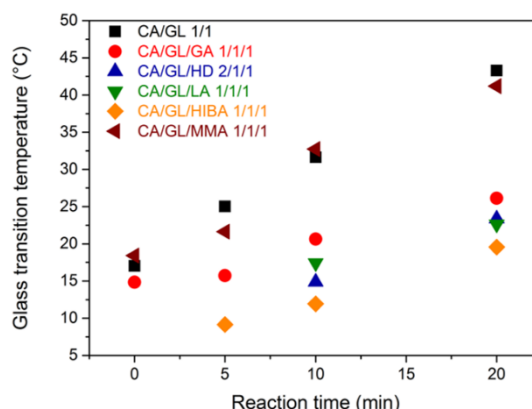


**Figure 6.10** Comparison of glass transition temperatures obtained by polycondensation of CA and GL with aliphatic bifunctional co-monomers.

The observation of two endothermic melting events, one of the additional co-monomer and the other from dissolution and reaction of the other monomers, implies that the amount of co-monomer used can only dissolve a limited amount of CA and GL. Increasing the amount of co-monomer allows more CA and GL to be dissolved at low temperature, but only results in an increase in linear segments within the polyester networks and a decrease in their glass transition temperature (Figure 6.11). This can in turn be overcome by elevated reaction temperatures or time (Figure 6.12).

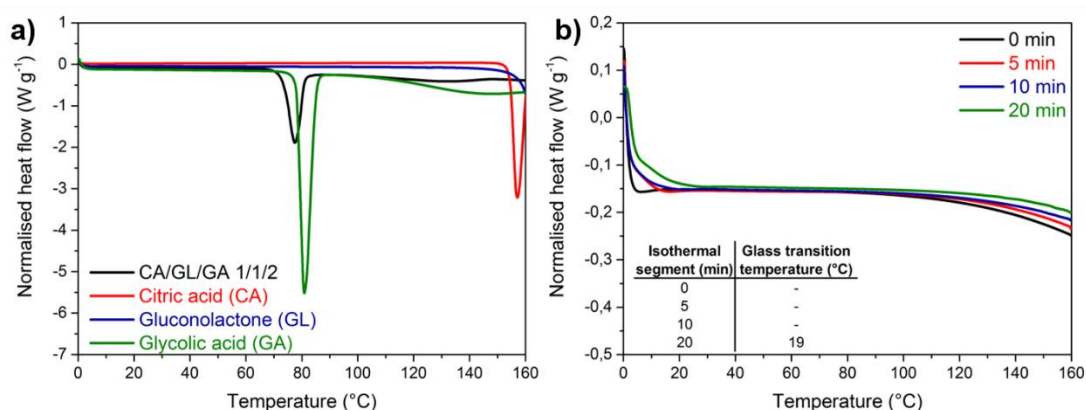


**Figure 6.11** DSC polymerisation of CA and GL with excess glycolic acid. a) First heating cycle. b) Second heating cycle.

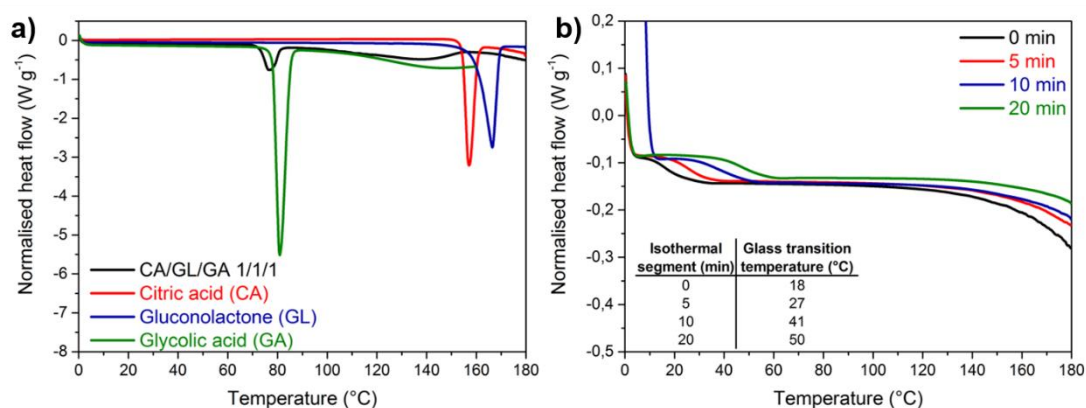


**Figure 6.12** DSC polymerisation of CA and GL with glycolic acid at higher temperature (180 °C). a) First heating cycle. b) Second heating cycle.

### 6.2.3. Aliphatic polyfunctional co-monomers

Subsequently, polyfunctional co-monomers (Figure 6.13) were evaluated. 1,1,1-Tri-methylolpropane (TMP,  $T_{\text{melt}} = 56 - 58$  °C) was tested in a CA/GL/TMP 2/1/1 ratio, and DL-malic acid (MA,  $T_{\text{melt}} = 131 - 133$  °C) and L-tartaric acid (TA,  $T_{\text{melt}} = 170 - 172$  °C) were tested in equimolar molar ratios with CA/GL.

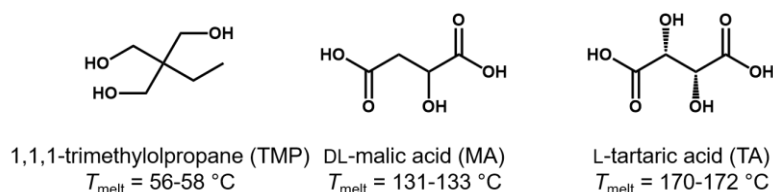


**Figure 6.13** Structures of aliphatic polyfunctional co-monomers.

TMP showed a similar behaviour on the first heating cycle as the bifunctional co-monomers with a sharp melting peak at the melting temperature of TMP (Figure 6.14a), followed by a further endothermic dissolution and reaction peak from 90 °C. For MA and TA no separate co-monomer peak was observed, only a broad endothermic melting and reaction peak, with melt onset temperatures at 118 °C and 130 °C for MA and TA, respectively (Figure 6.15a, 6.16a). Glass transition temperatures increase in the

order of  $TMP < MA < TA$  (Figures 6.14b – 6.16b), which can be explained by the length and flexibility of chains between the reacting groups, which determines the crosslinking density. A comparison overview is shown in Figure 6.17.

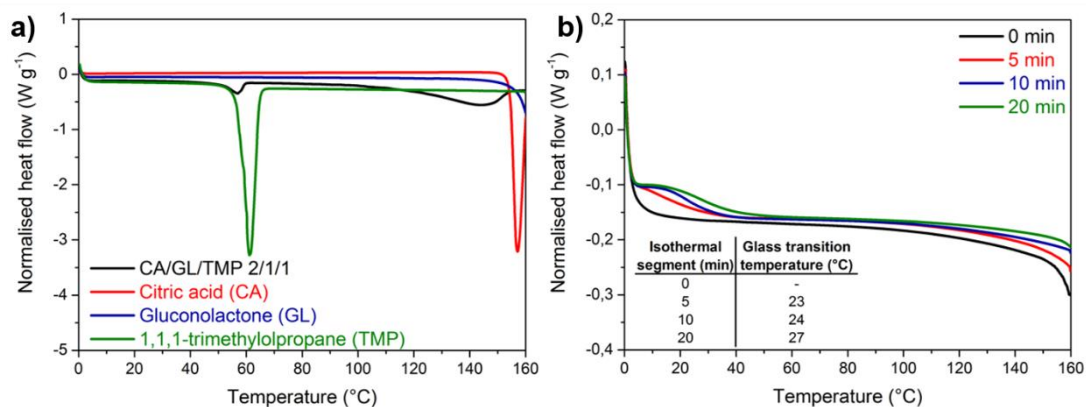


**Figure 6.14** DSC polymerisation of CA and GL with 1,1,1-trimethylolpropane. a) First heating cycle. b) Second heating cycle.

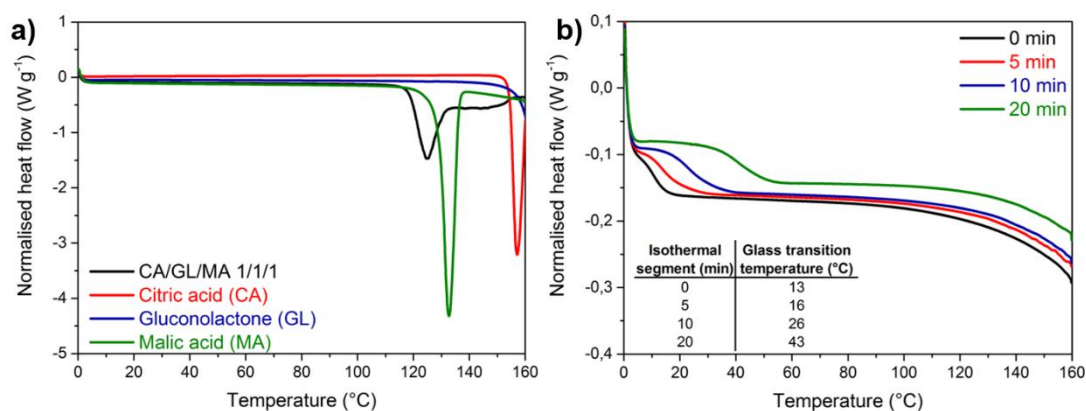


**Figure 6.15** DSC polymerisation of CA and GL with DL-malic acid. a) First heating cycle. b) Second heating cycle.

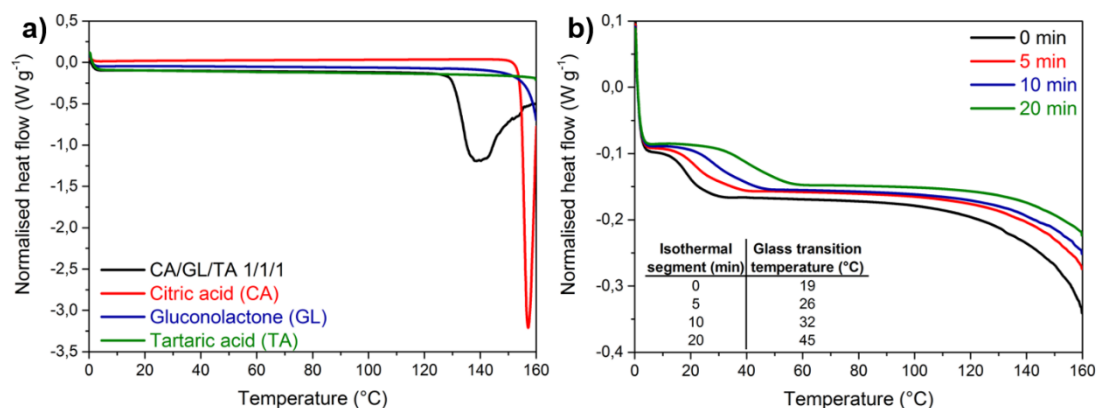


**Figure 6.16** DSC polymerisation of CA and GL with L-tartaric acid. a) First heating cycle. b) Second heating cycle.

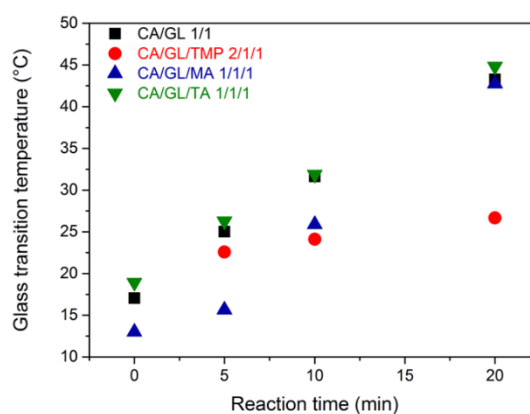


**Figure 6.17** Comparison of glass transition temperatures obtained by polycondensation of CA and GL with aliphatic polyfunctional monomers.

#### 6.2.4. Aromatic co-monomers

In addition to the aliphatic monomers tested, three aromatic monomers were also evaluated for the copolymerisation with CA and GL (Figure 6.18). 4-Hydroxybenzoic acid (HBA,  $T_{\text{melt}} = 213 - 217$  °C) and terephthalic acid (TPA,  $T_{\text{melt}} = 300$  °C) were copolymerised in equimolar ratios to CA and GL; 1,3,5-trihydroxybenzene (THB,  $T_{\text{melt}} = 215 - 220$  °C) was reacted in a CA/GL/THB 3/1/1 molar ratio to retain the same functional group stoichiometry.

Thermal study on polyester networks based on the renewable monomers citric acid and gluconolactone

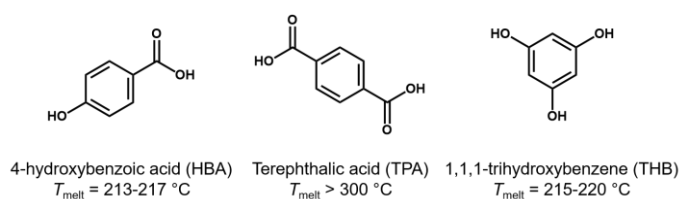


**Figure 6.18** Structures of aromatic co-monomers.

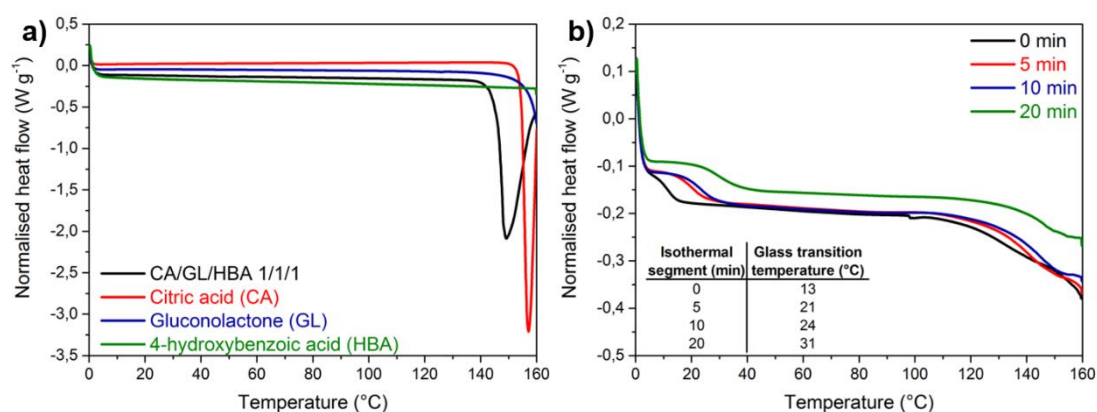


**Figure 6.19** DSC polymerisation of CA and GL with 4-hydroxybenzoic acid. a) First heating cycle. b) Second heating cycle.

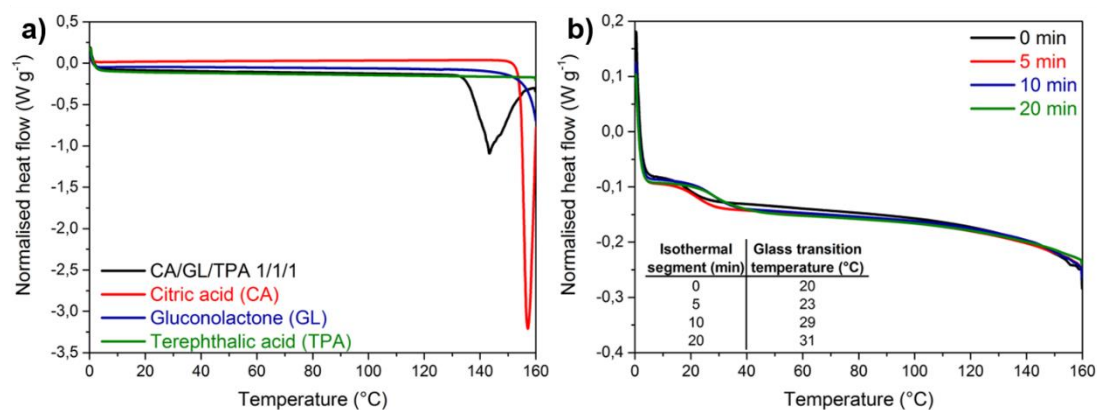


**Figure 6.20** DSC polymerisation of CA and GL with terephthalic acid. a) First heating cycle. b) Second heating cycle.

For short reaction times, all aromatic co-monomers resulted in glass transition temperatures close to the CA/GL system, but for long reaction times (20 min) it became clear

that the trifunctional THB results in higher glass transition temperatures compared to the bifunctional HBA and TPA monomers (Figures 6.19 – 6.22).

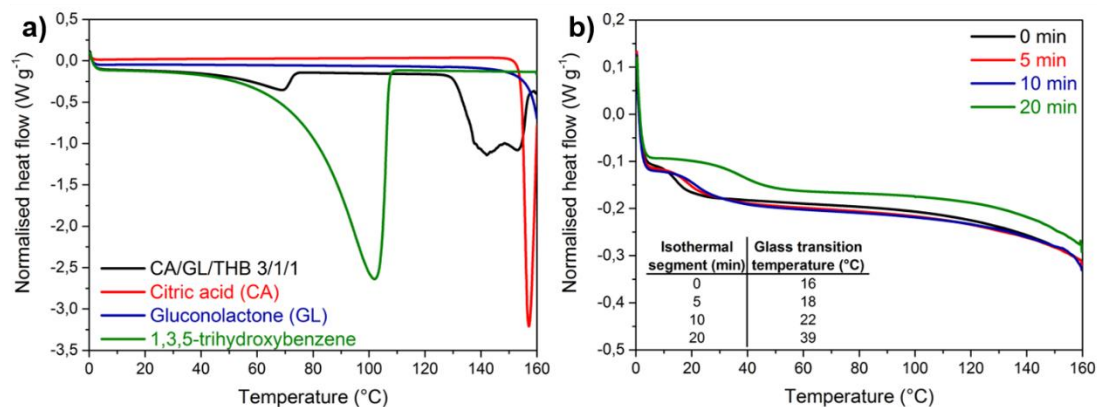


**Figure 6.21** DSC polymerisation of CA and GL with 1,3,5-trihydroxybenzene. a) First heating cycle. b) Second heating cycle.

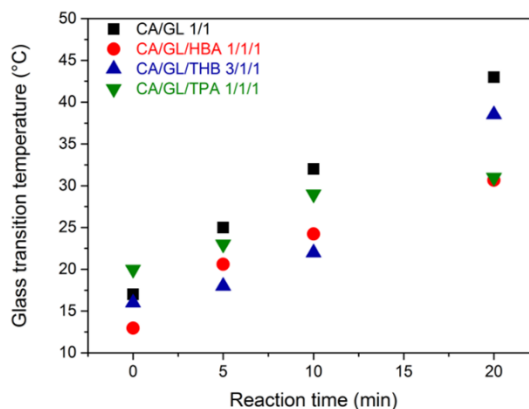


**Figure 6.22** Comparison of glass transition temperatures obtained by polycondensation of CA and GL with aromatic monomers.

### 6.2.5. Effect of ring-structured monomers

To investigate the influence of the ring-structure of GL on the polyester networks, CA was copolymerised with D-glucose (Glc,  $T_{\text{melt}} = 150 - 152$  °C) and D-fructose (Fru,  $T_{\text{melt}} = 119 - 122$  °C), in a 2/1 CA/polyol ratio (Figure 6.23). Both monomer combinations were found to melt at lower temperatures compared to the individual monomers,

with melt onset temperatures at 125 and 95 °C respectively for the Glc- and Fru-based systems (Figures 6.24a, 6.25a). This is in line with a report that CA can form deep eutectic solvents with different sugars, including glucose and sucrose.<sup>30</sup>

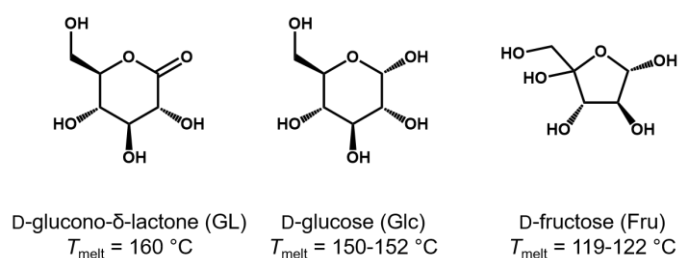


**Figure 6.23** Structures of the ring-structured monomers

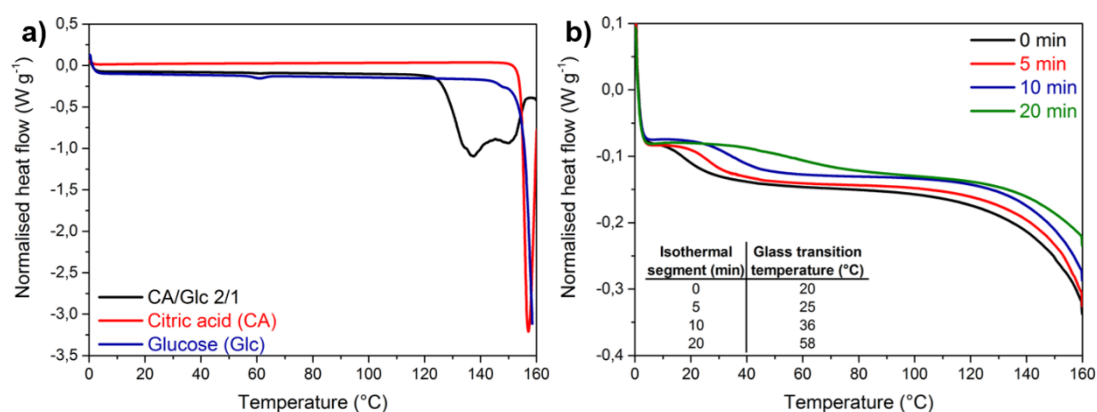


**Figure 6.24** DSC polymerisation of CA and D-glucose. a) First heating cycle. b) Second heating cycle.

The glass transition temperatures increased in the order of Fru < GL < Glc (Figures 6.24 – 6.26). This can be explained structurally as fructose has two primary, and therefore more flexible, hydroxyl groups. Glucose has one more hydroxyl group than GL, on the anomeric position, providing another reactive position, compared to the GL monomer. When compared to the other polyfunctional co-monomers, this shows that the rigid structure of these polyols has a significant influence on the material properties, compared to monomers without a rigid ring structure, and that their modification

has a higher impact on their glass transition temperature. The highest  $T_g$  was found to be 55 °C for a 20 min reaction with CA/Glu 2/1.

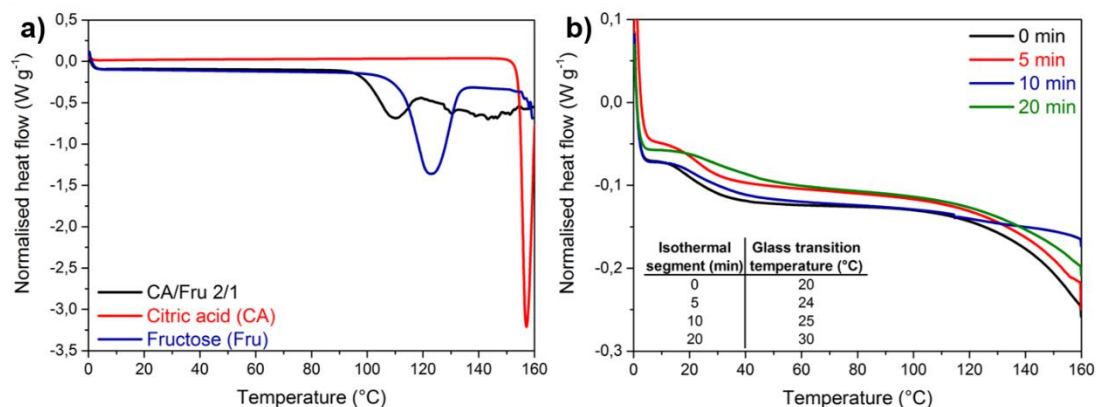


**Figure 6.25** DSC polymerisation of CA and D-fructose. a) First heating cycle. b) Second heating cycle.

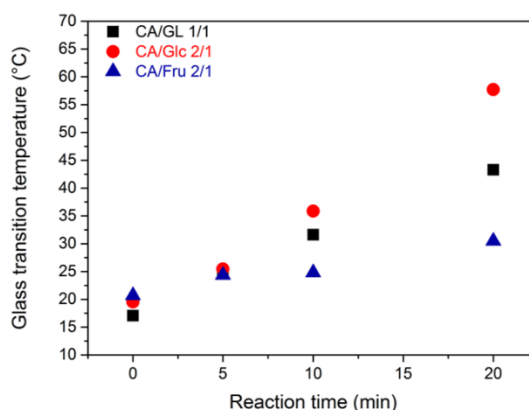


**Figure 6.26** Comparison of glass transition temperatures obtained by polycondensation of CA and ring-structured monomers.

### 6.2.6. Catalysts

A common method to enhance the synthesis of polyesters is the use of catalysts and there is a wide variety of metal-organic, organic and enzymatic catalysts that have been previously explored.<sup>31,32</sup> Herein, the use of two sets of catalysts on the polycondensation of CA/GL 1/1 were evaluated: catalysts based on zinc and a small selection of

non-zinc catalysts (Figure 6.27). The various zinc catalysts give variable results, but it is interesting to note that the safe complex zinc pyrithione<sup>33</sup> does improve the  $T_g$  even at low catalyst loadings. A more significant effect can be observed for the selected non-zinc catalysts. Scandium triflate is known to improve polycondensation reactions<sup>34</sup> and also significantly increases the  $T_g$  for CA/GL 1/1 polyesters. The largest improvement is obtained with sodium hypophosphite, which is also safe.<sup>35</sup> These results not only demonstrate that higher  $T_g$ s can be obtained by including catalysts, but also that there are safe catalysts that can be employed for this.

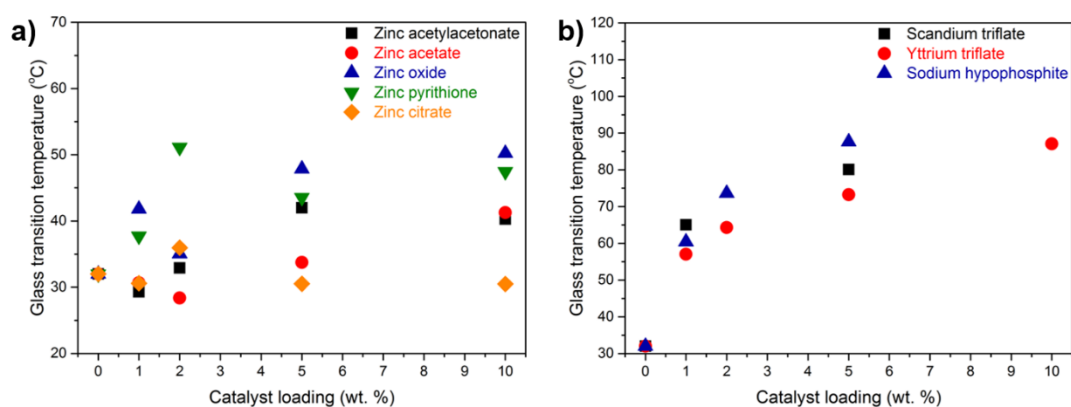


**Figure 6.27** Glass transition temperatures for the polycondensation of CA and GL in the presence of zinc catalysts (a) and other catalysts (b).

### 6.3. Conclusions

In this systematic study on polyester networks prepared by melt polycondensation from the renewable monomers citric acid and gluconolactone, it was first of all shown how reaction time and temperature influence the properties of the resulting networks. Increasing one or both yields materials with higher glass transition temperatures. Bi-functional monomers decrease this temperature, and even multifunctional monomers with flexible structures have the same result. It was found that aromatic co-monomers follow the same trend as aliphatic co-monomers. By evaluating other ring structured monomers, it was shown how the rigid structure of gluconolactone has a significant

influence on the resulting properties. Moreover, it is possible to obtain higher  $T_g$ s by using safe catalysts. The results in this study provide a general insight into this type of polycondensation and the results found can also be applied to polyester networks based on other materials.

## 6.4. Experimental

### 6.4.1. Materials

Citric acid (CA, 99.5%), D-glucono- $\delta$ -lactone (GL, 99%), glycolic acid (GA, 99%), 1,1,1-trimethylolpropane (TMP, 97%), methylmalonic acid (MMA, 99%), 2-hydroxyisobutyric acid (HIBA), DL-malic acid (MA, 99%), L-tartaric acid (TA, 99%), D-glucose (Glc, 99.5%), D-fructose (Fru, 99%), 4-hydroxybenzoic acid (HBA, 99%), 1,3,5-trihydroxybenzene (THB, 99%), terephthalic acid (TPA, 98%), scandium(III) triflate (99 %), zinc pyrithione ( $\geq 95$  %) and sodium hypophosphite ( $\geq 99$  %) were purchased from Sigma-Aldrich and used as received. L-lactic acid (LA, 98%) was obtained from VWR International and used as received. Glutaric acid (GLA, 99%) and 1,6-hexanediol (HD, 97%) were obtained from Merck and used as received.

### 6.4.2. Differential scanning calorimetry (DSC)

Polymerisations and thermal analysis by DSC were performed on a Mettler Toledo DSC1 differential scanning calorimeter in 40  $\mu$ L aluminium crucibles. Data was processed using Mettler Toledo STARe software. The melting and reaction behaviour was determined from the first heating segment, the thermal properties of the formed polyester networks were evaluated on the second heating cycle. The heating programs used are specified in Section 6.4.3.

### 6.4.3. Synthetic procedures

#### General polymerisation procedure

Monomers were mixed in the solid state and ground for homogenisation, in molar ratios as stated in the main text (approximating 1/1 ratios between the functional groups). A small amount of 10 - 15 mg was placed in a 40  $\mu\text{L}$  DSC crucible and subjected to the following DSC program (two heating/cooling cycles): 0 – 160 – ITS – 0 – 160 – 0  $^{\circ}\text{C}$  at 5  $^{\circ}\text{C min}^{-1}$ . The isothermal segment (ITS) on the first segment was set to 0, 5, 10 or 20 min at 160  $^{\circ}\text{C}$  to introduce different reaction times.

#### Determination of the minimum reaction temperatures for CA and GL

CA and GL were mixed in a 1/1 molar ratio and ground for homogenisation. A small amount of 10 - 15 mg was placed in a 40  $\mu\text{L}$  DSC crucible and subjected to the following DSC program (two heating/cooling cycles): 0 –  $T_{\text{react}}$  – 10 min ITS – 0 –  $T_{\text{react}}$  – 0  $^{\circ}\text{C}$  at 5  $^{\circ}\text{C min}^{-1}$ . The reaction temperature ( $T_{\text{react}}$ ) was set at 70, 90, 110, 130, 150 or 160  $^{\circ}\text{C}$ .

#### Determination of the eutectic melting temperature of CA and GL

CA and GL were mixed in the solid state in various ratios from 10 to 90 mol% GL in CA and ground for homogenisation. A small amount of 10-15 mg was placed in a 40  $\mu\text{L}$  DSC crucible and subjected to the following DSC program (two heating/cooling cycles): 0 – 160 – 0 – 160 – 0  $^{\circ}\text{C}$  at 5  $^{\circ}\text{C min}^{-1}$ . The melt onset temperature for each monomer mixture was determined from the first heating cycle.

#### Evaluation of catalysts

A stock mixture of CA/GL 1/1 was made. Catalysts were weighed out and an appropriate amount of the CA/GL stock mixture was added to obtain mixtures with 1, 2, 5 or 10 % w/w catalyst. These mixtures were ground for homogenisation. Mixtures were then used as described in the general polymerisation procedure.

## 6.5. References

- 1 M. Tsoskounoglou, G. Ayerides and E. Tritopoulou, *Energy Policy*, 2008, **36**, 3797–3806.
- 2 C. Vilela, A. F. Sousa, A. C. Fonseca, A. C. Serra, J. F. J. Coelho, C. S. R. Freire and A. J. D. Silvestre, *Polym. Chem.*, 2014, **5**, 3119–3141.
- 3 B. P. Mooney, *Biochem. J.*, 2009, **418**, 219–232.
- 4 H. Kobayashi and A. Fukuoka, *Green Chem.*, 2013, **15**, 1740–1763.
- 5 R. T. Mathers, *J. Polym. Sci. A Polym. Chem.*, 2012, **50**, 1–15.
- 6 K. Yao and C. Tang, *Macromolecules*, 2013, **46**, 1689–1712.
- 7 L. Karaffa and C. P. Kubicek, *Appl. Microbiol. Biotechnol.*, 2003, **61**, 189–196.
- 8 E. Alben and O. Erkmén, *Food Technol. Biotechnol.*, 2004, **42**, 19–22.
- 9 M. Roehr, *Food Technol. Biotechnol.*, 1998, **36**, 163–171.
- 10 Q. Chen, S. Liang and G. A. Thouas, *Prog. Polym. Sci.*, 2013, **38**, 584–671.
- 11 J. Yang, A. R. Webb and G. A. Ameer, *Adv. Mater.*, 2004, **16**, 511–516.
- 12 J. Yang, A. R. Webb, S. J. Pickerill, G. Hageman and G. A. Ameer, *Biomaterials*, 2006, **27**, 1889–1898.
- 13 Q. Liu, L. Jiang, R. Shi and L. Zhang, *Prog. Polym. Sci.*, 2012, **37**, 715–765.
- 14 R. Tran, Y. Zhang, D. Gyawali and J. Yang, *Recent Patents Biomed. Eng.*, 2009, **2**, 216–227.
- 15 K. M. Doll, R. L. Shogren, J. L. Willett and G. Swift, *J. Polym. Sci. A Polym. Chem.*, 2006, **44**, 4259–4267.
- 16 M. Adeli, B. Rasoulían, F. Saadatmehr and F. Zabihi, *J. Appl. Polym. Sci.*, 2013, **129**, 3665–3671.
- 17 S. Liu, M. Jian, S. Ye, X. Xu, P. Lu and J. Dong, *J. Appl. Polym. Sci.*, 2011, **124**, 3633–3640.
- 18 J. M. Halpern, R. Urbanski, A. K. Weinstock, D. F. Iwig, R. T. Mathers and H. A. Von Recum, *J. Biomed. Mater. Res. - Part A*, 2014, **102**, 1467–1477.
- 19 B. Tisserat, R. H. O’Kuru, H. Hwang, A. A. Mohamed and R. Holser, *J. Appl. Polym. Sci.*, 2012, **125**, 3429–3437.
- 20 I. Djordjevic, N. R. Choudhury, N. K. Dutta and S. Kumar, *Polymer*, 2009, **50**, 1682–1691.
- 21 I. Djordjevic, N. R. Choudhury, N. K. Dutta and S. Kumar, *Polym. Int.*, 2011, **60**, 333–343.

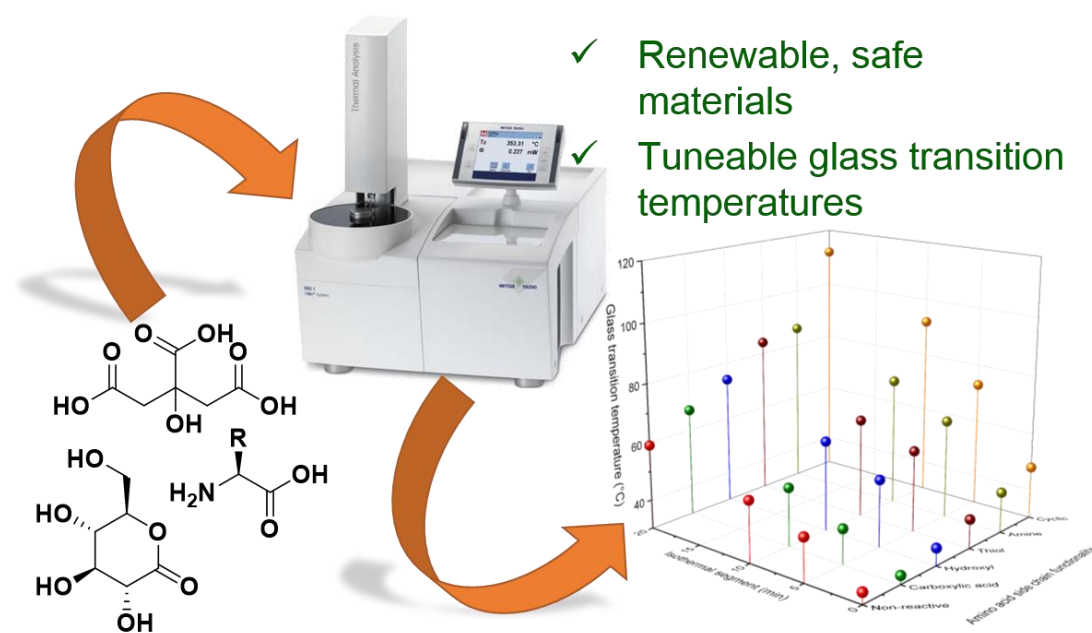
- 22 US Food and Drug Administration - Generally Recognized as Safe (GRAS), <https://www.fda.gov/Food/IngredientsPackagingLabeling/GRAS/default.htm> (Accessed May 2018).
- 23 D. Garlotta, *J. Polym. Environ.*, 2002, **9**, 63–84.
- 24 C. Hahn, S. Wesselbaum, H. Keul and M. Möller, *Eur. Polym. J.*, 2013, **49**, 217–227.
- 25 T. Kajiyama, H. Kobayashi, K. Morisaku, T. Taguchi, K. Kataoka and J. Tanaka, *Polym. Degrad. Stab.*, 2004, **84**, 151–157.
- 26 T. Kajiyama, T. Taguchi, H. Kobayashi, K. Kataoka and J. Tanaka, *Polym. Degrad. Stab.*, 2003, **81**, 525–530.
- 27 J. Telegdi, L. Trif, J. Mihály, E. Nagy and L. Nyikos, *J. Therm. Anal. Calorim.*, 2015, **121**, 663–673.
- 28 J. A. Galbis, M. de Gracia García-Martin, M. Violante de Paz and E. Galbis, *Chem. Rev.*, 2016, **116**, 1600–1636.
- 29 N. Tsutsumi, M. Oya and W. Sakai, *Macromolecules*, 2004, **37**, 5971–5976.
- 30 Y. H. Choi, J. van Spronsen, Y. Dai, M. Verberne, F. Hollmann, I. W. C. E. Arends, G.-J. Witkamp and R. Verpoorte, *Plant Physiol.*, 2011, **156**, 1701–1705.
- 31 S. Kobayashi, *Polym. Adv. Technol.*, 2015, **26**, 677–686.
- 32 X. Zhang, M. Fevre, G. O. Jones and R. M. Waymouth, *Chem. Rev.*, 2018, **118**, 839–885.
- 33 WO2011131450A2, 2011.
- 34 A. Takasu, T. Makino and S. Yamada, *Macromolecules*, 2010, **43**, 144–149.
- 35 US3173898A, 1961.

## Chapter 7

---

# High $T_g$ poly(ester amide)s by melt polycondensation of monomers from renewable resources: citric acid, D-glucono- $\delta$ -lactone and amino acids: A DSC study

---



This chapter has been published:

P.A.J.M. de Jongh, P.K.C. Paul, E. Khoshdel, P. Wilson, K. Kempe, D.M. Haddleton, *Eur. Polym. J.* **2017**, 94, 11-19

## 7.1. Introduction

Poly(ester amide)s (PEAs) have emerged as an interesting class of materials for a broad range of applications as they combine the degradability of polyesters<sup>1,2</sup> with the thermomechanical stability of polyamides<sup>3,4</sup> into one system and, as a result, they allow for a high level of functionality and fine-tuning of their properties. This has led to PEAs receiving an increasingly significant interest.<sup>5-9</sup> PEAs were first synthesised by Carothers and Hill in 1932 by the polycondensation of diacids, diols and diamines<sup>10</sup> and there are now a range of strategies available for their synthesis. Various methods including ring-opening of morpholine-2,5-diones,<sup>7-9</sup> acyclic diene metathesis (ADMET),<sup>11</sup> anionic random ring-opening copolymerisation of  $\epsilon$ -caprolactam with  $\epsilon$ -caprolactone,<sup>12,13</sup> ring-opening of cyclic anhydrides with diisopropanolamine,<sup>14</sup> ring-opening of bis(2-oxazolines) with dicarboxylic acids<sup>15</sup> and the spontaneous zwitterionic copolymerisation (SZWIP) of 2-oxazolines with acrylic acid<sup>16-18</sup> have been employed.

However, a more straightforward method, often applied in industrial applications, is the polycondensation between monomers bearing carboxylic acid, hydroxyl and amine groups as used in the original synthesis.<sup>10</sup> This polycondensation approach is often divided into three categories: (a) solution polymerisation, which takes place with all reagents dissolved in a single solvent or a mixture of miscible solvents, (b) interfacial polymerisation, a method based on Schotten-Baumann reaction conditions where two immiscible solvents are used and the reaction takes place at the interface of both solvents, and (c) melt polycondensation which takes place in the absence of any additional solvent and are therefore often considered to be a “green” approach.<sup>6,8</sup>

Amino acids (AAs) are a class of building blocks for PEAs that have received significant attention in literature.<sup>5-9,19</sup> Over 500 naturally occurring AAs are known,<sup>20</sup> of which 21 are proteinogenic  $\alpha$ -AAs and 20 are part of the genetic code. It is these naturally occurring proteinogenic  $\alpha$ -AAs that are most investigated for PEA synthesis as they are readily available and usually biocompatible. When considering the  $\alpha$ -AAs that have been used to produce PEAs via polycondensation, glycine,<sup>21-27</sup> alanine,<sup>22-25,28,29</sup> valine,<sup>23,30-32</sup> leucine,<sup>23,30,31,33</sup> isoleucine,<sup>30,31,33</sup> and phenylalanine<sup>23,28,30,31,33-40</sup> have been used extensively as their non-reactive side chains allow for their straightforward

incorporation into linear PEAs. AAs with reactive side chains have been employed in this context by protecting one of the reactive groups to yield linear PEAs with pendant reactive groups following deprotection. This strategy has been used for the polycondensation of serine,<sup>32</sup> tyrosine,<sup>41–44</sup> aspartic acid,<sup>28,35</sup> lysine,<sup>28,38–40,45</sup> and arginine.<sup>46,47</sup> Alternatively, unprotected AAs with reactive side chains have been employed for the synthesis of (hyper)branched PEAs. In this context, the trifunctional AAs aspartic acid,<sup>48,49</sup> glutamic acid<sup>48,50</sup> and lysine<sup>48</sup> have been used for the synthesis of PEA networks. Some other AAs that have received attention in the literature include  $\beta$ -alanine<sup>51–53</sup> and 4-hydroxyproline.<sup>54</sup>

Following on from studies reported by Tsutsumi *et al.*,<sup>55</sup> we investigated the melt polycondensation between citric acid (CA,  $T_{\text{melt}} = 153$  °C) and D-glucono- $\delta$ -lactone (GL,  $T_{\text{melt}} = 160$  °C) by differential scanning calorimetry (DSC), both derived from renewable resources and classified by the FDA as generally recognised as safe (GRAS).<sup>56</sup> It was found that polyesters were formed whose thermal properties could be tuned through a variation of reaction times, temperatures and copolymerising other polyacid/polyol monomers. From a sustainable and cost-effective chemistry point of view we were interested in short reaction times ( $\leq 20$  min) and relatively low reaction temperatures ( $\leq 160$  °C, just above the melting temperature of CA). Under these conditions the glass transition temperatures ( $T_g$ s) did not exceed 43 °C for a 20 min reaction of CA/GL 1/1.<sup>56</sup>

We were interested in forming small volumes of polymers, over very short timeframes, in confined spaces to give composite materials. The synthesis of polymers in DSC crucibles is not only a convenient way to combine synthesis and analysis into one step, but it also allows to demonstrate the benefits of polymerising in confined spaces with good thermal transfer through the material. There are numerous reports in literature that document the benefits of performing reactions in confined spaces, such as within polymersomes,<sup>57</sup> SiO<sub>2</sub> zeolite,<sup>58</sup> metal-organic frameworks (MOFs)<sup>59</sup> and polymerised high internal phase emulsion (polyHIPE) monoliths.<sup>60</sup> In addition to this, there are several publications where the polymerisation is studied by DSC, benefitting from its efficient heat transfer, including ring-opening polymerisation of cyclic esters<sup>61–63</sup> and free radical polymerisations of various monomers,<sup>64–66</sup> revealing insights into

polymerisations that cannot be obtained from conventional polymerisation methods mainly due to the insulation properties of the “plastic” product.

This Chapter reports an investigation on the effect of copolymerising various amino acids (AAs, Figure 7.1) with the GRAS monomers CA and GL on the thermal properties of the resulting PEAs with the aim of increasing the  $T_g$ s of the resulting polymers. The introduction of amines in the polycondensation, and thus the introduction of amide bonds in the resulting polymers, is generally known to increase the  $T_g$  of the resulting materials. Moreover, AAs are safe to use and most natural AAs are readily available, which further contributes to the “green” and cost effective approach adopted in this research. In line with our previous work we employed moderate reaction temperatures (160 °C) and short reaction times ( $\leq 20$  min). By polymerising in DSC crucibles (40  $\mu$ L) we demonstrate what can be achieved by polymerising small volumes in a confined space.

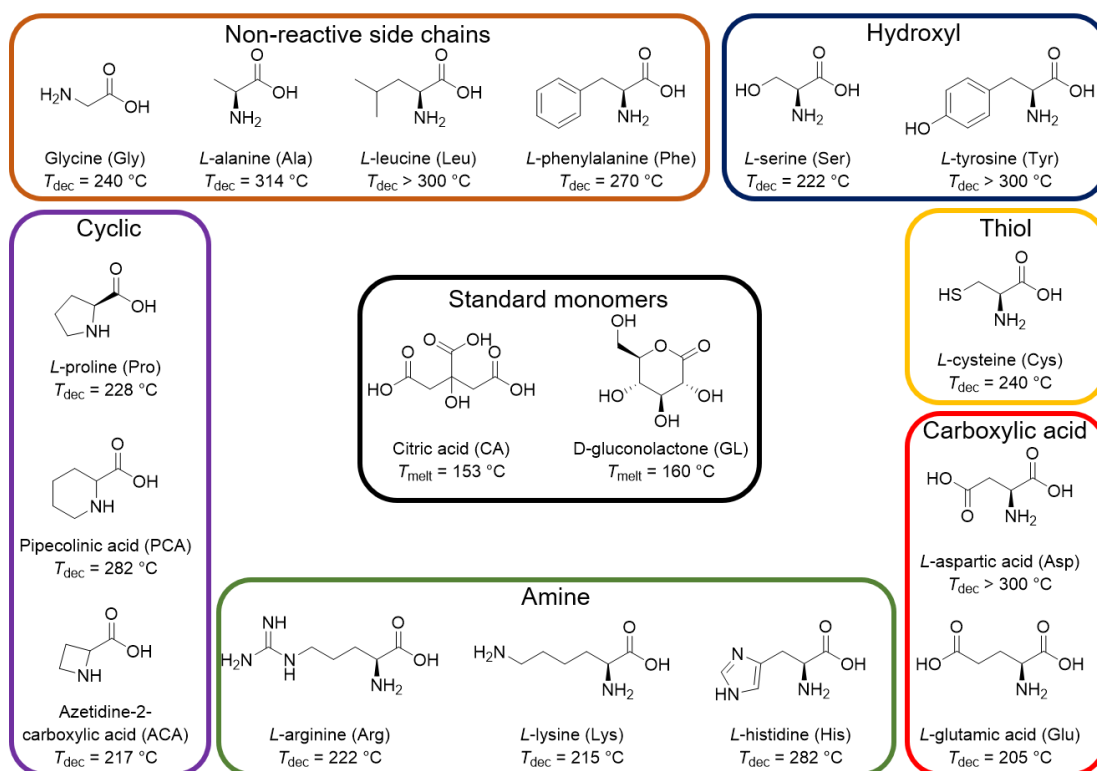


**Figure 7.1** Monomers studied and their melting ( $T_{melt}$ ) or decomposition ( $T_{dec}$ ) temperatures.

## 7.2. Results and discussion

The melt polycondensation between CA, GL and a range of AAs (Figure 7.) was studied by DSC. On the first heating cycle the melting temperature was determined and on the second cycle the glass transition temperature ( $T_g$ ) of the resulting PEAs evaluated. The reactions were carried out at 160 °C, just above the melting temperature of CA ( $T_{\text{melt}} = 153$  °C) with reaction times up to 20 min. Monomer conversions for these reactions cannot be determined by  $^1\text{H}$  NMR spectroscopy (overlapping signals) or SEC analysis (the hydrodynamic volumes of the polymers are near the lower exclusion limit and too low for triple detection SEC), but repeated heating cycles reveal increasing  $T_g$ s (data not shown), which suggests additional polymerisation took place. These low conversions at short reaction times are also expected when considering the modified Carothers equation for multifunctional monomers, shown in Equation 7.1.

$$p = \frac{2(N_0 - N_t)}{N_0 \cdot f_{av}} \quad (7.1)$$

In this equation, the conversion  $p$  is calculated from the initial number of monomers ( $N_0$ ), the number of molecules (monomers, oligomers and polymers) at a given time ( $N_t$ ) and the average functionality per monomer unit ( $f_{av}$ ), which is calculated with Equation 7.2, in which  $N_i$  is the number of molecules of type  $i$  and  $f_i$  is the functionality of monomer  $i$ .

$$f_{av} = \frac{\sum N_i \cdot f_i}{\sum N_i} \quad (7.2)$$

At short reactions times, such as the ones employed in this research,  $N_t$  will remain high and consequently the conversion  $p$  remains low, making unreacted monomers the dominant species as typically observed for polycondensation reactions. The average molecular weight then follows from Equation 7.3, demonstrating that the molecular weights remain low at these conversions.<sup>67</sup>

$$X_n = \frac{2}{2 - p \cdot f_{av}} \quad (7.3)$$

Furthermore, polycondensations involving multifunctional monomers allow for the formation of gels at a critical conversion. Using Flory's gel theory, it is possible to calculate the critical branching degree ( $\alpha_c$ ) based on the functionality of the monomers ( $f$ ) using Equation 7.4. With the hydroxyl group on CA effectively unreactive, CA contains three carboxylic acid groups and GL has four hydroxyl groups, so  $f$  equals 0.5 for CA and 0.33 for GL. The conversion at gel point can then be calculated using Equations 7.5 and 7.6 for CA and GL, respectively, in which  $P_i$  is the conversion of monomer  $i$ ,  $\alpha_{c,i}$  is the critical branching degree of this monomer and  $r$  is the ratio between the functionalities of the two monomers ( $r = f_i / f_j$ ). For the copolymerisation of CA and GL the gel point lies at 82 % conversion for CA and 50 % for GL, which further limits obtaining full conversion as gel formation will occur beforehand. As a result of the different reactivities of amines (from the AAs) compared to hydroxyl groups in the terpolymerisations studied in this work, Flory's model can no longer be applied to the polycondensations between CA, GL and AAs.<sup>68</sup> Gel formation remains possible, however, at the lower conversions obtained in this study gel formation was not observed.

$$\alpha_c = \frac{1}{f - 1} \quad (7.4)$$

$$P_{CA} = \sqrt{\frac{\alpha_{c,CA}}{r_{CA/GL}}} = \sqrt{\frac{0.5}{3/4}} = 0.82 \quad (7.5)$$

$$P_{GL} = \sqrt{\frac{\alpha_{c,GL}}{r_{GL/CA}}} = \sqrt{\frac{1/3}{4/3}} = 0.50 \quad (7.6)$$

The observed  $T_g$ s for all systems are reproducible within typical error for polycondensation reactions and reactions are easily scaled up, although it should be noted that the  $T_g$ s observed are dependent on the heating efficiency during the reaction.

---

All formulations were mixed in the solid state in ratios approximating equimolar amounts of functional groups (carboxylic acids vs. hydroxyl and amine groups), with the tertiary hydroxyl group of CA considered unreactive under the reaction conditions employed in this study. The AAs were chosen so as to cover the many different possible side chains, *i.e.* non-reactive, hydroxyl, thiol, carboxylic acid and amine side chains. In addition to the other AAs with non-reactive side chains, proline with its unique cyclic structure was evaluated for the synthesis of PEAs, as well as two structural analogues of proline. The molar ratios of the monomers (shown in the Figures below) are chosen appropriately to approach a stoichiometric balance between the functional groups.

### 7.2.1. Hydrophobic, non-reactive side chains

CA and GL were first copolymerised with four different AAs containing hydrophobic, non-reactive side chains: glycine (Gly), alanine (Ala), leucine (Leu) and phenylalanine (Phe). Their non-reactive side chains render these AAs bifunctional and therefore introduce short linear segments into the PEAs. The AAs were mixed in an equimolar ratio with CA and GL and melt polymerised at 160 °C. The first heating cycle revealed that including AAs into the CA/GL polycondensation does not have an effect on the melting and therefore reaction temperature (data not shown). It can be observed on the second heating cycle that all AAs result in an increased  $T_g$  compared to the CA/GL 1/1 system without AAs (Figure 7.2),<sup>56</sup> which can be attributed to the introduction of amide bonds into the resulting PEAs. The  $T_g$ s of all systems could be further modified by increasing the polymerisation time (0 – 20 min isothermal segment). There are, however, no significant differences between the different hydrophobic AAs as their side chain (proton, methyl, isopropyl or benzyl) does not participate in the reaction. Ala and Phe result in slightly higher  $T_g$ s than Gly and Leu, but the differences are too marginal to relate those to the structure of their side chain. The highest  $T_g$  obtained within a 20 min reaction is 64 °C for Ala. Surprisingly there is no significant effect of the benzyl side group of Phe, suggesting that the typical contributions of such groups on the  $T_g$  only become significant at higher conversions.

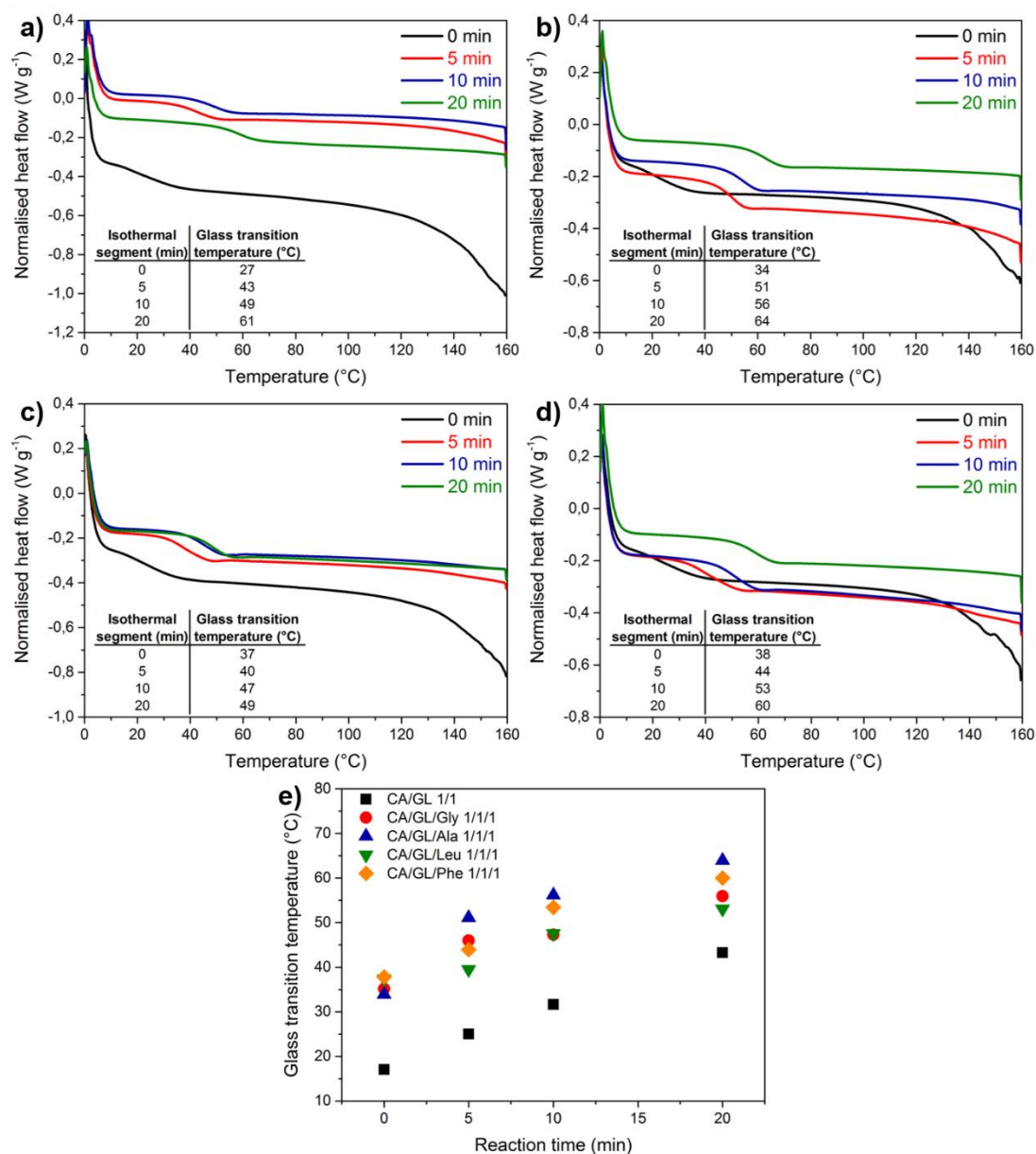


**Figure 7.2** Polycondensation of CA and GL with amino acids containing hydrophobic, non-reactive side chains. a) Glycine. b) L-alanine. c) L-leucine. d) L-phenylalanine. e) Comparison of the different amino acid co-monomers. The reaction times refer to the ITS.

### 7.2.2. Hydroxyl and thiol side chains

Two AAs with hydroxyl groups in their side chain were subsequently evaluated. Serine (Ser) contains an aliphatic primary alcohol group, whereas tyrosine (Tyr) has a phenolic side chain. The second heating cycle reveals very comparable  $T_g$ s for Ser and

Tyr, despite the distinctly different hydroxyl groups (Figure 7.3a,b). When compared to AAs containing hydrophobic, non-reactive side chains (*vide supra*), it was seen that the  $T_g$ s for the shortest reaction time (0 min Iso) are comparable at around 37 °C, but a significant increase is observed for longer reaction times with  $T_g$ s of 76 and 73 °C at 20 min reactions for Tyr and Ser, respectively. This can be attributed to the hydroxyl side chains being able to participate in the reaction by forming additional ester bonds and thereby increasing the crosslinking density, resulting in higher  $T_g$ s. Incorporation of Tyr and Ser leads to similar  $T_g$ s with those for Tyr marginally higher than Ser at every time point. The longer side chain of Tyr compared to Ser might be expected to result in lower  $T_g$ s, however, the presence of aromatic groups in the polymer backbone generally increase the  $T_g$ s of polymers and in this particular case the Tyr aromatic group effectively cancels this.

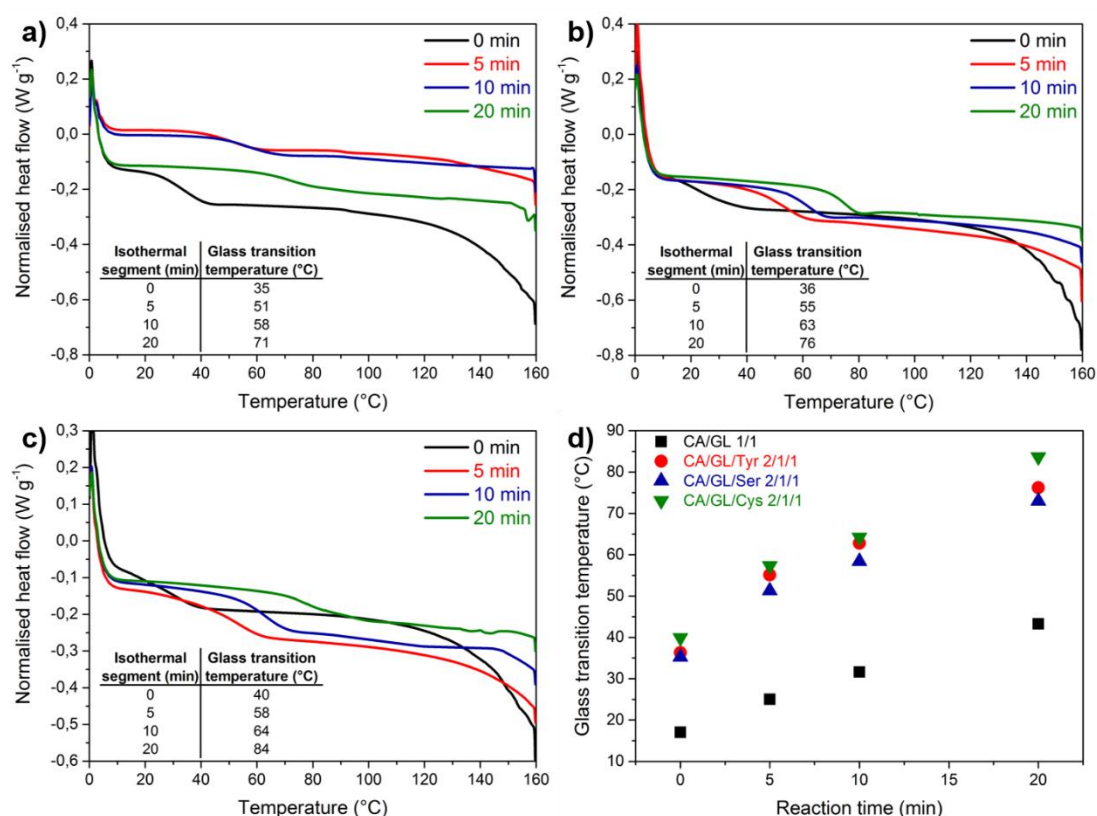


**Figure 7.3** Polycondensation of CA and GL with amino acids containing hydroxyl or thiol side chains. a) L-serine. b) L-tyrosine. c) L-cysteine. d) Comparison of the different amino acid co-monomers. The reaction times refer to the ITS.

Cysteine (Cys) is structurally similar to Ser, but contains a thiol group instead of the hydroxyl group. When copolymerised with CA/GL, the observed  $T_g$ s on the second heating cycle are slightly higher than for Ser, which is believed to be a result of the slightly more nucleophilic nature of thiols compared to hydroxyl groups (Figure 7.3c). A comparison of the different hydroxyl and thiol AAs is shown in Figure 7.3d.

### 7.2.3. Carboxylic acid side chains

There are two proteinogenic  $\alpha$ -AAs with a carboxylic acid group in their side chain: aspartic acid (Asp) and glutamic acid (Glu). Upon copolymerisation with CA and GL in equimolar ratios, the second heating cycle revealed distinctively different  $T_g$ s for the two AAs (Figure 7.4), with Asp-containing PEAs having significantly higher  $T_g$ s.

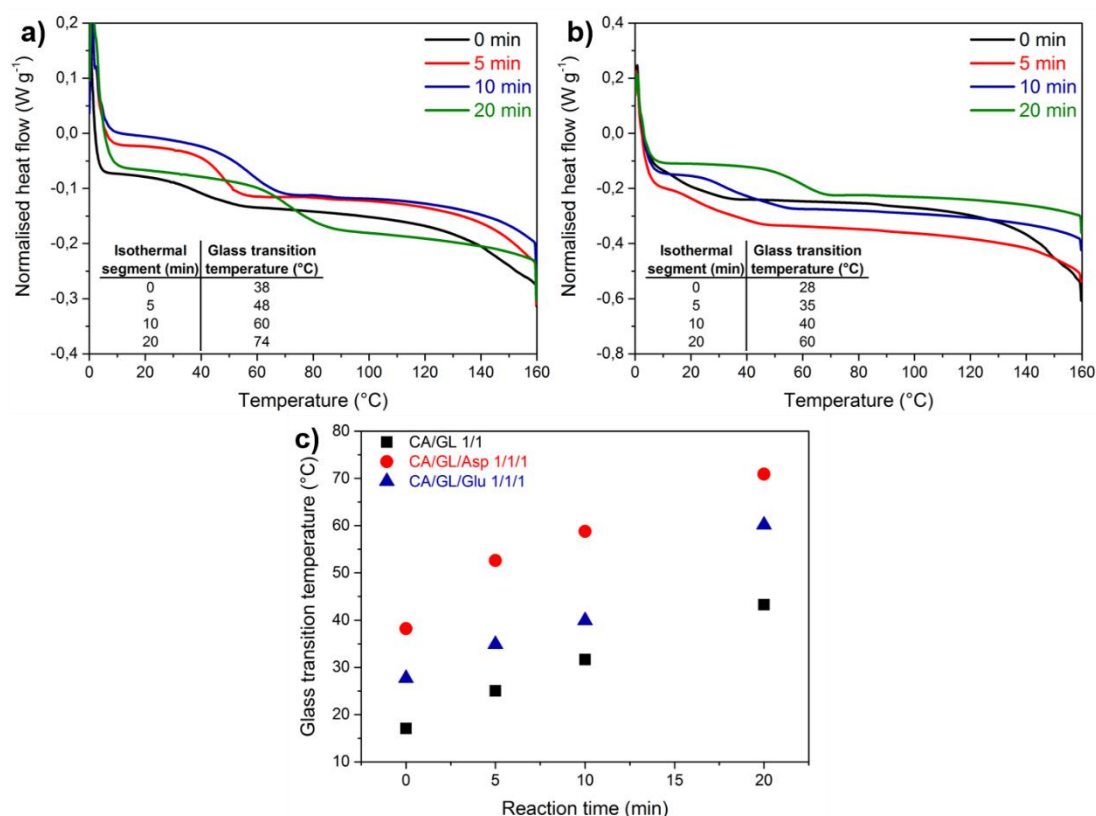


**Figure 7.4** Polycondensation of CA and GL with amino acids containing carboxylic acid side chains. a) L-aspartic acid. b) L-glutamic acid. c) Comparison of the different amino acid comonomers. The reaction times refer to the ITS.

The only structural difference between Asp and Glu is the additional methylene group in the Glu side chain. Thus, the side chain length of AAs with carboxylic acid side chains directly influences the  $T_g$  through the crosslinking densities of the resulting materials. The observed  $T_g$ s for Asp are comparable to those observed for Ser and Tyr, whereas the  $T_g$ s for Glu are actually slightly lower than for the AAs without reactive side chains. This observation suggests that having multifunctional monomers can yield lower  $T_g$ s if their crosslinking densities are too low, compared to short linear segments as introduced by the AAs without reactive side chains (*vide supra*).

#### 7.2.4. Amine and guanidine side chains

Lysine (Lys) is the only natural AA with a primary amine in its side chain whilst arginine (Arg) bears a guanidine group in its side chain, which can also act as a nucleophile *via* the guanidinium nitrogen. PEAs with Lys and Arg show comparable  $T_g$ s for all different reaction times, with  $T_g$ s as high as 91 and 82 °C for Arg and Lys, respectively, following a 20 min reaction (Figure 7.5a,b). This is a significant increase from Tyr and Ser with hydroxyl side chains, and Cys with its thiol side chain, which can be attributed to the higher reactivity of amines (Arg and Lys) compared to hydroxyl and thiol groups (Tyr, Ser and Cys). The guanidine amine from Arg is most likely slightly more reactive than the primary amine from Lys, which would explain why Arg results in slightly higher  $T_g$ s than Lys, despite a longer chain length and therefore lower crosslinking density.

Histidine (His) has an imidazole in its side chain, which consists of a secondary and a tertiary amine. When copolymerised with CA and GL in a 2/1/1 ratio (CA/GL/His; data not shown) lower  $T_g$ s were observed than for copolymerising in equimolar ratio, indicating that the imidazole secondary amine is not (significantly) participating in the polycondensation. This does, however, mean that the copolymerisation of His introduces (predominantly) linear segments and, consequently, the  $T_g$ s observed for His are lower than those observed for Lys and Arg (Figure 7.5c,d). The (negligible) reactivity of the of the imidazole's secondary amine is thought to be the result of its aromatic nature, as non-aromatic secondary amines are able to participate in the polycondensation (*vide infra*).

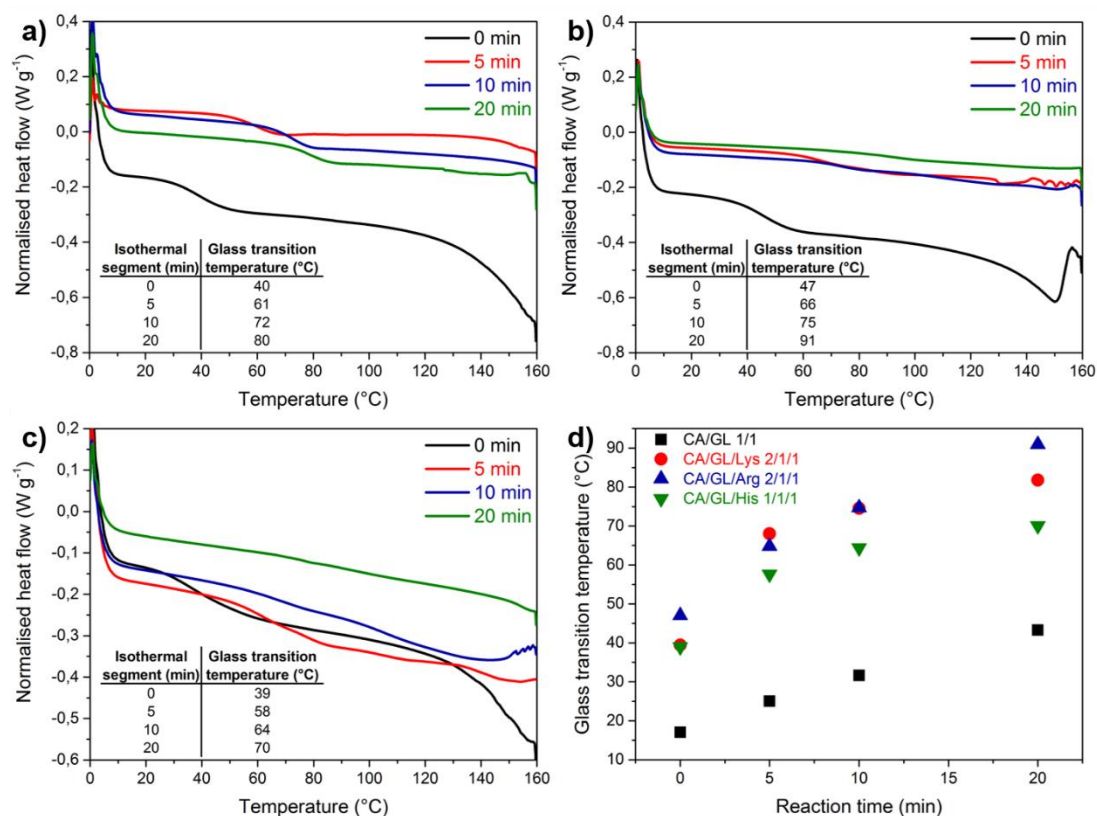


**Figure 7.5** Polycondensation of CA and GL with amino acids containing amine side chains. a) L-lysine. b) L-arginine. c) L-histidine. d) Comparison of the different amino acid co-monomers. The reaction times refer to the ITS.

### 7.2.5. Cyclic amino acids

The cyclic structure of proline (Pro) makes it unique compared to any other natural AA. Similar to the AAs with hydrophobic side chains discussed above, it is only bi-functional, but in the case of Pro the amine is secondary instead of primary, which changes its reactivity. In order to investigate the effect of this, Pro was copolymerised in an equimolar ratio with CA and GL. Compared to all other AAs, copolymerising Pro causes a significant increase in the  $T_g$ s of the resulting PEAs (Figure 7.6a). Unlike the AAs with hydroxyl, thiol, carboxylic acid or amine side chains, Pro does not have a reactive side chain that can participate in the reaction and increase the crosslinking density, however, the  $T_g$ s are up to twice as high as for the AAs with non-reactive, hydrophobic side chains. It was therefore hypothesised that this increased  $T_g$  results

from the cyclic structure which limits the rotational freedom within Pro, an effect that was previously also observed when comparing different sugar polyols to GL.<sup>56</sup>

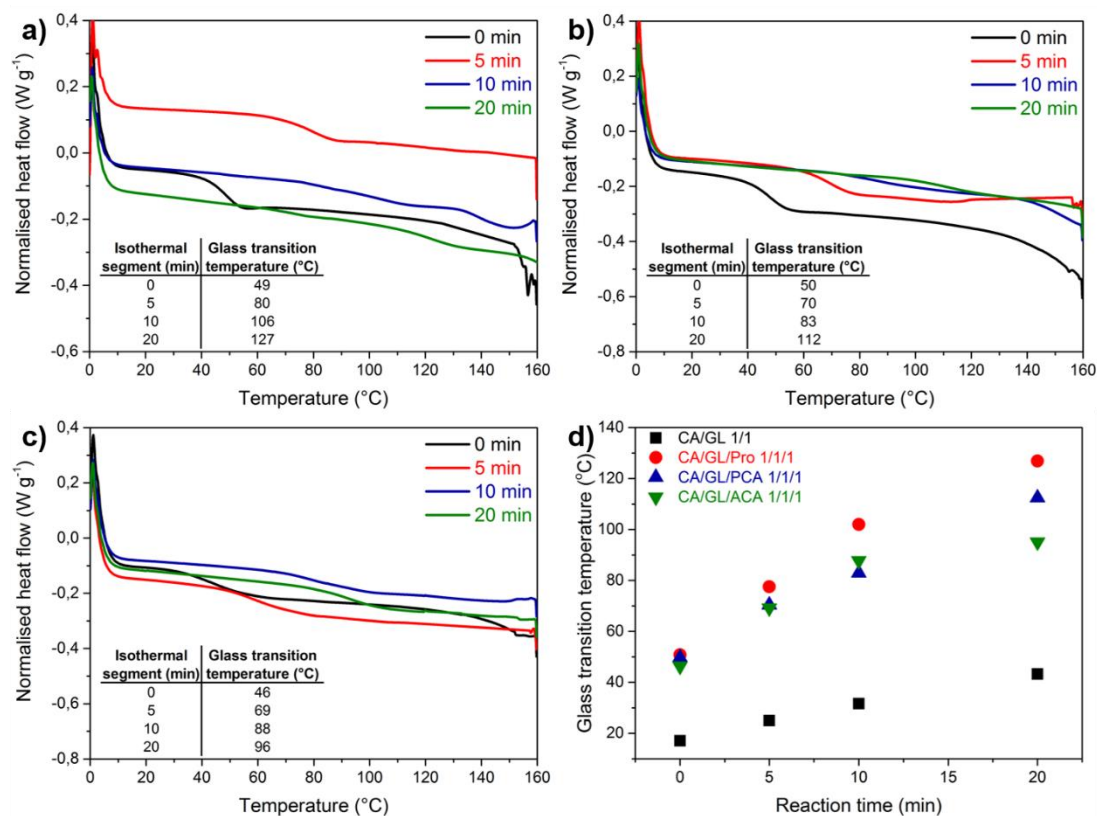


**Figure 7.6** Polycondensation of CA and GL with cyclic amino acids. a) L-proline. b) Pipecolinic acid. c) Azetidine-2-carboxylic acid. d) Comparison of the different amino acid comonomers. The reaction times refer to the ITS.

To further investigate this, CA and GL were copolymerised in equimolar ratios with pipecolinic acid (PCA) and azetidine-2-carboxylic acid (ACA), which are the six- and four-membered ring analogues of Pro, respectively. Similar to Pro, both PCA and ACA have higher  $T_g$ s than all other AAs tested in this work, although not as high as Pro itself (Figure 7.b,c). It is reasoned that the  $T_g$ s for PCA are slightly lower because of the more flexible six-membered ring compared to the five-membered ring of Pro, whereas in the case for ACA the more strained, four-membered ring reduces the reactivity of the secondary amine compared to Pro. Nevertheless, copolymerising PCA and

ACA clearly demonstrates that it is the ring structure in Pro that is responsible for the significant increase in  $T_g$ s compared to the other AAs (Figure 7.d).

### 7.3. Conclusions

This work systematically studied the synthesis of poly(ester amide)s (PEAs) by melt polycondensation of citric acid (CA), gluconolactone (GL) and various amino acids (AAs) by DSC, employing short reaction times ( $\leq 20$  min) and moderate reaction temperatures (160 °C). The copolymerisation of AAs with CA and GL leads to increased glass transition temperatures ( $T_g$ s) compared to CA/GL only and that the relative increase can be correlated to the monomer structure of the AA employed. AAs with non-reactive side chains resulted in the lowest  $T_g$ s, whereas AAs with hydroxyl, thiol, carboxylic acid and amine groups in their side chain yielded higher  $T_g$  materials as a result of an increased crosslinking density. Most interestingly, the cyclic structure of proline (and two analogues) provided the highest  $T_g$ s which is attributed to the reduced flexibility of the cyclic AA monomers. Overall, this study provides new insights into the copolymerisation of AAs into PEAs and their contribution to the thermal properties from monomers derived from sustainable feedstocks.

### 7.4. Experimental

#### 7.4.1. Materials

Citric acid (CA, 99.5 %), D-glucono- $\delta$ -lactone (GL, 99 %), glycine (Gly, 99 %), L-alanine (Ala, 99 %), L-leucine (Leu, 99 %), L-phenylalanine (Phe, 99 %), L-proline (Pro, 99.5 %), L-lysine (Lys, 97 %), L-aspartic acid (Asp, 98 %), L-cysteine (Cys, 98.5 %), L-histidine (His, 99.5 %) and pipercolinic acid (PCA, 98 %) were purchased from Sigma-Aldrich and used as received. L-glutamic acid (Glu, 98 %) and (S)-(-)-azetidine-2-carboxylic acid (ACA, 99 %) were obtained from Acros Organics and used as received. L-serine (Ser, 98 %) was obtained from IRIS Biotech and used as received.

L-tyrosine (Tyr, 99 %) and L-arginine (Arg, 99 %) were purchased from Avocado Research Chemicals and used as received.

### 7.4.2. Differential scanning calorimetry (DSC)

Polymerisations and thermal analysis by DSC were performed on a Mettler Toledo DSC1 differential scanning calorimeter in 40  $\mu$ L aluminium crucibles. Data was processed using Mettler Toledo STARe software. The melting and reaction behaviour was determined from the first heating segment, the thermal properties of the formed PEAs were evaluated on the second heating cycle.

### 7.4.3. Polymerisation procedure

Monomers were mixed in the solid state and ground for homogenisation, in molar ratios as stated in the main text (approximating 1/1 ratios between the functional groups). A small amount of 10 – 15 mg was placed in a 40  $\mu$ L DSC crucible and subjected to the following DSC program (two heating/cooling cycles): 0 – 160 – ITS – 0 – 160 – 0  $^{\circ}$ C at 10  $^{\circ}$ C  $\text{min}^{-1}$ . The isothermal segment (ITS) on the first segment was set to 0, 5, 10 or 20 min at 160  $^{\circ}$ C to introduce different reaction times. All reactions were performed under nitrogen atmosphere.

## 7.5. References

- 1 W. Amass, A. Amass and B. Tighe, *Polym. Int.*, 1998, **47**, 89–144.
- 2 J. Rydz, W. Sikorska, M. Kyulavska and D. Christova, *Int. J. Mol. Sci.*, 2015, **16**, 564–596.
- 3 K. Marchildon, *Macromol. React. Eng.*, 2011, **5**, 22–54.
- 4 M. Winnacker and B. Rieger, *Macromol. Rapid Commun.*, 2016, **37**, 1391–1413.
- 5 L. S. Nair and C. T. Laurencin, *Prog. Polym. Sci.*, 2007, **32**, 762–798.
- 6 A. C. Fonseca, M. H. Gil and P. N. Simões, *Prog. Polym. Sci.*, 2014, **39**, 1291–1311.
- 7 M. Winnacker and B. Rieger, *Polym. Chem.*, 2016, **7**, 7039–7046.

- 8 A. Rodriguez-Galan, L. Franco and J. Puiggali, *Polymers*, 2011, **3**, 65–99.
- 9 M. Okada, *Prog. Polym. Sci.*, 2002, **27**, 87–133.
- 10 W. H. Carothers and J. W. Hill, *J. Am. Chem. Soc.*, 1932, **54**, 1566–1569.
- 11 F. N. Führer and H. Schlaad, *Macromol. Chem. Phys.*, 2014, **215**, 2268–2273.
- 12 D. C. Christova, R. S. Velichkova and I. M. Panayotov, *Macromol. Chem. Phys.*, 1995, **196**, 3605–3613.
- 13 M. Gupta, F. Siegmund, E. Haberstroh, M. Rosenthal, D. A. Ivanov, M. W. M. Fijten, X. Zhu and M. Martin, *Macromol. Mater. Eng.*, 2014, **299**, 1343–1351.
- 14 R. A. T. M. van Benthem, *Prog. Org. Coatings*, 2000, **40**, 203–214.
- 15 B. M. Culbertson, *Prog. Polym. Sci.*, 2002, **27**, 579–626.
- 16 K. Kempe, P. A. J. M. de Jongh, A. Anastasaki, P. Wilson and D. M. Haddleton, *Chem. Commun.*, 2015, **51**, 16213–16216.
- 17 P. A. J. M. de Jongh, A. Mortiboy, G. S. Sulley, M. R. Bennett, A. Anastasaki, P. Wilson, D. M. Haddleton and K. Kempe, *ACS Macro Lett.*, 2016, **5**, 321–325.
- 18 P. A. J. M. de Jongh, M. R. Bennett, G. S. Sulley, P. Wilson, T. P. Davis, D. M. Haddleton and K. Kempe, *Polym. Chem.*, 2016, **7**, 6703–6707.
- 19 W. Khan, S. Muthupandian, S. Farah, N. Kumar and A. J. Domb, *Macromol. Biosci.*, 2011, **11**, 1625–1636.
- 20 I. Wagner and H. Musso, *Angew. Chem. Int. Ed.*, 1983, **22**, 816–828.
- 21 A. C. Fonseca, A. C. Serra, J. F. J. Coelho, M. H. Gil and P. N. Simões, *Polym. Int.*, 2013, **62**, 736–743.
- 22 L. Wang, Y. Wang, D. Cao, L. Wang, Y. Wang and D. Cao, *J. Macromol. Sci. Chem.*, 2009, **46**, 312–320.
- 23 Y. Fan, M. Kobayashi and H. Kise, *J. Polym. Sci. A Polym. Chem.*, 2001, **39**, 1318–1328.
- 24 J. Montané, E. Armelin, L. Asín, A. Rodriguez-Galan and J. Puiggali, *J. Appl. Polym. Sci.*, 2002, **85**, 1815–1824.
- 25 E. Armelin, N. Paracuellos, A. Rodriguez-Galan and J. Puiggali, *Polymer*, 2001, **42**, 7923–7932.
- 26 L. Asín, E. Armelin, J. Montané, A. Rodriguez-Galan and J. Puiggali, *J. Polym. Sci. A Polym. Chem.*, 2001, **39**, 4283–4293.
- 27 N. Paredes, A. Rodriguez-Galan and J. Puiggali, *J. Polym. Sci. A Polym. Chem.*, 1998, **36**, 1271–1282.
- 28 K. M. Atkins, D. Lopez, D. K. Knight, K. Mequanint and E. R. Gillies, *J.*

- Polym. Sci. A Polym. Chem.*, 2009, **47**, 3757–3772.
- 29 N. Paredes, A. Rodriguez-Galan, J. Puiggali and C. Peraire, *J. Appl. Polym. Sci.*, 1998, **69**, 1537–1549.
- 30 R. Katsarava, V. Beridze, N. Arabuli, D. Kharadze, C. C. Chu and C. Y. Won, *J. Polym. Sci. A Polym. Chem.*, 1999, **37**, 391–407.
- 31 S. Mallakpour and F. Zeraatpisheh, *Colloid Polym. Sci.*, 2011, **289**, 1055–1064.
- 32 M. Deng, J. Wu, C. A. Reinhart-king and C. Chu, *Acta Biomater.*, 2011, **7**, 1504–1515.
- 33 Z. Gomurashvili, H. R. Kricheldorf and R. Katsarava, *J. Macromol. Sci. Chem.*, 2000, **37**, 215–227.
- 34 X. Pang and C. Chu, *Biomaterials*, 2010, **31**, 3745–3754.
- 35 D. K. Knight, E. R. Gillies and K. Mequanint, *Acta Biomater.*, 2014, **10**, 3484–3496.
- 36 K. Guo and C. C. Chu, *J. Biomed. Res. B Appl. Biomater.*, 2009, **89B**, 491–500.
- 37 K. Guo and C. C. Chu, *Biomacromolecules*, 2007, **8**, 2851–2861.
- 38 M. A. de Wit, Z. Wang, K. M. Atkins, K. Mequanint and E. R. Gillies, *J. Polym. Sci. A Polym. Chem.*, 2008, **46**, 6376–6392.
- 39 M. Deng, J. Wu, C. A. Reinhart-king and C. Chu, *Biomacromolecules*, 2009, **10**, 3037–3047.
- 40 J. A. Horwitz, K. M. Shum, J. C. Bodle, M. Deng, C. Chu and C. A. Reinhart-king, *J. Biomed. Res. A*, 2010, **95A**, 371–380.
- 41 B. Kim, C. Lee and M. Gong, *Macromol. Res.*, 2003, **11**, 328–333.
- 42 A. Abdolmaleki, S. Mallakpour and R. N. Esmaeli, *Polym. - Plast. Technol. Eng.*, 2016, **55**, 911–919.
- 43 A. Abdolmaleki, S. Mallakpour and S. Borandeh, *Polym. Bull.*, 2012, **69**, 15–28.
- 44 A. Abdolmaleki and S. Mallakpour, *Amino Acids*, 2012, **42**, 1997–2007.
- 45 M. Vera, L. Franco and J. Puiggali, *J. Polym. Sci. A Polym. Chem.*, 2008, **46**, 661–667.
- 46 X. Pang, J. U. N. Wu, C. Reinhart-king and C. Chu, *J. Polym. Sci. A Polym. Chem.*, 2010, **48**, 3758–3766.
- 47 H. Song and C. C. Chu, *J. Appl. Polym. Sci.*, 2012, **124**, 3840–3853.
- 48 Y. Bao, J. He and Y. Li, *Polymer*, 2012, **53**, 145–152.
-

- 49 R. L. Shogren, K. M. Doll, J. L. Willett and G. Swift, *J. Polym. Environ.*, 2009, **17**, 103–108.
- 50 D. Lu, Z. Ren, T. Zhou, S. Wang and Z. Lei, *J. Appl. Polym. Sci.*, 2008, **107**, 3638–3643.
- 51 A. A. Mohammed, S. Salhi, S. Abid, R. El Gharbi and A. Fradet, *Eur. Polym. J.*, 2014, **53**, 160–170.
- 52 M. Abbas, S. Salhi, L. Lefevre, C. Delaite and S. Abid, *J. Macromol. Sci. Chem.*, 2015, **52**, 56–63.
- 53 N. Paredes, M. T. Casas and J. Puiggali, *Macromolecules*, 2000, **33**, 9090–9097.
- 54 R. Lee and J. Yang, *J. Appl. Polym. Sci.*, 2002, **86**, 1612–1621.
- 55 N. Tsutsumi, M. Oya and W. Sakai, *Macromolecules*, 2004, **37**, 5971–5976.
- 56 P. A. J. M. de Jongh, P. K. C. Paul, E. Khoshdel, P. Wilson, K. Kempe and D. M. Haddleton, *Polym. Int.*, 2017, **66**, 59–63.
- 57 A. Küchler, M. Yoshimoto, S. Luginbühl, F. Mavelli and P. Walde, *Nat. Nanotechnol.*, 2016, **11**, 409–420.
- 58 D. Scelta, M. Ceppatelli, M. Santoro, R. Bini, F. A. Gorelli, A. Perucchi, M. Mezouar, A. Van Der Lee and J. Haines, *Chem. Mater.*, 2014, **26**, 2249–2255.
- 59 T. Wang, M. Farajollahi, S. Henke, T. Zhu, S. R. Bajpe, S. Sun, J. S. Barnard, J. S. Lee, J. D. W. Madden, A. K. Cheetham and S. K. Smoukov, *Mater. Horiz.*, 2017, **4**, 64–71.
- 60 M. Chen, F. Sun, W. Xu, L. Zhou and F. Zhang, *J. Mater. Sci.*, 2016, **51**, 5113–5121.
- 61 N. G. Sedush, Y. Y. Strelkov and S. N. Chvalun, *Polym. Sci. Ser. B*, 2014, **56**, 35–40.
- 62 N. G. Sedush and S. N. Chvalun, *Eur. Polym. J.*, 2015, **62**, 198–203.
- 63 R. Mazarro, A. De Lucas, I. Gracia and J. F. Rodríguez, *Macromol. Chem. Phys.*, 2008, **209**, 818–824.
- 64 G. Ye, Y. Cui, X. Liu and H. Zhou, *J. Therm. Anal. Calorim.*, 2013, **112**, 1499–1506.
- 65 M. T. Viciosa, J. Quiles Hoyo, M. Dionísio and J. L. Gómez Ribelles, *J. Therm. Anal. Calorim.*, 2007, **90**, 407–414.
- 66 D. S. Achilias, *J. Therm. Anal. Calorim.*, 2014, **116**, 1379–1386.
- 67 W. H. Carothers, *Trans. Faraday Soc.*, 1936, **32**, 39–49.
- 68 J. Flory, *J. Am. Chem. Soc.*, 1941, **63**, 3083–3090.

## Chapter 8

---

### Conclusions and outlook

---



## 8.1. The potential of polyester-based materials

Polyester-based materials have received significant attention from the scientific community for a plethora of applications. One major reason for this is their degradability, which is interesting for applications ranging from food packaging to drug delivery. Another important aspect is that a wide range of monomers that can be used for polyester synthesis can be directly found in Nature or synthesised from renewable precursors. The combination of polyesters and polyamides into poly(ester amide)s (PEA)s and poly(aminoester)s (PAEs) opens up many opportunities to modify the properties of the materials. This thesis investigated the synthesis and properties of novel polyester-based materials by spontaneous zwitterionic copolymerisation (SZWIP) and polycondensation. This Chapter summarises the main conclusions and provides a main outlook for the work in this thesis.

## 8.2. *N*-acylated poly(aminoester)s by SZWIP

The majority of the work in this thesis revolved around *N*-acylated poly(aminoester) (NPAE) macromonomers synthesised by SZWIP of cyclic imino ethers (CIEs) and acrylic acid (AA) and their corresponding comb polymers. Initially, the SZWIP between these monomers was studied to identify the effect of several experimental parameters. Different solvents and reaction temperatures had negligible effect on the resulting macromonomers and in all cases oligomers with typical DPs of 3-4 were obtained. However, through alteration of the monomer feed ratios it was possible to modify the  $\omega$ -end groups from 50 % carboxylic acid and 50 % amide to (near-)quantitative introduction of carboxylic acid groups. Interestingly, elemental analysis and MALDI-ToF analysis suggested the presence of homopropagation of the CIEs as a side reaction to the SZWIP mechanism. An in-depth mass spectrometry was subsequently conducted to further investigate the presence of various structures that could not be identified by NMR analysis. Tandem mass spectrometry investigations revealed the presence of several microstructures. Apart from the expected alternating structures, homopropagation of the CIEs was shown to be a competing reaction. Semi-quantitative analysis allowed to establish an extended mechanism for the SZWIP of CIEs and

AA in which cationic ring-opening polymerisation of the CIE was added as the main competing event. Furthermore, these studies demonstrated the effect of the different CIEs and monomer feed ratios on the extent of homopropagation and  $\omega$ -end groups. Interestingly, the use of a six-membered CIE almost completely prevented homopropagation and thus furnished macromonomers with almost defect-free alternating structures. Similar in-depth studies for other monomer pairs suitable for SZWIP would be interesting to gain a better understanding of this polymerisation technique as a whole.

The quantitative introduction of  $\alpha$ -acrylate end groups on these NPAE oligomers was then explored to synthesise well-defined comb polymers by aqueous redox-initiated RAFT polymerisation. Comb polymers derived from 2-ethyl-2-oxazoline (EtOx) and 2-ethyl-2-oxazine (EtOz) showed a pH-dependant LCST behaviour. Their cloud points could be tuned through the use of different monomers, DPs of the comb polymers, medium pH and salts. It was demonstrated that these comb polymers can be used as scaffolds for post-polymerisation functionalisation using three model amines. The potential of these comb polymers for biological applications was investigated next. Although degradable in forced conditions, the comb polymers showed a remarkable stability in biologically relevant conditions. No significant cytotoxicity or haemolysis was observed. Flow cytometry revealed that the relative interaction of the comb polymers with cells appeared to be dictated by hydrophobicity. Surprisingly, cell uptake experiments showed that the comb polymers localise within the mitochondria. Finally, in the context of potential applications, the anti-fouling behaviour on gold surfaces was studied and revealed significant reductions in fouling against model enzymes.

The investigations into the synthesis of the comb polymers and their properties are one of the first examples into the applications of SZWIP-derived polymers and only form the foundation for a plethora of possibilities. Mahmoud *et al.* have explored the synthesis of more hydrophobic NPAEs and corresponding amphiphilic block copolymers and studied their self-assembly into micelles in aqueous solution.<sup>1</sup> Their non-cytotoxic nature could make them interesting alternatives for common biocompatible polymers in drug delivery applications, in particular the non-biodegradable poly(ethylene glycol) and poly(2-oxazoline)s, where the dual-responsiveness in aqueous solution could

be exploited for targeted drug delivery. Another interesting study would be on the synthesis of higher molecular weight linear NPAEs to replace the polyacrylate backbone currently present in the comb polymers and create a fully degradable polymer. Finally, the degradation profile of these materials should be investigated further.

### **8.3. Branched polyesters from renewable materials**

The latter part of this thesis investigated the synthesis of branched polyesters and PEAs by melt polycondensations involving the renewable monomers citric acid (CA) and gluconolactone (GL). Differential scanning calorimetry (DSC) was employed as a highly efficient tool to combine the synthesis and thermal analysis of these materials into one step. The polycondensation of CA and GL could be easily tuned to furnish polyesters with tuneable glass transition temperatures ( $T_g$ s) by simple variation of the reaction conditions such as reaction temperature and time. The copolymerisation with other polyacid and polyol co-monomers further extended this toolbox and revealed that the use of multifunctional, ring-structured monomers resulted in higher  $T_g$ s. Furthermore, there are safe catalysts that are able to catalyse these polycondensations to yield higher  $T_g$  materials. This synthesis of polyesters was then extended to PEAs by copolymerising CA and GL with amino acids. The introduction of amide bonds significantly increased the  $T_g$ s of the resulting materials, in particular when side-chain functional amino acids are employed. The use of cyclic amino acids, proline and derivatives thereof, significantly enhances the  $T_g$ . This is in line with the previous observation that cyclic monomers provide a major contribution to the thermal properties of the resulting polyesters and PEAs.

These systematic studies provide clear insights in structure-thermal property relationships between the monomers employed for the synthesis of these branched polyesters/PEAs and their  $T_g$ s. The use of DSC demonstrated the potential of monitoring reactions by thermal behaviour and polymerisations on small scale (10 – 15 mg). Scaling up these syntheses has not been investigated but should demonstrate the same trends as observed on the small scale. However, on large scale the heating transfer

during the reaction will be less efficient and therefore reaction times and/or temperatures will need to be adjusted to obtain the same thermal properties.

## 8.4. Overall outlook

There is significant potential for polyester-based materials for a wide range of applications as mentioned above. The high tuneability of these materials in terms of structures, architectures and their resulting properties makes them very versatile materials. The synthesis of diverse classes of polyesters, PEAs and PAEs has been demonstrated in this thesis to provide interesting materials for different applications, with many more possibilities available for the future. It is for these reasons that continued research on polyester-based materials is an important subject for the scientific community.

## 8.5. References

- 1 A. M. Mahmoud, A. Rajakanthan and K. Kempe, *Polym. Chem.*, 2018, **9**, 1562–1566.

## About the author

Patrick obtained his Bachelor of Applied Science (BSc.) degree in Chemistry from the Avans University of Applied Sciences (Breda, The Netherlands, 2007-2011). During this time, he carried out industrial placements at DSM and Mercachem. He then moved to the Radboud University Nijmegen (The Netherlands) to start his premaster and Master of Science (MSc.) in Chemistry degree, during which he carried out two placements. The first was under supervision of Prof. Jan van Hest and the second at Monash University (Australia) under supervision of Prof. Sébastien Perrier and Dr. Michael Whittaker. After graduating with a MSc. in Chemistry in 2014 (*cum laude*), he moved to the University of Warwick (UK) to start his PhD research under supervision of Prof. David Haddleton and Dr. Kristian Kempe, investigating the synthesis and properties of novel polyester-based materials. During his PhD, he completed the Postgraduate Award Teaching and Learning in Higher Education and spent three months as a visiting researcher at Monash University, working with Dr. Angus Johnston. As of July 2018, he is working as a post-doctoral researcher in the group of Prof. Charlotte Williams at the University of Oxford (UK).

---

## List of publications

Spontaneous zwitterionic copolymerisation: an undervalued and efficacious technique for the synthesis of functional degradable oligomers and polymers

P.A.J.M. de Jongh, D.M. Haddleton, K. Kempe, *Prog. Polym. Sci.* **2018**, DOI: 10.1016/j.progpolymsci.2018.08.002

Unraveling the Spontaneous Zwitterionic Copolymerisation Mechanism of Cyclic Imino Ethers and Acrylic Acid

J. Steinkoenig, P.A.J.M. de Jongh, D.M. Haddleton, A.S. Goldmann, C. Barner-Kowollik, K. Kempe, *Macromolecules* **2018**, 51, 318-327

Thiol-reactive (co)polymer scaffolds comprised of organic arsenical acrylamides

C. Footman, P.A.J.M. de Jongh, J. Tanaka, R. Peltier, K. Kempe, T.P. Davis, P. Wilson, *Chem. Commun.* **2017**, 53, 8447-8450

High T<sub>g</sub> poly(ester amide)s by melt polycondensation of monomers from renewable resources; citric acid, D-glucono- $\delta$ -lactone and amino acids: A DSC study

P.A.J.M. de Jongh, P.K.C. Paul, E. Khoshdel, P. Wilson, K. Kempe, D.M. Haddleton, *Eur. Polym. J.* **2017**, 91, 11-19

Thermal study on polyester networks based on the renewable monomers citric acid and gluconolactone

P.A.J.M. de Jongh, P.K.C. Paul, E. Khoshdel, P. Wilson, K. Kempe, D.M. Haddleton, *Polym. Int.* **2017**, 66, 59-63

Facile one-pot/one-step synthesis of heterotelechelic N-acylated poly(aminoester) macromonomers for carboxylic acid decorated comb polymers

P.A.J.M. de Jongh, M.R. Bennett, G.S. Sulley, P. Wilson, T.P. Davis, D.M. Haddleton, K. Kempe, *Polym. Chem.* **2016**, 7, 6703-6707

Dual Stimuli-Responsive Comb Polymers from Modular *N*-Acylated Poly(aminoester)-Based Macromonomers

P.A.J.M. de Jongh, A. Mortiboy, G.S. Sulley, M.R. Bennett, A. Anastasaki, P. Wilson, D.M. Haddleton, K. Kempe, *ACS Macro Lett.* **2016**, 5, 321-326

Novel comb polymers from alternating *N*-acylated poly(aminoester)s obtained by spontaneous zwitterionic copolymerisation

K. Kempe, P.A.J.M. de Jongh, A. Anastasaki, P. Wilson, D.M. Haddleton, K. Kempe, *Chem. Commun.* **2015**, 51, 16213-16216

## Appendix

---

### Supplementary information for Chapter 3

---

The data in this appendix has been published:

J. Steinkoenig, P.A.J.M. de Jongh, D.M. Haddleton, A.S. Goldmann, C.Barner-Kowollik, K. Kempe, *Macromolecules* **2018**, 51, 318-327

**Table A.1** Quantitative calculations for MeOx:AA 1:1 based on the calibration curve (Figure 3.10) referred to the overview spectrum (Figure 3.1a). Calculated using Equation 3.1.

Repeat unit H <sup>+</sup>			Repeat unit Na <sup>+</sup>		
<i>m/z</i> <sup>exp</sup>	Intensity [a.u.]	$\chi$	<i>m/z</i> <sup>exp</sup>	Intensity [a.u.]	$\chi$
230.1019	2.20E+07	0.18 ± 0.03	252.0836	8.03E+07	0.14 ± 0.02
315.1543	2.08E+08	0.39 ± 0.06	337.1365	4.72E+08	0.29 ± 0.04
387.1756	6.39E+07	0.25 ± 0.04	409.1575	1.49E+08	0.17 ± 0.03
472.2285	2.99E+08	0.43 ± 0.06	494.2094	5.02E+08	0.32 ± 0.05
544.2496	9.95E+07	0.32 ± 0.05	566.2314	1.31E+08	0.24 ± 0.04
629.3008	1.88E+08	0.49 ± 0.07	651.2829	3.02E+08	0.36 ± 0.05
701.3233	5.02E+07	0.43 ± 0.06	723.3045	7.44E+06	0.05 ± 0.01
786.3755	7.18E+07	0.55 ± 0.08	808.3581	1.01E+08	0.39 ± 0.06
858.3955	1.90E+07	0.55 ± 0.08	880.3782	2.57E+07	0.44 ± 0.07
943.4495	2.43E+07	0.61 ± 0.09	965.4294	3.09E+07	0.43 ± 0.06

**Table A.2** Quantitative calculations for MeOx:AA 1:2 based on the calibration curve (Figure 3.10) referred to the overview spectrum (Figure 3.1b). Calculated using Equation 3.1.

Repeat unit H <sup>+</sup>			Repeat unit Na <sup>+</sup>		
<i>m/z</i> <sup>exp</sup>	Intensity [a.u.]	$\chi$	<i>m/z</i> <sup>exp</sup>	Intensity [a.u.]	$\chi$
230.1019	9.50E+07	0.77 ± 0.12	252.0835	4.34E+08	0.76 ± 0.11
315.1543	1.96E+08	0.37 ± 0.06	337.1365	4.02E+08	0.25 ± 0.04
387.1747	1.74E+08	0.67 ± 0.10	409.1575	6.33E+08	0.73 ± 0.11
472.2282	2.10E+08	0.30 ± 0.05	494.2095	4.56E+08	0.29 ± 0.04
544.2492	1.84E+08	0.60 ± 0.09	566.2300	3.36E+08	0.62 ± 0.09
629.3022	9.79E+07	0.25 ± 0.04	651.2831	1.80E+08	0.21 ± 0.03
701.3223	5.33E+07	0.46 ± 0.07	723.3049	1.03E+08	0.68 ± 0.10
786.3748	2.36E+07	0.18 ± 0.03	808.3559	3.80E+07	0.15 ± 0.02
858.3947	1.10E+07	0.32 ± 0.05	880.3789	1.66E+07	0.29 ± 0.04
943.4485	4.99E+06	0.12 ± 0.02	965.4338	5.64E+06	0.08 ± 0.01

**Table A.3** Quantitative calculations for MeOx:AA 2:1 based on the calibration curve (Figure 3.10) referred to the overview spectrum (Figure 3.1c). Calculated using Equation 3.1.

Repeat unit H <sup>+</sup>			Repeat unit Na <sup>+</sup>		
<i>m/z</i> <sup>exp</sup>	Intensity [a.u.]	$\chi$	<i>m/z</i> <sup>exp</sup>	Intensity [a.u.]	$\chi$
230.1019	5.81E+06	0.05 ± 0.01	252.0835	5.84E+07	0.10 ± 0.02
315.1543	1.27E+08	0.24 ± 0.04	337.1363	7.50E+08	0.46 ± 0.07
387.1753	2.08E+07	0.08 ± 0.01	409.1573	8.08E+07	0.09 ± 0.01
472.2274	1.82E+08	0.26 ± 0.03	494.2104	6.32E+08	0.40 ± 0.06
544.2482	2.42E+07	0.08 ± 0.01	566.2310	7.44E+07	0.14 ± 0.02
629.3011	1.00E+08	0.26 ± 0.04	651.2823	3.56E+08	0.42 ± 0.06
701.3215	1.29E+07	0.11 ± 0.02	723.3039	4.06E+07	0.27 ± 0.04
786.3760	3.50E+07	0.27 ± 0.04	808.3573	1.18E+08	0.46 ± 0.07
858.3961	4.80E+06	0.14 ± 0.02	880.3773	1.56E+07	0.27 ± 0.04
943.4503	1.08E+07	0.27 ± 0.04	965.4319	3.49E+07	0.49 ± 0.07

**Table A.4** Quantitative calculations for MeOx:AA 1:1 based on the calibration curve (Figure 3.10) referred to the overview spectrum (Figure 3.2a). Calculated using Equation 3.1.

<b>Repeat unit</b>			
<b>Label</b>	$m/z^{\text{exp}}$	<b>Intensity [a.u.]</b>	$\chi$
	230.1019	2.20E+07	0.18 ± 0.03
●	315.1543	2.08E+08	0.39 ± 0.05
△	324.1047	6.22E+06	0.12 ± 0.02
▼	328.1862	5.64E+07	0.29 ± 0.04
●	387.1756	6.39E+07	0.25 ± 0.04
▼	400.2073	1.84E+08	0.45 ± 0.07
●	472.2285	2.99E+08	0.43 ± 0.06
△	481.1780	1.32E+07	0.10 ± 0.02
▼	485.2593	5.55E+07	0.42 ± 0.06
●	544.2496	9.95E+07	0.32 ± 0.05
▼	557.2800	1.54E+08	0.49 ± 0.07
●	629.3008	1.88E+08	0.49 ± 0.07
△	638.2519	9.66E+06	0.21 ± 0.03
▼	642.3334	4.56E+07	0.50 ± 0.08
●	701.3233	5.02E+07	0.43 ± 0.06
▼	714.3548	8.28E+07	0.54 ± 0.08
●	786.3755	7.18E+07	0.55 ± 0.08
△	795.3271	7.11E+06	0.17 ± 0.03
▼	799.4059	2.50E+07	0.59 ± 0.09
●	858.3955	1.90E+07	0.55 ± 0.08
▼	871.4288	3.46E+07	0.59 ± 0.09

**Table A.5** Quantitative calculations for MeOx:AA 1:2 based on the calibration curve (Figure 3.10) referred to the overview spectrum (Figure 3.2b). Calculated using Equation 3.1.

<b>Repeat unit</b>			
<b>Label</b>	$m/z^{\text{exp}}$	<b>Intensity [a.u.]</b>	$\chi$
	230.1019	9.31E+07	0.77 ± 0.12
●	315.1543	1.27E+08	0.24 ± 0.04
△	324.1047	4.23E+07	0.82 ± 0.12
▼	328.1861	3.86E+07	0.20 ± 0.03
●	387.1753	1.74E+08	0.67 ± 0.03
▼	400.2064	1.21E+08	0.30 ± 0.05
●	472.2285	2.10E+08	0.30 ± 0.05
△	481.1780	1.13E+08	0.87 ± 0.13
▼	485.2593	3.25E+07	0.25 ± 0.04
●	544.2496	1.84E+08	0.60 ± 0.09
▼	557.2800	7.65E+07	0.24 ± 0.04
●	629.3008	9.79E+07	0.25 ± 0.04
△	638.2519	3.11E+07	0.69 ± 0.10
▼	642.3334	1.60E+07	0.17 ± 0.03
●	701.3233	5.33E+07	0.46 ± 0.07
▼	714.3548	2.59E+07	0.17 ± 0.03
●	786.3755	2.36E+07	0.18 ± 0.03
△	795.3271	3.28E+07	0.77 ± 0.12
▼	799.4059	2.67E+06	0.06 ± 0.01
●	858.3955	1.10E+07	0.32 ± 0.05
▼	871.4288	6.46E+06	0.11 ± 0.02

**Table A.6** Quantitative calculations for MeOx:AA 2:1 based on the calibration curve (Figure 3.10) referred to the overview spectrum (Figure 3.2c). Calculated using Equation 3.1.

<b>Repeat unit</b>			
<b>Label</b>	$m/z^{\text{exp}}$	<b>Intensity [a.u.]</b>	$\chi$
	230.1019	5.81E+06	0.05 ± 0.01
●	315.1543	1.96E+08	0.37 ± 0.06
△	324.1045	2.94E+06	0.06 ± 0.01
▼	328.1860	9.99E+07	0.51 ± 0.08
●	387.1747	2.08E+07	0.08 ± 0.01
▼	400.2071	1.00E+08	0.25 ± 0.04
●	472.2285	1.82E+08	0.26 ± 0.04
△	481.1780	4.40E+06	0.03 ± 0.01
▼	485.2593	4.36E+07	0.33 ± 0.05
●	544.2496	2.42E+07	0.08 ± 0.01
▼	557.2800	8.59E+07	0.27 ± 0.04
●	629.3008	1.00E+08	0.26 ± 0.04
△	638.2519	4.39E+06	0.10 ± 0.02
▼	642.3334	3.03E+07	0.33 ± 0.05
●	701.3233	1.29E+07	0.11 ± 0.02
▼	714.3548	4.48E+07	0.29 ± 0.04
●	786.3755	3.50E+07	0.27 ± 0.04
△	795.3271	2.48E+06	0.06 ± 0.01
▼	799.4059	1.46E+07	0.34 ± 0.05
●	858.3955	4.80E+06	0.14 ± 0.02
▼	871.4288	1.76E+07	0.30 ± 0.05

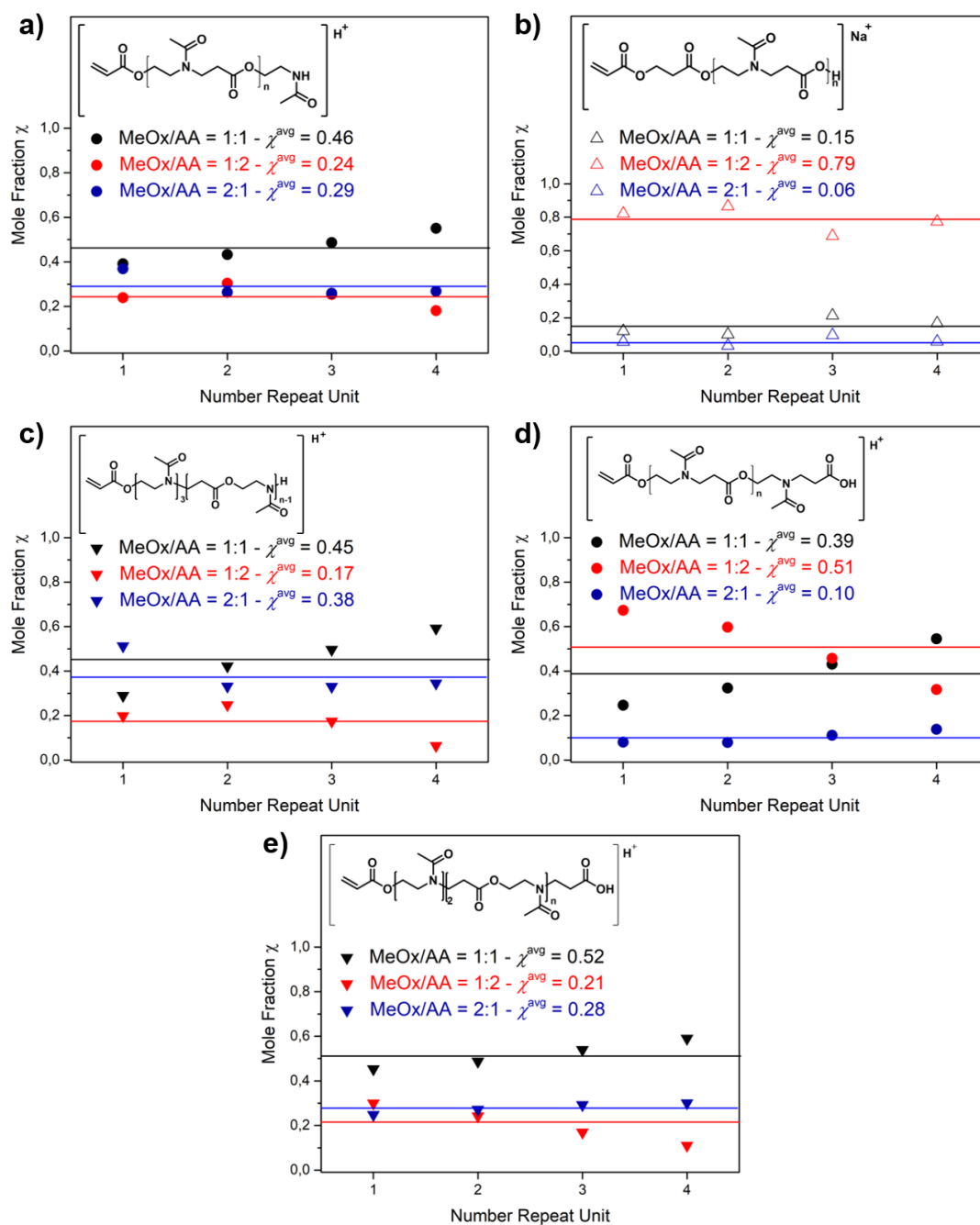


**Figure A.1** Mole fractions of the various microstructures of MeOx/AA oligomers. a)  $\text{H}^+$  ionised  $\bullet$  species. b)  $\text{Na}^+$  ionised  $\triangle$  species. c)  $\text{H}^+$  ionised  $\blacktriangledown$  species. d)  $\text{H}^+$  ionised  $\bullet$  species. e)  $\text{H}^+$  ionised  $\blacktriangledown$  species.

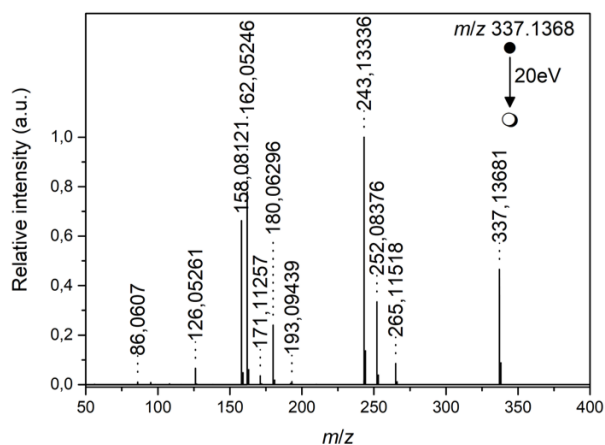
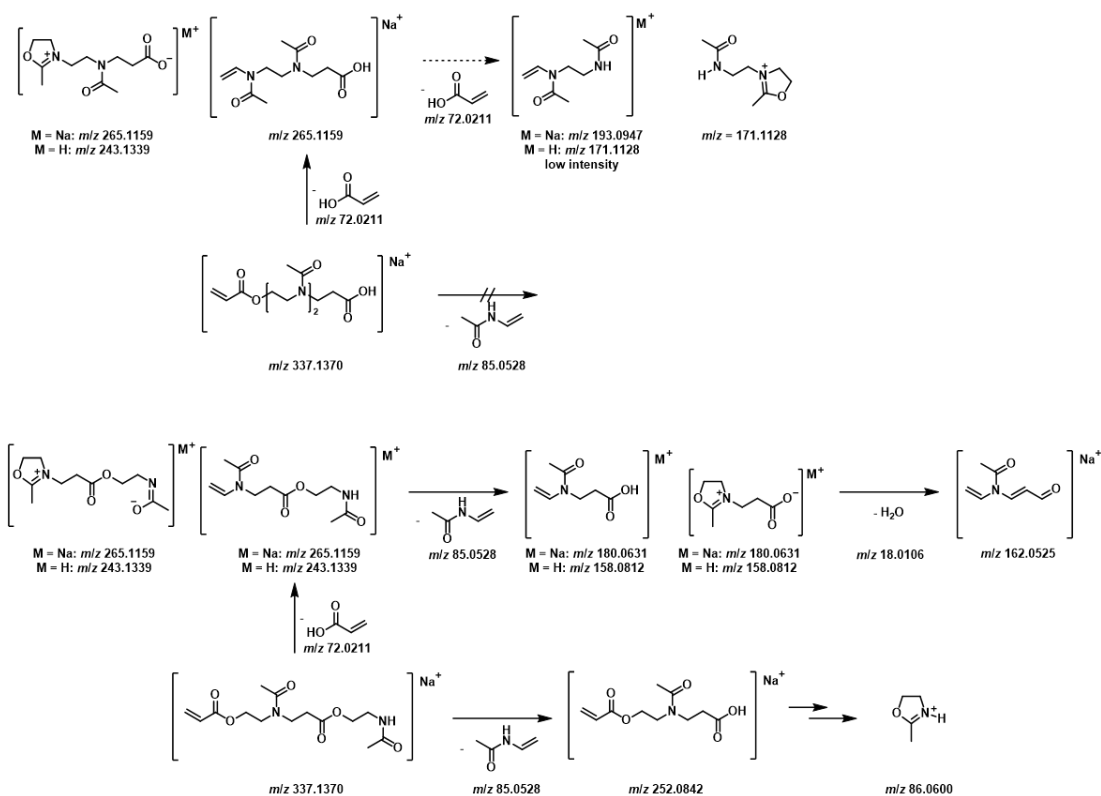


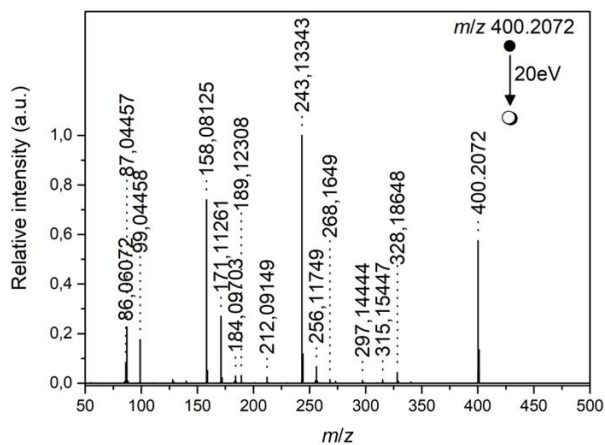
**Figure A.2** ESI MS/MS (positive mode) of MeOx/AA (1/1) isolating a species at  $m/z^{\text{exp}} = 337.1368$  with an HCD of 20 eV.

**Table A.7** Peak assignment of ESI MS/MS experiment of a MeOx/AA species at  $m/z^{\text{exp}} = 337.1368$  (Figure A.2).

$m/z^{\text{exp}}$	$m/z^{\text{theo}}$	$\Delta m/z$	Error [ppm]
337.1368	337.1370	0.0002	0.59
265.1152	265.1159	0.0007	2.64
252.0837	252.0842	0.0005	1.98
243.1333	243.1337	0.0006	1.65
193.0944	193.0947	0.0003	1.55
180.0630	180.0631	0.0001	0.56
171.1126	171.1128	0.0002	1.17
162.0525	162.0525	0.0000	0.00
158.0812	158.0812	0.0000	0.00
126.0526	126.0525	0.0001	0.79
86.0607	86.0600	0.0007	8.13



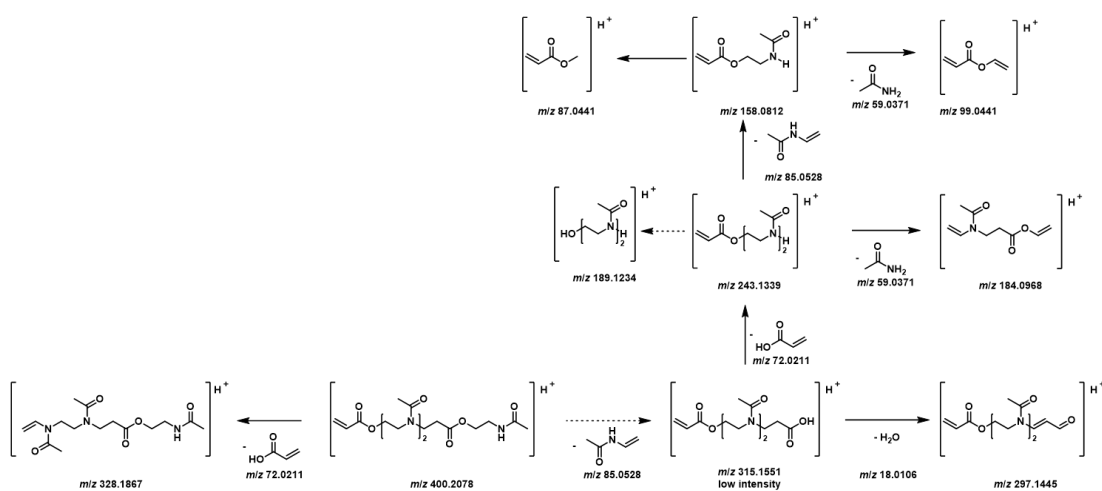
**Scheme A.1** Fragmentation scheme for MeOx/AA precursor at  $m/z^{\text{exp}} = 337.1368$ .

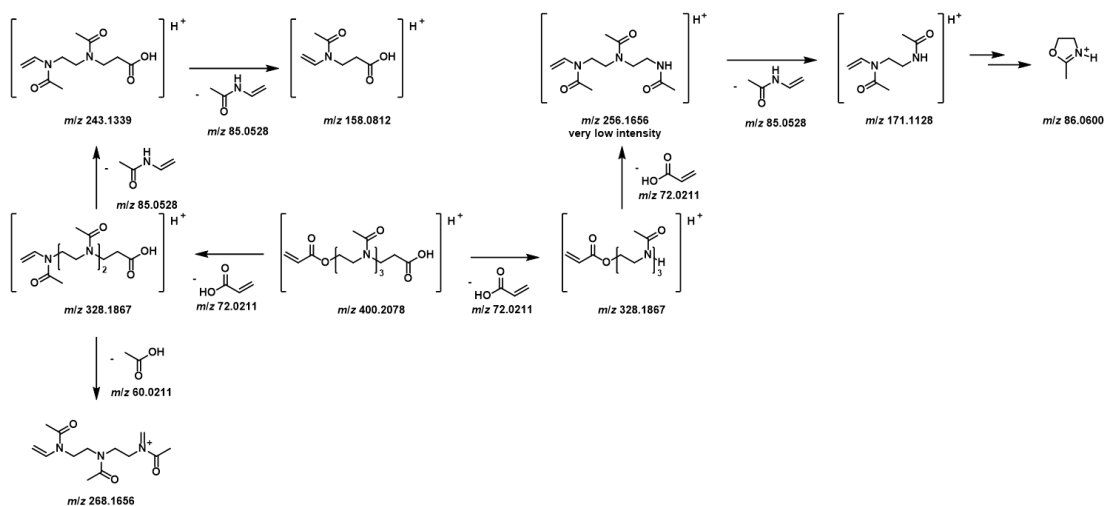


**Figure A.3** ESI MS/MS (positive mode) of MeOx/AA (1/1) isolating a species at  $m/z^{\text{exp}} = 400.2072$  with an HCD of 20 eV.

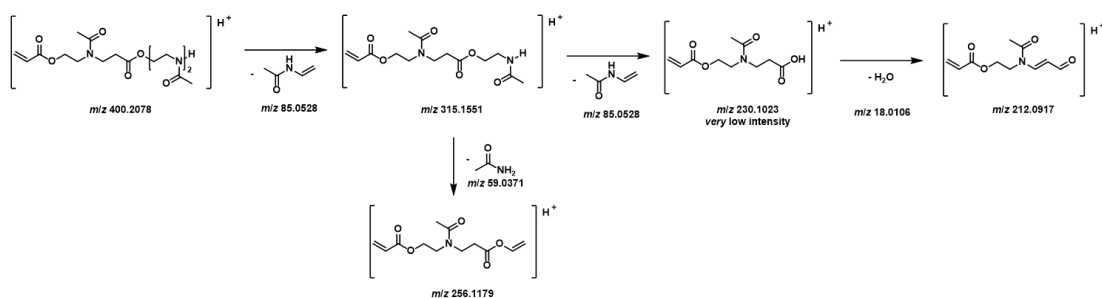
**Table A.8** Peak assignment of ESI MS/MS experiment of a MeOx/AA species at  $m/z^{\text{exp}} = 400.2072$  (Figure A.3).

$m/z^{\text{exp}}$	$m/z^{\text{theo}}$	$\Delta m/z$	Error [ppm]
400.2072	400.2078	0.0006	1.50
328.1865	328.1867	0.0002	0.61
315.1545	315.1551	0.0006	1.90
297.1444	297.1445	0.0001	0.34
268.1649	268.1656	0.0007	2.61
256.1653	256.1656	0.0003	1.17
256.1175	256.1179	0.0004	1.56
243.1334	243.1339	0.0005	2.06
212.0915	212.0917	0.0002	0.94
189.1231	189.1234	0.0003	1.59
184.0970	184.0968	0.0002	1.09
171.1126	171.1128	0.0002	1.17
158.0813	158.0812	0.0001	0.63
99.0446	99.0441	0.0005	5.05
87.0446	87.0441	0.0005	5.74
86.0607	86.0600	0.0007	8.13

**Scheme A.2** Fragmentation scheme for MeOx/AA precursor at  $m/z^{\text{exp}} = 400.2072$  based on an ABA oligomer (A=MeOx, B=AA).



**Scheme A.3** Fragmentation scheme for MeOx/AA precursor at  $m/z^{\text{exp}} = 400.2072$  based on an AAAB oligomer (A=MeOx, B=AA).



**Scheme A.4** Fragmentation scheme for MeOx/AA precursor at  $m/z^{\text{exp}} = 400.2072$  based on an ABAA oligomer (A=MeOx, B=AA).

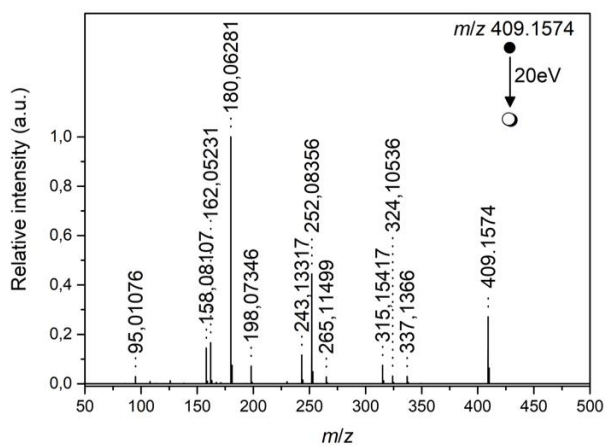


**Figure A.4** ESI MS/MS (positive mode) of MeOx/AA (1/1) isolating a species at  $m/z^{\text{exp}} = 409.1574$  with an HCD of 20 eV.

**Table A.9** Peak assignment of ESI MS/MS experiment of a MeO<sub>x</sub>/AA species at  $m/z^{\text{exp}} = 409.1574$  (Figure A.4).

$m/z^{\text{exp}}$	$m/z^{\text{theo}}$	$\Delta m/z$	Error [ppm]
409.1574	409.1581	0.0007	1.71
337.1366	337.1370	0.0004	1.19
324.1054	324.1053	0.0001	0.31
315.1542	315.1551	0.0009	2.86
265.1150	265.1159	0.0009	3.39
252.0836	252.0842	0.0006	2.38
243.1332	243.1339	0.0007	2.88
198.0735	198.0737	0.0002	1.01
180.0628	180.0631	0.0003	1.67
162.0523	162.0525	0.0002	1.23
158.0811	158.0812	0.0001	0.63
95.0108	95.0104	0.0004	4.21



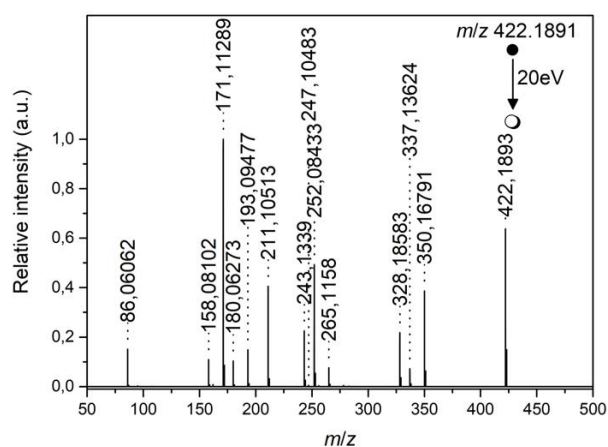
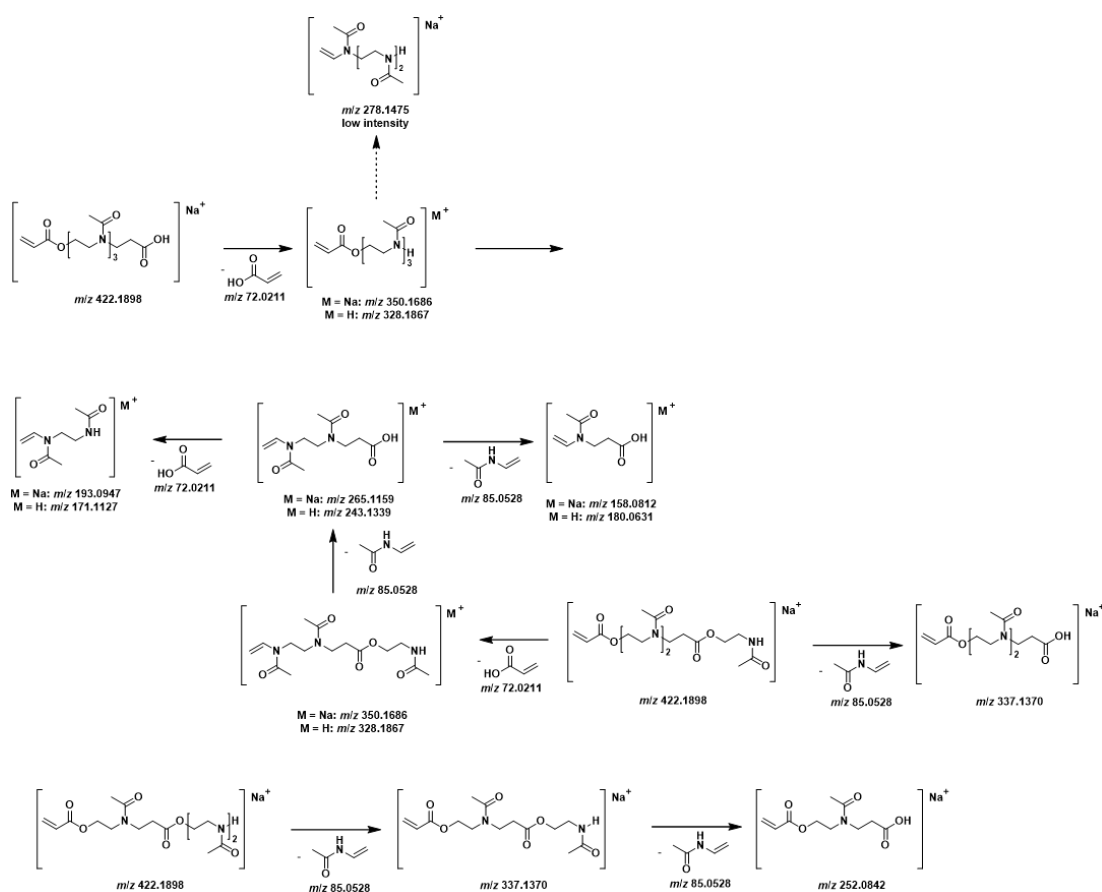


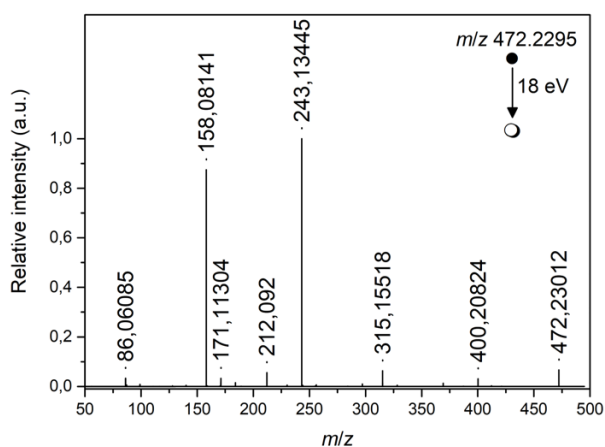
**Figure A.5** ESI MS/MS (positive mode) of MeOx/AA (1/1) isolating a species at  $m/z^{\text{exp}} = 422.1891$  with an HCD of 20 eV.

**Table A.10** Peak assignment of ESI MS/MS experiment of a MeOx/AA species at  $m/z^{\text{exp}} = 422.1891$  (Figure A.5).

$m/z(\text{exp})$	$m/z(\text{theo})$	$\Delta m/z$	Error / ppm
422.1891	422.1898	0.0007	1.66
350.1679	350.1686	0.0007	2.00
337.1362	337.1370	0.0008	2.37
315.1542	315.1551	0.0009	2.86
265.1150	265.1159	0.0009	3.39
252.0836	252.0842	0.0006	2.38
243.1332	243.1339	0.0007	2.88
198.0735	198.0737	0.0002	1.01
180.0628	180.0631	0.0003	1.67
162.0523	162.0525	0.0002	1.23
158.0811	158.0812	0.0001	0.63
95.0108	95.0104	0.0004	4.21



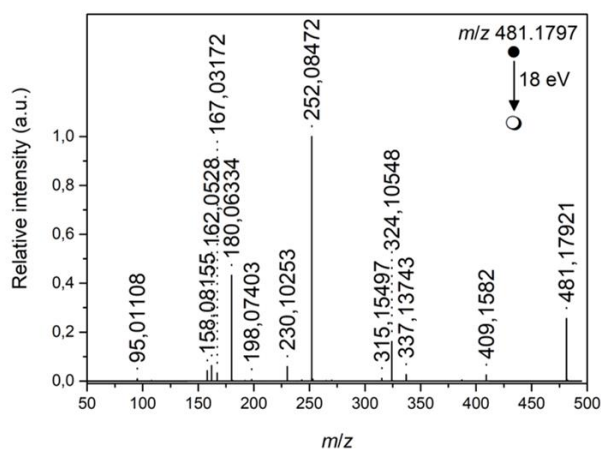
**Scheme A.6** Fragmentation scheme for MeOx/AA precursor at  $m/z^{\text{exp}} = 422.1898$ .



**Figure A.6** ESI MS/MS (positive mode) of MeOx/AA (1/1) isolating a species at  $m/z^{\text{exp}} = 472.2295$  with an HCD of 20 eV.

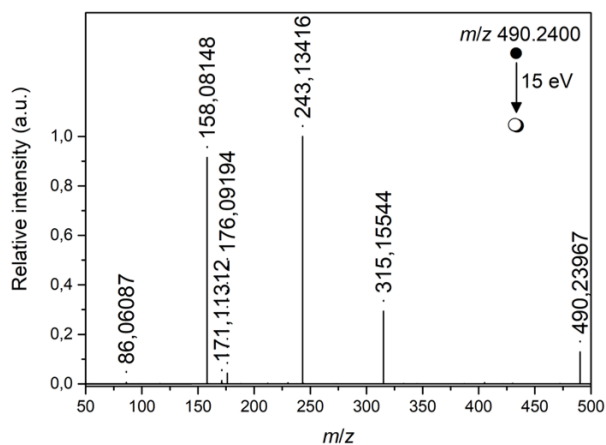
**Table A.11** Peak assignment of ESI MS/MS experiment of a MeO<sub>x</sub>/AA species at  $m/z^{\text{exp}} = 472.2295$  (Figure A.6).

$m/z^{\text{exp}}$	$m/z^{\text{theo}}$	$\Delta m/z$	Error [ppm]
472.2295	472.2290	0.0005	1.06
400.2082	400.2078	0.0004	1.00
315.1552	315.1551	0.0001	0.32
243.1345	243.1339	0.0006	2.47
212.0920	212.0917	0.0003	1.41
171.1130	171.1128	0.0002	1.17
158.0814	158.0812	0.0002	1.27
86.0609	86.0600	0.0009	10.46

**Figure A.7** ESI MS/MS (positive mode) of MeO<sub>x</sub>/AA (1/1) isolating a species at  $m/z^{\text{exp}} = 481.1797$  with an HCD of 18 eV.

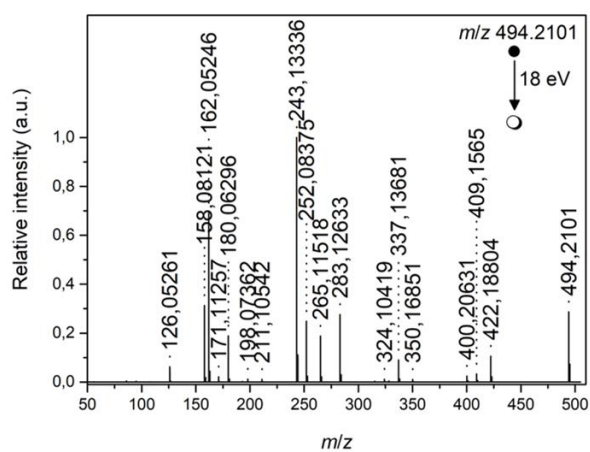
**Table A.12** Peak assignment of ESI MS/MS experiment of a MeO<sub>x</sub>/AA species at  $m/z^{\text{exp}} = 481.1797$  (Figure A.7).

$m/z^{\text{exp}}$	$m/z^{\text{theo}}$	$\Delta m/z$	Error [ppm]
481.1797	481.1793	0.0004	0.83
409.1582	409.1581	0.0001	0.24
337.1374	337.1370	0.0004	1.19
324.1055	324.1053	0.0002	0.62
315.1550	315.1551	0.0001	0.32
252.0847	252.0842	0.0005	1.98
230.1025	230.1023	0.0002	0.87
198.0740	198.0737	0.0003	1.51
180.0633	180.0631	0.0002	1.11
167.0317	167.0315	0.0002	1.20
162.0528	162.0525	0.0003	1.85
158.0816	158.0812	0.0004	2.53
95.0111	95.0104	0.0007	7.37

**Figure A.8** ESI MS/MS (positive mode) of MeO<sub>x</sub>/AA (1/1) isolating a species at  $m/z^{\text{exp}} = 490.2400$  with an HCD of 15 eV.

**Table A.13** Peak assignment of ESI MS/MS experiment of a MeO<sub>x</sub>/AA species at  $m/z^{\text{exp}} = 490.2400$  (Figure A.8).

$m/z^{\text{exp}}$	$m/z^{\text{theo}}$	$\Delta m/z$	Error /ppm
490.2400	490.2395	0.0005	1.02
315.1554	315.1551	0.0003	0.95
243.1342	243.1339	0.0003	1.23
176.0919	176.0917	0.0002	1.14
171.1131	171.1128	0.0003	1.75
158.0815	158.0812	0.0003	1.90
86.0609	86.0600	0.0009	10.46

**Figure A.9** ESI MS/MS (positive mode) of MeO<sub>x</sub>/AA (1/1) isolating a species at  $m/z^{\text{exp}} = 494.2101$  with an HCD of 18 eV.

**Table A.14** Peak assignment of ESI MS/MS experiment of a MeO<sub>x</sub>/AA species at  $m/z^{\text{exp}} = 494.2101$  (Figure A.9).

$m/z^{\text{exp}}$	$m/z^{\text{theo}}$	$\Delta m/z$	Error [ppm]
494.2101	494.2109	0.0008	1.62
422.1880	422.1898	0.0018	4.26
409.1565	409.1581	0.0016	3.91
400.2063	400.2078	0.0015	3.75
350.1685	350.1686	0.0001	0.29
337.1368	337.1370	0.0002	0.59
324.1042	324.1053	0.0011	3.39
283.1263	283.1264	0.0001	0.35
265.1152	265.1159	0.0007	2.64
252.0838	252.0842	0.0004	1.59
243.1334	243.1339	0.0005	2.06
211.1054	211.1053	0.0001	0.47
198.0736	198.0737	0.0001	0.50
180.0630	180.0631	0.0001	0.56
171.1126	171.1128	0.0002	1.17
162.0525	162.0525	0.0000	0.00
158.0812	158.0812	0.0000	0.00
126.0526	126.0525	0.0001	0.79

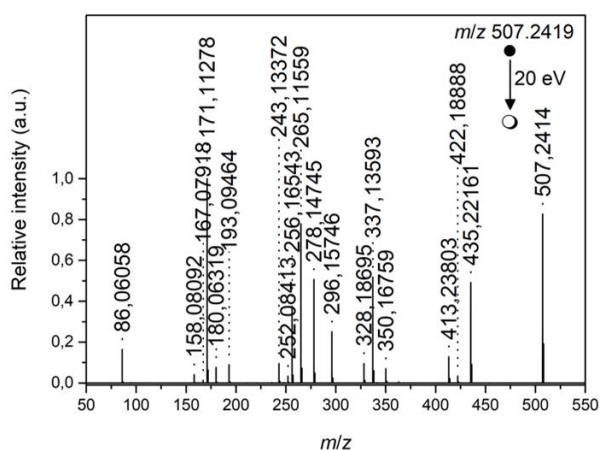


**Figure A.10** ESI MS/MS (positive mode) of MeOx/AA (1/1) isolating a species at  $m/z^{\text{exp}} = 507.2419$  with an HCD of 20 eV.

**Table A.15** Peak assignment of ESI MS/MS experiment of a MeOx/AA species at  $m/z^{\text{exp}} = 507.2419$  (Figure A.10).

$m/z^{\text{exp}}$	$m/z^{\text{theo}}$	$\Delta m/z$	Error [ppm]
507.2419	507.2425	0.0006	1.18
435.2216	435.2214	0.0002	0.46
422.1888	422.1898	0.0010	2.37
413.2380	413.2395	0.0015	3.63
350.1676	350.1686	0.0010	2.86
337.1359	337.1370	0.0011	3.26
328.1870	328.1867	0.0003	0.91
296.1575	296.1581	0.0006	2.03
278.1475	278.1475	0.0000	0.00
265.1156	265.1159	0.0003	1.13
256.1654	256.1656	0.0002	0.78
252.0841	252.0842	0.0001	0.40
243.1337	243.1339	0.0002	0.82
193.0946	193.0947	0.0001	0.52
180.0632	180.0631	0.0001	0.56
171.1128	171.1128	0.0000	0.00
167.0792	?		
158.0809	158.0812	0.0003	1.90
86.0606	86.0600	0.0006	6.97

**Table A.16** Quantitative calculations for EtOx:AA 1:1 based on the calibration curve (Figure 3.10) referred to the overview spectrum (Figure 3.2a). Calculated using Equation 3.1.

Repeat unit H <sup>+</sup>			Repeat unit Na <sup>+</sup>		
<i>m/z</i> <sup>exp</sup>	Intensity [a.u.]	$\chi$	<i>m/z</i> <sup>exp</sup>	Intensity [a.u.]	$\chi$
244.1174	1.75E+07	0.36 ± 0.05	266.0990	9.86E+07	0.26 ± 0.04
343.1860	1.62E+08	0.68 ± 0.10	365.1674	5.45E+08	0.60 ± 0.09
415.2069	5.47E+07	0.45 ± 0.07	437.1882	2.38E+08	0.29 ± 0.04
514.2745	2.78E+08	0.79 ± 0.12	536.2565	9.58E+08	0.67 ± 0.10
586.2967	8.20E+07	0.57 ± 0.09	608.2778	2.68E+08	0.40 ± 0.06
685.3636	1.71E+08	0.86 ± 0.13	707.3464	6.75E+08	0.77 ± 0.12
757.3850	4.14E+07	0.72 ± 0.11	779.3661	1.53E+08	0.50 ± 0.08
856.4545	5.65E+07	0.89 ± 0.13	878.4362	2.16E+08	0.80 ± 0.12
928.4753	1.28E+07	0.54 ± 0.08	950.4554	4.63E+07	0.61 ± 0.09
244.1174	1.75E+07	0.36 ± 0.05	266.0990	9.86E+07	0.26 ± 0.04

**Table A.17** Quantitative calculations for EtOx:AA 1:2 based on the calibration curve (Figure 3.10) referred to the overview spectrum (Figure 3.2b). Calculated using Equation 3.1.

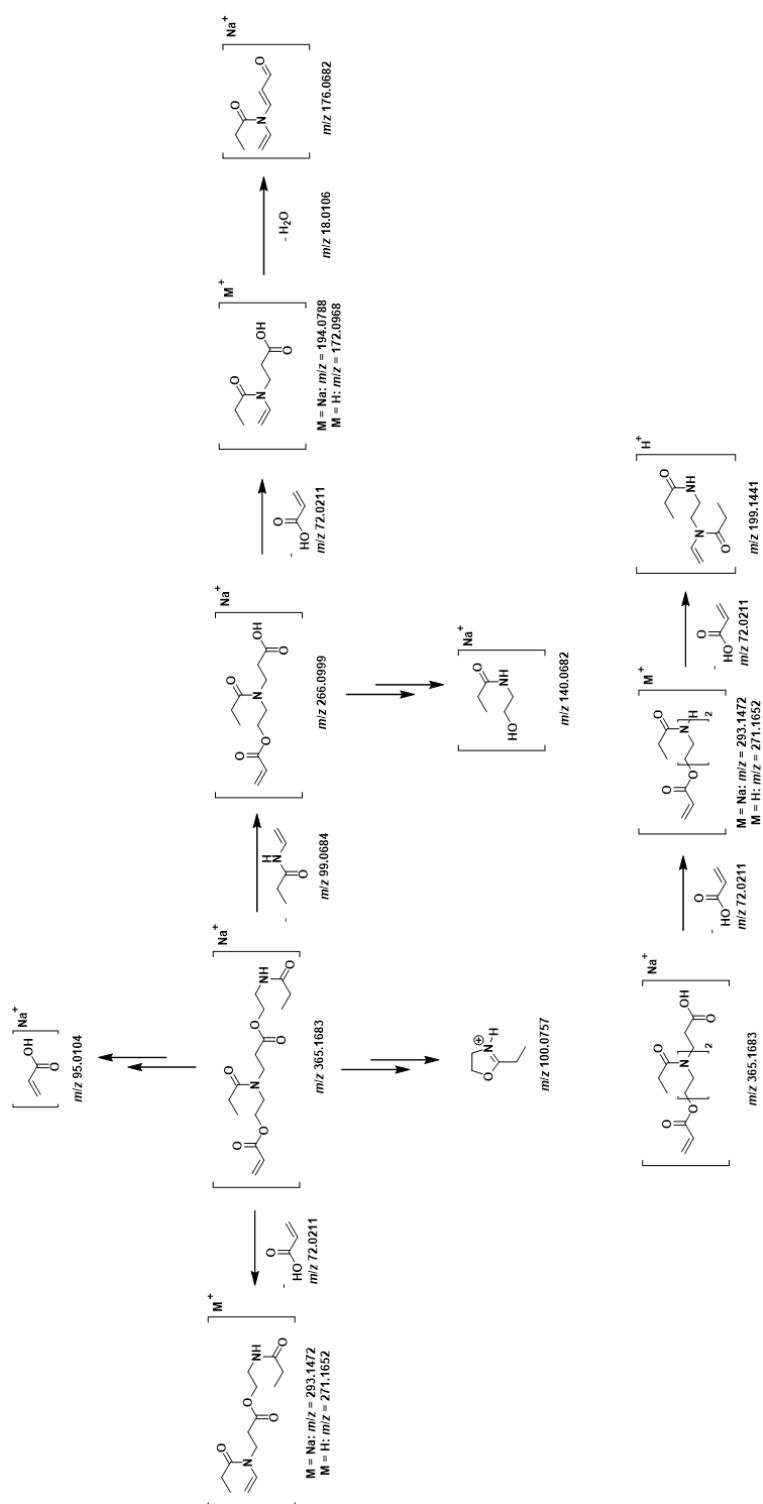
Repeat unit H <sup>+</sup>			Repeat unit Na <sup>+</sup>		
<i>m/z</i> <sup>exp</sup>	Intensity [a.u.]	$\chi$	<i>m/z</i> <sup>exp</sup>	Intensity [a.u.]	$\chi$
244.1174	3.17E+07	0.64 ± 0.09	266.0992	2.74E+08	0.74 ± 0.11
343.1855	7.48E+07	0.32 ± 0.05	365.1676	3.65E+08	0.40 ± 0.06
415.2062	6.67E+07	0.55 ± 0.08	437.1885	5.89E+08	0.71 ± 0.11
514.2748	7.50E+07	0.21 ± 0.03	536.2567	4.79E+08	0.33 ± 0.05
586.2952	6.23E+07	0.43 ± 0.06	608.2780	4.03E+08	0.60 ± 0.09
685.3638	2.83E+07	0.14 ± 0.02	707.3443	2.06E+08	0.23 ± 0.03
757.3851	1.59E+07	0.28 ± 0.04	779.3662	1.55E+08	0.50 ± 0.08
856.4515	7.08E+06	0.11 ± 0.02	878.4332	5.30E+07	0.20 ± 0.03
928.4753	1.10E+07	0.46 ± 0.07	950.4553	3.01E+07	0.39 ± 0.05
244.1174	3.17E+07	0.64 ± 0.10	266.0992	2.74E+08	0.74 ± 0.11

**Table A.18** Overview of species associated with homopropagation in EtOx/AA spectra and their respective mole fractions.

EtOx:AA feed	Repeat units [n]	$m/z^{\text{exp}}$	Intensity [a.u.]	$\chi$
<b>1:1</b>	2	271.1647	1.44E+08	$0.70 \pm 0.11$
	3	370.2330	4.15E+07	$0.83 \pm 0.12$
	4	469.3013	7.09E+06	$0.88 \pm 0.13$
	5	568.3695	5.30E+05	$1.00 \pm 0.15$
<b>1:2</b>	2	271.1647	6.16E+07	$0.30 \pm 0.05$
	3	370.2330	8.64E+06	$0.17 \pm 0.03$
	4	469.3013	1.00E+06	$0.12 \pm 0.02$
	5	568.3695	0.00E+00	$0.00 \pm 0.01$

**Table A.19** Peak assignment of ESI MS/MS experiment of an EtOx/AA species at  $m/z^{\text{exp}} = 365.1670$  (Figure 3.9a).

$m/z^{\text{exp}}$	$m/z^{\text{theo}}$	$\Delta m/z$	Error [ppm]
365.1670	365.1683	0.0013	3.56
293.1464	293.1472	0.0012	2.73
271.1643	271.1652	0.0009	3.32
266.0992	266.0999	0.0007	2.63
199.1436	199.1441	0.0005	2.51
194.0784	194.0788	0.0004	2.06
176.0677	176.0682	0.0005	2.84
172.0964	172.0968	0.0004	2.32
140.0679	140.0682	0.0003	2.14
100.0759	100.0757	0.0002	2.00
95.0106	95.0104	0.0002	2.11

Scheme A.7 Fragmentation scheme for EtOx/AA precursor at  $m/z^{\text{exp}} = 365.1683$ .

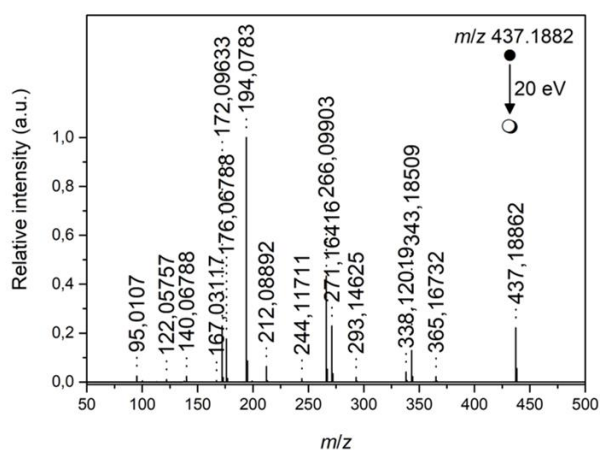
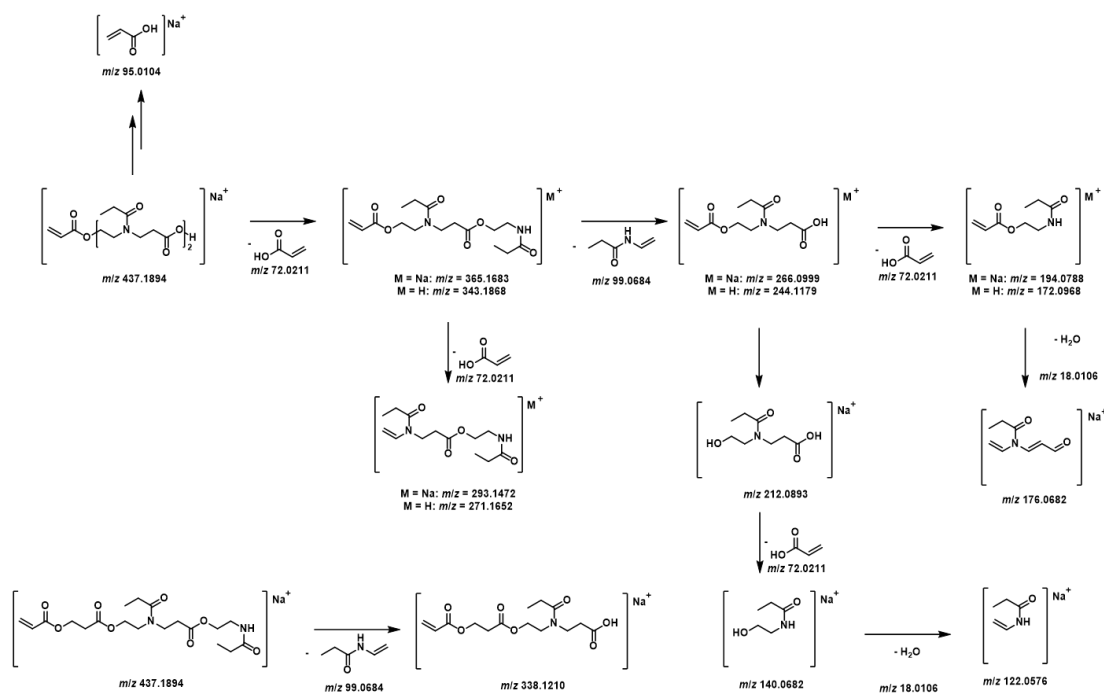


**Figure A.11** ESI MS/MS (positive mode) of EtOx/AA (1/1) isolating a species at  $m/z^{\text{exp}} = 437.1882$  with an HCD of 20 eV.

**Table A.20** Peak assignment of ESI MS/MS experiment of an EtOx/AA species at  $m/z^{\text{exp}} = 437.1882$  (Figure A.11).

$m/z^{\text{exp}}$	$m/z^{\text{theo}}$	$\Delta m/z$	Error [ppm]
437.1882	437.1894	0.0012	2.74
365.1673	365.1683	0.0010	2.74
343.1851	343.1868	0.0017	4.95
338.1202	338.1210	0.0002	2.37
293.1463	293.1472	0.0009	3.07
271.1642	271.1652	0.0010	3.69
266.0990	266.0999	0.0009	3.38
244.1171	244.1179	0.0008	3.28
212.0889	212.0893	0.0004	1.89
194.0783	194.0788	0.0005	2.58
176.0678	176.0682	0.0004	2.27
172.0963	172.0968	0.0005	2.91
167.0312	?		
140.0678	140.0682	0.0004	2.86
122.0576	122.0576	0.0000	0.00
95.0107	95.0104	0.0003	3.16



**Scheme A.8** Fragmentation scheme for EtOx/AA precursor at  $m/z^{\text{exp}} = 437.1894$ .

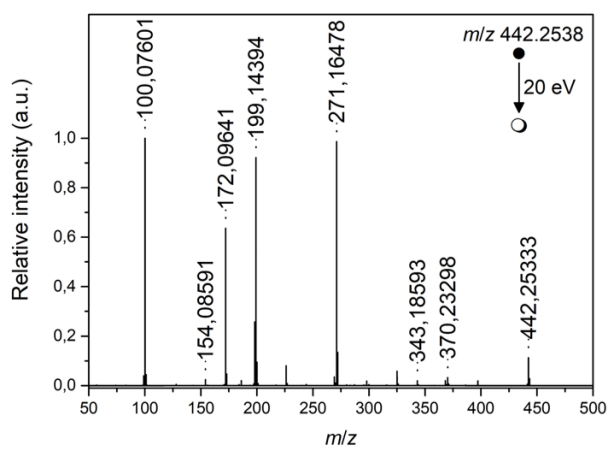


**Figure A.12** ESI MS/MS (positive mode) of EtOx/AA (1/1) isolating a species at  $m/z^{\text{exp}} = 442.2538$  with an HCD of 20 eV.



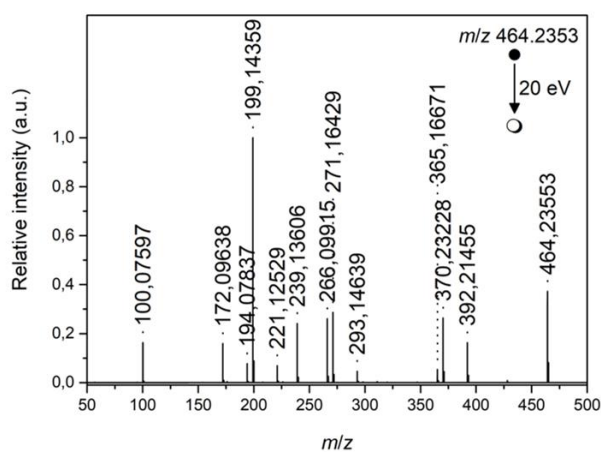


**Figure A.13** ESI MS/MS (positive mode) of EtOx/AA (1/1) isolating a species at  $m/z^{\text{exp}} = 464.2353$  with an HCD of 20 eV.

**Table A.22** Peak assignment of ESI MS/MS experiment of an EtOx/AA species at  $m/z^{\text{exp}} = 464.2353$  (Figure A.13).

$m/z^{\text{exp}}$	$m/z^{\text{theo}}$	$\Delta m/z$	Error [ppm]
464.2353	464.2367	0.0014	3.02
392.2146	392.2156	0.0010	2.55
370.2323	370.2336	0.0013	3.51
365.1667	365.1683	0.0016	4.38
293.1464	293.1472	0.0008	2.73
271.1643	271.1652	0.0009	3.32
266.0992	266.0999	0.0007	2.63
239.1361	239.1366	0.0005	2.09
221.1253	221.1260	0.0007	3.17
199.1436	199.1441	0.0005	2.51
194.0784	194.0788	0.0004	2.06
172.0964	172.0968	0.0004	2.32
100.0760	100.0757	0.0003	3.00

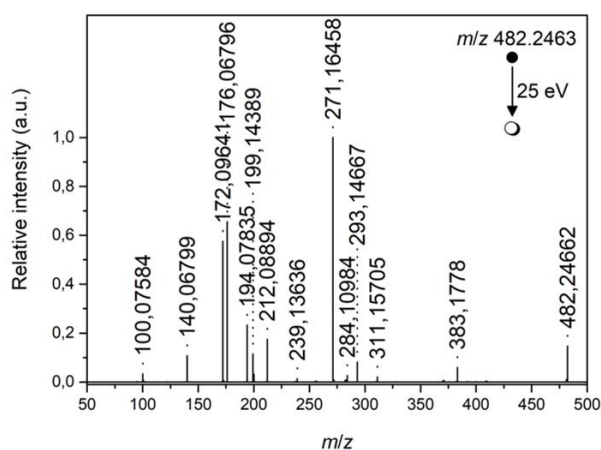
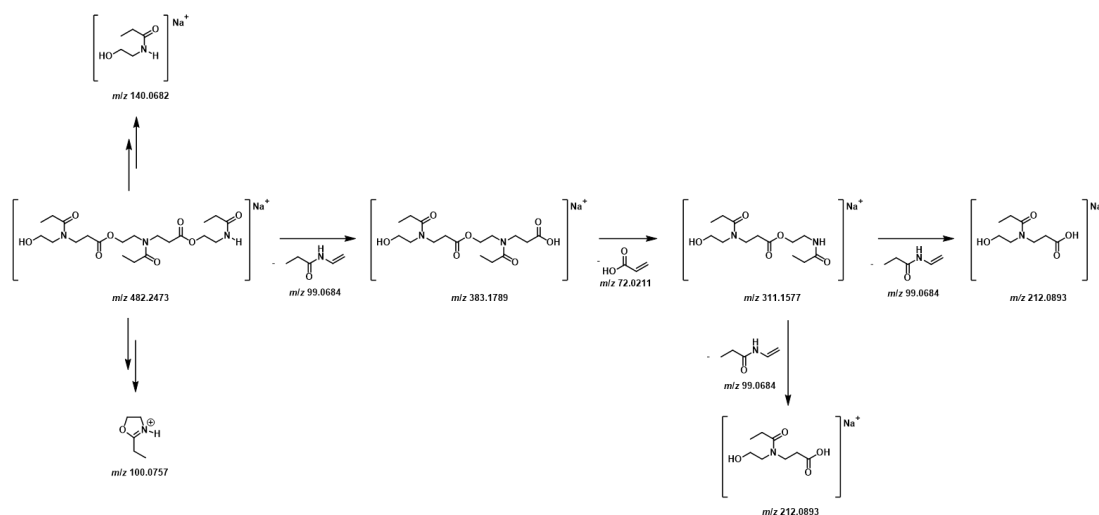


**Figure A.14** ESI MS/MS (positive mode) of EtOx/AA (1/1) isolating a species at  $m/z^{\text{exp}} = 482.2463$  with an HCD of 25 eV.

**Table A.23** Peak assignment of ESI MS/MS experiment of an EtOx/AA species at  $m/z^{\text{exp}} = 482.2463$  (Figure A.14).

$m/z^{\text{exp}}$	$m/z^{\text{theo}}$	$\Delta m/z$	Error [ppm]
482.2463	482.2473	0.0009	2.07
383.1778	383.1789	0.0011	2.87
311.1571	311.1577	0.0006	1.93
293.1467	293.1472	0.0005	1.71
284.1098	284.1105	0.0007	2.46
271.1646	271.1652	0.0006	2.21
239.1364	239.1366	0.0002	0.84
212.0889	212.0893	0.0004	1.89
199.1439	199.1441	0.0002	1.00
194.0784	194.0788	0.0004	2.06
176.0680	176.0682	0.0002	1.14
172.0964	172.0968	0.0004	2.32
140.0680	140.0682	0.0002	1.43
100.0760	100.0757	0.0003	3.00



**Scheme A.10** Fragmentation scheme for EtOx/AA precursor at  $m/z^{\text{EXP}} = 482.2463$ .

**Table A.24** Quantitative calculations for EtOz:AA 1:1 based on the calibration curve (Figure 3.10) referred to the overview spectrum (Figure 3.3a). Calculated using Equation 3.1.

Repeat unit $\text{H}^+$			Repeat unit $\text{Na}^+$		
$m/z^{\text{EXP}}$	Intensity [a.u.]	$\chi$	$m/z^{\text{EXP}}$	Intensity [a.u.]	$\chi$
258.1330	4.17E+07	$0.27 \pm 0.04$	280.1148	1.04E+08	$0.35 \pm 0.05$
371.2173	2.05E+08	$0.46 \pm 0.07$	393.1988	2.37E+08	$0.48 \pm 0.07$
443.2381	1.59E+08	$0.23 \pm 0.03$	465.2193	1.70E+08	$0.26 \pm 0.04$
556.3218	2.44E+08	$0.53 \pm 0.08$	578.3040	4.25E+08	$0.55 \pm 0.08$
628.3434	1.49E+08	$0.26 \pm 0.04$	650.3240	1.91E+08	$0.30 \pm 0.05$
741.4259	1.31E+08	$0.60 \pm 0.09$	763.4082	2.99E+08	$0.68 \pm 0.06$
813.4469	7.34E+07	$0.33 \pm 0.05$	835.4305	1.21E+08	$0.41 \pm 0.06$
926.5327	5.01E+07	$0.68 \pm 0.10$	948.5127	1.03E+08	$0.77 \pm 0.12$
998.5529	2.58E+07	$0.39 \pm 0.06$			

**Table A.25** Quantitative calculations for EtOz:AA 1:2 based on the calibration curve (Figure 3.10) referred to the overview spectrum (Figure 3.3b). Calculated using Equation 3.1.

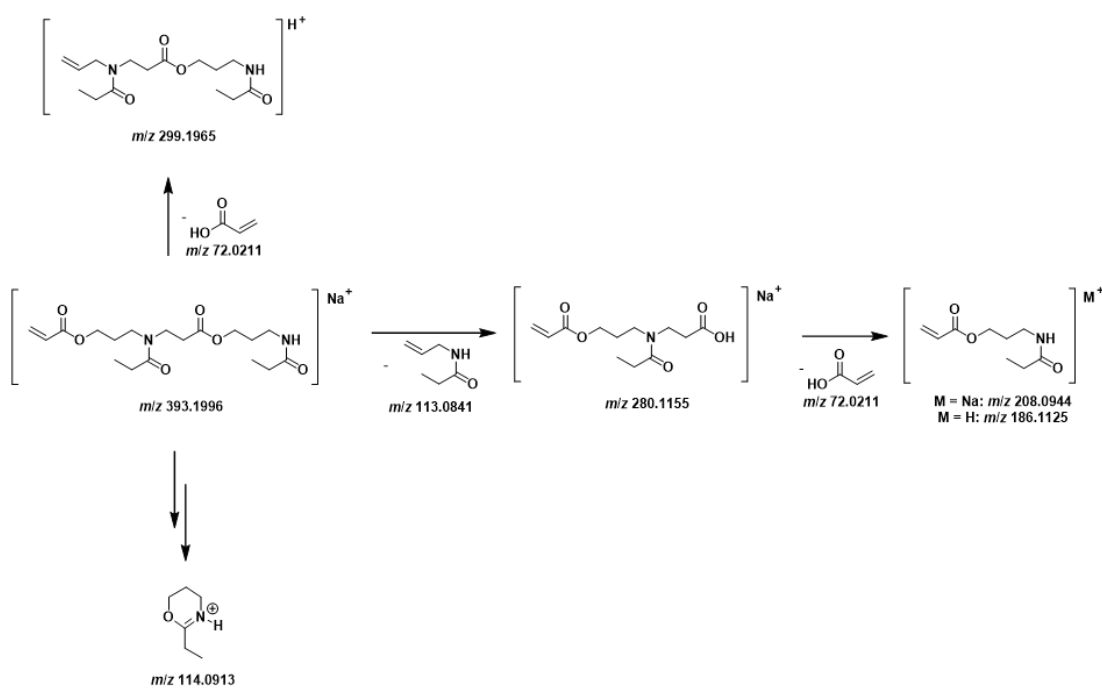
Repeat unit H <sup>+</sup>			Repeat unit Na <sup>+</sup>		
$m/z^{\text{exp}}$	Intensity [a.u.]	$\chi$	$m/z^{\text{exp}}$	Intensity [a.u.]	$\chi$
258.1333	1.12E+08	0.73 ± 0.11	280.1151	1.91E+08	0.65 ± 0.10
371.2169	2.46E+08	0.54 ± 0.08	393.1984	2.60E+08	0.52 ± 0.08
443.2376	5.28E+08	0.77 ± 0.12	465.2200	4.86E+08	0.74 ± 0.11
556.3226	2.14E+08	0.47 ± 0.07	578.3031	3.41E+08	0.45 ± 0.07
628.3423	4.22E+08	0.74 ± 0.11	650.3246	4.49E+08	0.70 ± 0.11
741.4265	8.94E+07	0.40 ± 0.06	763.4088	1.43E+08	0.32 ± 0.05
813.4474	1.50E+08	0.67 ± 0.10	835.4284	1.77E+08	0.59 ± 0.09
926.5330	2.35E+07	0.32 ± 0.05	948.5131	3.10E+07	0.23 ± 0.03
998.5530	4.09E+07	0.61 ± 0.09			

**Table A.26** Overview of species associated with homopropagation in EtOz/AA spectra and their respective mole fractions.

EtOz:AA	Repeat units	$m/z^{\text{exp}}$	Intensity	$\chi$
feed	[n]		[a.u.]	
<b>1:1</b>	2	299.1960	3.64E+07	0.48 ± 0.07
	3	412.2797	2.35E+06	0.89 ± 0.13
	4	525.3640	1.88E+04	1.00 ± 0.15
	5	638.4487	0.00E+00	0.00 ± 0.01
<b>1:2</b>	2	299.1960	3.93E+07	0.52 ± 0.08
	3	412.2797	2.97E+05	0.11 ± 0.02
	4	525.3640	0.00E+00	0.00 ± 0.01
	5	638.4487	0.00E+00	0.00 ± 0.01

**Table A.27** Peak assignment of ESI MS/MS experiment of an EtOz/AA species at  $m/z^{\text{exp}} = 393.1995$  (Figure 3.9b).

$m/z^{\text{exp}}$	$m/z^{\text{theo}}$	$\Delta m/z$	Error [ppm]
393.1995	393.1996	0.0001	0.25
299.1968	299.1965	0.0003	1.00
280.1156	280.1155	0.0001	0.36
208.0946	208.0944	0.0002	0.96
186.1126	186.1125	0.0001	0.54
114.0918	114.0913	0.0005	4.38

**Scheme A.11** Fragmentation scheme for EtOz/AA precursor at  $m/z^{\text{exp}} = 393.1995$ .

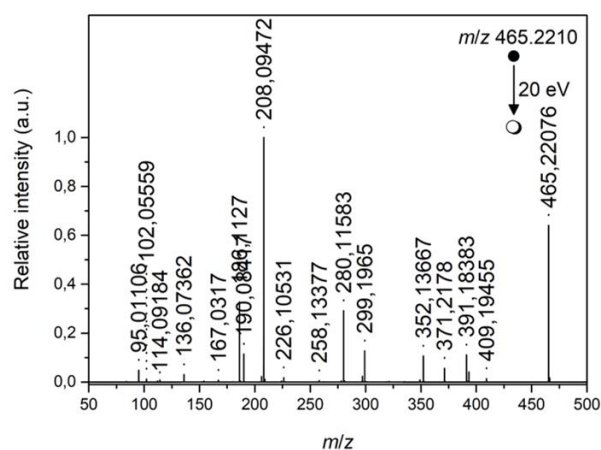


**Figure A.15** ESI MS/MS (positive mode) of EtOz/AA (1/1) isolating a species at  $m/z^{\text{exp}} = 465.2210$  with an HCD of 20 eV.

**Table A.28** Peak assignment of ESI MS/MS experiment of an EtOz/AA species at  $m/z^{\text{exp}} = 465.2210$  (Figure A.15).

$m/z^{\text{exp}}$	$m/z^{\text{theo}}$	$\Delta m/z$	Error [ppm]
465.2210	465.2207	0.0003	0.25
409.1946	299.1965	0.0003	1.00
280.1156	280.1155	0.0001	0.36
208.0946	208.0944	0.0002	0.96
186.1126	186.1125	0.0001	0.54
114.0918	114.0913	0.0005	4.38

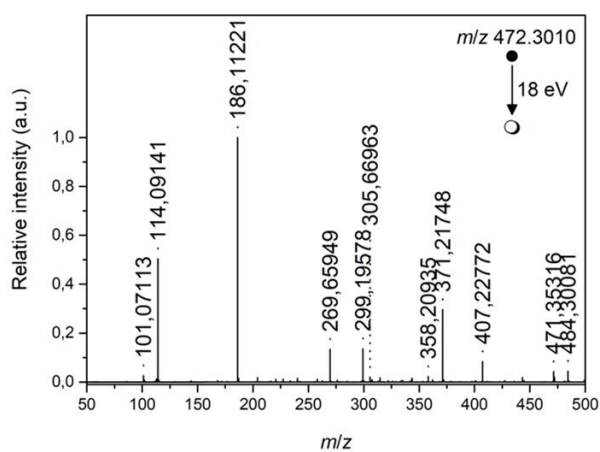


**Figure A.16** ESI MS/MS (positive mode) of EtOz/AA (1/1) isolating a species at  $m/z^{\text{exp}} = 472.3010$  with an HCD of 18 eV.

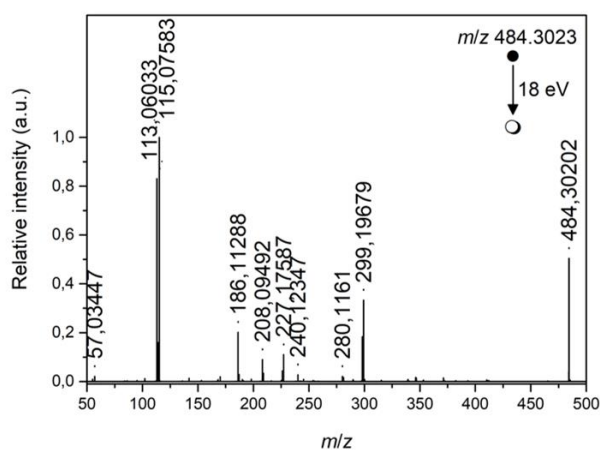


**Figure A.17** ESI MS/MS (positive mode) of EtOz/AA (1/1) isolating a species at  $m/z^{\text{exp}} = 484.3023$  with an HCD of 18 eV.